AN EXPERIMENTAL AND COMPUTATIONAL INVESTIGATION OF THE EFFECT OF PRIMARY INTAKE RUNNER GEOMETRY ON THE PERFORMANCE OF A SINGLE CYLINDER ENGINE

A Thesis

Presented in Partial Fulfillment of the Requirements for

the Degree Master of Science in the

Graduate School of The Ohio State University

By

Vincent Edward Mariucci, B.S.M.E.

****

The Ohio State University
2006

Master's Examination Committee:

Dr. Ahmet Selamet, Advisor

Dr. Rajendra Singh

Keith D. Miazgowicz

Approved by:

_____
Advisor

Graduate Program in Mechanical Engineering

ABSTRACT

The present study investigates the effects of various intake configurations on a firing single cylinder research engine. Eighteen different intake configurations were tested and modeled including a straight baseline case, tapers, varying inlet radii, bends, and S-bends. All of the intakes include a bellmouthed flange at the entrance and retain the same length to the bellmouth, transducer locations, and downstream diameter in an effort to identify the effect of the intake geometry only. An experimental study was conducted where each intake was instrumented with three pressure transducers. One of the pressure transducers was located near the entrance of the intake; the others were located downstream of the barrel throttle. Volumetric efficiency, brake power, and intake and exhaust pressures for each configuration are presented to determine the effect of each geometry on engine performance.

Each intake configuration was modeled using a quasi-one-dimensional finite difference engine simulation code, MANDY. The volumetric efficiencies and pressures obtained experimentally are compared to the predictions to assess the code's ability to predict the effects of the various intake configurations on engine performance.

Taper area ratios above 1.5 were found to have a detrimental effect on volumetric efficiency at high-speed tuning peaks. The inlet flow losses for the sharpest bellmouth

studied ($R_i/D = 0.05$) had a measurable negative effect on volumetric efficiency, while those of larger-radiused inlets were negligible. The flow losses associated with the bends and S-bends also had a detrimental effect on volumetric efficiency compared to the straight pipe. In general, MANDY showed a good agreement with the experiments for each intake configuration for both volumetric efficiency and intake pressure near the valves at the main tuning peak speeds.

Dedicated to My Wife, Jennifer

ACKNOWLEDGMENTS

I would like to thank my advisor, Dr. Ahmet Selamet, for his expertise and guidance over the past two years. I am grateful to Dr. Rajendra Singh for taking time to be a member of my examination committee. I would also like to thank Ford Motor Company for supporting my work by supplying all the test pieces and the single cylinder engine and for giving me an opportunity to continue what I love doing after graduation. Specifically, I would like to thank Dr. Kevin Tallio for supporting the procurement of the single cylinder engine, Zafar Shaikh for his assistance as the supervisor of the Ford single cylinder lab, Mike Magnan for designing and fabricating the intake configurations, Graham Hoare and Frank Fsadni for supporting the single-cylinder related Ford University Research Program proposal, Dr. Nolan Dickey for his knowledge and assistance with the engine simulation code, and Keith Miazgowicz for his MANDY assistance, outstanding overall support of the project, and for serving as a member of my examination committee.

For the past two years, I have had the privilege to work with an outstanding group of team members at the Center for Automotive Research. Special thanks go to Cam Giang, Dr. Iljae Lee, Adam Christian, Jacques Paul, Shankar Kumar, Dr. Emel Selamet,

and Don Williams who have all helped me through various stages of the project.

Last, but certainly not least, I would like to thank my wife, Jennifer, for providing encouragement and support from the very beginning of my graduate career.

VITA

September 21, 1982……... Born – Toledo, Ohio

2004……... B.S. Mechanical Engineering,
The Ohio State University

2004 – Present……Graduate Research Associate,
The Ohio State University

FIELDS OF STUDY

Major Field: Mechanical Engineering

TABLE OF CONTENTS

LIST OF FIGURES

LIST OF TABLES

NOMENCLATURE

A	cross-sectional area
c	speed of sound
CAD	crank angle [degrees]
$C_{b\text{-}b}$	bend-bend interaction factor
C_θ	bend angle correction factor
D	intake duct diameter
D_t	inlet diameter of taper
EVC	exhaust valves close
EVO	exhaust valves open
f	frequency, Fanning friction factor
IV	intake valve
IVC	intake valves close
IVO	intake valves open
K_{90}	loss factor of 90° bend
$K_{b\text{-}b}$	bend-bend loss factor
K_t	total bend loss factor

K_θ	loss factor of bend angle θ
l	effective intake length
L_t	length of tapered section
$\dot{m}_a$	mass flow rate of air into cylinder
N	engine speed, number of species
OSPL	overall sound pressure level
p	pressure
$\wp$	perimeter
P_{rms}	root-mean-square of pressure
q	ratio of pipe frequency to engine frequency
$\dot{q}$	heat transfer rate
QSW	quasi standing wave
R_c	radius of curvature
r_c	compression ratio
Re	Reynolds number
R_i	inlet radius
SPL	sound pressure level
U	velocity
V_d	displaced volume
WOT	wide-open throttle
y_j	mass fraction of species j
γ	ratio of specific heats

δ	end correction length
θ	bend angle
ρ	density
τ_w	wall shear stress

CHAPTER 1

INTRODUCTION

1.1 Background

For almost as long as the internal combustion (IC) engine has existed, designers have been trying to optimize it. Whether the motivating factor was more power or better fuel economy, several techniques have been employed throughout the years to improve the IC engine. One of the most well-known and used methods of enhancing an engine's performance is by intake or exhaust tuning. Due to the unsteady nature of the gas exchange process in the IC engine, pressure fluctuations are generated when the engine takes in air or exhausts combustion gasses. During the intake stroke of a single cylinder engine with intake pipe leading from atmosphere to the cylinder, for example, as the piston draws in fresh charge, an expansion wave propagates toward the inlet of the intake pipe. When this expansion wave reaches the inlet of the pipe, it is partially reflected as a compression wave. If this compression wave arrives back at the intake valve while it is open to the cylinder, it can aid the breathing process of the engine, thus increasing the volumetric efficiency defined as

$$\eta_v = \frac{\text{mass of air trapped in cylinder}}{\text{mass of air contained in swept volume of cylinder at inlet air density}}, \qquad (1.1)$$

an important parameter for comparing and evaluating different designs for similar engines. This charging effect will happen at certain engine speeds, giving rise to "tuning peaks." Conversely, an expansion wave may reach the valve at an inopportune time, causing what is generally referred to as "anti-tuning." A similar effect occurs in the exhaust of the engine, and is usually called "exhaust scavenging."

Predicting what engine speed this tuning effect will be most effective or most detrimental has been an important focus of engine designers from the early 20th century to the present. Predictive engine design tools have been used in several different forms from linear acoustic lumped and distributed Helmholtz resonator approximations of the intake and cylinder to complicated computer codes that solve nonlinear quasi-one-dimensional fluid conservation equations using numerical methods. Some predict only where the tuning peak will occur; others, such as the quasi-1D computer codes, can predict, in addition to the location of peaks, their magnitudes and several variables including pressure, temperature, and velocity of the working fluids anywhere in the intake or exhaust system.

1.2 Literature Survey

The idea of optimizing an engine's intake, exhaust, and other systems for power or volumetric efficiency gains has been around almost as long as the IC engine itself. One of the first mentions of engine optimization was made by Koester in 1904. His conclusions on how to optimize a steam engine included minimizing flow losses in the

intake by keeping the runners as short as possible and minimizing the bends, and by keeping the intake valve open as long as possible during the intake stroke. Most of his ideas were directly applicable to IC engines.

In 1924, Matthews and Gardiner, working with a one-cylinder diesel engine, found that the engine would not start unless the compression pressure was increased. They found that a long suction pipe attached to the inlet port gave them the pressure increase they needed, and proceeded to test several lengths of pipe up to 70 in. in addition to the case where no pipe was present from 500 to 1800 RPM; they noticed an increase in compression pressure of 17 % with the 62 in pipe compared to no inlet pipe. This study was purely experimental and did not attempt to explain the reason for the increase in pressure.

Capetti (1929) developed a method for determining the optimum length of pipe for intake tuning. He proposed that the maximum tuning effect occurred when the maximum of the compression wave reached the piston while it was at bottom dead center (BDC). The maximum of the compression wave is produced by the reflection of the maximum of the expansion wave; the generation of the maximum of the expansion wave, Capetti said, would occur at mid stroke when the piston is at its maximum speed. Therefore, the ideal length of intake pipe was one that allowed the return trip of the compression wave in one half of a stroke, or 90 crank angle degrees (CAD). In other words,

$$l = 7.5\frac{c}{N}, \tag{1.2}$$

where l [m] is the length of intake pipe, c [m/s] is the speed of sound, and N [rpm] is the engine speed. This formula, if correct, would have given engine designers a powerful, easy-to-use tool for predicting engine performance; however, when comparing the earlier results of Matthews and Gardiner to his theory, Capetti discovered that the actual optimum lengths were less than that given by Eq. (1.2).

Dennison (1933) attempted to develop his own theory for predicting the optimum tuning length of an intake pipe by thinking of the column of air in the pipe as a reservoir of kinetic energy. Despite being more complex than Capetti's method, Dennison's theory over-predicted the optimum length of pipe by 50 percent and over-predicted the maximum volumetric efficiency gain by 9.4 percent when compared to his test results. Also, both Capetti's and Dennison's methods do not account for cylinder volume or pipe diameter, two dimensions which are known to be important for accurate tuning peak predictions. Dennison only mentioned that the smallest pipe would give the largest supercharging effect as long as it was not too small as to let friction negate any positive effects. He also stated that "theoretical (volumetric) efficiency must be corrected by about 10 percent in the size of the engine tested. In larger engines, the correction will be smaller, and in small engines larger."

Morse *et al.* (1938) developed another theory of intake pipe tuning based on the "organ pipe" assumption that Capetti and others used. Their theory stated that when a fundamental firing frequency of the engine equals one of the resonant frequencies of the intake pipe when the valve is closed, then the pressure fluctuations at the valve will be large. Sometimes, a lower-than-average pressure will be present at the intake valve shortly before closing, which will decrease the engine's power; other times, a higher-

than-average pressure will be present, and this will cause the supercharging effect. They determined that positive intake tuning occurred when the ratio of pipe frequency to engine firing frequency equaled 3, 4, or 5. This method of prediction was echoed by Lichty (1951). Morse *et al.* also proposed a method for determining the volumetric efficiency of the engine with the tuned intake and the pressure traces near the intake port; their predictions correlated well with their experiments. Their work admits one shortcoming: "in this analysis we have made no mention of the effect on the results of a change of valve timing. It is clear that such a change may have a considerable effect on the results."

In 1935, Kadenacy patented an adjustable length exhaust which was set to optimize a certain speed at which the engine would operate under normal conditions. He explained the exhaust scavenging effect by the column of air exiting the exhaust pipe, which, by Kadenacy's reasoning had the properties of a resilient body, would create a partial vacuum in the cylinder that would aid the intake process. Mucklow (1940) investigated the exhaust pressure pulsations of an IC engine and their effect on volumetric efficiency. He investigated both the effect of different exhaust lengths as well as different intake and exhaust valve timing in an effort to obtain the maximum air consumption of the engine.

DeHaller (1945) applied the Method of Characteristics (MC) to the mass and momentum equations governing unsteady flow in pipes of varying cross-section, like those found in the intake and exhaust of IC engines. This method of solving the quasi-1D unsteady flow equations served as the basis for a computer code developed in the 1960s by Benson *et al.* (1964). This code was one of the first quasi-1D engine simulation

programs. Using MC to solve the mass, momentum, and energy conservation equations, Benson's code was capable of predicting the pressure and temperature fluctuations in the exhaust pipe of a single cylinder two-stroke engine, and allowed for friction, heat transfer, and gradual area changes. Although the code outlined in the 1964 paper was only for one cylinder and included the exhaust valve and exhaust duct, other more sophisticated programs soon followed.

In the later half of the 20th century, Engelman and his coworkers developed an intake tuning prediction tool based on a lumped Helmholtz resonator; they modeled the intake and cylinder as shown in Fig. 1.1, treating the air in the cylinder as a spring, and the air in the runner as a mass. The tuning peak is assured to occur when the resonant frequency of the Helmholtz system is around twice the piston frequency. Engelman (1973) stated that for a case of a single cylinder with an intake runner open to atmosphere, the lumped method predicts that the tuning peak will occur at,

$$N_t(RPM) = \frac{955}{K} c \left(\frac{A}{l\, V_{eff}} \right)^{1/2} \tag{1.3}$$

where c [m/s] is the speed of sound, A [cm²] is the effective cross-sectional area of the intake, l [cm] is the effective length of the inlet system, K is a factor usually equal to 2.1, but that varies from 2.0 to 2.5 depending upon valve timing and other factors, and,

$$V_{eff} = \frac{V_d (r_c + 1)}{2(r_c - 1)} \quad [\text{cm}^3] , \tag{1.4}$$

where V_d [cm^3] is the displaced volume and r_c is the compression ratio. This method provides a simple tool for calculating the location of an intake tuning peak, but gives no insight into its magnitude. Even though it incorporates extra parameters over the organ

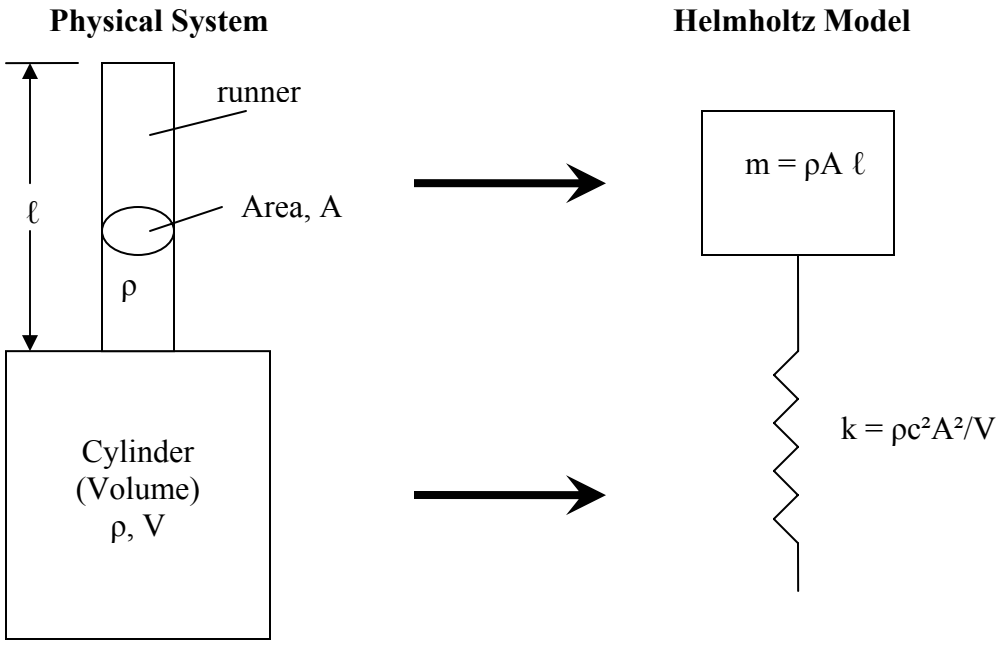

Figure 1.1: Lumped Helmholtz Resonator Model of Cylinder and Runner.

pipe method such as the pipe area and cylinder volume, the value for K is slightly ambiguous until experimental data can be obtained, which decreases this method's usefulness. In his thesis, Thompson (1968) proposed

$$\frac{L}{A}_{effective} = \int_0^L \frac{dx}{A} \cong \sum_{j=1}^{N} \frac{L_j}{A_j} \tag{1.5}$$

to account for tapers and other geometries with varying cross-sections when using Eq. (1.3).

Others have expanded on the Helmholtz approximation for cylinder breathing. Driels (1975) added a valve model to the Helmholtz system between the intake pipe and cylinder volume and developed a time-dependent method of predicting intake pressure

traces. Chapman *et al.* (1983) developed a computer code that treats the pipes and volumes of a manifold as a system of nonlinear coupled Helmholtz resonators. This model consisted not only of the system of Helmholtz resonators to predict flow in the intake and exhaust systems but also a thermodynamic in-cylinder model and valve boundaries that provide conditions to drive the Helmholtz resonators. The system of ordinary differential equations derived by this method was solved using a fourth order Runge-Kutta integration. This model predicted intake pressure very well at low engine speeds, but became increasingly inaccurate at higher speeds. It predicted the volumetric efficiency of a four-cylinder engine fairly accurately.

Winterbone and Yoshitomi (1990) developed a Helmholtz resonator model of an engine intake where, instead of being considered a volume as in Engelman's method, the cylinder and intake pipe were considered to be two connected pipes, with the larger pipe (the cylinder) having a closed end. Using this method, the gas in both the pipe and the cylinder have compressibility and inertia, whereas Engelman's method assumes the gas in the pipe has no compressibility and the gas in the cylinder has no inertia. A computer simulation model was created from this method which predicted intake pressures and volumetric efficiency. In general, the intake pressure compared well with the experiment, with a growing phase shift as the engine speed increased; the overall trend of the volumetric efficiency curve was predicted adequately, but the absolute magnitudes were generally over-predicted when compared with the experiment. Winterbone and Pearson (1999) mentioned a simpler version of this method, by allowing the cylinder to be a lumped element as Engelman had and letting the pipe be a distributed element.

As computing power increased, attempting to solve with numerical methods the quasi-1D, nonlinear conservation equations through the entire gas exchange process of an engine, as Benson had done, gained more support. Ledger (1975) applied a finite-difference approach to the problem of exhaust gas dynamics in a turbocharged diesel engine. This particular model did not include friction and assumed the flow in the exhaust pipe was homentropic; it compared very well to results given by Benson's MC-based code run under the same assumptions. In 1979, Lakshminarayanan *et al.* detailed another finite-difference approach to predict the gas exchange process using the Runge-Kutta method. Another finite difference code, developed by Chapman *et al.* (1982) is based on a FRAM algorithm. Takizawa *et al.* (1982) developed a two-step Lax-Wendroff-based finite difference code. They found that their finite difference method, being second order accurate in both time and space, provided more accurate results than the classic method of characteristics, which is essentially first-order accurate, when compared to their experimental results.

In recent years, three-dimensional computational fluid dynamics (3D CFD) codes have been coupled to the quasi-1D codes to better predict the gas exchange process in areas that give rise to three-dimensional flow effects, such as air boxes, plenums, bellmouths, etc. Usually, the quasi-1D code is allowed to run to convergence by itself, then in the appropriate section, the 1D code passes boundary conditions to the 3D CFD model, which computes new boundary conditions to pass back to the 1D code. Arias *et al.* (2000), Sinclair *et al.* (2000), Borghi *et al.* (2001), Maynes *et al.* (2002), and Riegler and Bargende (2002) have published works on 1D/3D coupled engine simulation, and most commercially available quasi-1D codes have the option for 3D CFD coupling.

1.3 Objective

The first objective of this thesis is to investigate the effect of intake geometry on the overall engine performance. Eighteen intake geometries were fabricated at Ford Motor Company using laser stereo-lithography for this study and have the characteristics representative of intake systems in production engines. Besides the straight baseline configuration, the test pieces can be categorized into four groups: tapers, bellmouths, bends, and double-bends or S-bends. In order to isolate the effects of the intake geometries, each test piece is the same length to the inlet radius, and in all cases except the bellmouth group the inlet radius is the same; further characteristics of the test pieces will be provided in Chapter 2. Each of these intake geometries was tested on a single cylinder research engine from operating speeds of 1000 to 5500 RPM by 250 RPM increments with additional points obtained at speeds of relative importance, like volumetric efficiency peaks.

Despite the many predictive tools available to the designer to approximate the behavior in the intake of an IC engine, most of the literature has focused on varying the area and length of straight ducts only. Although quasi-1D engine simulation codes can theoretically handle tapers and bends, it is somewhat unclear if these geometries can be modeled accurately in one dimension, or if they generate 3D flow effects that alter the tuning characteristics of the intake. For example, some designers using quasi-1D simulation in industry have noted that the predicted effect of the tapered geometry is over-estimated when compared to engine experiments. The second objective of this study is to find a systematic way of modeling the intake geometries in 1D alone that

better captures the physics, or if there are strong multi-dimensional effects present in certain geometries, to use 1D-3D coupled simulation code to obtain better predictions and be able to visualize the flow effects in these intakes.

Following this introduction, the experimental setup is described in Chapter 2, starting with the engine and DC dynamometer pair. The engine intake and exhaust systems are depicted next followed by the details of the 18 intake prototype configurations. Finally, the transducer locations and procedure for determining volumetric efficiency are outlined.

Chapter 3 compares the experimental results only. The effect of tapers, inlet bellmouths, and bends are investigated as groups. Volumetric efficiency, brake power, and pressure in both the time and frequency domains are presented.

Chapter 4 details the various intake models used for this study. First, results from simple one-dimensional, linear models are presented, including the organ pipe and lumped parameter Helmholtz approximations. Also, the details of the quasi-1D engine simulation code are given, as well as the calibraton parameters used for this work and the baseline calibration results.

Chapter 5 compares the results of the quasi-1D engine simulation to the experimental results. Volumetric efficiency and intake pressures are compared. Any modeling techniques not required for the baseline case, such as using loss factors to approximate the effects of the bends and S-bends, are also presented. Finally, Chapter 6 includes final remarks and recommendations for future work.

CHAPTER 2

EXPERIMENTAL SETUP

2.1 Engine Description and Engine Control

All experiments for this work were performed on a single cylinder research engine designed by Ford Motor Company, shown with the intake and exhaust setup used in this study in Fig. 2.1. This is a 4-valve spark-ignition engine designed to mimic one cylinder of the Jaguar 3.0L V6 X200 engine, including the combustion chamber, bore and stroke, piston geometry, valve timing, and intake and exhaust ports. Although the Jaguar engine has variable cam phasing, the single cylinder engine does not. The only engine accessory is a dry sump oil pump which is run off the timing belt; the water pump is electric and not powered by the engine. The camshaft follower is a direct-acting mechanical bucket. The overall engine specifications are given in Table 2.1.

The fuel and spark delivery to the engine is controlled by the Haltech E6K programmable engine control unit. It is connected to the engine through a custom-built wiring harness and programmed through a computer running PC-DOS. The spark timing for all experiments was set to a conservative amount close to peak torque. The air-fuel ratio was set to 12.5:1 for all experiments and monitored with a Horiba Mexa-110λ AFR Analyzer.

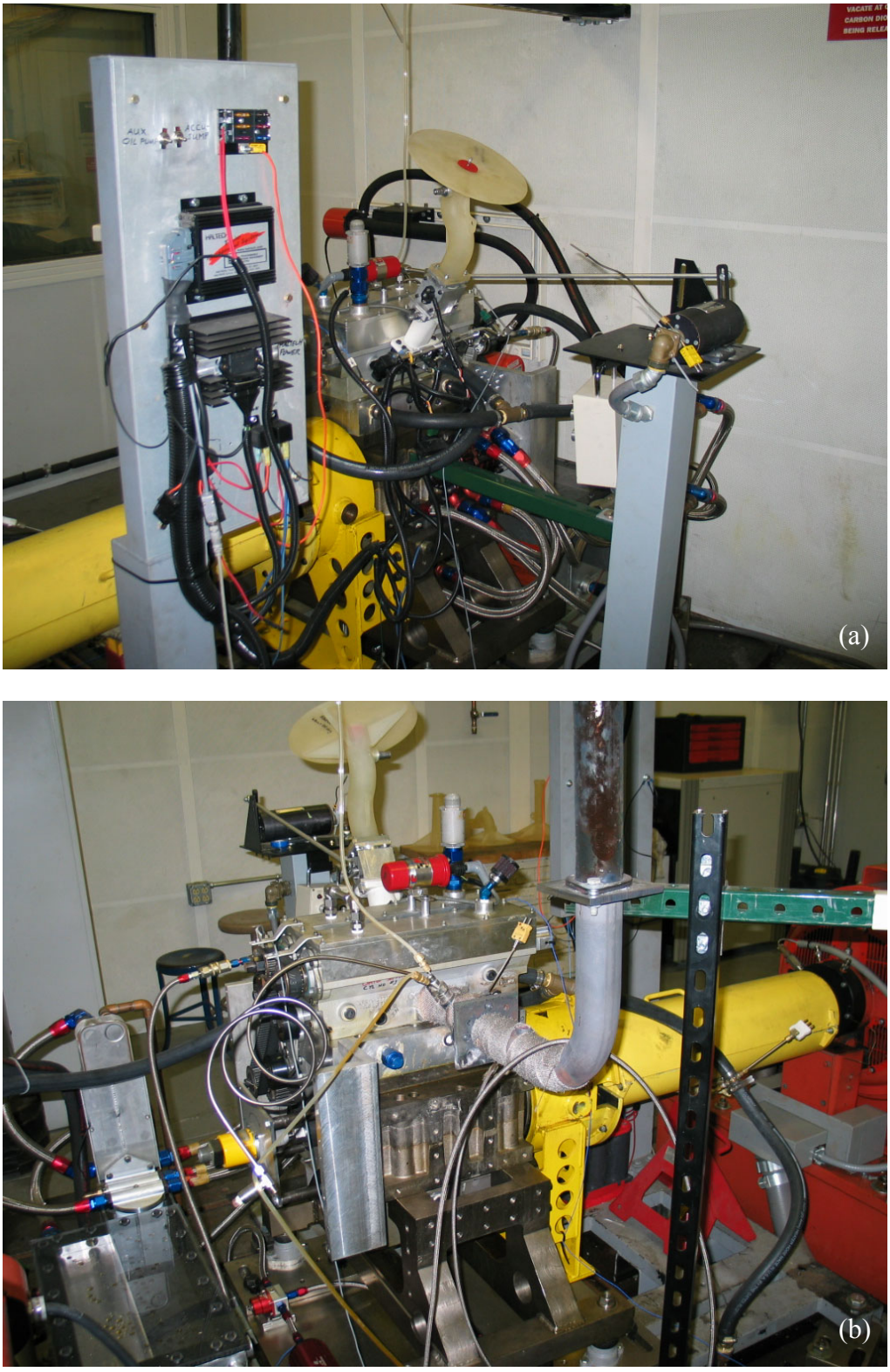

Figure 2.1: OSU Single Cylinder Research Engine with S-Bend Intake Configuration: (a) Intake Side and (b) Exhaust Side.

Bore	8.90 cm
Stroke	7.95 cm
Rod Length	13.81 cm
Compression Ratio	10.5:1
Clearance Volume	47.10 cm^3
Maximum Valve Lift	
Intake	0.914 cm
Exhaust	0.937 cm
Valve Timing	
Intake Open	308.0 CAD
Intake Duration	286.0 CAD
Exhaust Open	86.5 CAD
Exhaust Duration	326.0 CAD

Table 2.1: Single Cylinder Research Engine Specifications.

The single cylinder engine was connected to a General Electric DC engine dynamometer (dyno) capable of both motoring the engine and absorbing the load while firing at a specific speed. It is capable of delivering 134 kW as a motor and absorbing 142 kW as a dynamometer; the maximum speed is 6300 RPM. The dyno was computer-controlled by Horiba Systems EDTCS-1000. Each intake was tested from 1000 to 5500 RPM in 500 RPM increments from 1000 to 2000 RPM, then in 250 RPM increments from 2000 to 5500 RPM. Additional points were tested around the volumetric efficiency peaks for each intake configuration. All experiments were performed at wide-open throttle (WOT).

For each experiment, the engine oil and water was held at 200°F. Below 3000 RPM, the oil and water needed to be heated in order to maintain proper operating temperatures. The oil and water were each heated with their own Watlow brand 5000 W

circulation heaters controlled by Watlow PID controllers. Above 3000 RPM, the single cylinder engine was capable of heating the oil and water above the operating temperature; during this time, the oil and water were cooled with water from a large outdoor cooling tower. The cooling system was also controlled by PID controllers.

2.2 Engine Intake and Exhaust

The intake of the single cylinder engine, shown schematically in Fig. 2.2, consisted of the intake port, a fuel rail block, an adapter section, a barrel-style throttle, and the test piece. The intake port was a split-port design with a diameter of 3.02 cm at each valve; the port stayed separated for 6.48 cm, then the two branches came together in an oval of 14.32 cm^2, or an equivalent diameter of 4.27 cm, for 3.52 cm until the head face. The fuel rail block bolted between the head face and the adapter section; it housed the fuel injector and held the fuel rail. It was 5.14 cm long and has a slight taper from an oval with a 4.27 cm equivalent diameter to an oval with a 4.31 cm equivalent diameter. The adapter section was 12.0 cm long and provided a smooth transition from the oval shape of the fuel rail block to the 4.20 cm diameter barrel throttle. Although all experiments were done at WOT, a barrel throttle was used in case the engine needed to be throttled due to unexpected knocking or other engine-damaging phenomena. The throttle was made such that at WOT, there would be no obstruction in the flow and thus no unwanted reflection of the pressure waves to be measured. The barrel throttle had a length of 8.67 cm and a diameter of 4.20 cm. The only component of the intake that varied for each experiment was the test piece, which will be described in detail in the next section.

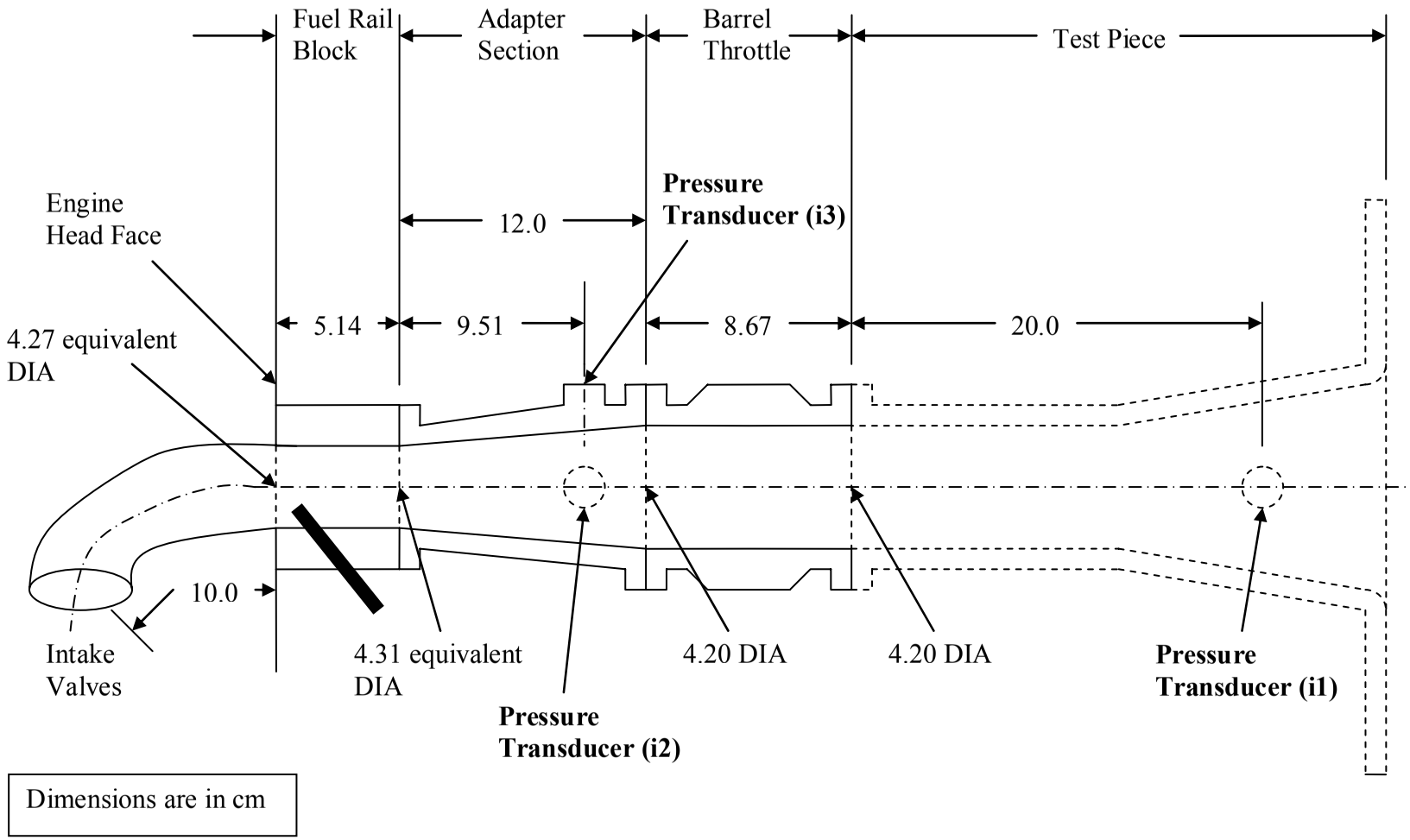

Figure 2.2: Schematic of Single Cylinder Intake

The exhaust, shown schematically in Fig. 2.3, was designed to lead the exhaust gas outside as efficiently as possible while keeping external noise to an acceptable level. It is made of 6.03 cm diameter straight pipe and mandrel-bent 90° elbows with bend radii of 19.4 cm. The exhaust port is a split-port design with a diameter of 2.54 cm at each valve; the port stayed separated for 4.86 cm, and then came together into a 10.18 cm^2 oval for a length of 3.48 cm until the head face. A 16.5 cm long adapter, shown in Fig. 2.4, provided a smooth transition from the oval exhaust port of 10.18 cm^2 to the rest of the exhaust with a diameter of 6.03 cm. A production three-pass muffler was located between the exit of the 6.03 cm diameter section of the exhaust and the large tube that routes the exhaust gas outside; the muffler was installed to ensure reasonable sound levels for the buildings surrounding the test site.

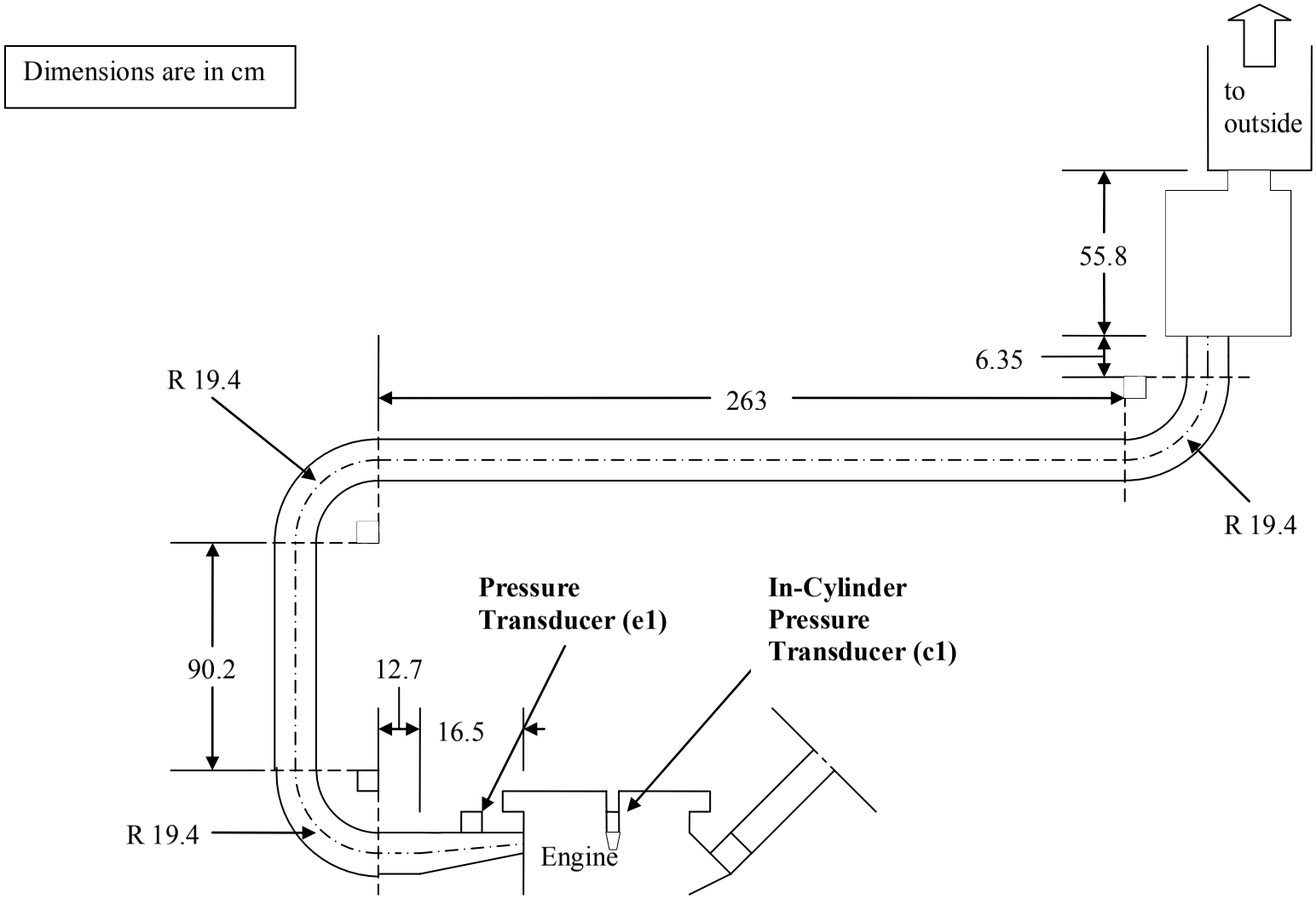

Figure 2.3: Schematic of Single Cylinder Exhaust

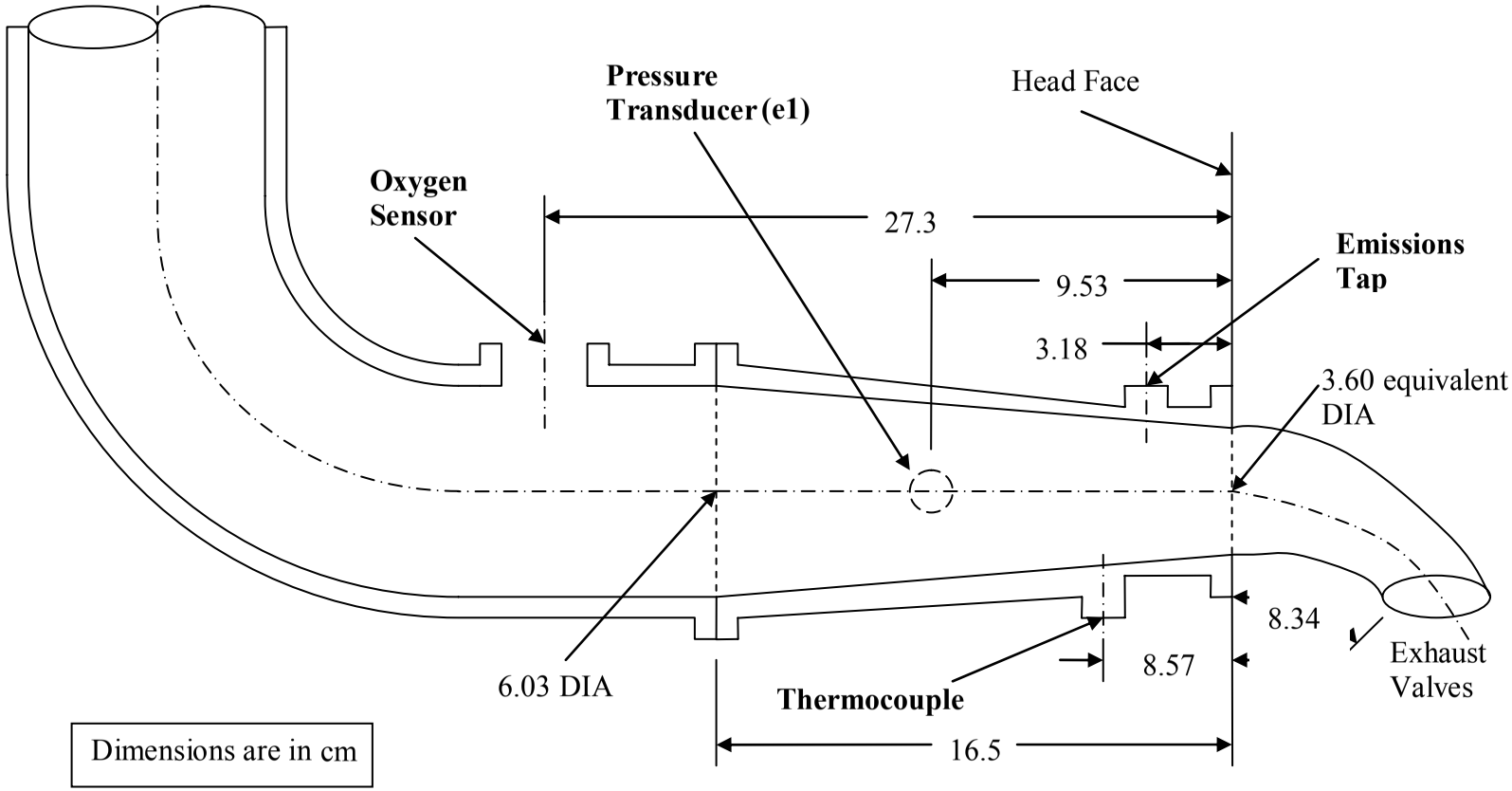

Figure 2.4: Adapter Section of Single Cylinder Exhaust

2.3 Intake Test pieces

The intake configurations were all designed using IDEAS CAD software and fabricated using laser stereolithography techniques. Laser stereolithography is the process where an ultraviolet laser is used to harden a thin layer of a liquid photopolymer. This is done by shining the laser onto a pool of liquid photopolymer; the photopolymer hardens into an 0.08 mm thick cross-section of the final part. This layer is then lowered deeper into the pool, and another layer is hardened on top of it. This process continues until the part is complete; then the plastic part is bathed in ultraviolet light to cure any uncured photopolymer. By fabricating the test pieces in this way, good accuracy was achieved on dimensions such as bellmouth radii, bend radii, and surface finish.

The 18 configurations consisted of a baseline case and four groups of geometries: tapers, bellmouths, single bends, and double "S" bends. The baseline case was designated intake #1. The tapers consisted of intakes #2 - #8; the bellmouth pieces #9 - #12; #13 - #15 the single bend group, and #16 - #18 were the S-bend group. One characteristic common to all test pieces was the large flange at the entrance to the piece, which ensured a hemispherical propagation of the pressure waves leaving the duct. A color photograph for each of these configurations is given in Appendix A.

The baseline piece, shown in Fig. 2.5a, was a straight duct 26.45 cm long with an inner diameter of 4.20 cm. At the inlet of the baseline piece was a 1.45 cm radius bellmouth and the large flange at the inlet.

The taper group, shown in Fig. 2.5b, all had an overall length of 26.45 cm and met the barrel throttle with a diameter of 4.20 cm. The length of the tapered section, L_t, and the taper inlet diameter, D_t, varied for each taper. A table of the dimensional

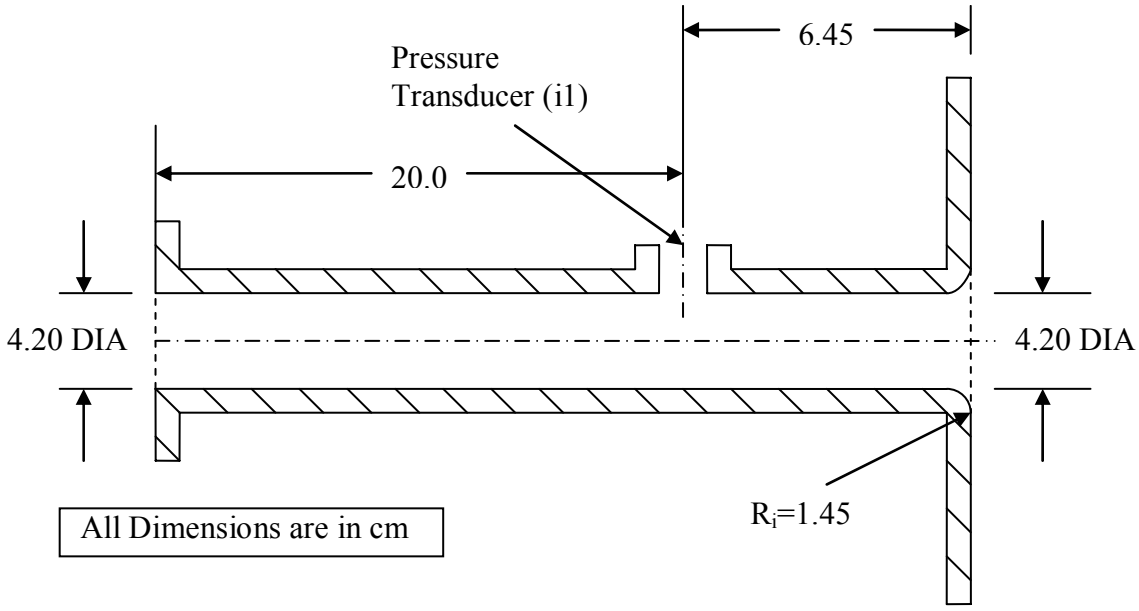

(a)

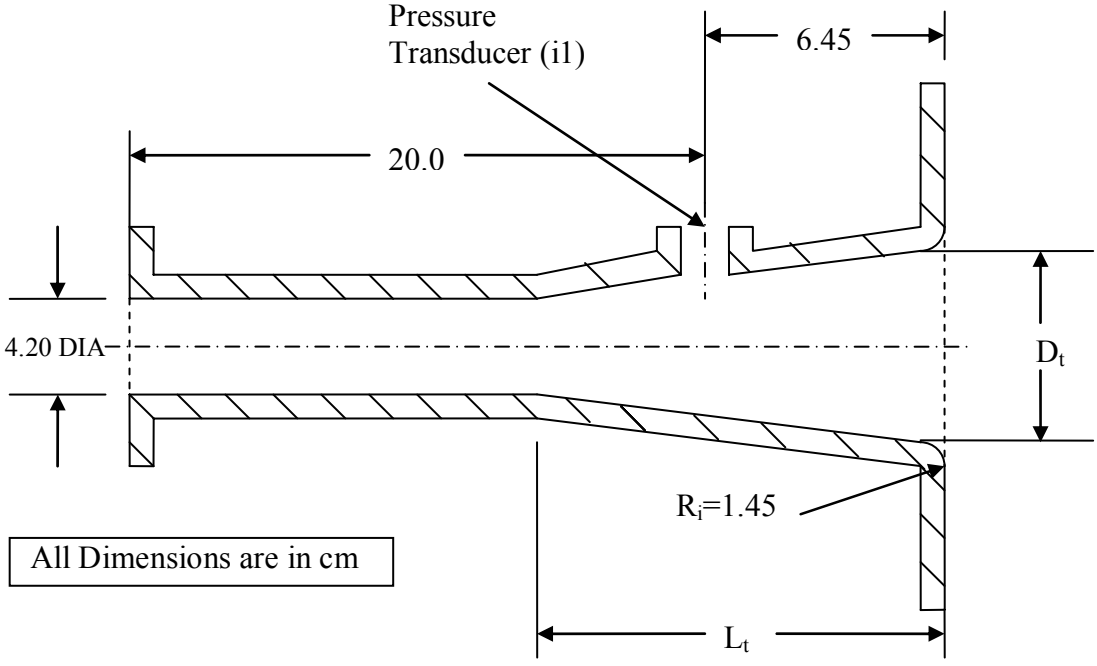

(b)

Figure 2.5: Intake test pieces: (a) baseline, (b) taper group, (c) bellmouth group, (d) bend group, (e) S-bend group.

Figure 2.5 continued

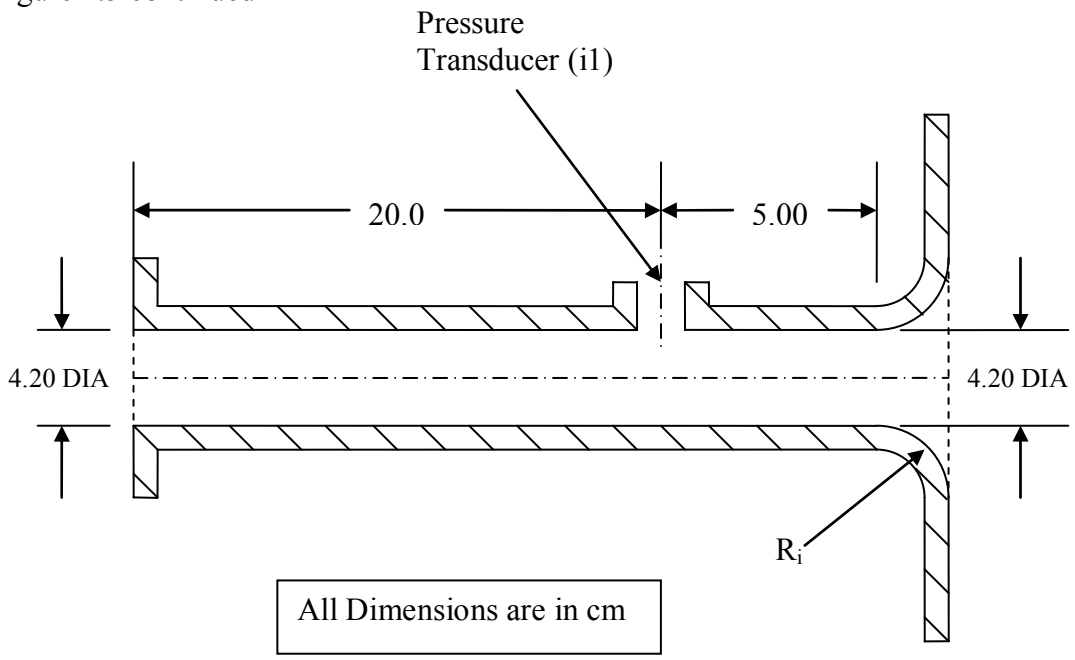

(c)

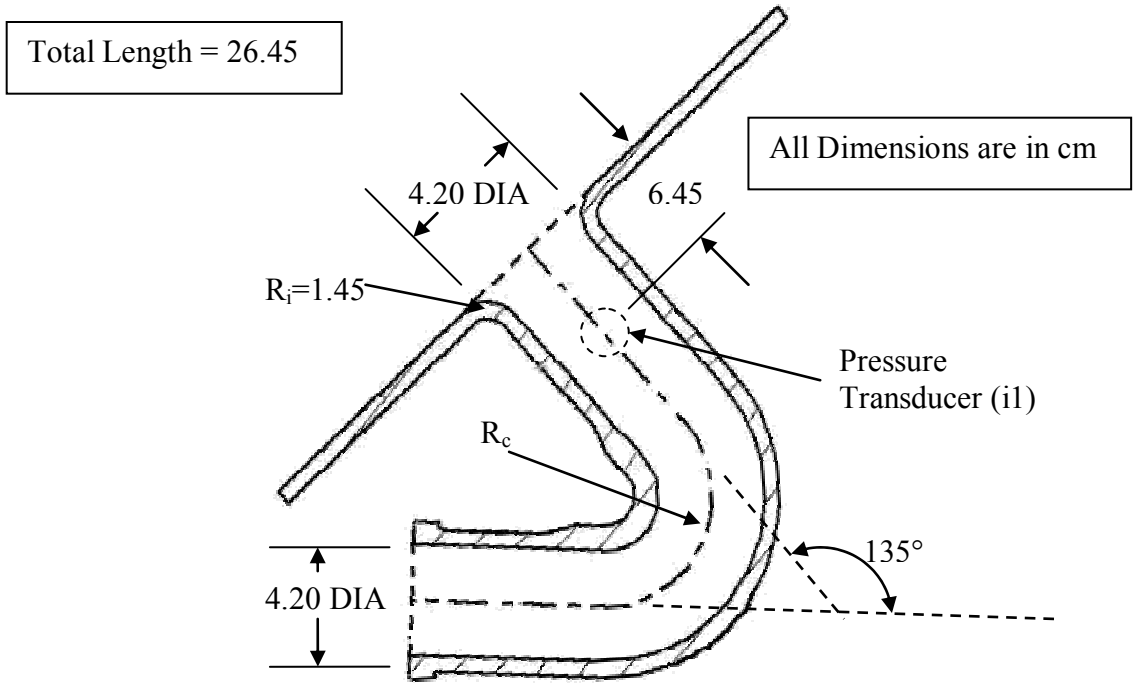

(d)

Figure 2.5 (cont'd.): Intake test pieces: (a) baseline, (b) taper group, (c) bellmouth group, (d) bend group, (e) S-bend group.

Figure 2.5 continued

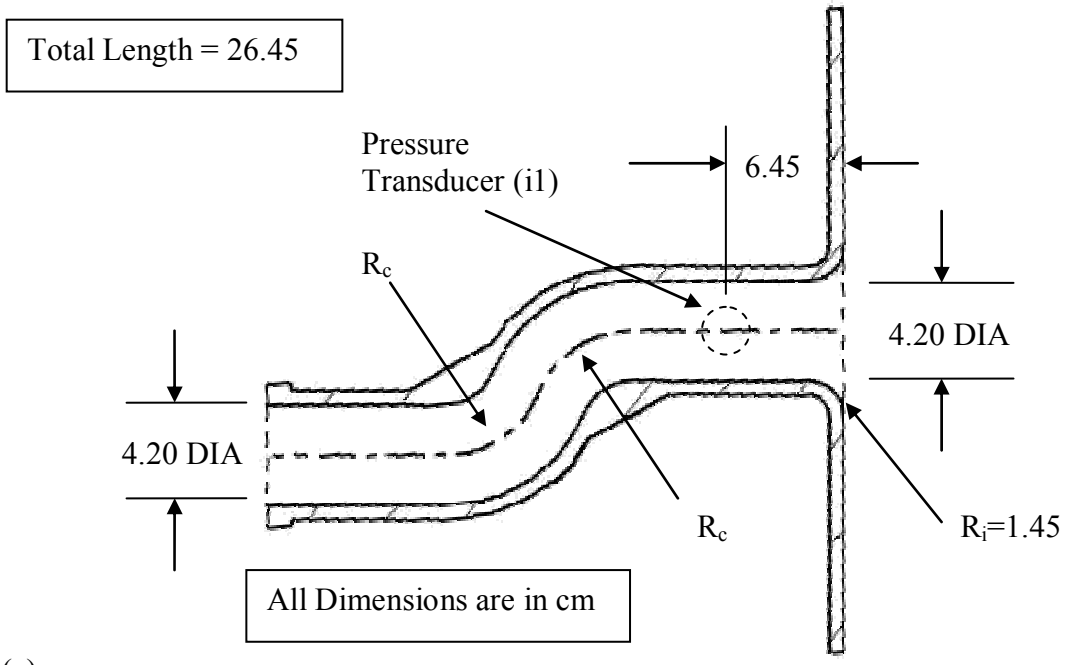

(e)

Figure 2.5 (cont'd.): Intake test pieces: (a) baseline, (b) taper group, (c) bellmouth group, (d) bend group, (e) S-bend group.

differences for each taper is shown in Table 2.2. Intake #2 had a taper over 25% of its length and an area ratio of 1.5. Intake #3 had a taper over 50% of its length and an area ratio of 1.5. Intake #4 had a taper over 100% of its length and an area ratio of 1.5. Intakes #5 and #6 had an area ratio of 2 over 50% and 100% of their lengths, respectively. Intakes #7 and #8 were tapered for 100% of their lengths with an area ratio of 2.5 and 3, respectively.

Figure 2.5c shows schematically the bellmouth group, with the dimensions given in Table 2.3. Each intake in the bellmouth group was a straight pipe with a 4.20 cm inner diameter, and a distance of 25.00 cm to the start of the bellmouth. Since each intake

Intake	L_t (cm)	D_t (cm)	Taper Area Ratio
#2	6.613	5.14	1.5
#3	13.23		
#4	26.45		
#5	13.23	5.94	2
#6	26.45		
#7	26.45	6.62	2.5
#8		7.26	3

Table 2.2: Taper Group Dimensions.

in this group had a different inlet radius, R_i, the overall lengths are different for each intake. Intake #9 had an R_i of 0.21 cm ($R_i/D = 0.05$) for an overall length of 25.21 cm. Intake #10 had an R_i of 0.84 cm ($R_i/D = 0.2$) for an overall length of 25.84 cm. Intake #11 had an R_i of 2.10 cm ($R_i/D = 0.5$) for an overall length of 27.10 cm, and intake #12 had an R_i of 4.20 cm ($R_i/D = 1.0$) for an overall length of 29.20 cm.

Intake	R_i (cm)	R_i/D	Overall Length (cm)
#9	0.21	0.05	25.21
#10	0.84	0.2	25.84
#11	2.10	0.5	27.10
#12	4.20	1.0	29.20

Table 2.3: Bellmouth Group Dimensions.

The single bend group, shown schematically in Fig. 2.5d, consisted of three intakes, each with an overall length of 26.45 cm, inlet radius of 1.45 cm, and 4.20 cm diameter. The radius of curvature, R_c, for each intake are shown in Table 2.4. Each bend

was 135° and was oriented on the engine such that the inlet was pointing downward. Intakes #13 – 15 had R_c = 8.4, 6.3, and 4.2 cm for R_c/D = 2.0, 1.5, and 1.0, respectively.

Single Bend Intake	R_c (cm)	R_c/D	S-Bend Intake	R_c (cm)	R_c/D
#13	8.4	2.0	#16	8.4	2.0
#14	6.3	1.5	#17	6.3	1.5
#15	4.2	1.0	#18	4.2	1.0

Table 2.4: Single Bend and S-bend Group Radii of Curvature.

The S-bend group, shown in Fig. 2.5e, had an overall length of 26.45 cm, an inlet radius of 1.45 cm, and 4.20 cm diameter. Each S-bend was such that the two straight sections of the test piece, one at the inlet and one at the transition to the barrel throttle, were parallel. Table 2.4 also shows the radius of curvature, R_c, of the S-bends. Intakes #16 - 18 had R_c = 8.40, 6.30, and 4.20 cm, for R_c/D = 2.0, 1.5, and 1.0, respectively.

2.4 Experimental Measurements

The intake of the single cylinder engine was outfitted with three Kistler piezoresistive pressure transducers with a 0-2 bar range (model 4045A2). Each of these transducers was connected through a Kistler 4603A Amplifier to a Concurrent high-speed data acquisition system (model MC68040). This system is capable of acquiring data at a sampling rate of 2 MHz from 32 channels simultaneously. The pressure transducers labeled i2 and i3 were both located in the adapter section of the intake, 14.65 cm from the head face as shown in Fig. 2.2. Both transducers were flush with the inner wall of the adapter piece, and both were perpendicular to and pointed toward the centerline of the

duct. The pressure transducer labeled i1 was located in the test piece. An aluminum bushing was made to push into each test piece and fish-mouthed to fit flush with the inner wall of the duct. The transducer threaded tightly into this bushing and also was flush with the inner wall of the duct and was perpendicular to and pointed toward its centerline. For each piece, the i1 transducer was located 20.00 cm following the duct from the surface that mated with the barrel throttle. The pressure traces acquired at locations i1, i2, and i3 had a resolution of 1 point per CAD and averaged for 64 engine cycles. Above the inlet of the intake duct was a thermocouple for the purpose of measuring ambient air temperature.

The exhaust of the single cylinder engine was fitted with a pressure transducer, an emissions tap, a thermocouple, and a wide-band oxygen sensor (recall Fig. 2.4). The pressure transducer, e1, was a Kistler piezoresistive pressure transducer with a 0-5 bar range (model 4045A5). This transducer threaded into a water jacket which was supplied with cooling water. The water jacket was threaded into its bung in the adapter section such that it was flush with the inner wall of the duct. The e1 transducer was located 9.53 cm from the head face. As with the intake pressure traces, the exhaust pressure traces at e1 had a resolution of 1 point per CAD and averaged for 64 engine cycles. The thermocouple was located 8.57 cm from the head face. The wide-band oxygen sensor was located 27.3 cm from the head face and connected to a Horiba MEXA-110λ AFR Analyzer. The emissions tap was connected first through stainless steel tube and then macroline to a Horiba MEXA-7100 Motor Exhaust Gas Analyzer. Both the MEXA-110λ and the MEXA-7100 were connected to the Horiba dyno controller computer. The data from these two devices was averaged for one minute for each engine speed.

A PCB Piezotronics in-cylinder pressure transducer (model 145A07), labeled c1 in Fig. 2.3, was located in the top center section of the combustion chamber, fitting flush with its inner surface, between the spark plug and the rearward-most intake and exhaust valves. It was amplified via a Kistler dual-mode amplifier (model 5010), and its output was recorded using the Concurrent data-acquisition system. Due to the cycle-to-cycle variations in combustion normally associated with internal combustion engines, the in-cylinder pressure traces were averaged for 256 engine cycles. Since there is a signal offset associated with the in-cylinder transducer, the recorded relative pressures must be "pegged" to a known absolute value. The intake pressure at location i2 at BDC was assumed to closely approximate the pressure in the cylinder at that time for a certain engine speed (Randolph, 1994). Thus, the in-cylinder pressure at that crank angle was made to match the average of the i2 pressure at BDC and one CAD before and after it.

The engine brake and motoring torques were measured with a Revere Transducers, Inc. load cell (model 606555-24) and acquired with the Horiba dyno controller computer. As with the Mexa-7100, this data was averaged for one minute for each engine speed. The fuel flow was metered with the Pierburg Instruments PII401*11863 Fuel Measurement System. The output of this meter was sent to the Horiba dyno controller computer and averaged for one minute.

Using the air-fuel ratio obtained from the MEXA-7100 and the fuel flow rate, the volumetric efficiency was calculated for each engine speed by (Heywood, 1988)

$$\eta_v = \frac{2\dot{m}_a}{\rho_{a,i} V_d}, \tag{2.1}$$

where $\dot{m}_a$ [g/s] is the mass flow rate of air into the cylinder, V_d [cm^3] is the displaced volume, and $\rho_{a,i}$ [g/cm^3] is the inlet air density. Knowing the fuel flow rate and the air-fuel ratio, the mass flow rate of air was obtained. The inlet air density was known from barometer readings, measured ambient temperature, and ideal gas relations.

CHAPTER 3

EXPERIMENTAL RESULTS AND DISCUSSION

3.1 Introduction

In this chapter, the experimental results for each intake configuration are presented. Section 3.2 covers the taper group, Section 3.3 the bellmouth group, Section 3.4 the bend group, and Section 3.5 the S-bends. Intake pressure was taken at three locations, i1, i2, and i3, as described in Section 2.4. i2 and i3 are located at the same distance from the valves, and pressures measured at both locations were found to be identical. i2 and i3 are significantly closer to the valves than i1 and thus the magnitudes of the pressure fluctuations are larger, are more indicative of volumetric efficiency trends, and the shifts in ambient pressure are less noticeable. Therefore, only intake pressure at i2 will be compared in this chapter. For each group of intakes, the volumetric efficiencies, corrected brake powers, intake pressures at location i2, and exhaust pressures at location e1 are compared. The intake pressures are presented in both the crank-angle resolved time domain where 0 CAD is defined as the top-dead center of the compression stroke, and the frequency domain. Data was converted to the frequency domain using a Discrete Fourier Transform and expressed as sound pressure level (SPL),

$$SPL = 20\log_{10}\left(\frac{P_{rms}}{P_{ref}}\right), \tag{3.1}$$

where P_{rms} is the root-mean-square value of pressure, $P_{ref} = 2\text{x}10^{-5}$ Pa, and SPL is in decibels (dB). The frequency spectra are presented as functions of engine order, where the mth order is defined as $m \times \frac{N[RPM]}{60}$. In-cylinder pressure (c1) will not be compared. During a study of intake tapers on a motoring engine, Howard (2003) discovered that the in-cylinder pressure data was not of sufficient accuracy for comparisons. With a firing engine, the thermal effects after combustion are believed to decrease transducer accuracy at WOT (Kothamasu, 1998). In-cylinder pressure was used effectively, however, in the calibration of the quasi-1D model (discussed in Section 4.3.1).

3.2 Taper Group

Seven tapers were tested against the baseline case using the experimental setup described in Chapter 2. The taper group was comprised of intakes #2 through 8 as outlined in Table 2.2 and shown schematically in Fig. 2.5b. The effect of the different tapers on the volumetric efficiency and brake power of the engine is discussed next in Section 3.2.1. Section 3.2.2 contains comparisons of the intake pressure at i2 for the seven tapers and baseline case. Section 3.2.3 contains a discussion of exhaust measurements.

3.2.1 Volumetric Efficiency and Brake Power

The measured volumetric efficiency of the engine for each taper (intakes #2-8), and the corrected brake power are compared to the baseline case in this section as a

function of engine speed. All intakes that are tapered over their full length (intakes #4, 6, 7, and 8) are also compared to show the overall trend of increasing taper area ratio.

Figure 3.1a compares the volumetric efficiencies of the baseline intake #1 with intake #2. There is very little difference in the performance of these two intakes; the $L/A_{effective}$ as defined by Eq. (1.5) goes from 4.49 cm^{-1} for intake #1 to only 4.41 cm^{-1} for intake #2, a difference of 1.8%. Equation (1.3) then suggests the main tuning peak speed should only increase by 37 RPM. The main tuning peaks for each taper are predicted using these equations and presented in Chapter 4. In the experiments, the tuning peaks at 3750 and 4750 RPM for intake #1 have actually shifted to 3850 and 4850 RPM for intake #2. The tuning peak at 3000 RPM has diminished for intake #2. The overall magnitudes of volumetric efficiency are similar for both intakes. Figure 3.1b shows the brake power for intakes #1 and 2. As can be inferred by the volumetric efficiency comparison, the power for both intakes is similar, with a slight shift of the power for intake #2 toward higher speeds. The peak power of both intakes is similar.

Figure 3.2a compares volumetric efficiency for intakes #1 and 3; the tuning peak shift is more noticeable as $L/A_{effective}$ has now a difference of 3.9% between the two intakes. The tuning peaks once located at 3000, 3750, and 4750 RPM for intake #1 have moved to 3250, 3850, and 5000 RPM for intake #3. The overall magnitudes of the peaks are similar to intake #1. The brake power for intakes #1 and 3 are compared in Fig. 3.2b. Compared to the baseline, the power for intake #3 has shifted toward higher engine speeds. The peak power for both intakes is similar, but there are power gains for intake #3 at 4000, 5000, and 5250 RPM of 1.4, 1.0, and 1.5 kW, respectively.

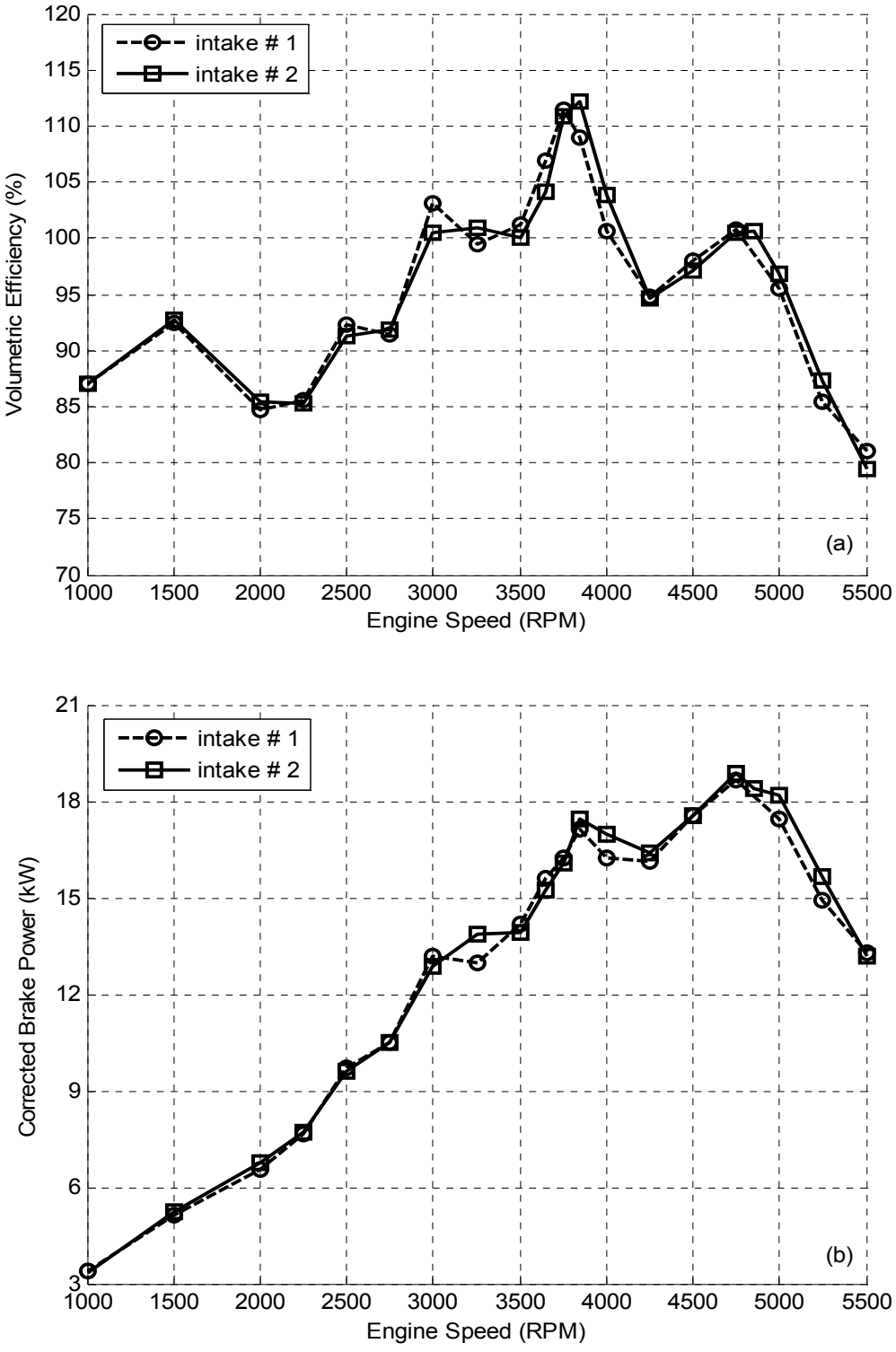

Figure 3.1: Experimental (a) Volumetric Efficiency and (b) Brake Power for Intake #1 and Intake #2.

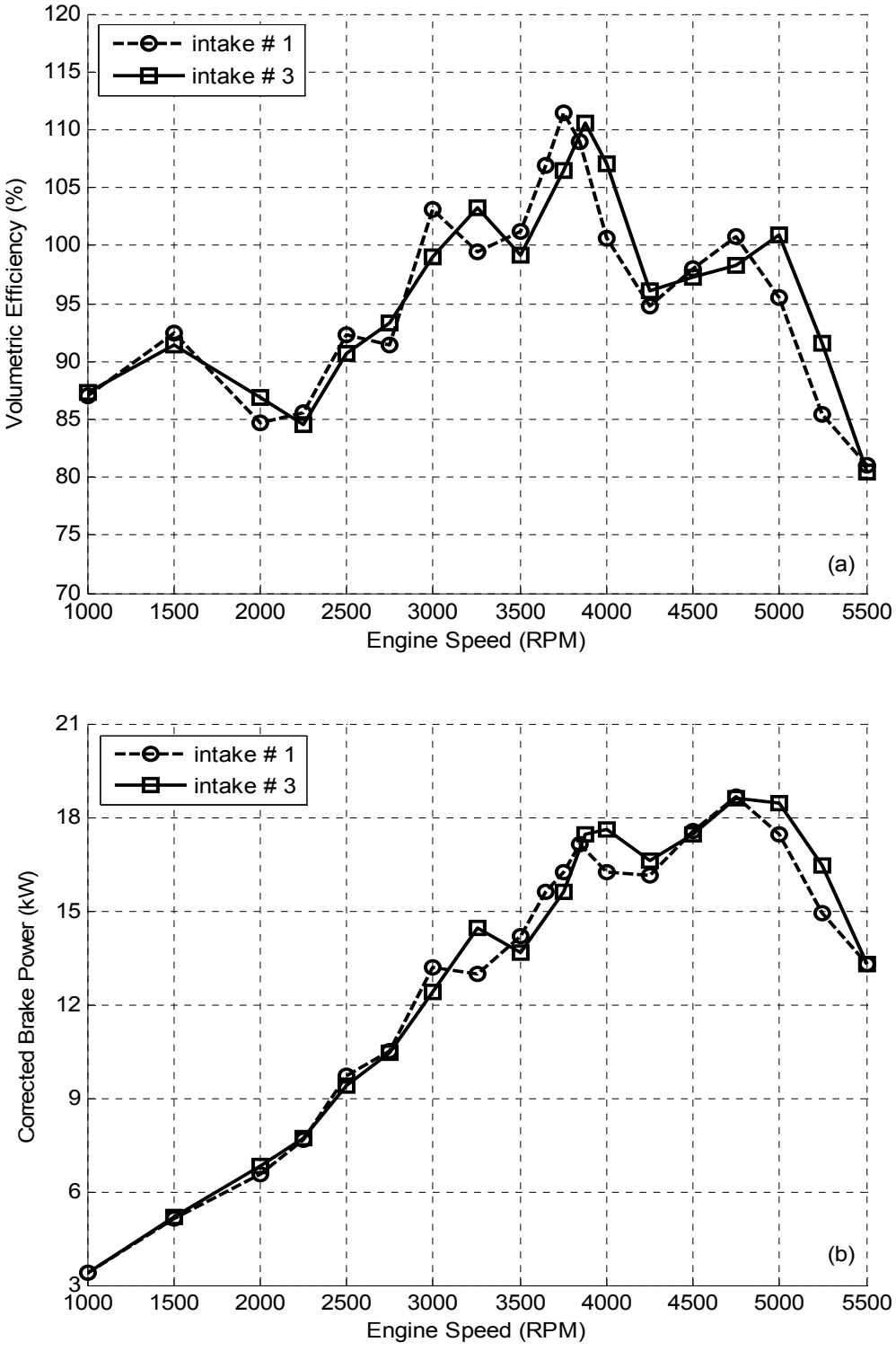

Figure 3.2: Experimental (a) Volumetric Efficiency and (b) Brake Power for Intake #1 and Intake #3.

The volumetric efficiency of intake #4 is compared to intake #1 in Fig. 3.3a. The average area of the intake continues to grow, and as expected, the location of the tuning peaks continues to shift to higher speeds, moving from 3000, 3750, and 4750 RPM for intake #1 to 3250, 4000, and 5000 RPM for intake #4. Unlike with intakes #2 and 3, there is a slight increase compared to intake #1 in the magnitude of the first tuning peak. Figure 3.3b shows the brake power for intakes #1 and 4. The peak power is similar for both intakes, but the location has shifted from 4750 RPM for intake #1 to 5000 RPM for intake #4. There is a 3.3 kW gain in power for intake #4 at 5250 RPM.

Figure 3.4a shows the volumetric efficiencies for intakes #1 and 5. Intake #5 has tuning peak locations similar to intake #4; $L/A_{effective}$ of 4.15 and 4.21 cm^{-1} for intakes #4 and #5, respectively, suggest that they are nearly equivalent in terms of engine tuning. The brake power for intakes #1 and 5 are shown in Fig. 3.4b. Since the volumetric efficiencies for intakes #4 and 5 are similar, the power curves are also similar.

Figure 3.5a compares the volumetric efficiency of intake #6 with intake #1. The tuning peaks continue to shift to higher speeds, from 3000, 3750, and 4750 RPM to 3500, 4125, and 5250 RPM. The first peak has increased in magnitude, but the last two peaks have decreased by about 2%. This may be because the tuning effect is weakened due to flow losses having a more pronounced effect as the engine speeds of the peaks increase. Another possibility is that as the intake becomes wider, the flow velocity becomes slower, and inertial effects of the air begin to diminish due to weaker reflected compression waves. The brake power for intakes #1 and 6 are shown in Fig. 3.5b. The peak power for intake #6 occurs near the peak volumetric efficiency, thus reducing the peak power speed from 4750 RPM for the baseline case to 4250 RPM. However,

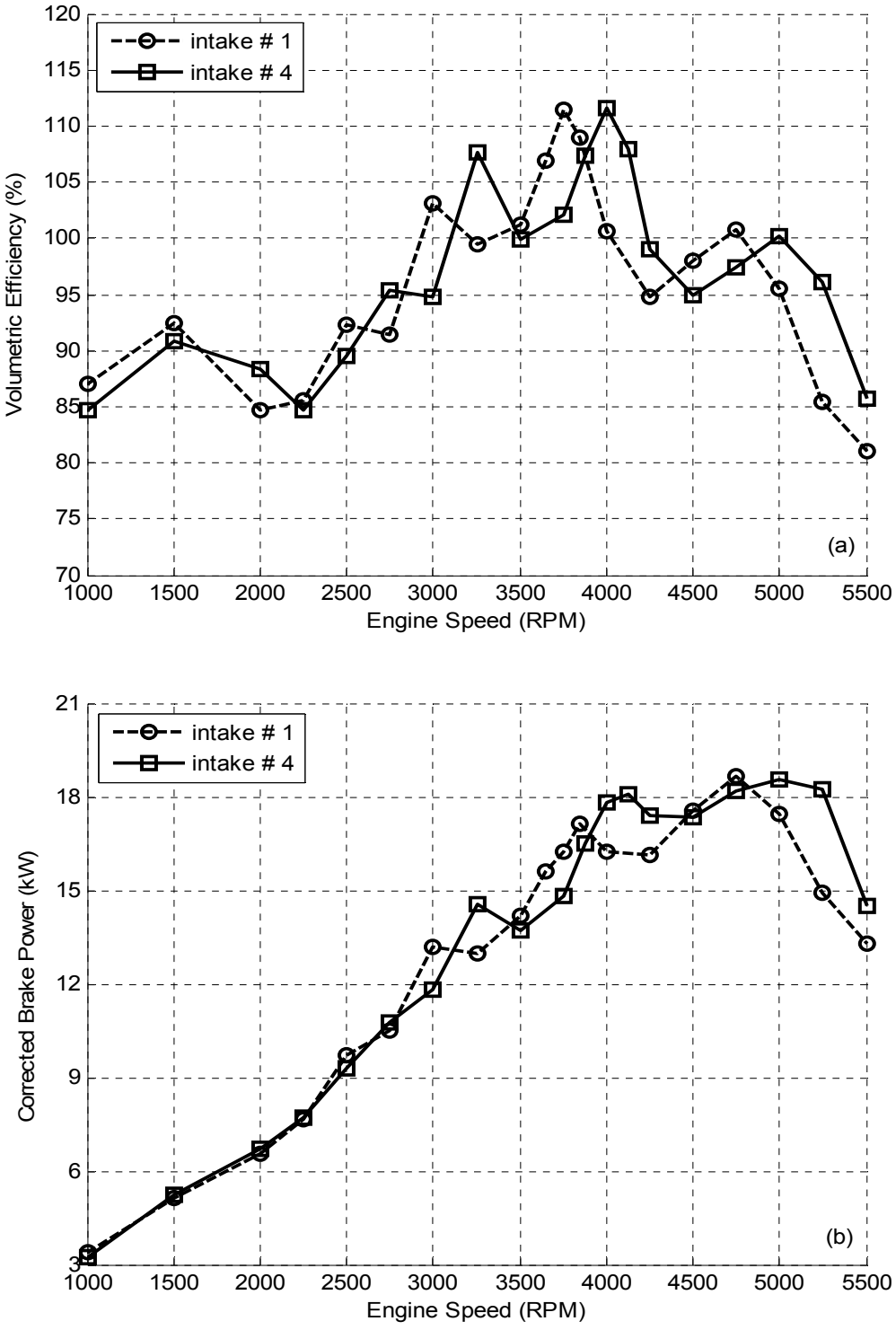

Figure 3.3: Experimental (a) Volumetric Efficiency and (b) Brake Power for Intake #1 and Intake #4.

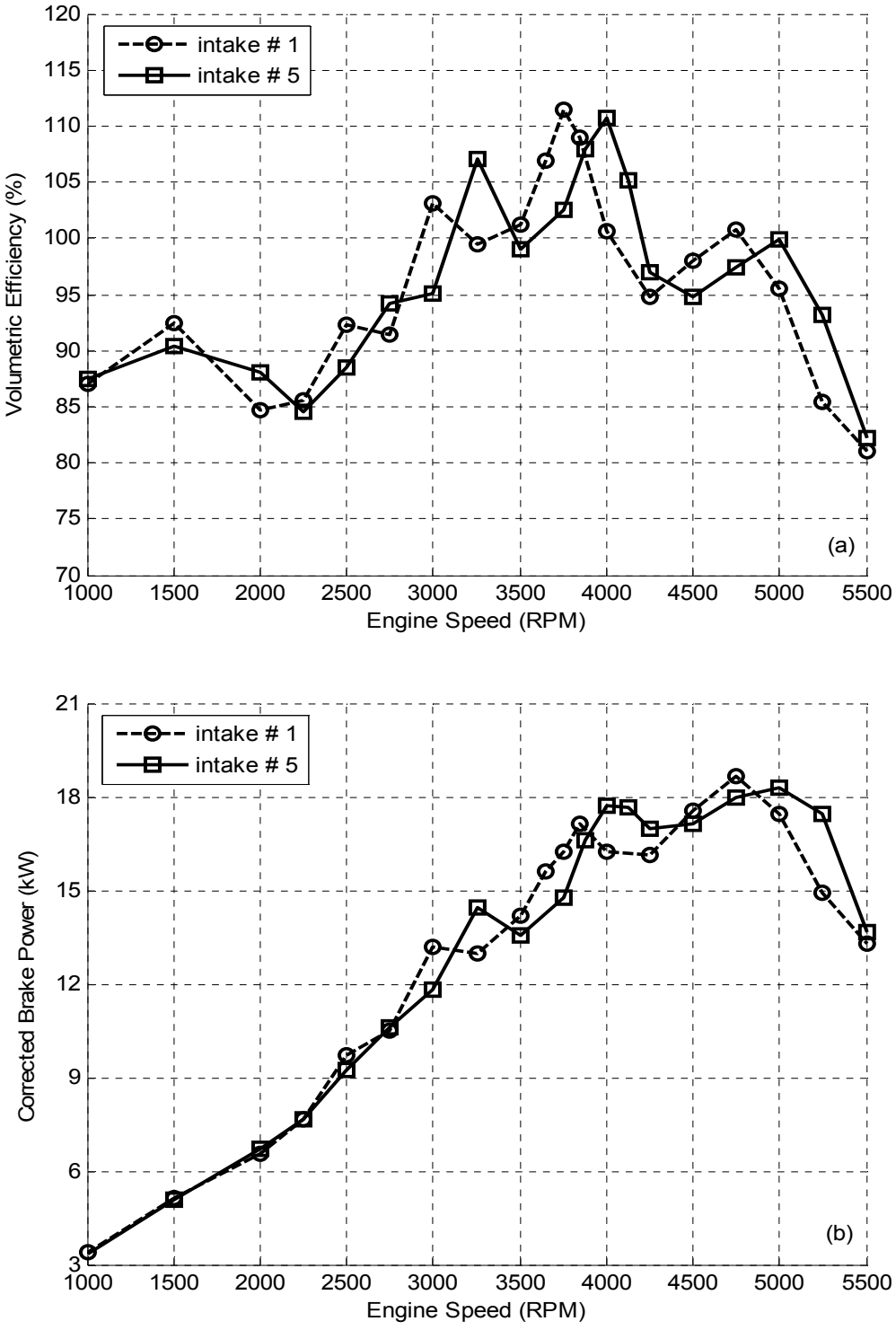

Figure 3.4: Experimental (a) Volumetric Efficiency and (b) Brake Power for Intake #1 and Intake #5.

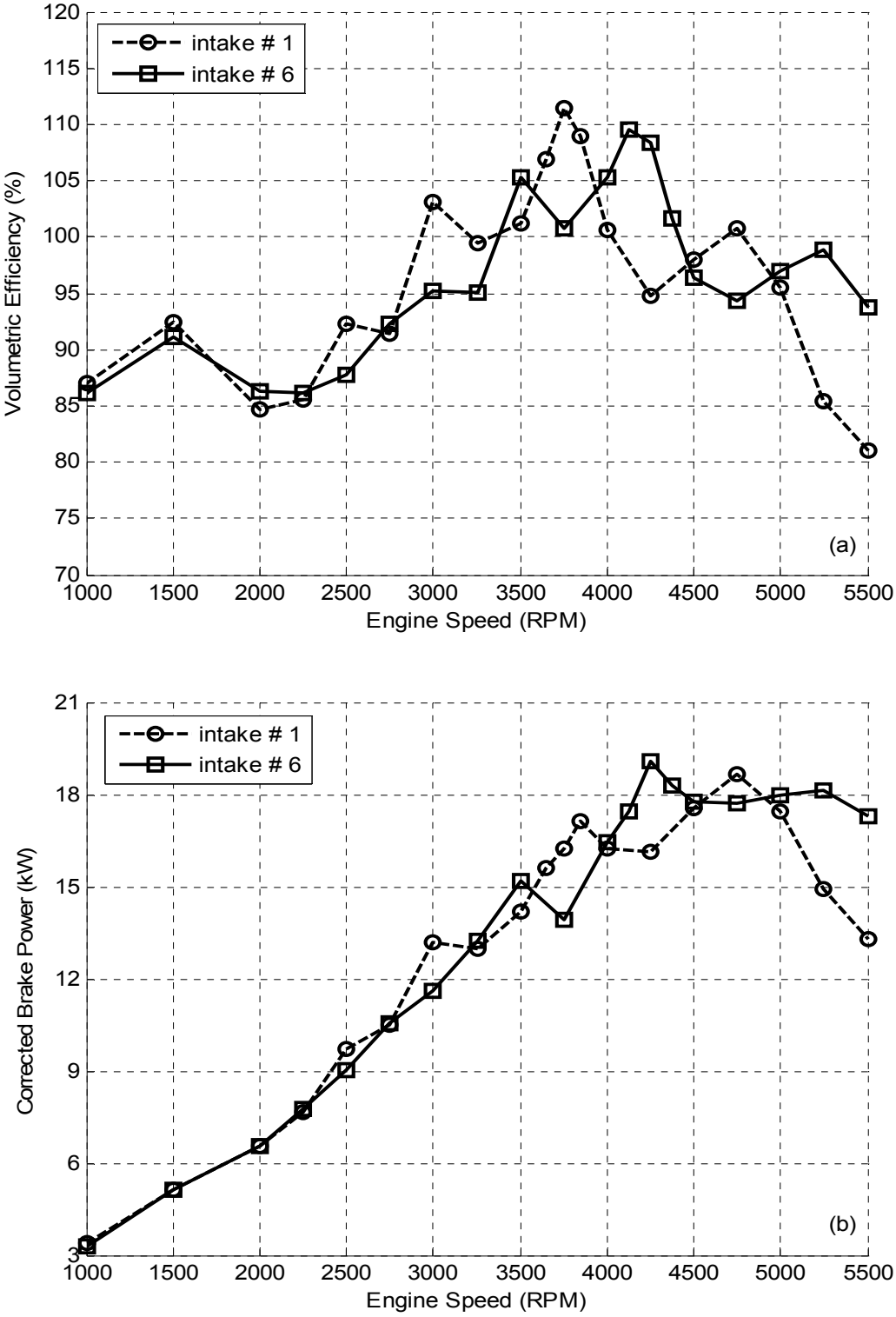

Figure 3.5: Experimental (a) Volumetric Efficiency and (b) Brake Power for Intake #1 and Intake #6.

the power for intake #6 remains fairly constant from 4500 to 5500 RPM and does not drop off after 4750 RPM as it does for the baseline, resulting in a 3.2 kW gain in power at 5250 RPM and a 3.8 kW gain at 5500 RPM. The peak power for intake #6 is slightly higher than that of intake #1.

The volumetric efficiency of intake #7 is compared to intake #1 in Fig. 3.6a. The tuning peaks continue to move toward higher engine speeds as $L/A_{effective}$ of the intake continues to increase. Intake #7 has substantial tuning peaks at 3500, 4250, and 5500 RPM. While the first tuning peak has increased in magnitude slightly compared to the baseline, the second and third peaks have decreased by 3.0% and 3.6%. Again, this could be caused by the increase in flow losses associated with higher engine speeds and the reduction of the inertia effect of intake flow caused by the increase in area. Figure 3.6b shows the brake power for intakes #1 and 7. The peak power for intake #7 occurs at 4375 RPM, close to the volumetric efficiency peak. As observed with intake #6, the power for intake #7 stays fairly constant from 4500 to 5500 RPM, resulting in a power gain of 3.2 kW at 5250 RPM and 4.8 kW at 5500 RPM when compared to the baseline. The peak power for intake #7 has increased by 0.7 kW.

Figure 3.7a shows the comparison of volumetric efficiency for intakes #1 and 8. The only noticeable tuning peak for intake #8 is at 4375 RPM. The highest-speed tuning peak is beyond the range of experimentation, as confirmed by quasi-1D engine simulation. The reduction in peak volumetric efficiency observed with intakes #6 and 7 continues, as the peak at 4375 has decreased to 107.5% from 111.7% for the 3750 RPM peak of intake #1. Figure 3.7b shows engine brake power for intakes #1 and 8. The

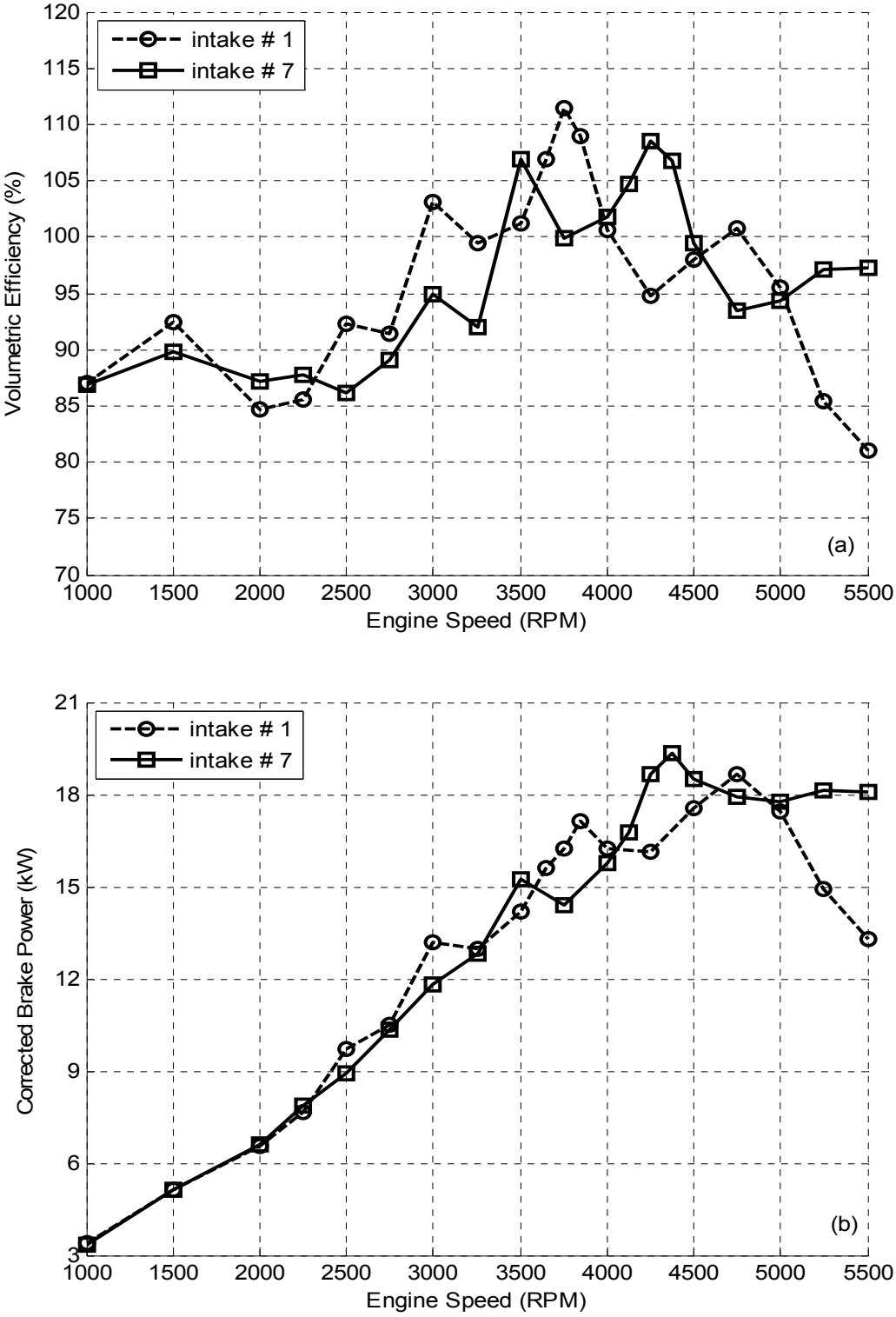

Figure 3.6: Experimental (a) Volumetric Efficiency and (b) Brake Power for Intake #1 and Intake #7.

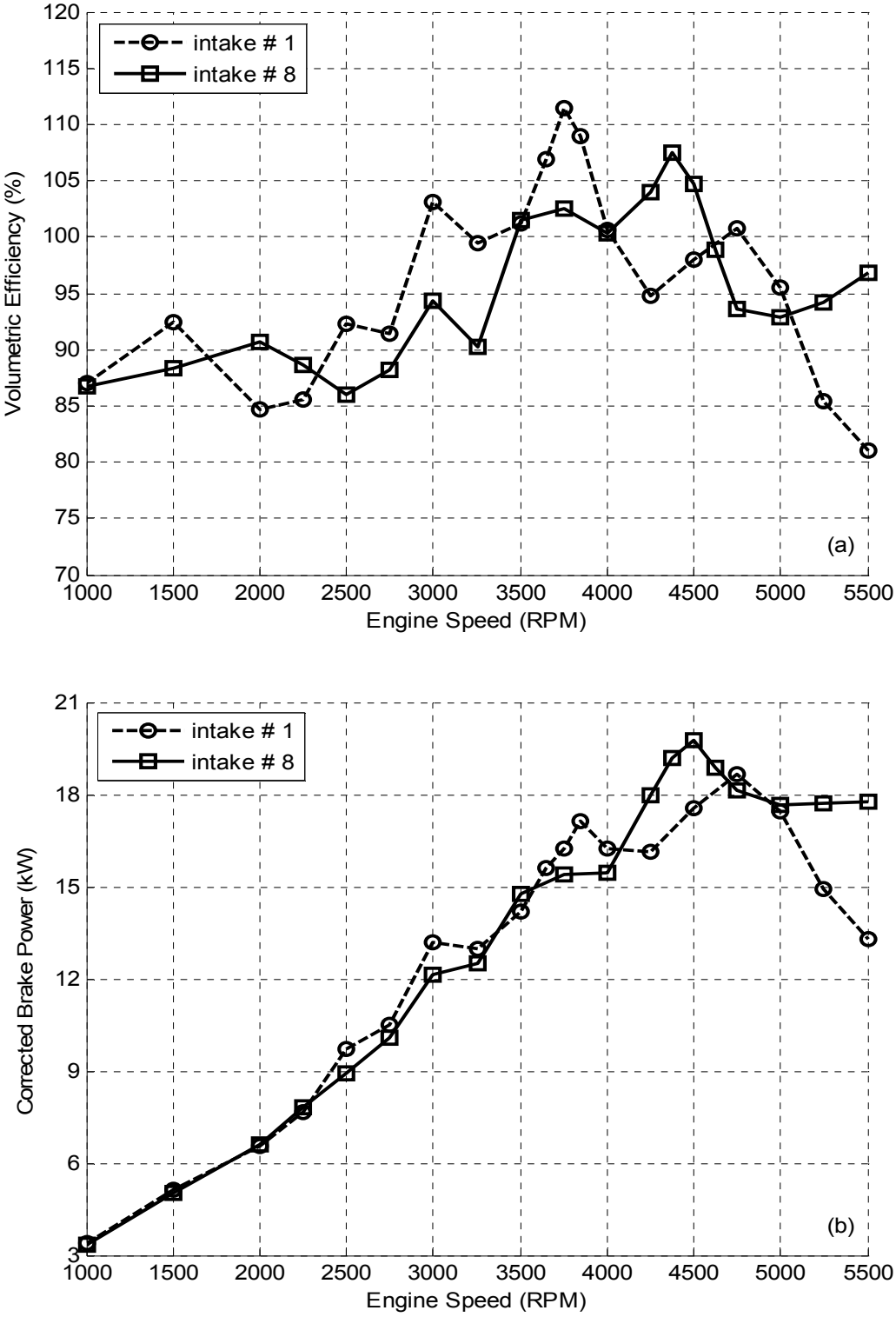

Figure 3.7: Experimental (a) Volumetric Efficiency and (b) Brake Power for Intake #1 and Intake #8.

peak power for intake #8 occurs at 4500 RPM and is 1.1 kW higher than that of the baseline. Power gains of 2.2, 2.8 and 4.5 kW can be seen at 4500, 5250 and 5500 RPM, respectively, for intake #8 when compared to intake #1.

Figure 3.8 compares all the intakes that are tapered over their entire length (intakes #4, 6, 7, and 8) with the baseline intake #1. There is a clear tradeoff between shifting the tuning peaks to higher speeds and reducing the magnitudes of the volumetric efficiency peaks as the taper angle increases. It appears that a taper area ratio of 1.5 (intake #4) is the most beneficial for engine breathing, and anything larger begins to weaken the tuning effects as any larger taper gives a reduction in the magnitude of the largest tuning peak. The power for the various tapers show that the peak power increases as taper area ratio increases for intakes #6 through 8. Even though the volumetric efficiency peaks for these intakes begin to decrease, the power continues to increase because the locations of the tuning peaks continue to increase in engine speed. By adding a taper to the intake geometry, substantial gains in power can be had at high engine speeds, but only at the sacrifice of engine performance at lower speeds.

3.2.2 Intake Pressure

For brevity, only the i2 location will be compared for a select set that includes intakes #1, 4, 6, 7, and 8. These intakes were chosen because of their significant differences in volumetric efficiency with respect to one another. Comparisons are presented for speeds corresponding to the main tuning peak of the baseline case, 3750 RPM, and the main tuning peak of each of the other intakes. Each pressure trace is presented in the crank-angle resolved time domain, as well as the frequency domain.

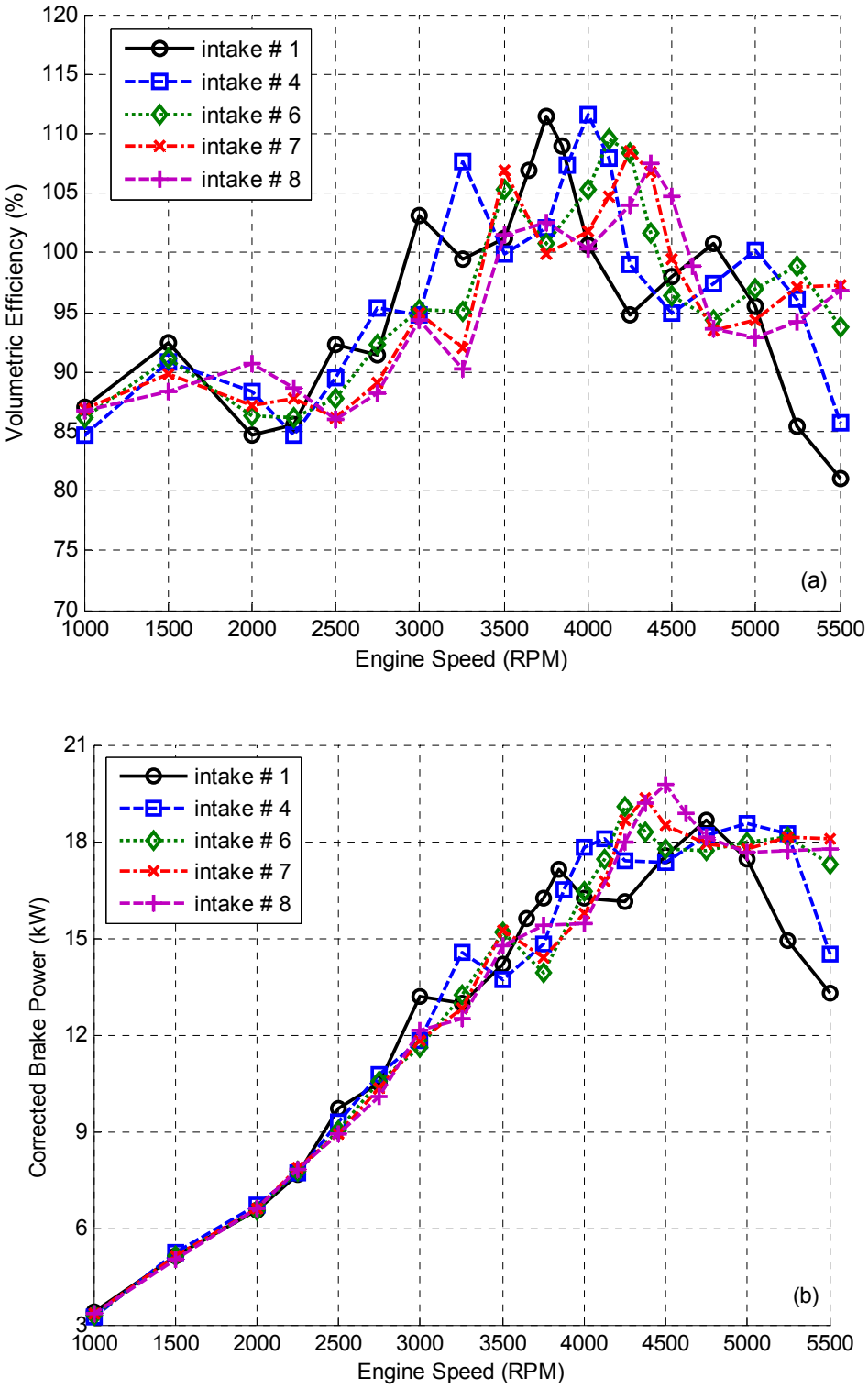

Figure 3.8: Experimental (a) Volumetric Efficiency and (b) Brake Power for Intake #1 and Intakes Tapered Over Entire Length.

Figure 3.9 shows the pressure at i2 at 3750 RPM for intakes #1 and 4. For intake #4, the compression wave returning to i2 near IVC is reduced in magnitude by 0.166 bar (12.6%) at its peak, which decreases the effectiveness of intake tuning; At the same speed, Fig. 3.3 shows a reduction in volumetric efficiency of 9.4% from intake #1 to intake #4. The dominant frequency of the "quasi standing wave" (QSW), defined as the pressure wave in the intake during the IV closed period, has increased for intake #4, going from about 136 Hz for the baseline to 150 Hz; any dominant frequencies of the QSW presented in this Chapter were calculated by measuring the CAD between peaks of the QSW. For the straight baseline case, the dominant frequency of the QSW is similar to the first resonance frequency of a closed-end quarter-wave silencer,

$$f = \frac{c}{4l}, \tag{3.2}$$

where c [m/s] is the speed of sound and l [m] is the effective length of the intake duct. Using c = 348 m/s and l = 0.6226 m, f = 140 Hz, a 3% difference with respect to the measured frequency. The increase in average intake area for the tapered case has a similar effect on the frequency of the QSW as shortening the effective length of the intake. The frequency spectra are similar in form for intakes #1 and 4. There is a 5.5 dB reduction in SPL at order 2, the dominant order. Figure 3.10 shows the pressure at i2 at the main tuning peak speed for intake #4, 4000 RPM. At this speed, the peak magnitude of the compression wave near IVC is larger for the baseline case than for intake #4; however, it occurs 18 CAD later for intake #1 and right at IVC. Thus it seems that this compression wave is slightly late in getting from i2 to the back of the valves, while

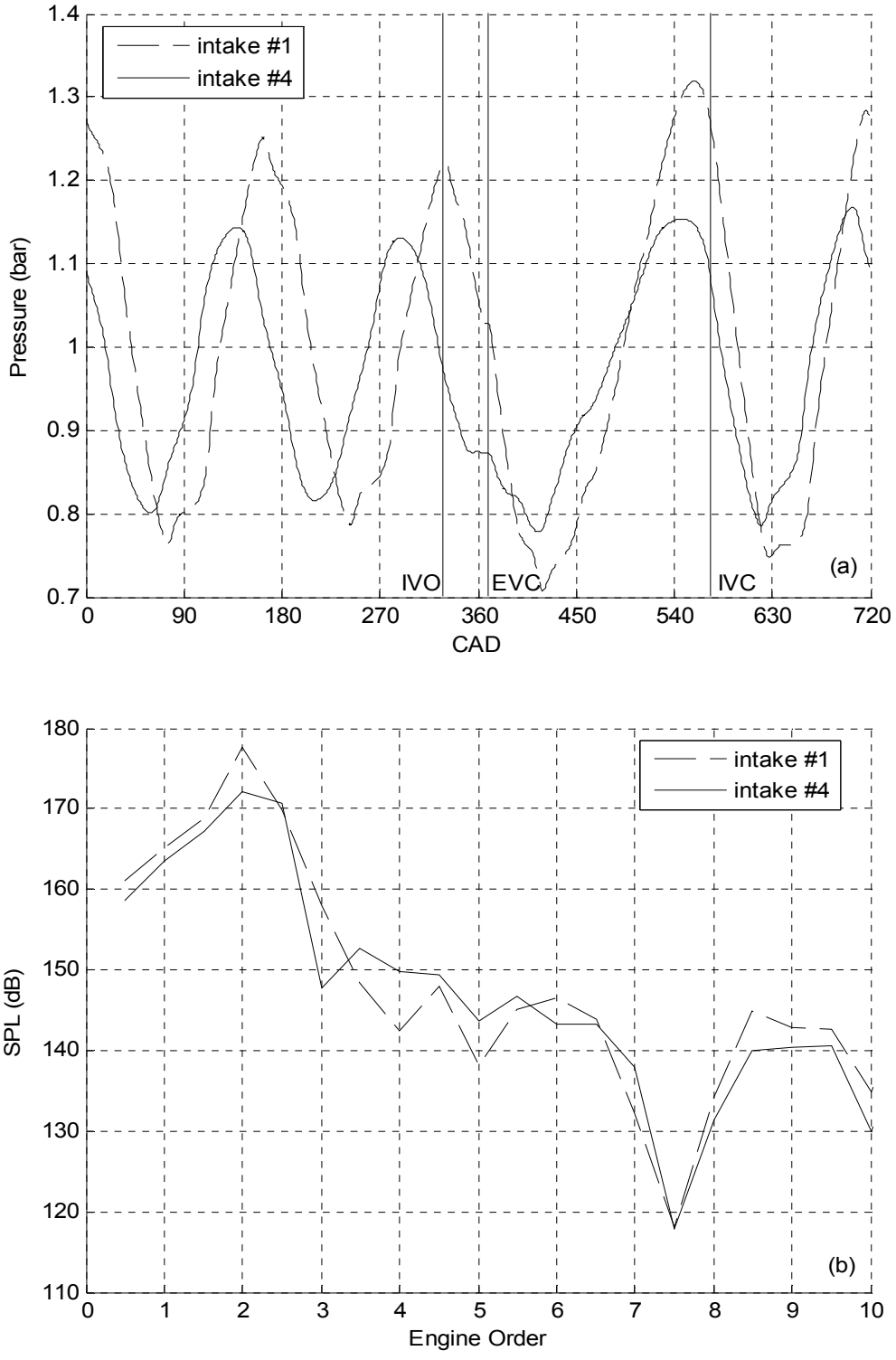

Figure 3.9: Experimental Intake Pressure at i2 at 3750 RPM for Intakes #1 and 4 in the (a) Time Domain and (b) Frequency Domain.

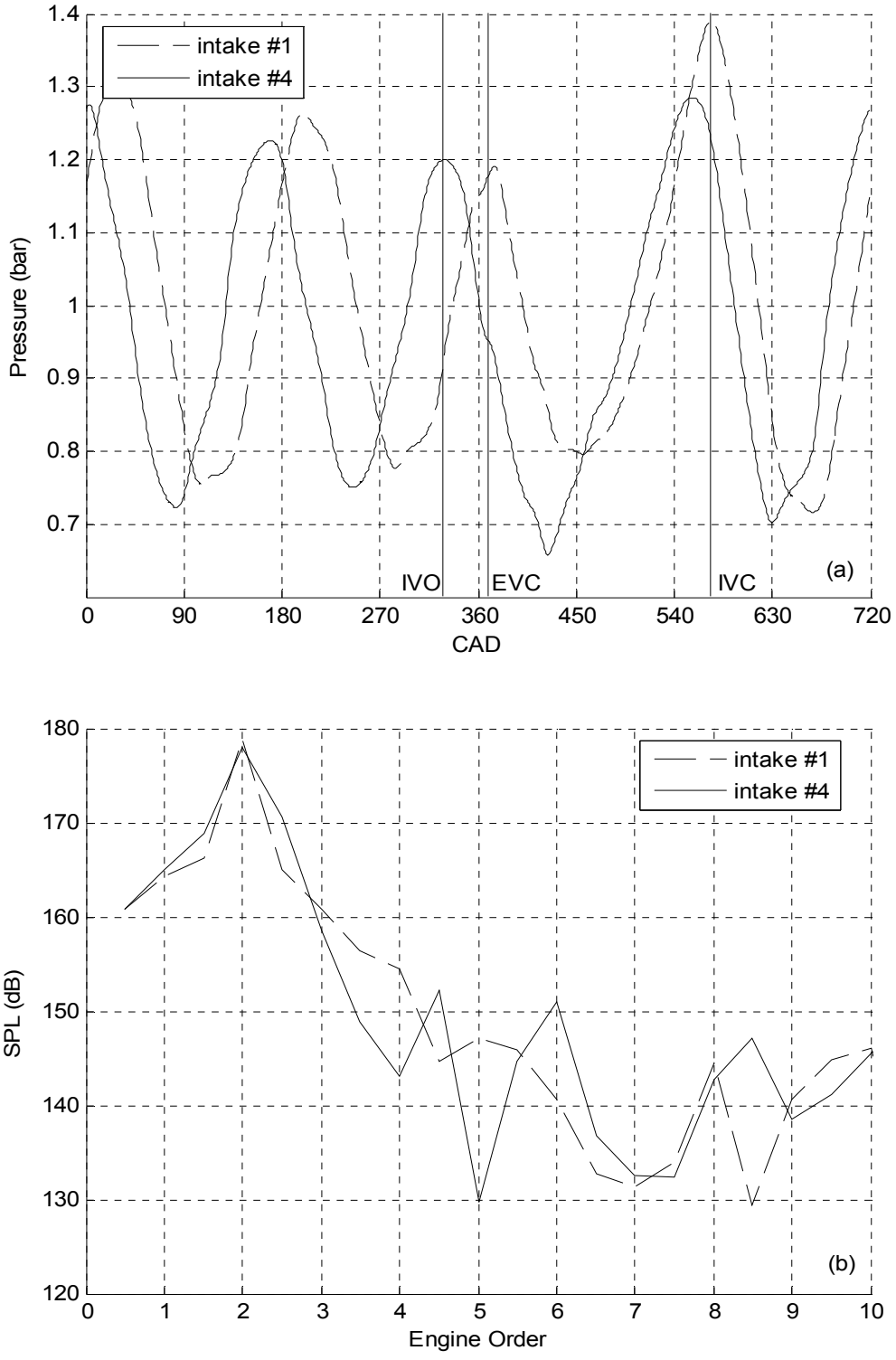

Figure 3.10: Experimental Intake Pressure at i2 at 4000 RPM for Intakes #1 and 4 in the (a) Time Domain and (b) Frequency Domain.

the compression wave for intake #4 is early enough to affect positive intake tuning, giving a rise of 11% in volumetric efficiency over the baseline case (recall Fig. 3.3). The approximate time in CADs required for the compression wave to travel from i2 to the back of the intake valves may be calculated from

$$\Delta CAD = \frac{6\ \Delta\ell\ \ N}{c}, \tag{3.3}$$

where $\Delta\ell$ is the distance from i2 to the back of the valves (= 0.2465 m for this study), N [RPM] is the engine speed, and c [m/s] is the speed of sound. Equation (3.3) gives ΔCAD = 16° at 3750 RPM, 17° at 4000 RPM, and 18° at 4250 RPM. At 4000 RPM, the dominant frequency of the QSW has increased for the taper case just as it had for 3750 RPM. The peak SPL of intake #4 has decreased by 0.5 dB compared to intake #1, while those of neighboring orders have increased.

Figure 3.11 compares intake pressures at i2 at 3750 RPM for intakes #1 and 6. For intake #6, the compression wave arriving at i2 near IVC has been drastically reduced, by 0.182 bar (13.8%), at its peak. At the same speed, Fig. 3.5 shows that volumetric efficiency is reduced by 11% compared to the baseline. As with intake #4, an increase in the dominant frequency of the QSW is observed for intake #6 when compared to the baseline: about 150 Hz for intake #6 versus 136 Hz for the baseline. The peak SPL for intake #6 has moved from order 2 to 2.5 and reduced by 5.9 dB compared to intake #1. A direct comparison of pressure at the intake #6 tuning peak speed of 4125 RPM is not possible since that speed was not acquired for the baseline case, so 4250 RPM is presented in Fig. 3.12. The peak magnitudes of the compression waves occurring during the IV open period are similar for both intakes #6 and 1, but the peak occurs 10°

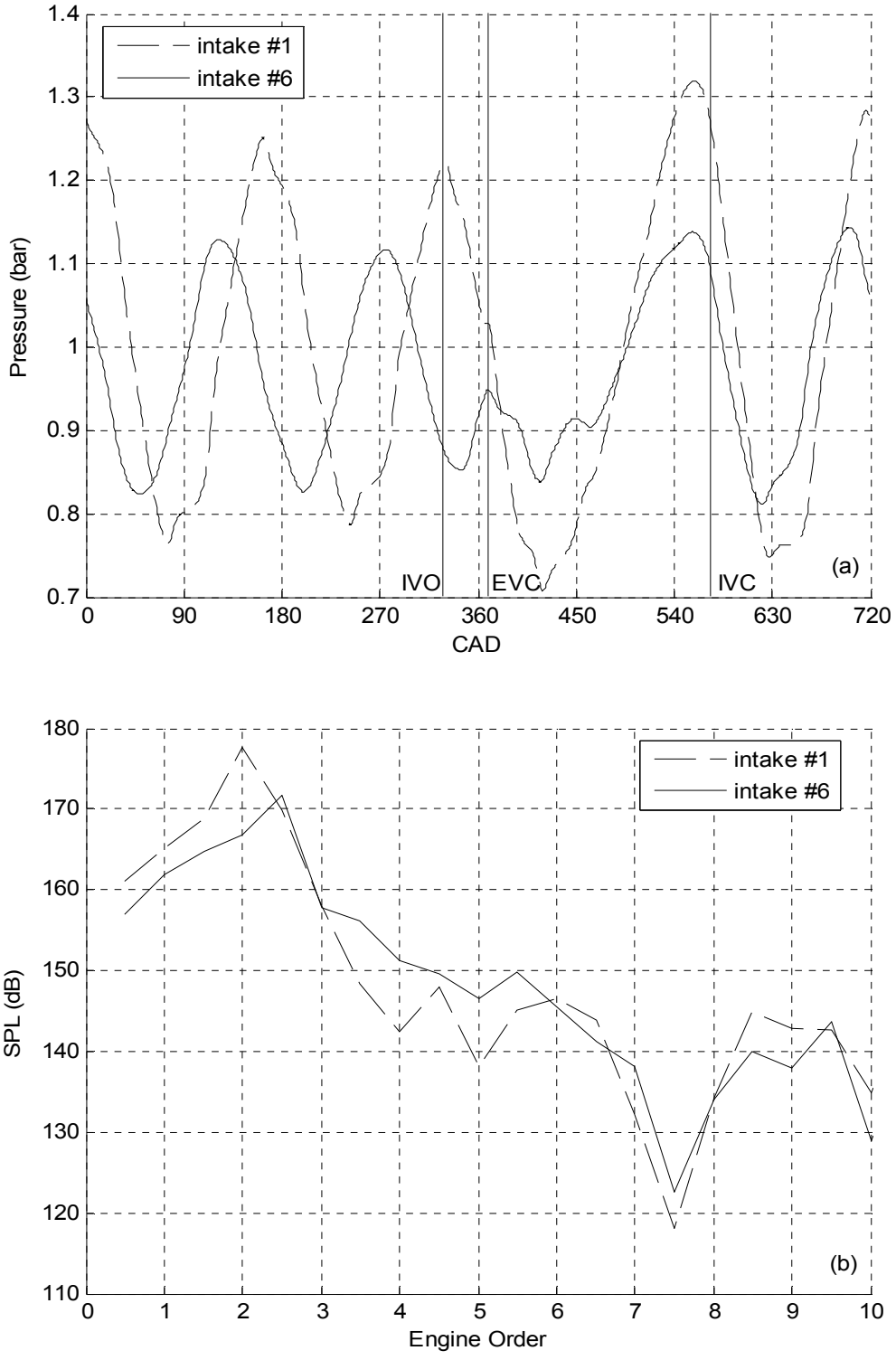

Figure 3.11: Experimental Intake Pressure at i2 at 3750 RPM for Intakes #1 and 6 in the (a) Time Domain and (b) Frequency Domain.

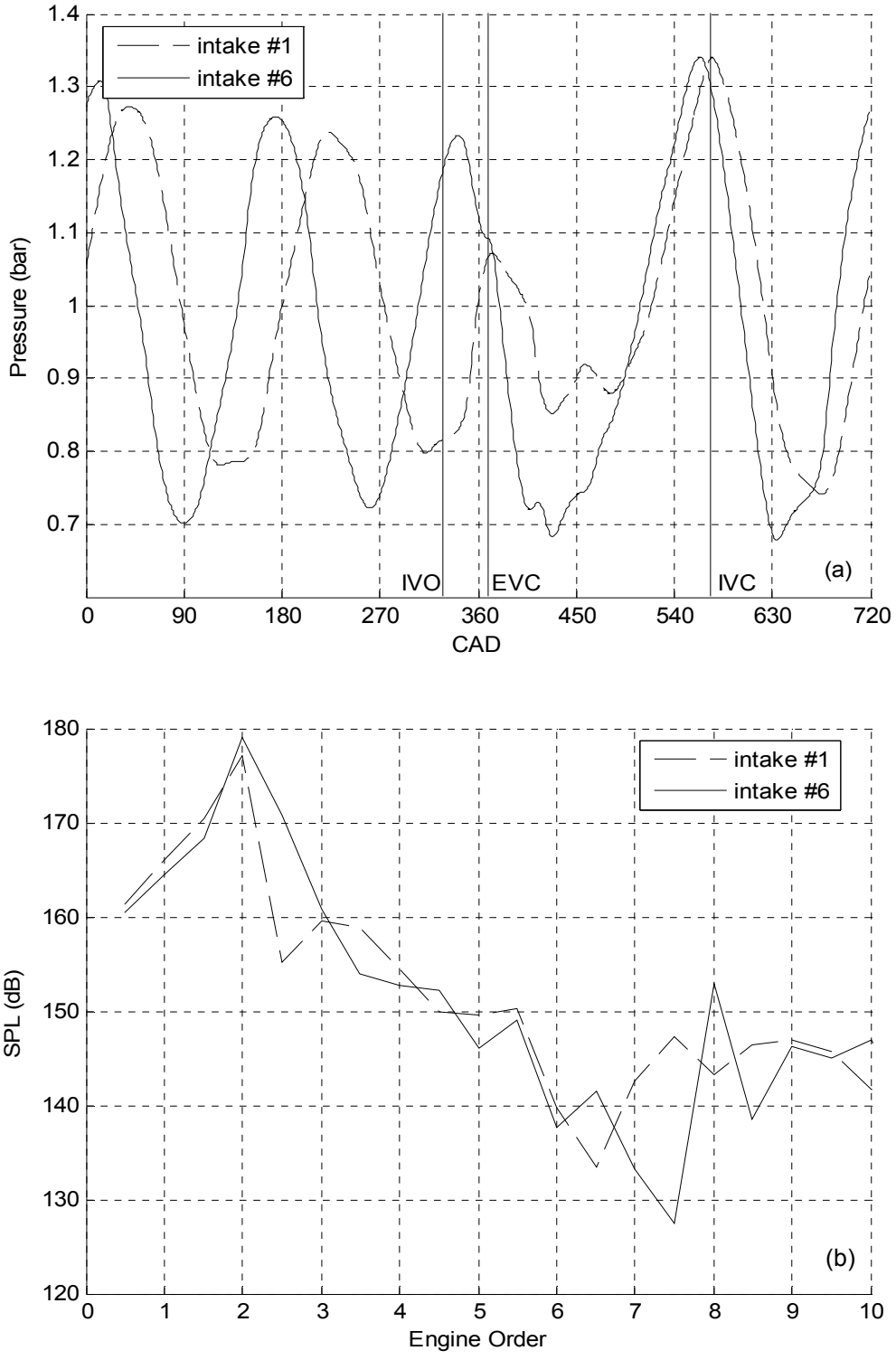

Figure 3.12: Experimental Intake Pressure at i2 at 4250 RPM for Intakes #1 and 6 in the (a) Time Domain and (b) Frequency Domain.

sooner for intake #6, while the peak for the baseline case arrives at i2 right at IVC and thus its effect on intake tuning has decreased. Also, the average pressure between IVO and EVC (also known as the valve overlap period) is higher for intake #6. This may mean the difference between pulling fresh charge into the cylinder (increasing volumetric efficiency) and reversion of exhaust gas (decreasing volumetric efficiency) during the overlap, and may be another reason for the 13% increase in volumetric efficiency for intake #6 over intake #1 at 4250 RPM. Compared to the baseline, the frequency spectrum shows a decrease in SPL from order 0.5 to 1.5 and an increase from orders 2 to 3 for the taper, with the largest increase (15.5 dB) at order 2.5.

The pressure at i2 at 3750 RPM for intake #7 is compared to the baseline in Fig. 3.13. The peak pressure of intake #1 is 0.15 bar (11.4%) higher than intake #7. Also, the average pressure at i2 during valve overlap is higher for intake #1. Both of these phenomena likely contribute to the 11% reduction in volumetric efficiency for intake #7 (Fig. 3.6). The frequency spectra show that the peak SPL has shifted from order 2 to 2.5 and reduced by 4.6 dB for intake #7. The magnitudes from order 0.5 to 2 are reduced, and those from orders 2.5 to 5.5 have increased for intake #7. Figure 3.14 compares the same intakes at the main tuning peak speed of 4250 RPM for intake #7. The peak magnitude of the compression wave near IVC is lower for intake #7 than for intake #1; however, the compression wave for the baseline arrives at i2 later and right at IVC, thus reducing its effect on volumetric efficiency and allowing higher volumetric efficiency for intake #7 at this speed. Compared to the baseline, the SPL for intake #7 is 15.5 dB higher at order 2.5 and slightly lower from orders 0.5 to 2. A large change in trend is noted at order 4, with the SPL of intake #7 dipping 22.5 dB below that of intake #1.

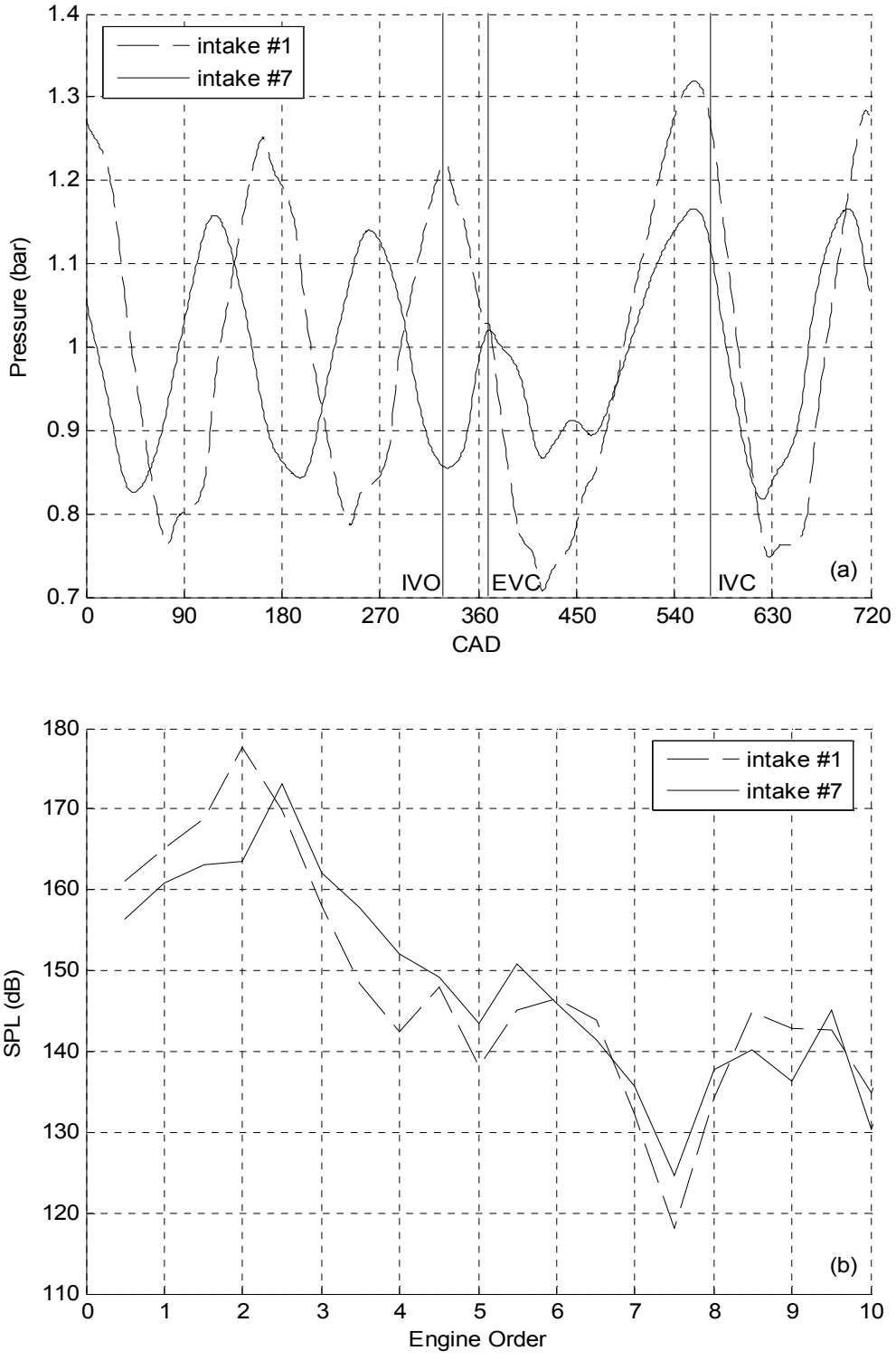

Figure 3.13: Experimental Intake Pressure at i2 at 3750 RPM for Intakes #1 and 7 in the (a) Time Domain and (b) Frequency Domain.

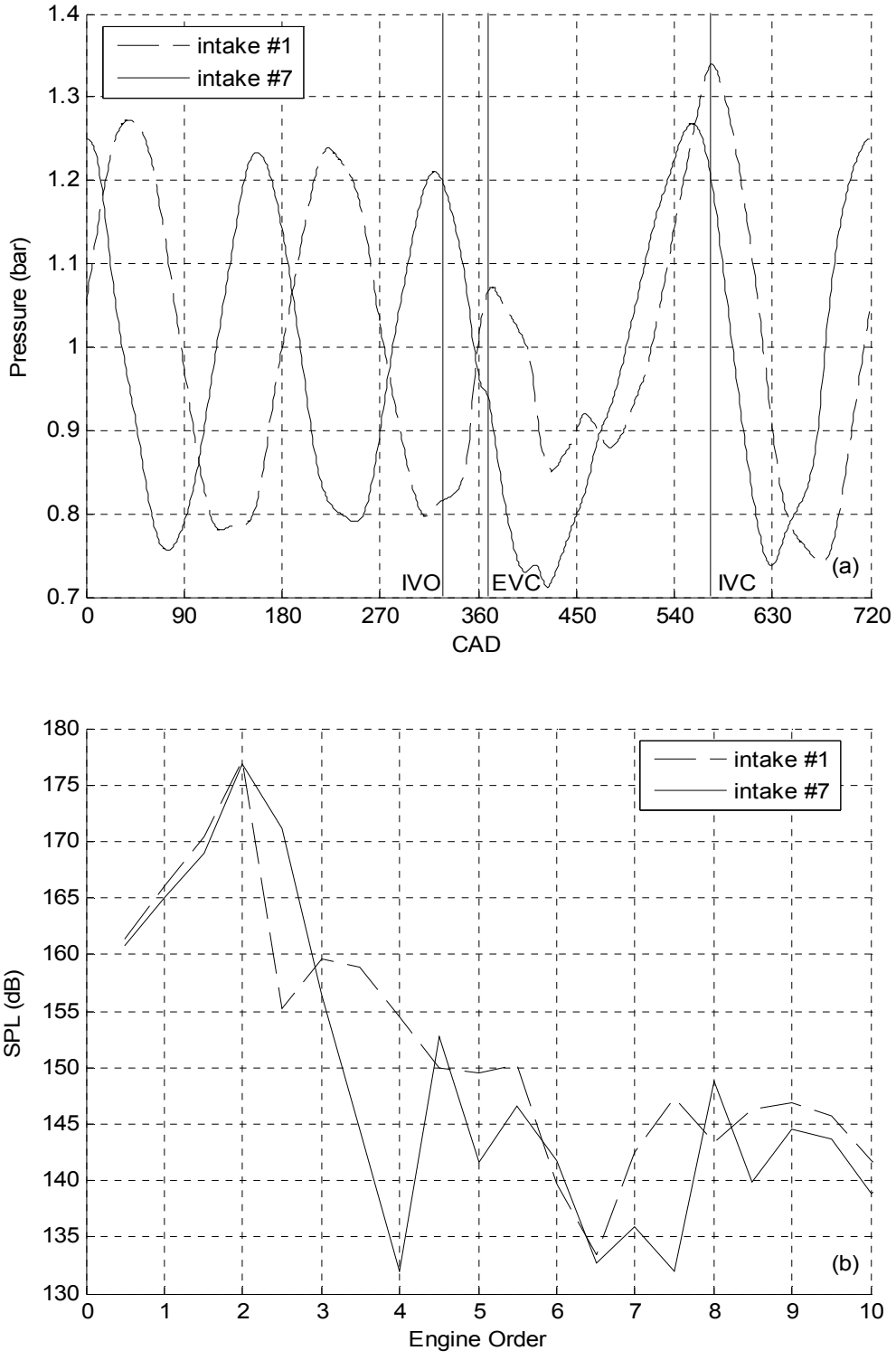

Figure 3.14: Experimental Intake Pressure at i2 at 4250 RPM for Intakes #1 and 7 in the (a) Time Domain and (b) Frequency Domain.

Figure 3.15 shows the pressure at i2 of the largest tapered intake (D_t = 7.26 cm), intake #8, compared to intake #1 at the main tuning peak of intake #1, 3750 RPM. A reduction of 0.14 bar (10.6%) can be seen in the peak pressure for intake #8, which decreases its effectiveness on intake tuning at this speed, contributing to a 9% reduction in volumetric efficiency when compared to baseline. As with the other tapered cases, the dominant frequency of the QSW has increased for intake #8, from about 136 Hz for the baseline to about 161 Hz, an increase of 18.4% over the baseline and 7.3% over intake #6. When compared to intake #1, the frequency spectrum for intake #8 shows a decrease in SPL from orders 0.5 to 2 followed by an increase from orders 2.5 to 4, with the peak SPL moving from order 2 to 2.5. Data was not acquired for the baseline case for the exact volumetric efficiency peak speed for intake #8 of 4375 RPM, so pressure at i2 is presented at 4250 RPM instead in Fig. 3.16. The peak pressure of intake #8 is 0.132 bar (9.9%) lower than that of the baseline, but it occurs 25° earlier, which is early enough to give the cylinder a super-charging effect before IVC, aiding in the 8% increase in volumetric efficiency observed for intake #8 (Fig. 3.7). The SPL from orders 0.5 to 2, have decreased for intake #8, while that of order 2.5 has increased by 16.0 dB when compared to intake #1.

3.2.3 Exhaust Pressure

Exhaust pressure was taken in one location in the exhaust, e1 (shown in Fig. 2.3). The geometric differences of any intake configuration had only a minimal effect on the exhaust pressures, with intake #8 having the most pronounced differences when compared to the baseline. Thus this section is limited to the discussion of exhaust

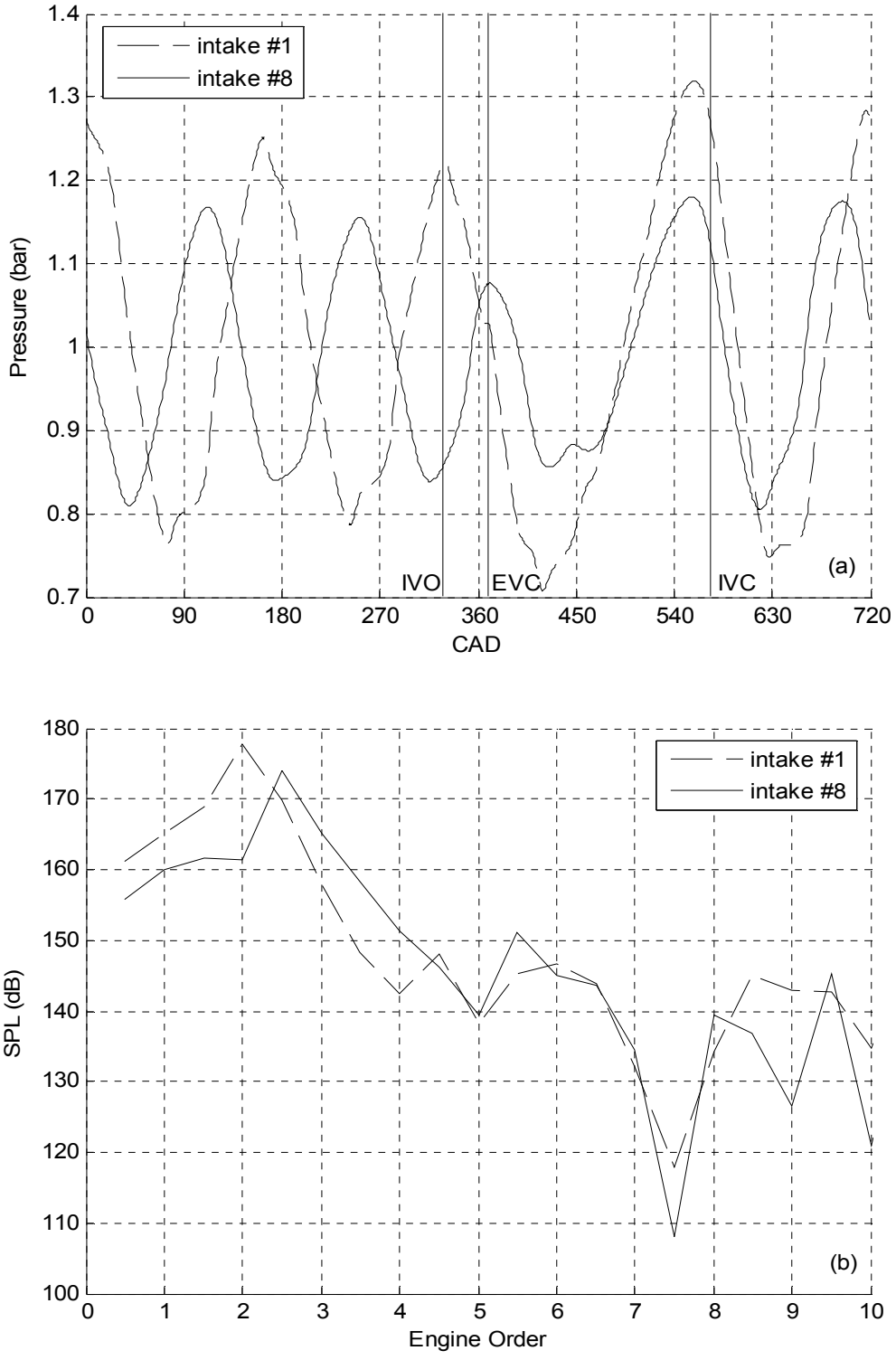

Figure 3.15: Experimental Intake Pressure at i2 at 3750 RPM for Intakes #1 and 8 in the (a) Time Domain and (b) Frequency Domain.

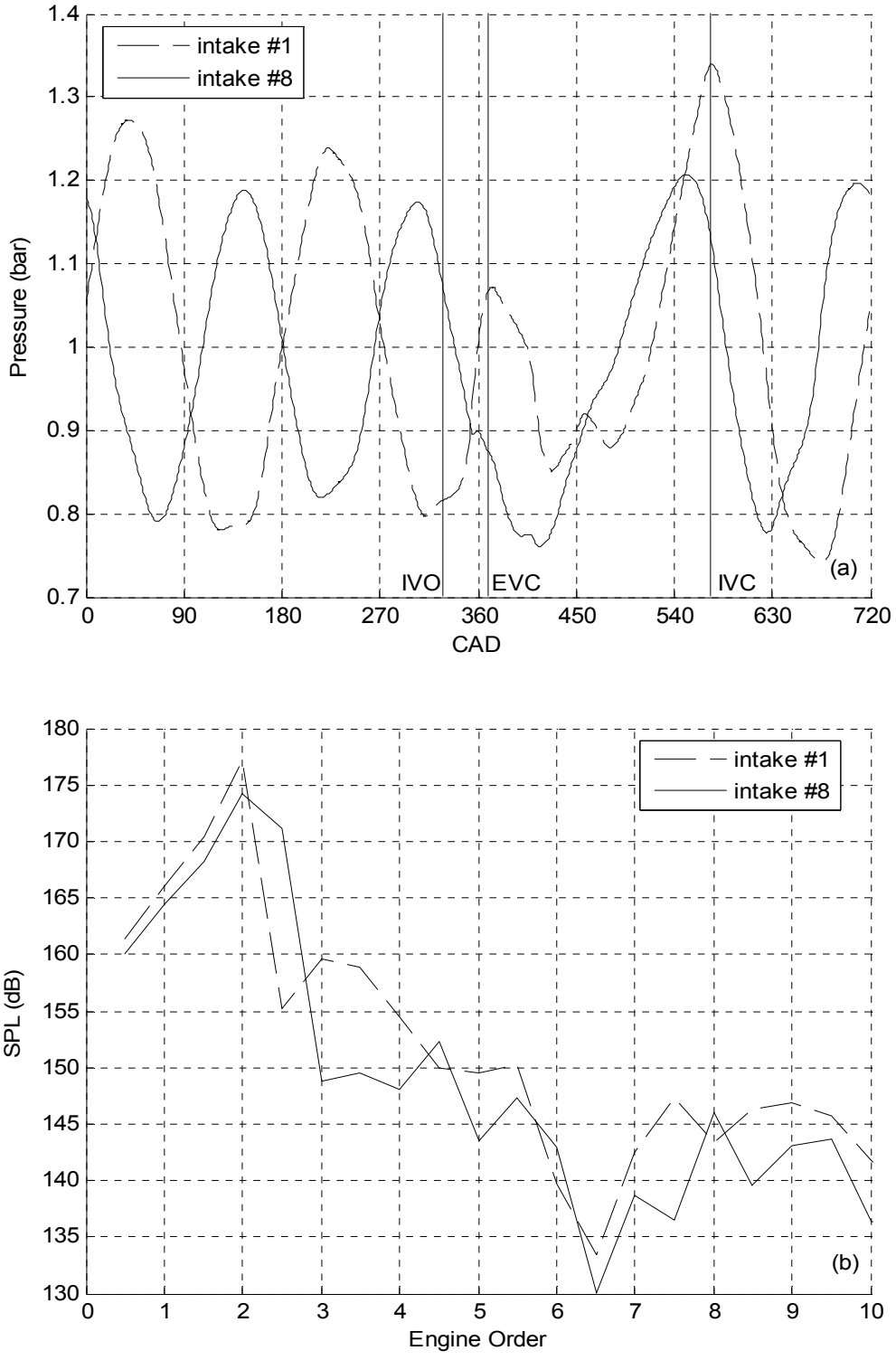

Figure 3.16: Experimental Intake Pressure at i2 at 4250 RPM for Intakes #1 and 8 in the (a) Time Domain and (b) Frequency Domain.

pressures resulting from intakes #1 and 8, and the remaining sections in this chapter will not include exhaust pressure comparisons. The variance in exhaust pressure between the two intakes does not change much as a function of engine speed. Therefore, for brevity, engine speeds from 2000 to 5500 RPM are presented by 500 RPM increments. The precise acquisition of pressures at 1000 and 1500 RPM was hampered by excessive engine vibration; thus, those speeds were omitted.

Figures 3.17-3.20 show the comparisons of the exhaust pressures at e1 for intakes #1 and 8 at speeds 2000 to 5500 RPM. In general, the pressures are very similar for the two intakes. Any changes in the time that the peak of the largest expansion pulse returns to e1 are less than 7 CAD and are most likely due to subtle differences in exhaust temperature between the two intakes at any given speed. Most deviations in pressures between intakes #1 and 8 are within 0.05 bar. The most noticeable difference in exhaust pressure between the two intakes occurs at 5500 RPM, where the peak pressure during the exhaust event is 0.1 bar higher for intake #8 than for intake #1. This is the largest difference in pressures at e1 between the baseline and all other intake configurations and thus the reason intake #8 was chosen for comparison.

3.3 Bellmouth Group

Four intakes of varying inlet bellmouths were tested against the baseline case using the experimental setup described in Chapter 2. The bellmouth group was comprised of intakes #9 through 12 as outlined in Table 2.3 and shown schematically in Fig. 2.5c. The effect of the inlet bellmouths on the volumetric efficiency and brake

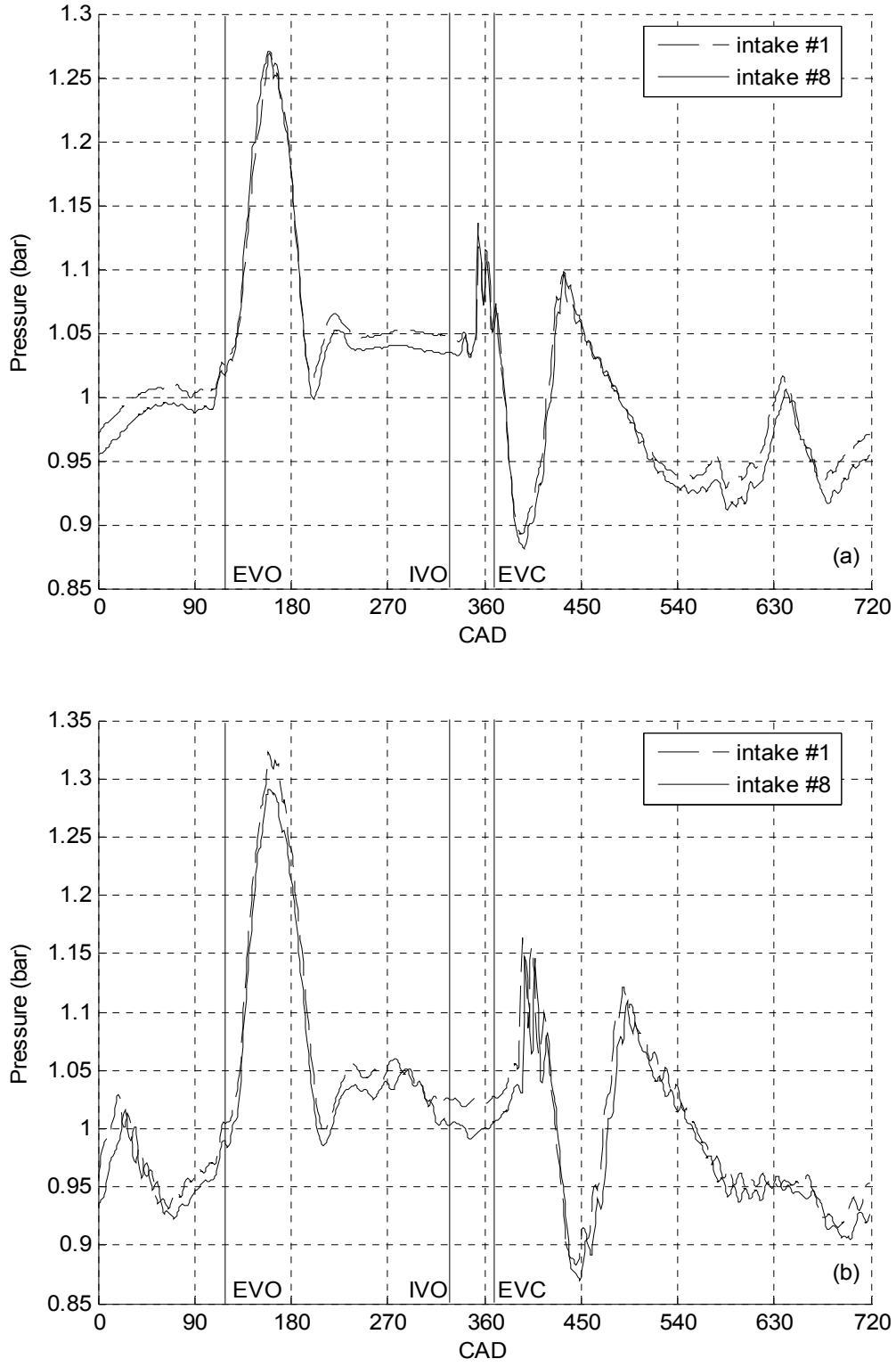

Figure 3.17: Experimental Exhaust Pressure at e1 for Intakes #1 and 8 at (a) 2000 RPM and (b) 2500 RPM.

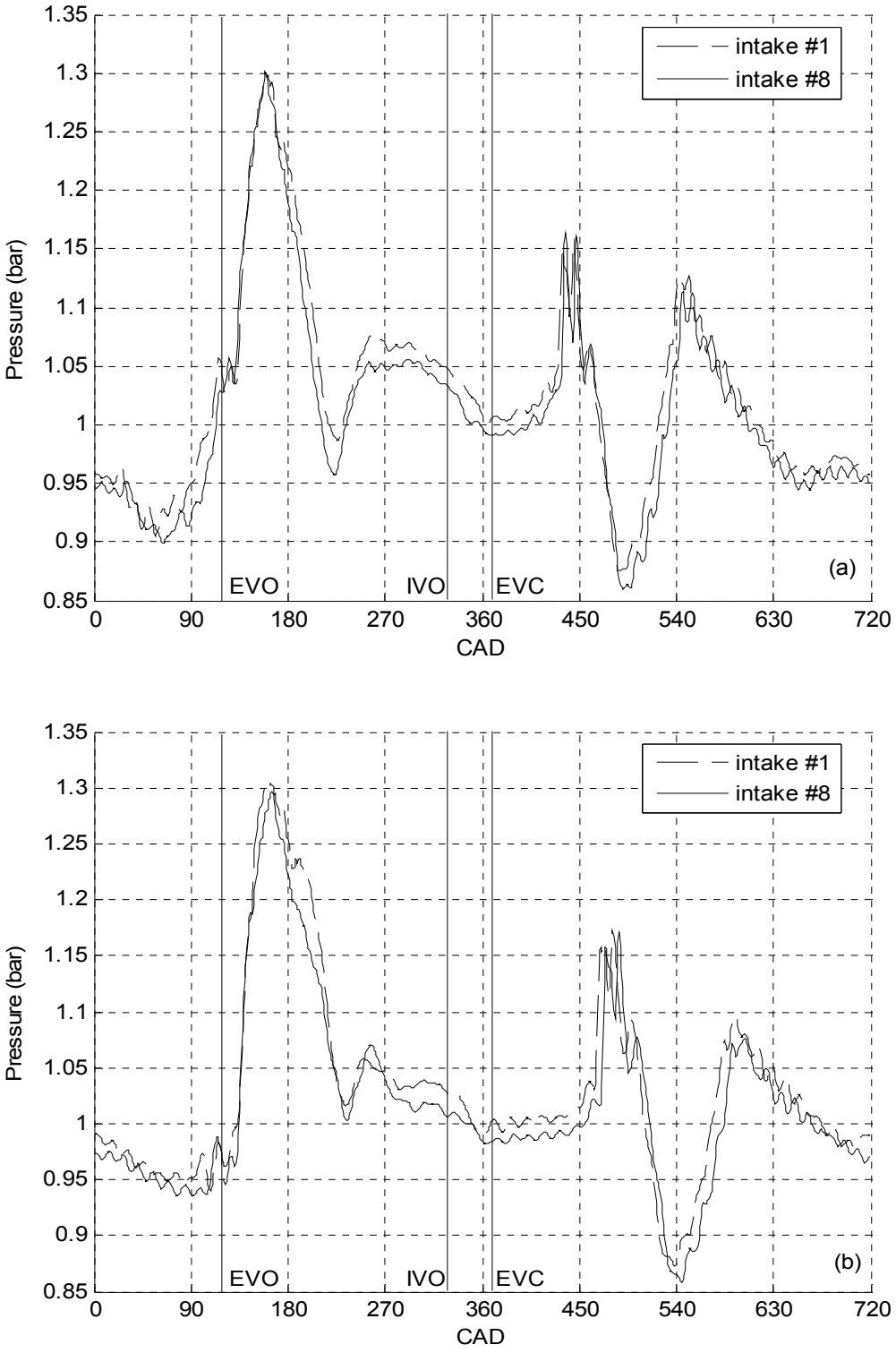

Figure 3.18: Experimental Exhaust Pressure at e1 for Intakes #1 and 8 at (a) 3000 RPM and (b) 3500 RPM.

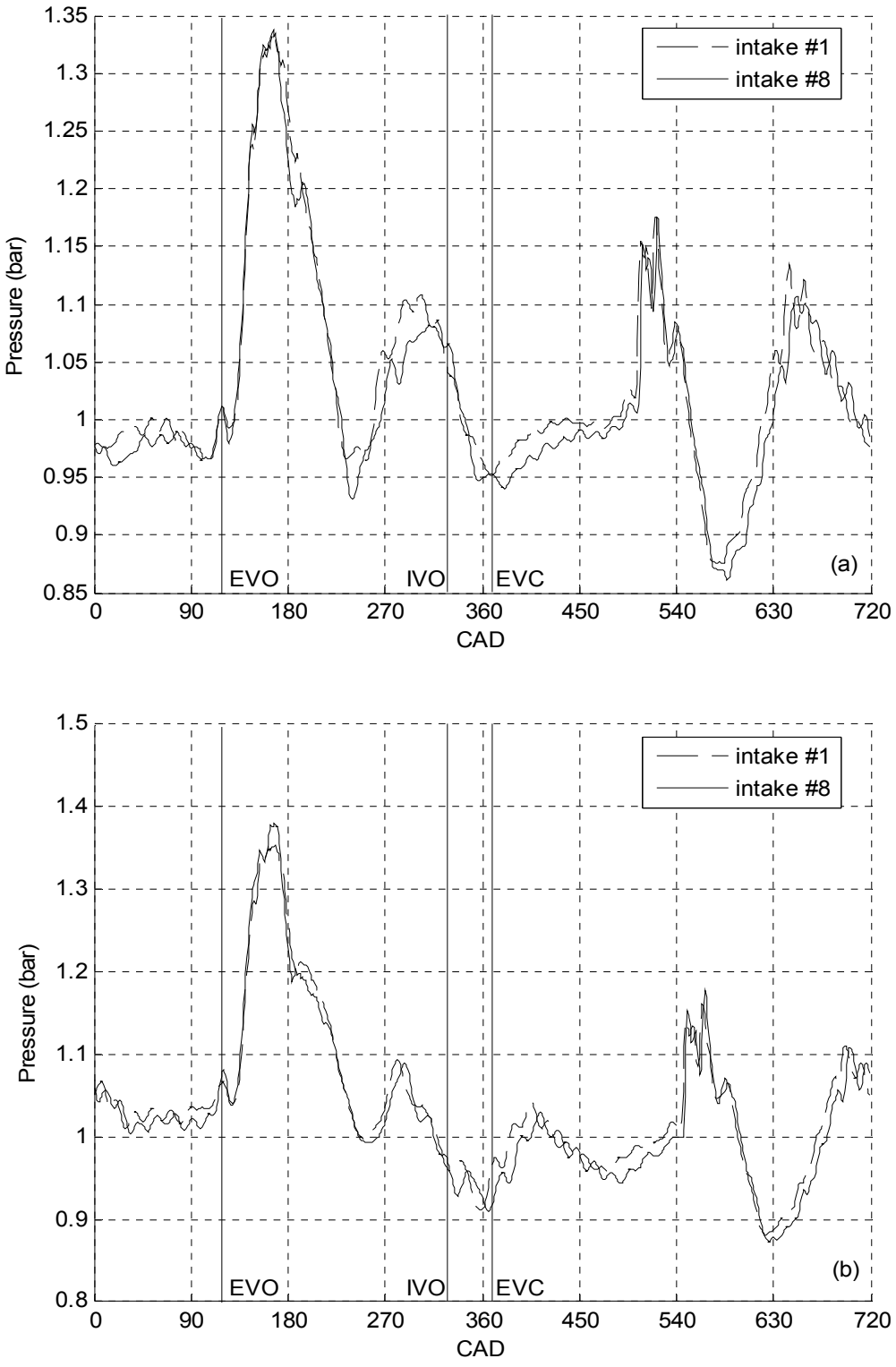

Figure 3.19: Experimental Exhaust Pressure at e1 for Intakes #1 and 8 at (a) 4000 RPM and (b) 4500 RPM.

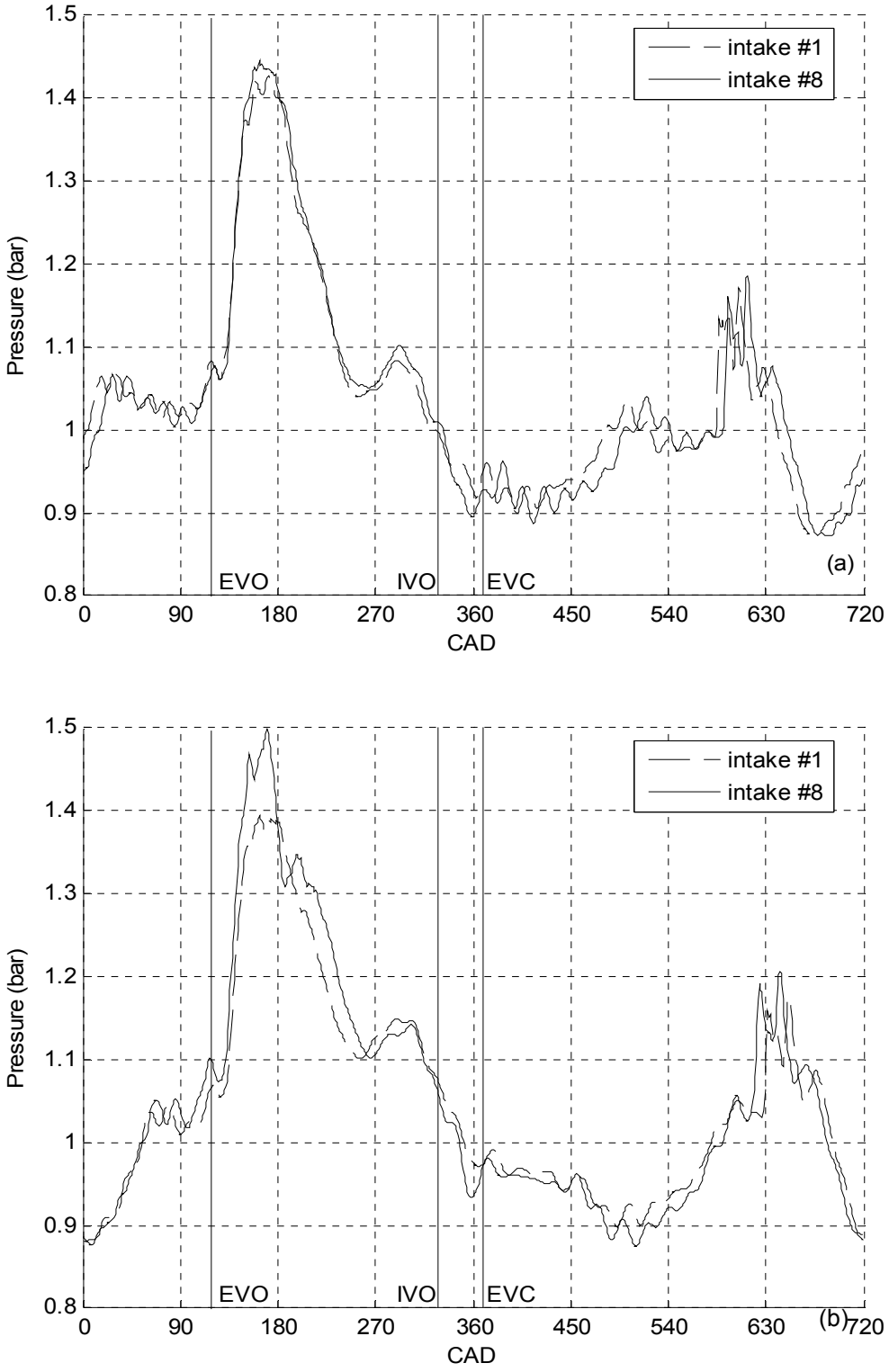

Figure 3.20: Experimental Exhaust Pressure at e1 for Intakes #1 and 8 at (a) 5000 RPM and (b) 5500 RPM.

power of the engine is discussed next in Section 3.3.1. Section 3.3.2 provides comparisons of the intake pressure at i2 for four bellmouths and the baseline.

3.3.1 Volumetric Efficiency and Brake Power

The volumetric efficiency and corrected brake power for each bellmouth is compared to the baseline in this section as a function of engine speed. Figure 3.21 shows a comparison of intakes #1 and 9. Intake #9 has the smallest bellmouth at $R_i = 0.21$ cm. The volumetric efficiency at each tuning peak has decreased, with the magnitudes at 3000, 3750, and 4750 RPM, lowered by 3.1%, 3.8%, and 3.5%, respectively. For intake #9, $R_i/D = 0.05$ results in an inlet loss coefficient of about 0.2 (Miller, 1990), which is measurably detrimental to the overall engine performance. The peak power for intake #9 has reduced slightly when compared to the baseline, and an increase in power at 5250 to 5500 RPM is noticeable corresponding to the increase in volumetric efficiency at those speeds.

Intakes #1 and 10 ($R_i/D = 0.20$) are compared in Fig. 3.22. Fox and McDonald (1998) suggest that for an $R_i/D > 0.15$, the inlet loss is almost negligible. This appears to be the case as both the volumetric efficiency and brake power compare well between the two intakes.

Figure 3.23 shows intake #11 ($R_i/D = 0.5$) compared with the baseline; it appears that the volumetric efficiency of intake #11 has shifted toward lower speeds slightly, increasing at 3650 RPM and decreasing at 3850, 4000, and 4750-5500 RPM. Selamet *et al.* (2001) have shown that for a duct with flanged bellmouth, as R_i/D increases, the length of the end correction, a fictitious length of pipe attached to the inlet of the duct to

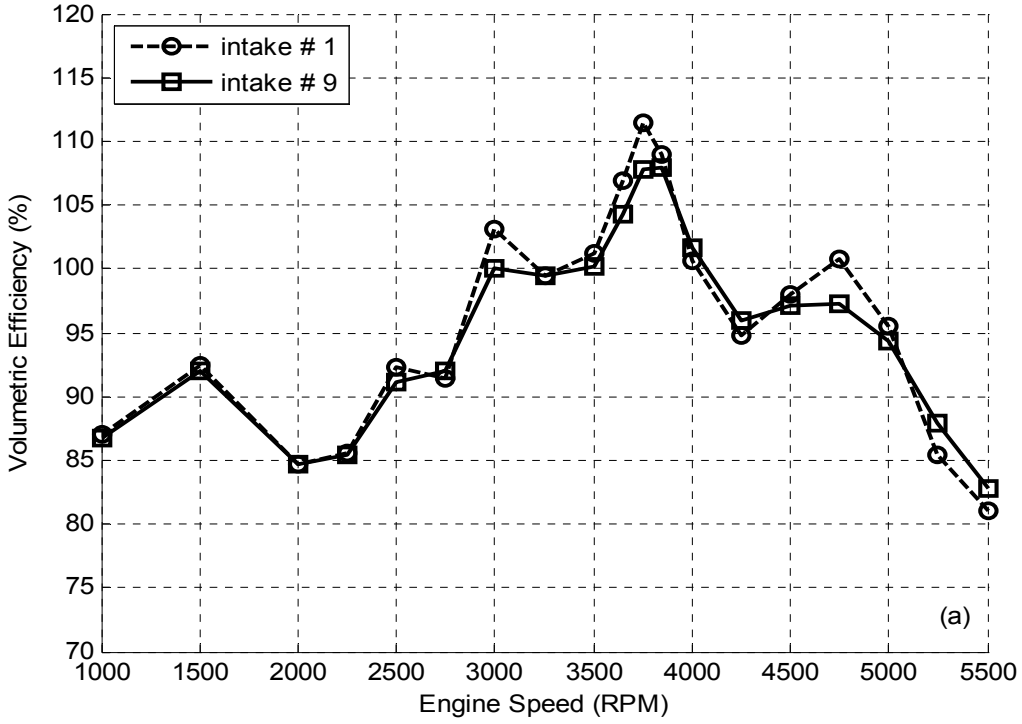

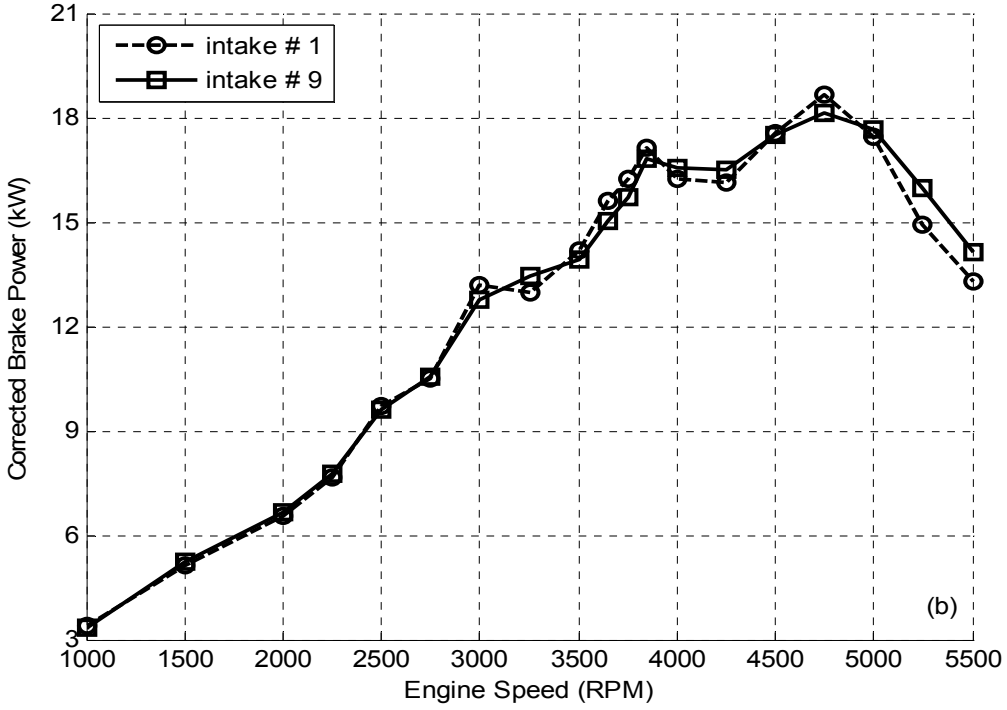

Figure 3.21: Experimental (a) Volumetric Efficiency and (b) Brake Power for Intake #1 and Intake #9.

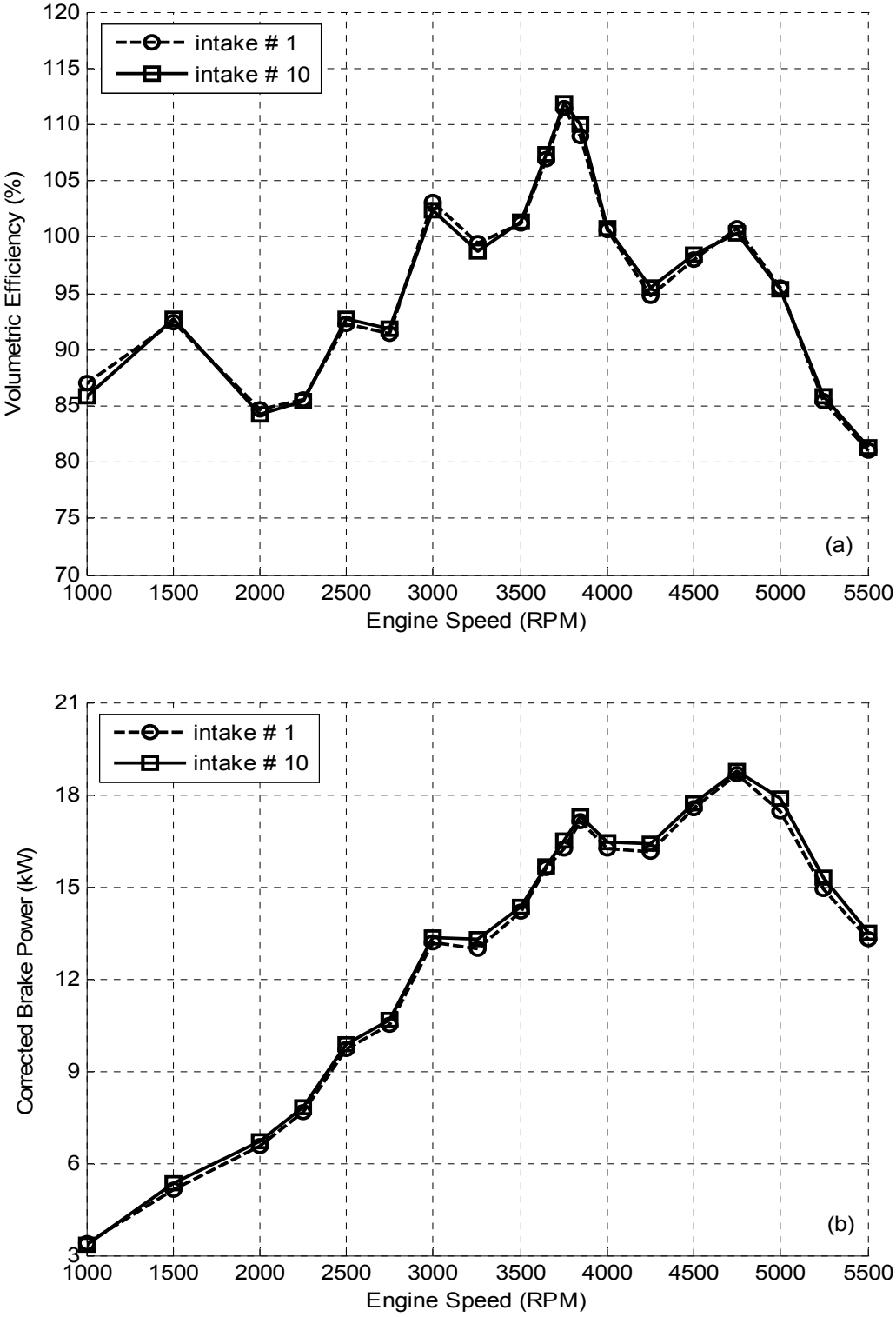

Figure 3.22: Experimental (a) Volumetric Efficiency and (b) Brake Power for Intake #1 and Intake #10.

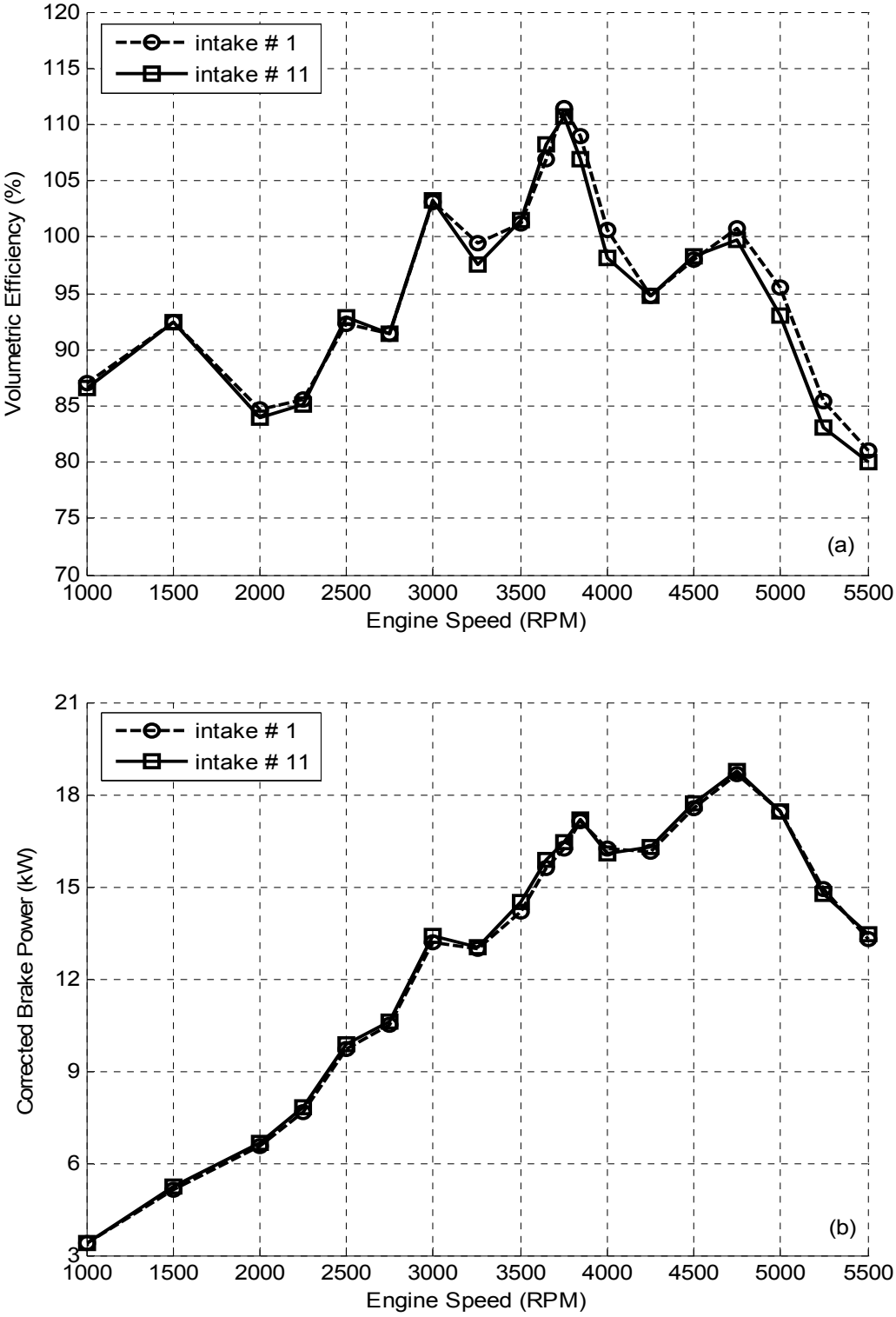

Figure 3.23: Experimental (a) Volumetric Efficiency and (b) Brake Power for Intake #1 and Intake #11.

account for inertial effects of the air, increases for frequencies low enough to affect engine tuning. This gives a longer effective length for intake #11 compared to intake #1 despite both intakes having equal distance to the bellmouth, causing the shift in volumetric efficiency toward lower speeds for the former. End corrections will be discussed in further detail in Chapter 4. The slight shift in volumetric efficiency between the two intakes does not have much influence on the brake power.

Volumetric efficiencies for intakes #1 and 12 ($R_i/D = 1.0$) are compared in Fig. 3.24a. Since the bellmouth is larger, the end correction of intake #12 is larger than that for the baseline and intake #11; therefore the overall length of the intake is longer, and the volumetric efficiency continues to shift toward lower speeds for intake #12 compared to the baseline or intake #11, with tuning peaks moving from 3750 and 4750 RPM for the baseline to 3650 and 4650 RPM for intake #12. Figure 3.24b shows corrected brake power for intakes #1 and 12. The power, following the trend of volumetric efficiency, has shifted toward lower engine speeds for intake #12, while the peak power remains similar.

3.3.2 Intake Pressures

Figure 3.25 shows the pressure at i2 at 3000 RPM for the smallest R_i, intake #9, and the baseline. The peak of the compression wave returning to i2 near 540 CAD has reduced by 0.042 bar (3.5%) for intake #9, and the peak pressure during the valve overlap decreased by about 0.069 bar (6.0%). Such reductions in pressure suggest a decrease in volumetric efficiency for intake #9 at this speed, which can be observed in Fig. 3.21. The pressures of intake #9 lead those of the baseline by about 5 CAD based on the peaks and

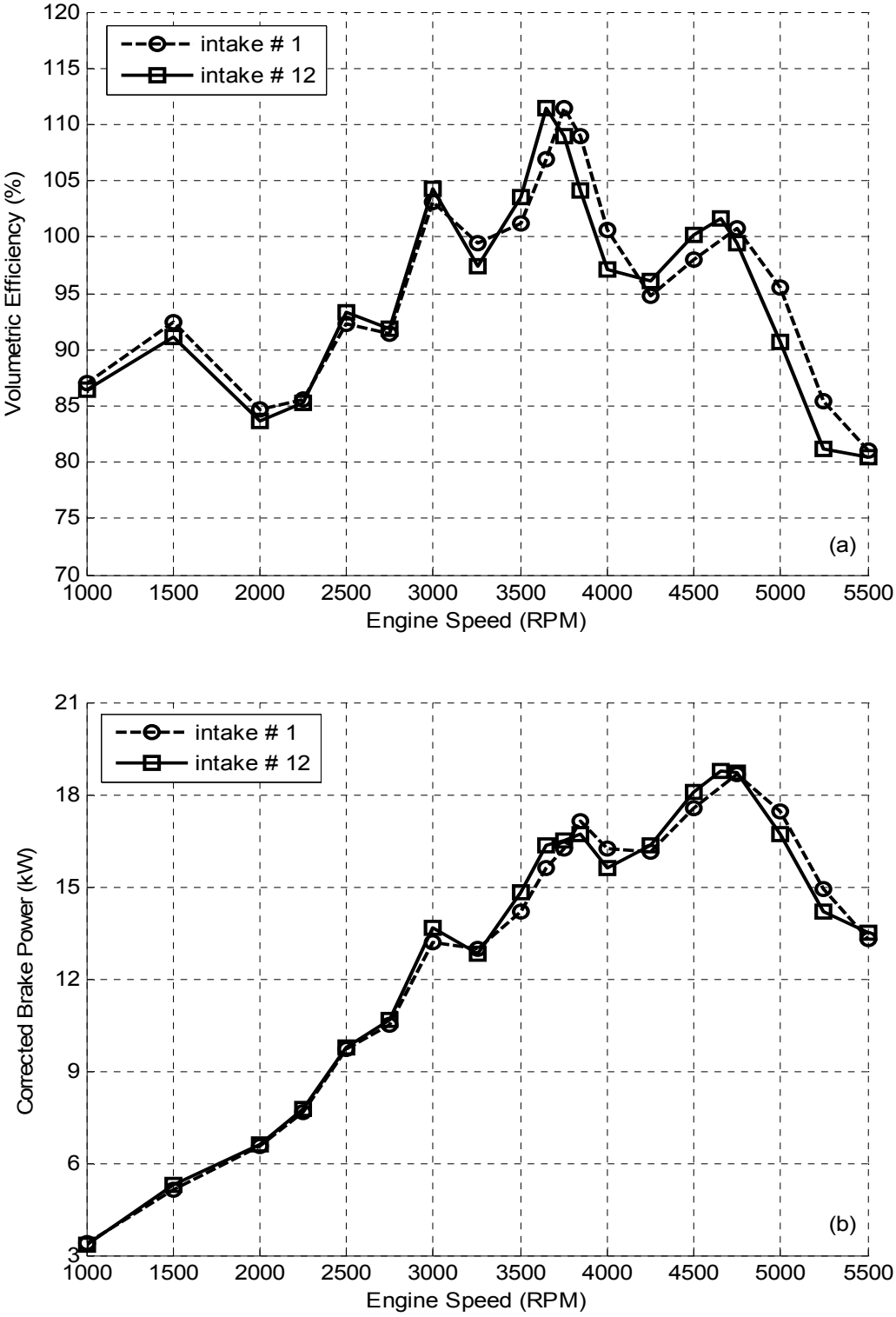

Figure 3.24: Experimental (a) Volumetric Efficiency and (b) Brake Power for Intake #1 and Intake #12.

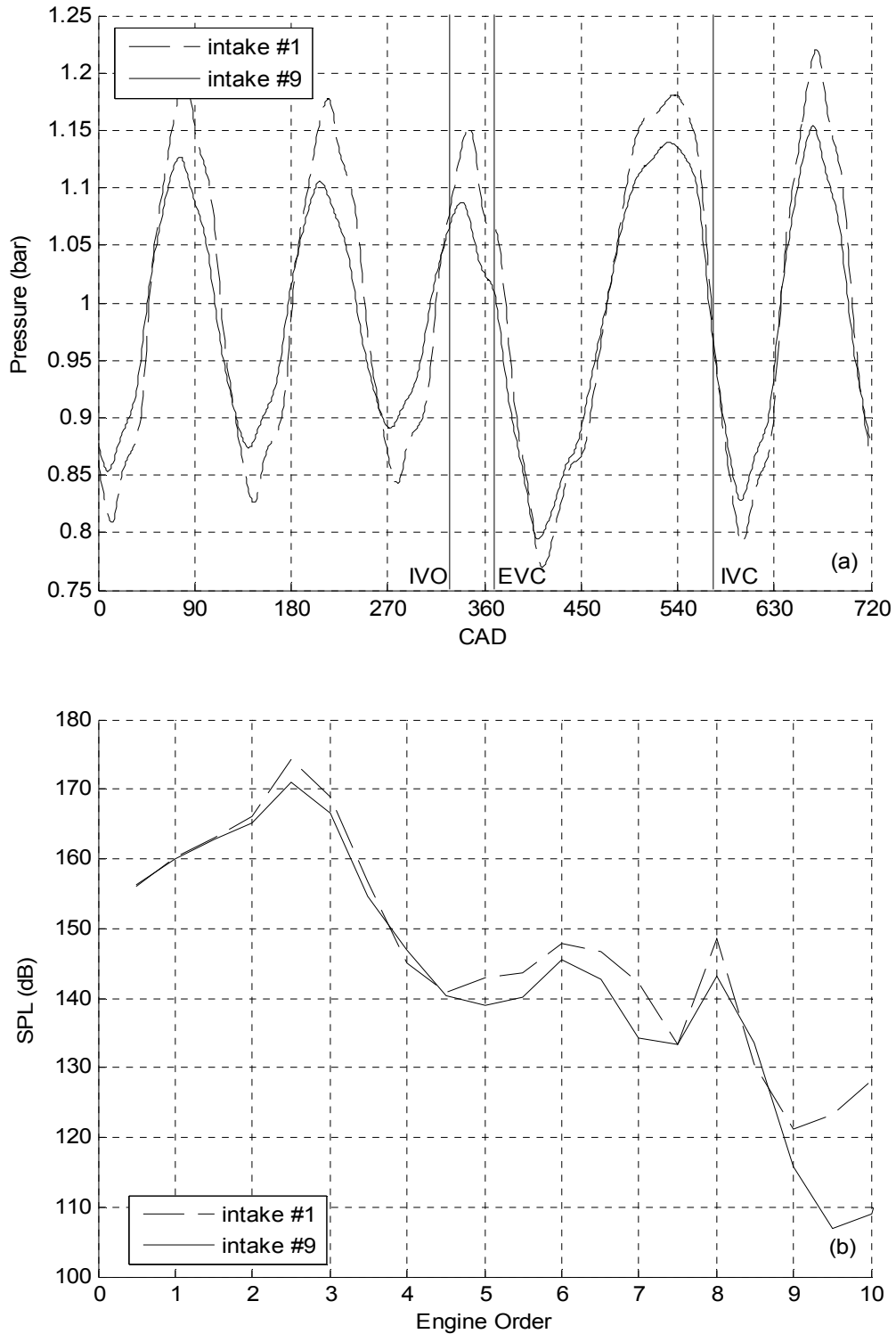

Figure 3.25: Experimental Intake Pressure at i2 at 3000 RPM for Intakes #1 and 9 in the (a) Time Domain and (b) Frequency Domain.

valleys of the wave, suggesting that intake #9 may have a smaller end correction than the baseline. Chapter 4 will show that this is indeed true. The frequency spectra for the two intakes are similar in shape, with intake #9 having similar or lower SPL over almost the entire order range, with exceptions at orders 4 and 8.5. Figure 3.26 shows the pressure at i2 for the volumetric efficiency peak speed of 3750 RPM of intake #1. The peak pressure near IVC of intake #9 is 0.063 bar (4.8%) lower than that of the baseline, and the pressures have also decreased during valve overlap. These reductions in pressure contribute to a drop in volumetric efficiency of 4% for intake #9. A trend similar to that of 3000 RPM is observed for the frequency spectra between these two intakes at 3750 RPM; the overall behavior is similar for both intakes, with similar or lower SPL for intake #9 for most orders. The pressures at i2 at 4750 RPM for intakes #1 and 9 are shown in Fig. 3.27. The peak pressure for intake #9 is 0.056 bar (3.8%) lower than that of intake #1. This indicates that volumetric efficiency should be lower for intake #9 at 4750 RPM, which is indeed the case. The peak SPL of intake #9 is 2.1 dB lower than that of the baseline; both peaks occur at order 1.5. The overall trend of the frequency spectra are similar for both intakes through order 5, after which somewhat of a crossing pattern is observed.

Figures 3.28-3.30 show the intake pressures at i2 for intakes #1 and 10 at 3000, 3750, and 4750 RPM, respectively. Since the volumetric efficiencies for these two intakes are nearly identical, it is expected that the intake pressures should also be nearly identical. This proves to be the case, as only the subtlest of differences can be seen in

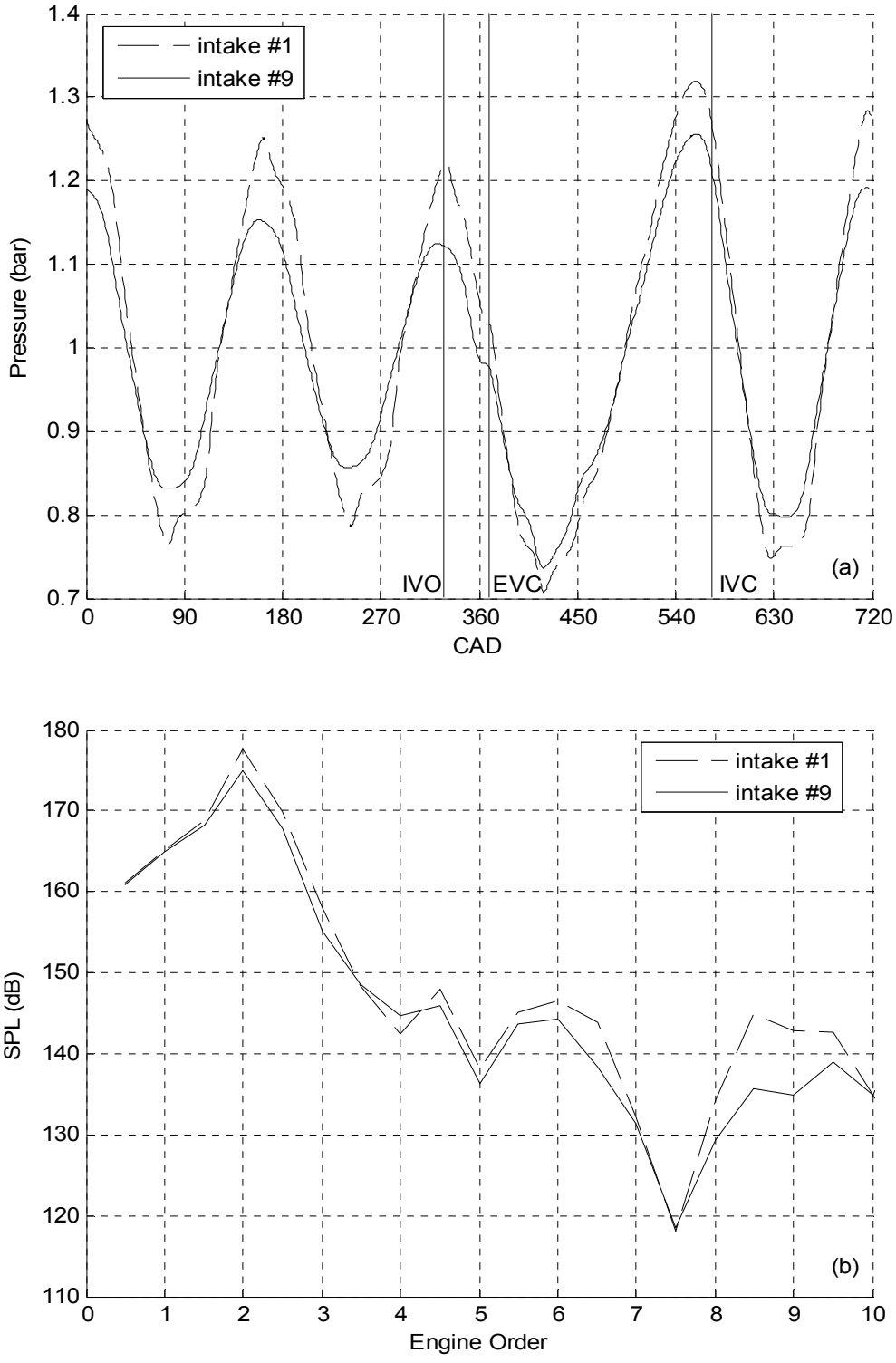

Figure 3.26: Experimental Intake Pressure at i2 at 3750 RPM for Intakes #1 and 9 in the (a) Time Domain and (b) Frequency Domain.

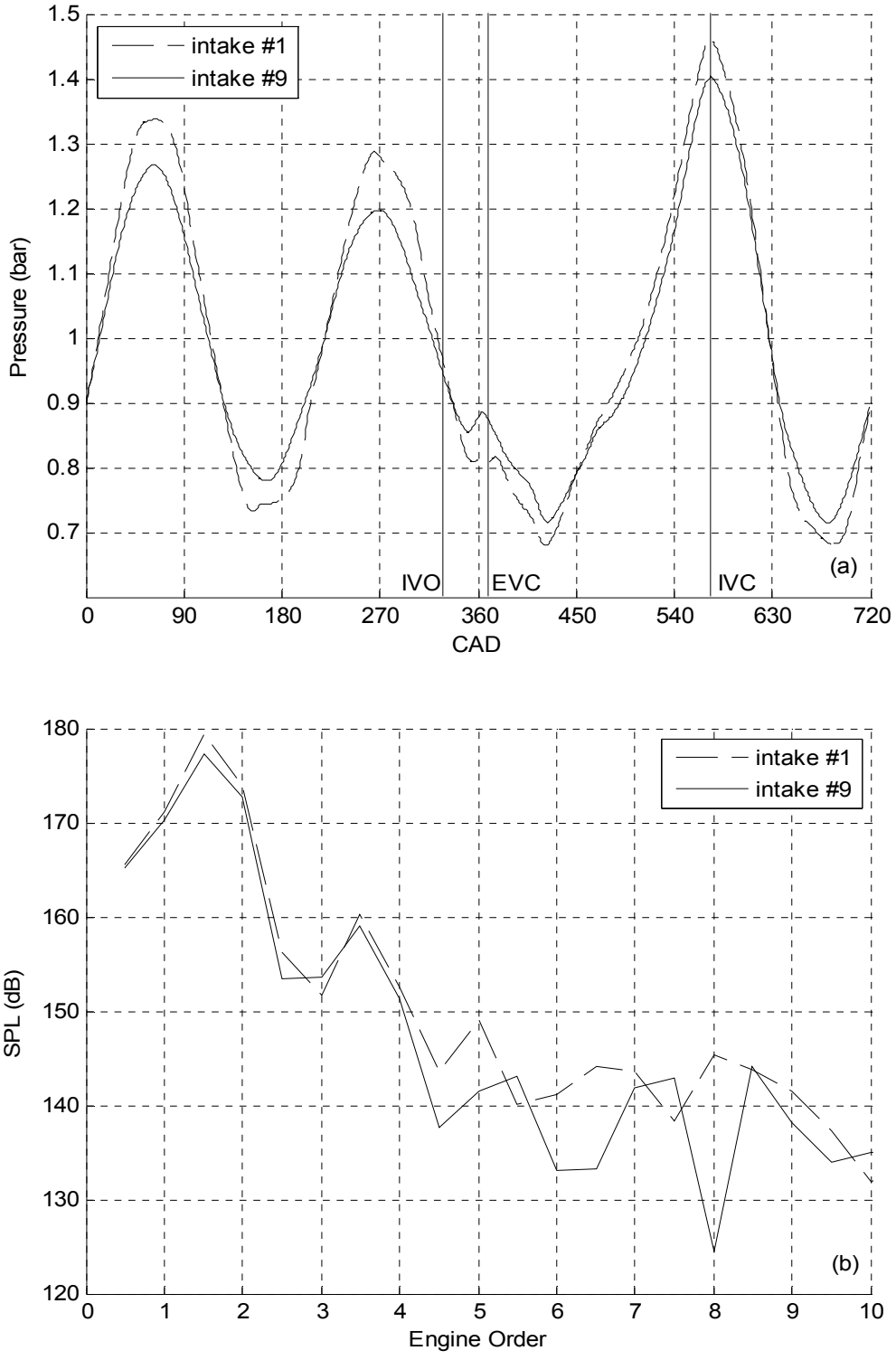

Figure 3.27: Experimental Intake Pressure at i2 at 4750 RPM for Intakes #1 and 9 in the (a) Time Domain and (b) Frequency Domain.

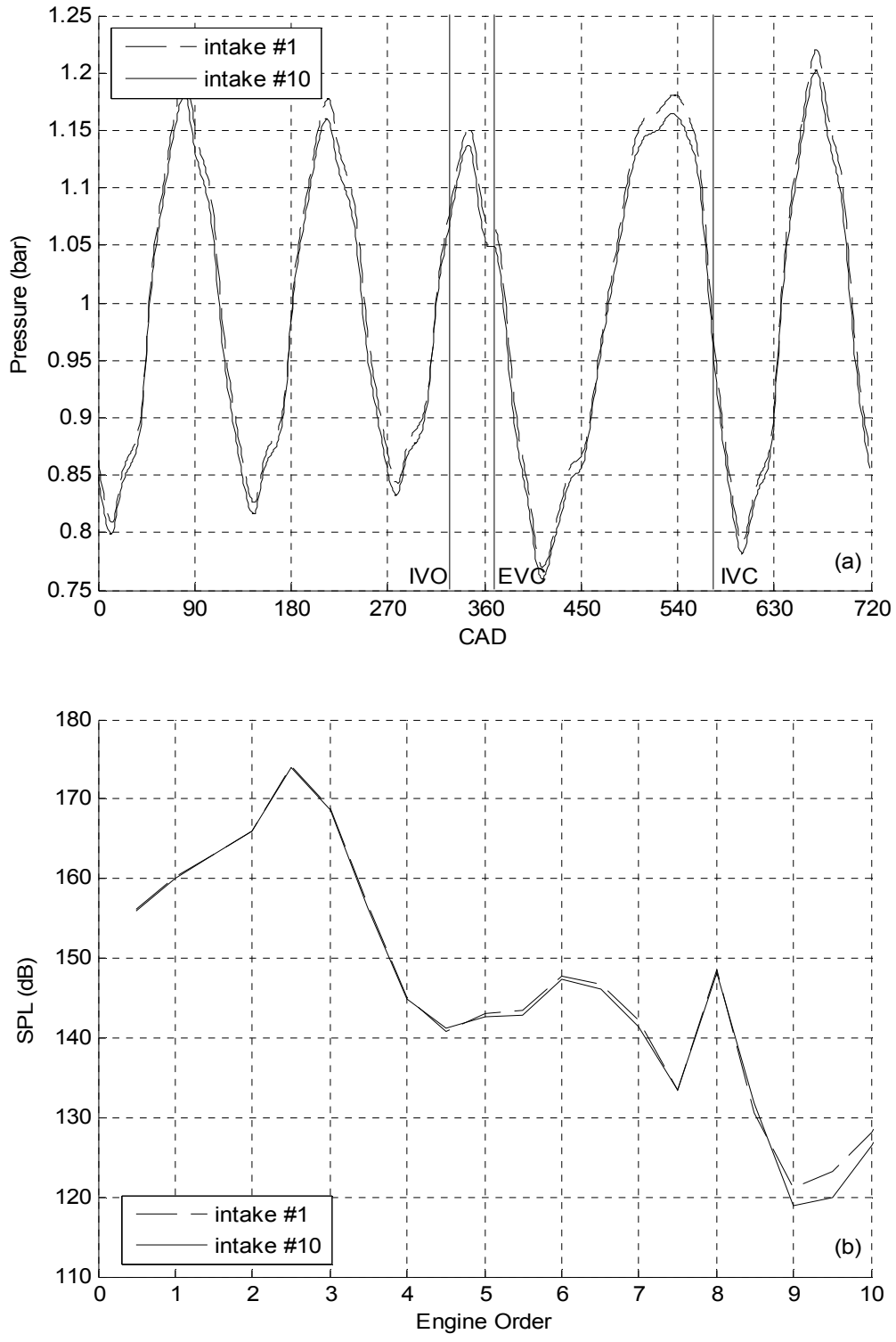

Figure 3.28: Experimental Intake Pressure at i2 at 3000 RPM for Intakes #1 and 10 in the (a) Time Domain and (b) Frequency Domain.

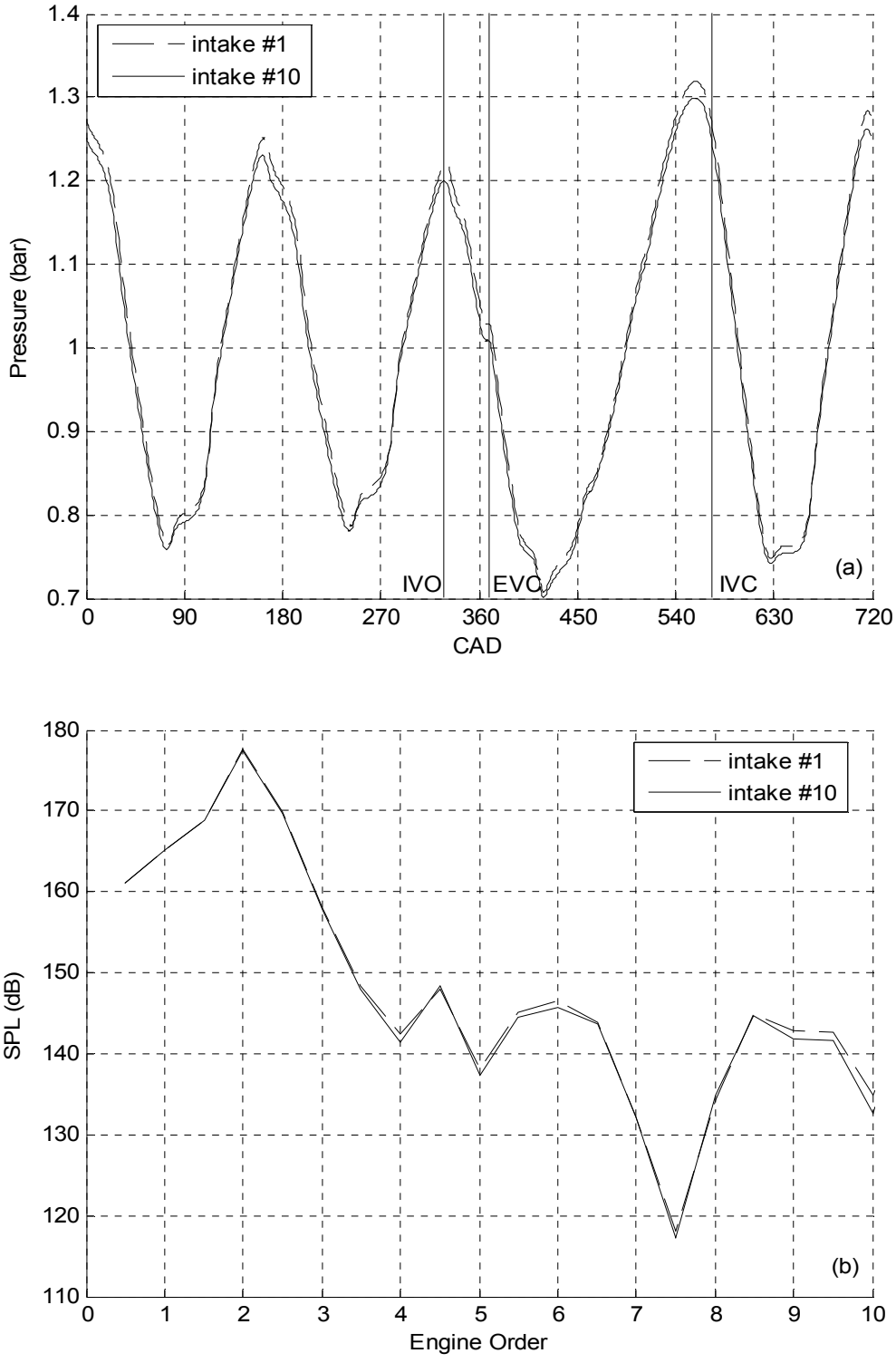

Figure 3.29: Experimental Intake Pressure at i2 at 3750 RPM for Intakes #1 and 10 in the (a) Time Domain and (b) Frequency Domain.

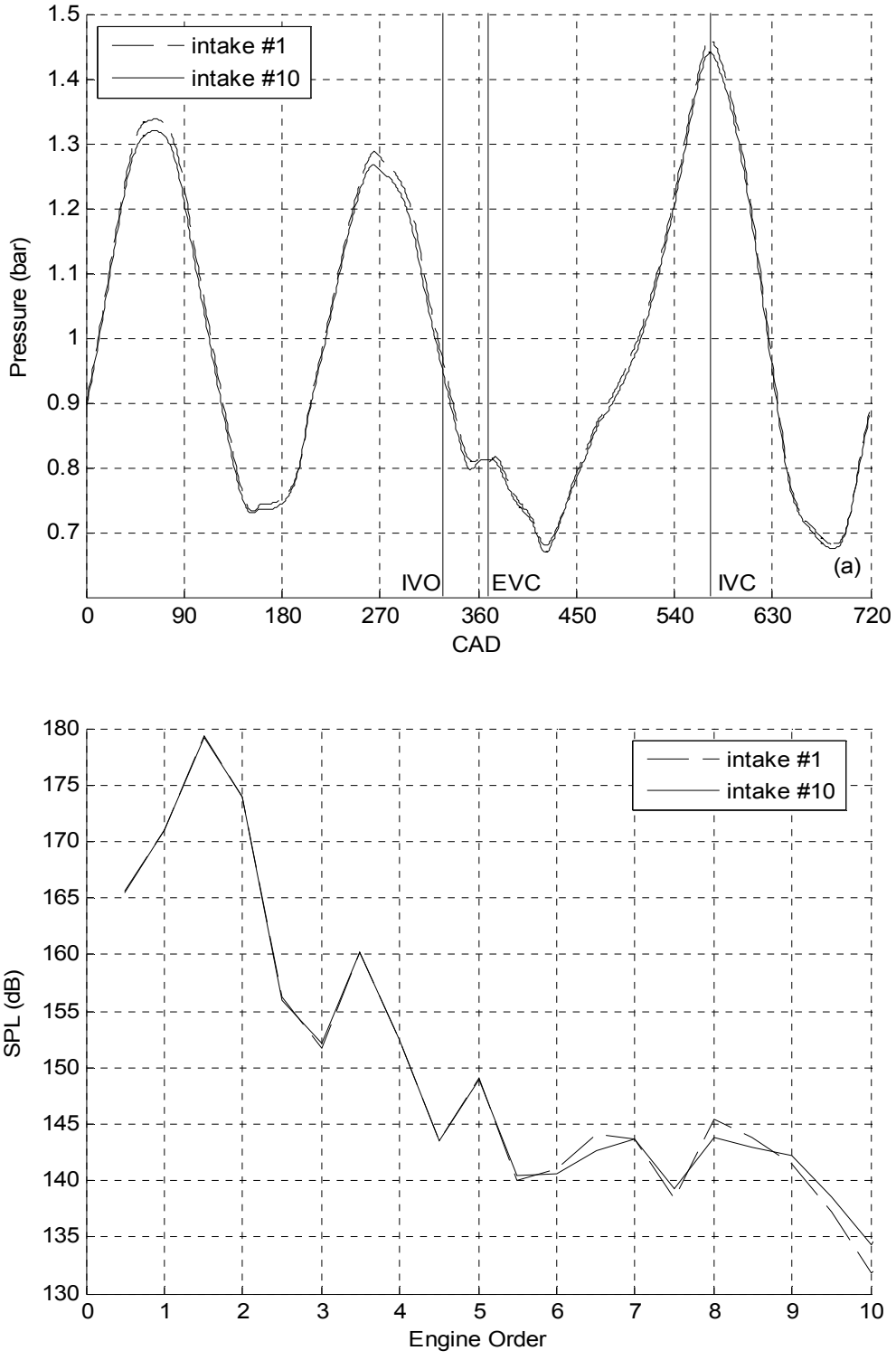

Figure 3.30: Experimental Intake Pressure at i2 at 4750 RPM for Intakes #1 and 10 in the (a) Time Domain and (b) Frequency Domain.

both the time and frequency domain and are most likely due to the change in barometric pressure between experiments, with that of intake #1 being 0.013 bar higher.

The pressures at i2 are compared for intakes #1 and 11 in Figs. 3.31-3.33 for the baseline tuning peak speeds of 3000, 3750, and 4750 RPM, respectively. At 3000 RPM, the pressures at i2 are similar in magnitude for both intakes #1 and 11; the volumetric efficiency at 3000 RPM, shown in Fig. 3.23, for both intakes is also similar. The peaks and valleys of the wave for intake #11 trail those of the baseline by 2 to 4 CAD at this speed, indicating that the effective length of this intake is slightly longer. The frequency spectra show that the SPL of the dominant engine orders are virtually the same at 3000 RPM for both intakes; as are the overall trends, with subtle differences at high engine orders. At 3750 RPM, trends similar to those at 3000 RPM are observed for the pressures between the same two intakes; the magnitudes are similar and again a small phase lag is noticeable for intake #11. At this speed, the volumetric efficiencies for both intakes are also similar. The frequency spectra for intakes #1 and 11 are almost identical for the dominant engine orders (from 0.5 to 2.5), while the overall behavior of SPL for higher orders are similar. At 4750 RPM, the pressures for intakes #1 and 11 are nearly identical. At this speed, the volumetric efficiencies for both intakes are also similar. The pressures for both intakes are comprised of similar frequency components (within 1 dB) from orders 0.5 to 5.

Figures 3.34-3.36 compare the intake pressure at i2 for the largest bellmouth ($R_i/D = 1.0$), intake #12, to the baseline for its tuning peak speeds of 3000, 3750, and 4750 RPM, respectively. At 3000 RPM, the peak pressure of the compression wave near IVC is similar for both intakes, suggesting that the volumetric efficiency at this speed

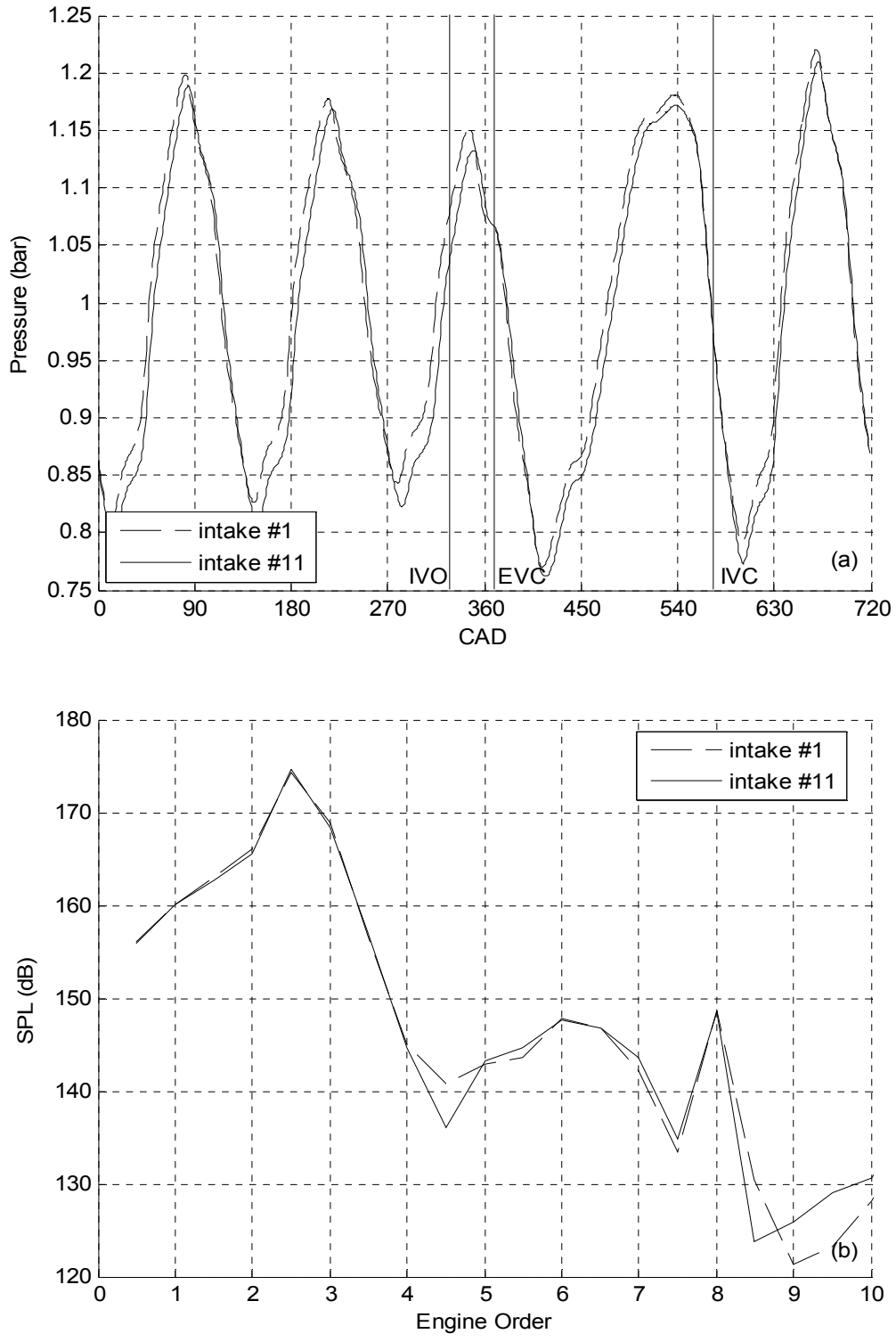

Figure 3.31: Experimental Intake Pressure at i2 at 3000 RPM for Intakes #1 and 11 in the (a) Time Domain and (b) Frequency Domain.

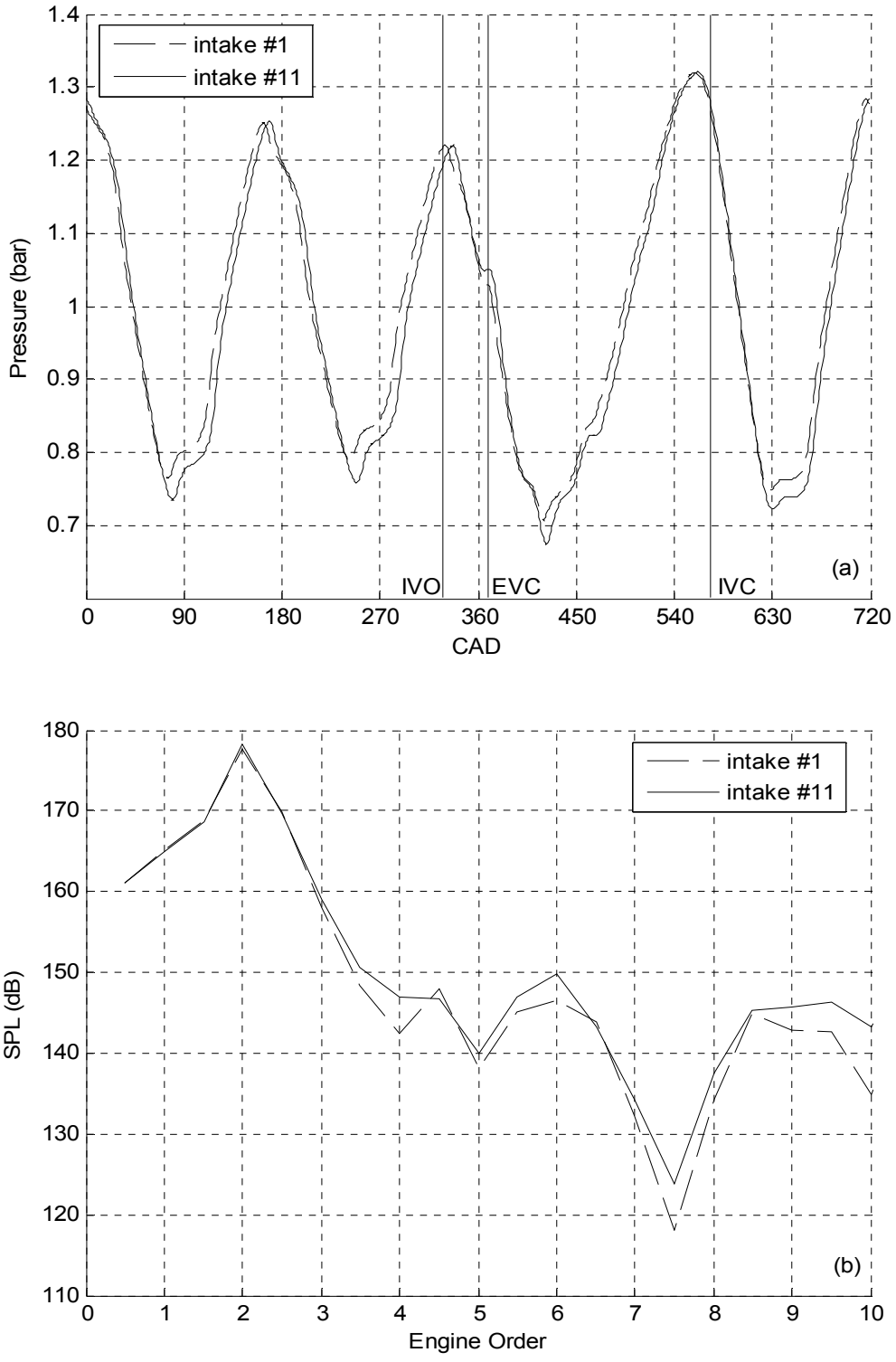

Figure 3.32: Experimental Intake Pressure at i2 at 3750 RPM for Intakes #1 and 11 in the (a) Time Domain and (b) Frequency Domain.

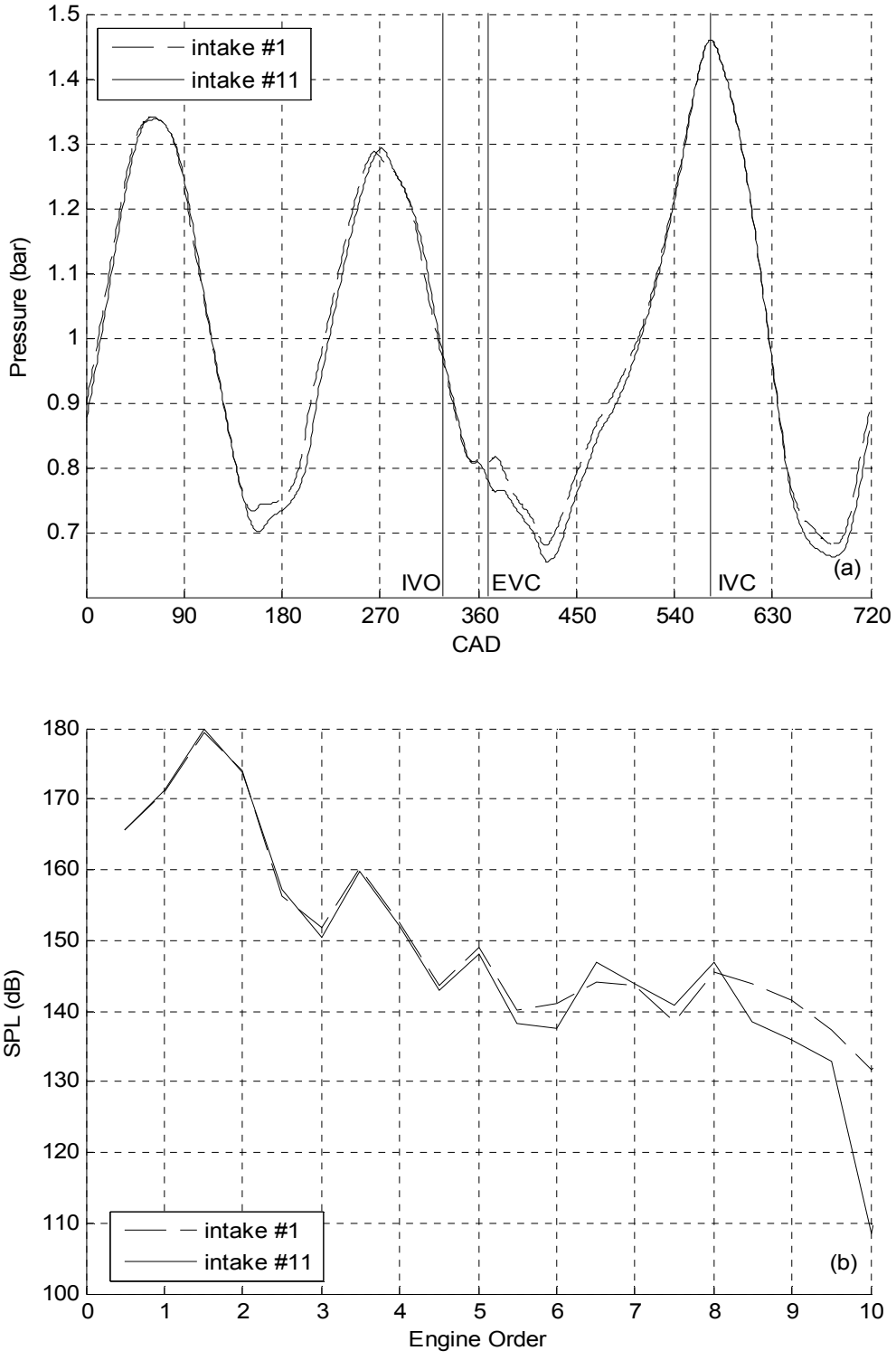

Figure 3.33: Experimental Intake Pressure at i2 at 4750 RPM for Intakes #1 and 11 in the (a) Time Domain and (b) Frequency Domain.

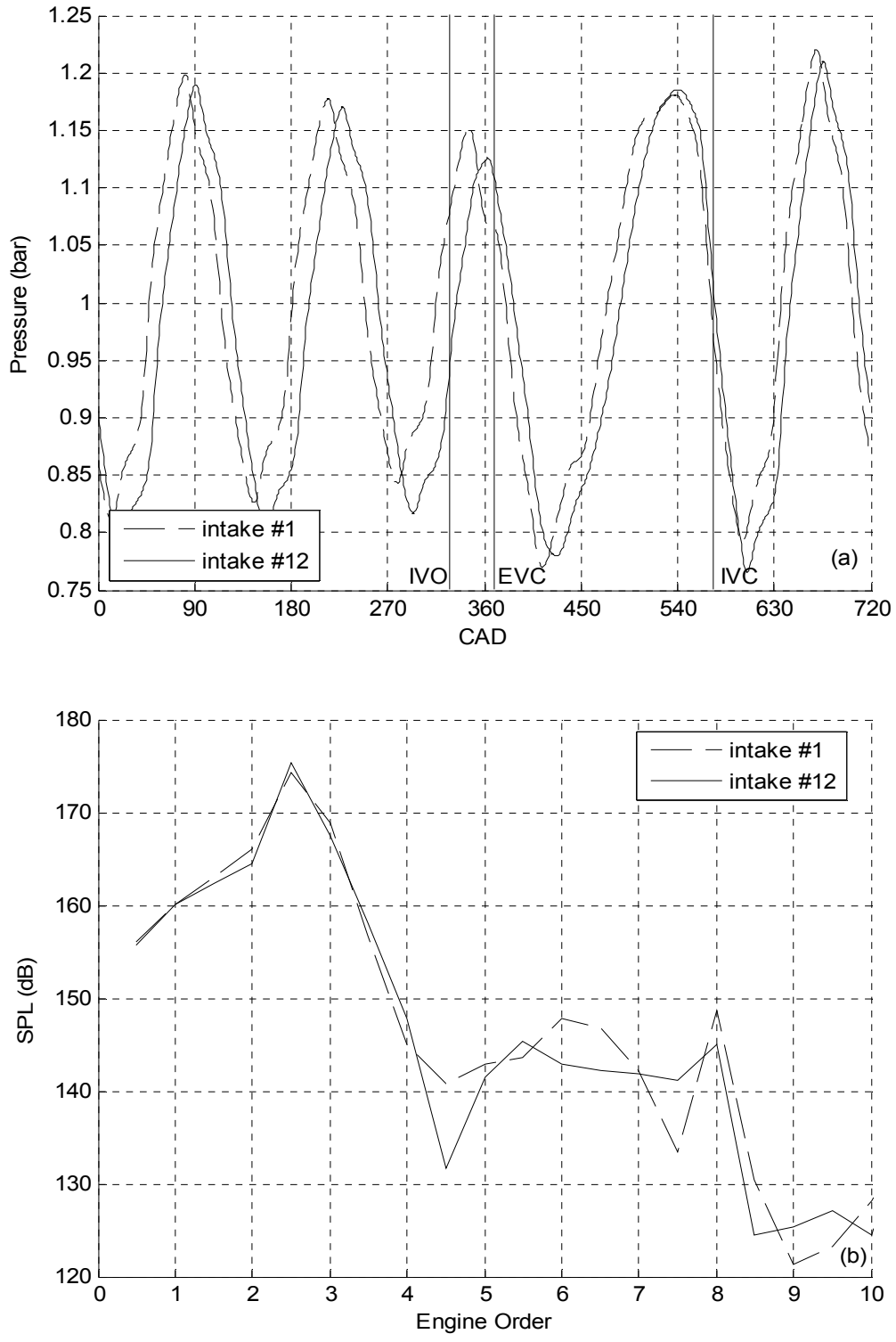

Figure 3.34: Experimental Intake Pressure at i2 at 3000 RPM for Intakes #1 and 12 in the (a) Time Domain and (b) Frequency Domain.

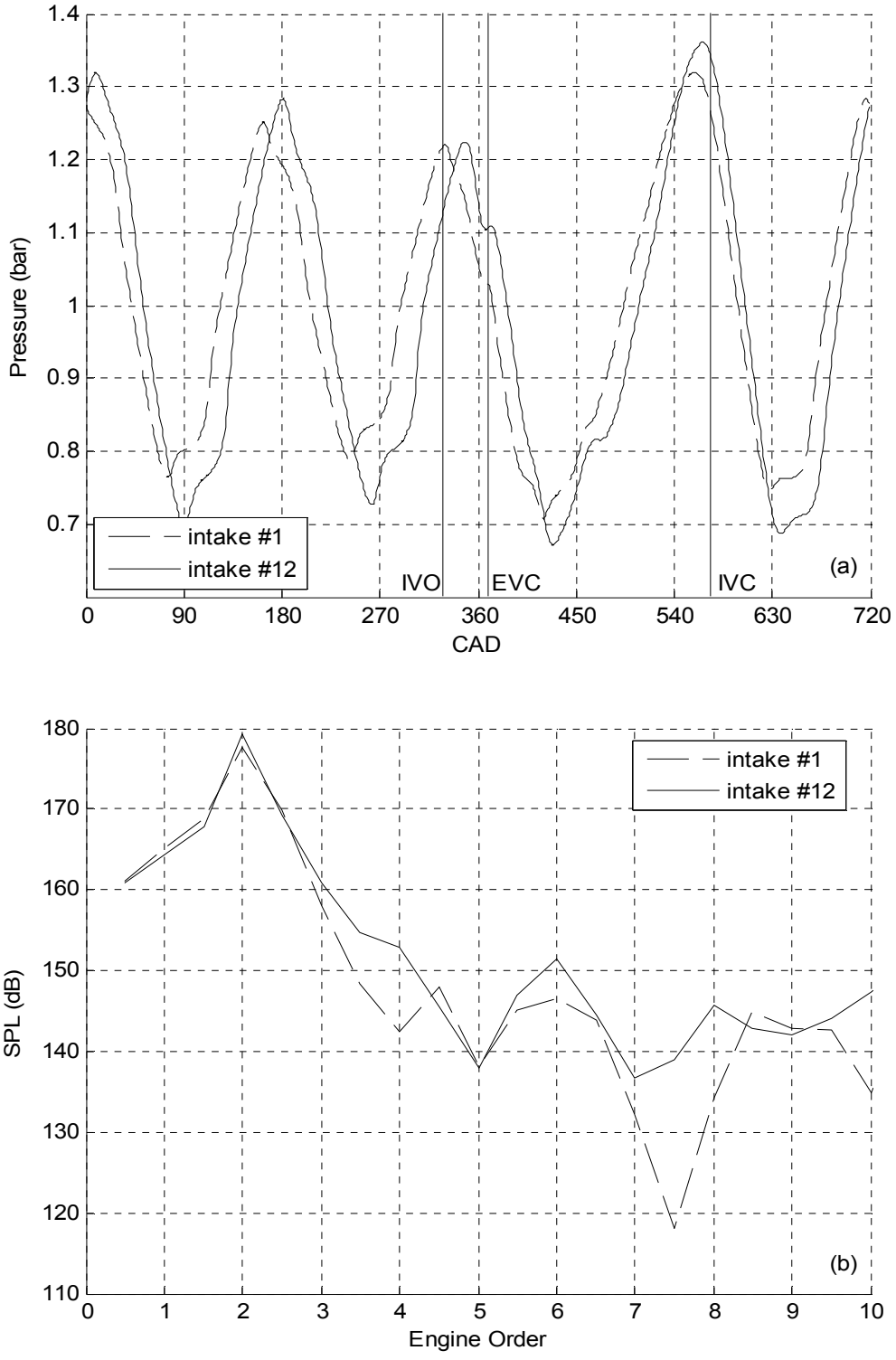

Figure 3.35: Experimental Intake Pressure at i2 at 3750 RPM for Intakes #1 and 12 in the (a) Time Domain and (b) Frequency Domain.

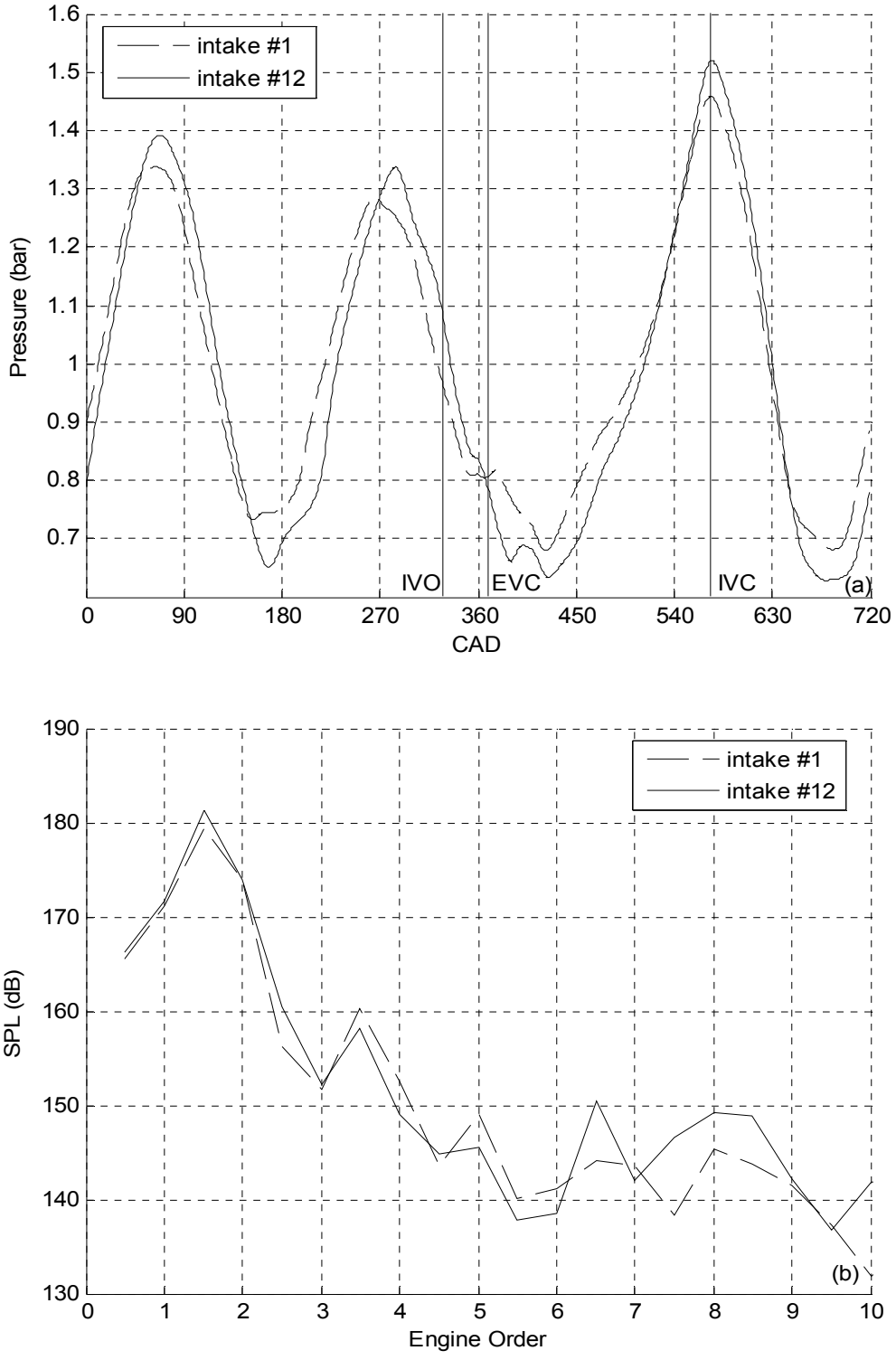

Figure 3.36: Experimental Intake Pressure at i2 at 4750 RPM for Intakes #1 and 12 in the (a) Time Domain and (b) Frequency Domain.

should be similar; Fig. 3.24 shows they are within 1%. The dominant frequency of the QSW, again determined by measuring the time between peaks, is noticeably lower for intake #12 than it is for the baseline, by approximately 5 Hz, indicating that the effective length of intake #12 is longer than that of the baseline, despite both intakes having the same length to the bellmouth; the phase lag from intake #1 to intake #12 is also considerably larger (5 to 15 CAD) than for intake #11. This suggests that, generally, a longer end correction is needed as R_i/D increases; this trend is explored further in Chapter 4. The frequency spectrum for intake #12 at this speed is within 1.5 dB of intake #1 for orders 0.5 to 3.5, with some differences at less significant, higher orders. At 3750 RPM, the peak pressure is higher for intake #12 than for intake #1, but it occurs 7 CAD later for intake #12 (and only 10 CAD before IVC), which appears to reduce its effect on intake tuning, as volumetric efficiency for intake #12 is 5% lower than intake #1 at this speed. A phase lag similar to that of 3000 RPM between the two intakes is observed at this speed as well. At this speed, the SPL of these two intakes are within 1 dB from orders 0.5 to 2.5. At 4750 RPM, the peak pressure is higher for intake #12 than for intake #1, but both peaks occur at IVC while it takes about 20 CAD at this speed to travel from i2 to the back of the valves, and pressures are similar from 520 to 560 CAD. At this speed, volumetric efficiencies for these two intakes are within 1.2%.

3.4 Bend Group

Three intakes of varying radii of curvature, R_c, were tested against the baseline using the experimental setup described in Chapter 2. The bend group was comprised of intakes #13 - 15, and is shown schematically in Fig. 2.5d. The effect of R_c on the

volumetric efficiency and brake power of the engine is discussed next in Section 3.4.1. Section 3.4.2 contains comparisons of the intake pressures at i2 for three bends and the baseline.

3.4.1 Volumetric Efficiency and Brake Power

Figure 3.37a shows the volumetric efficiency of the intake with the largest radius of curvature ($R_c/D = 2.0$), intake #13, compared to the baseline case. Since the length and cross-sectional area of both intakes are the same, there is no noticeable shift of the peak locations. Due to increased flow losses compared to the straight case, the bend has a slight negative impact on the volumetric efficiency magnitude of the tuning peaks, reducing by 3.3%, 1.7%, and 2.1% at 3000, 3750, and 4750 RPM, respectively. The corrected brake power for intakes #1 and 13 are shown in Fig. 3.37b. The power curves for both intakes are similar from 1000 to 4750 RPM, and intake #13 actually seems to make slightly more power from 5000 to 5500 RPM than the baseline despite similar volumetric efficiencies at those speeds. This may possibly be due to secondary swirling flows developed in the bends (Miller, 1990). These secondary flows may help with in-cylinder mixing and charge motion, thus speeding up the combustion process resulting in higher in-cylinder pressures (confirmed by c1 measurements), hence leading to higher power output when compared to a straight pipe.

Figure 3.38a compares the volumetric efficiency of the $R_c/D = 1.5$ bend, intake #14, with baseline. Again, there are no noticeable shifts in tuning peak locations. Volumetric efficiencies for intakes #13 and 14 are within 1% from 2500 to 5500 RPM. The steady flow loss coefficients at Reynolds numbers typical of engine operation for the

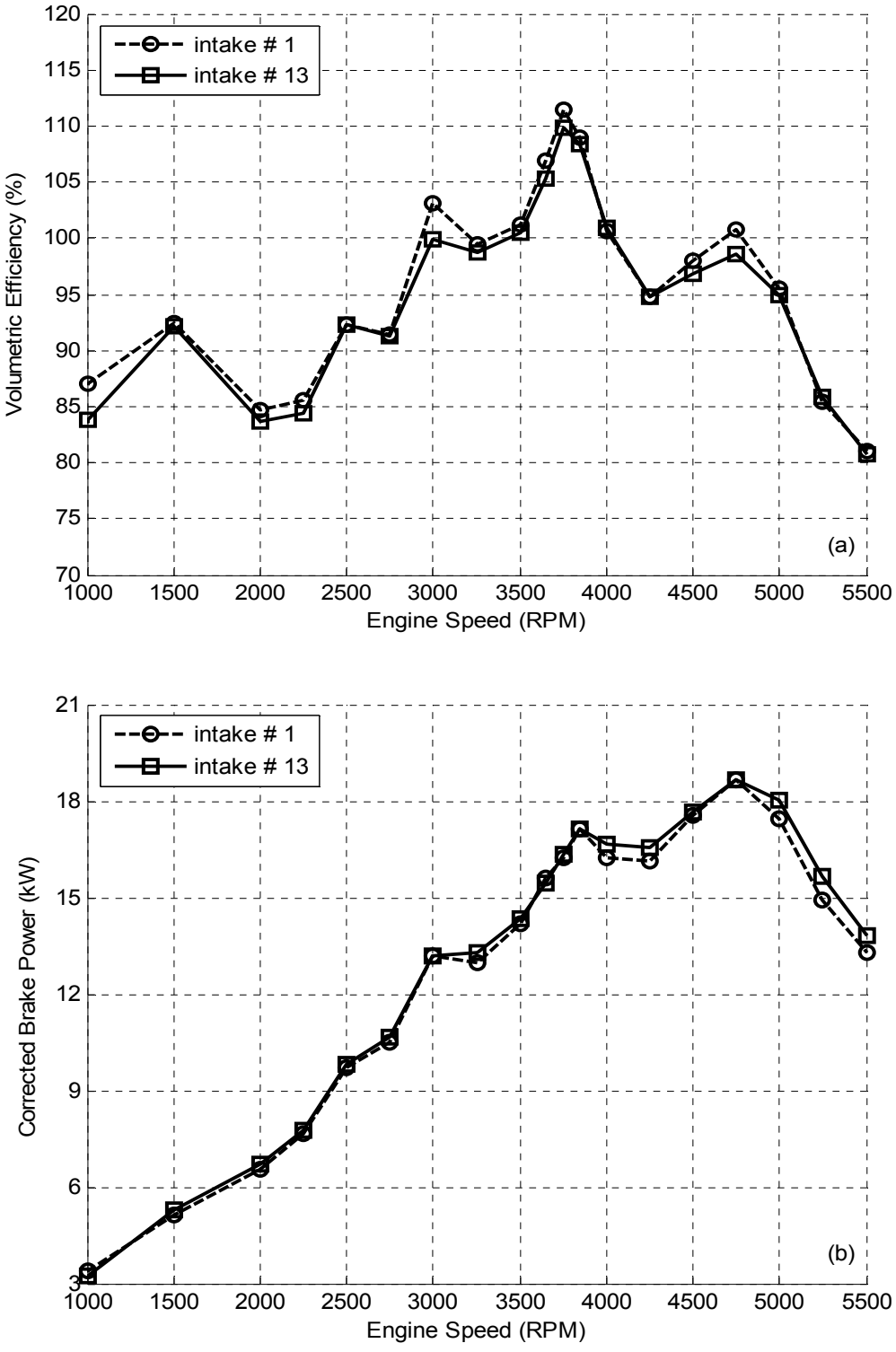

Figure 3.37: Experimental (a) Volumetric Efficiency and (b) Brake Power for Intake #1 and Intake #13.

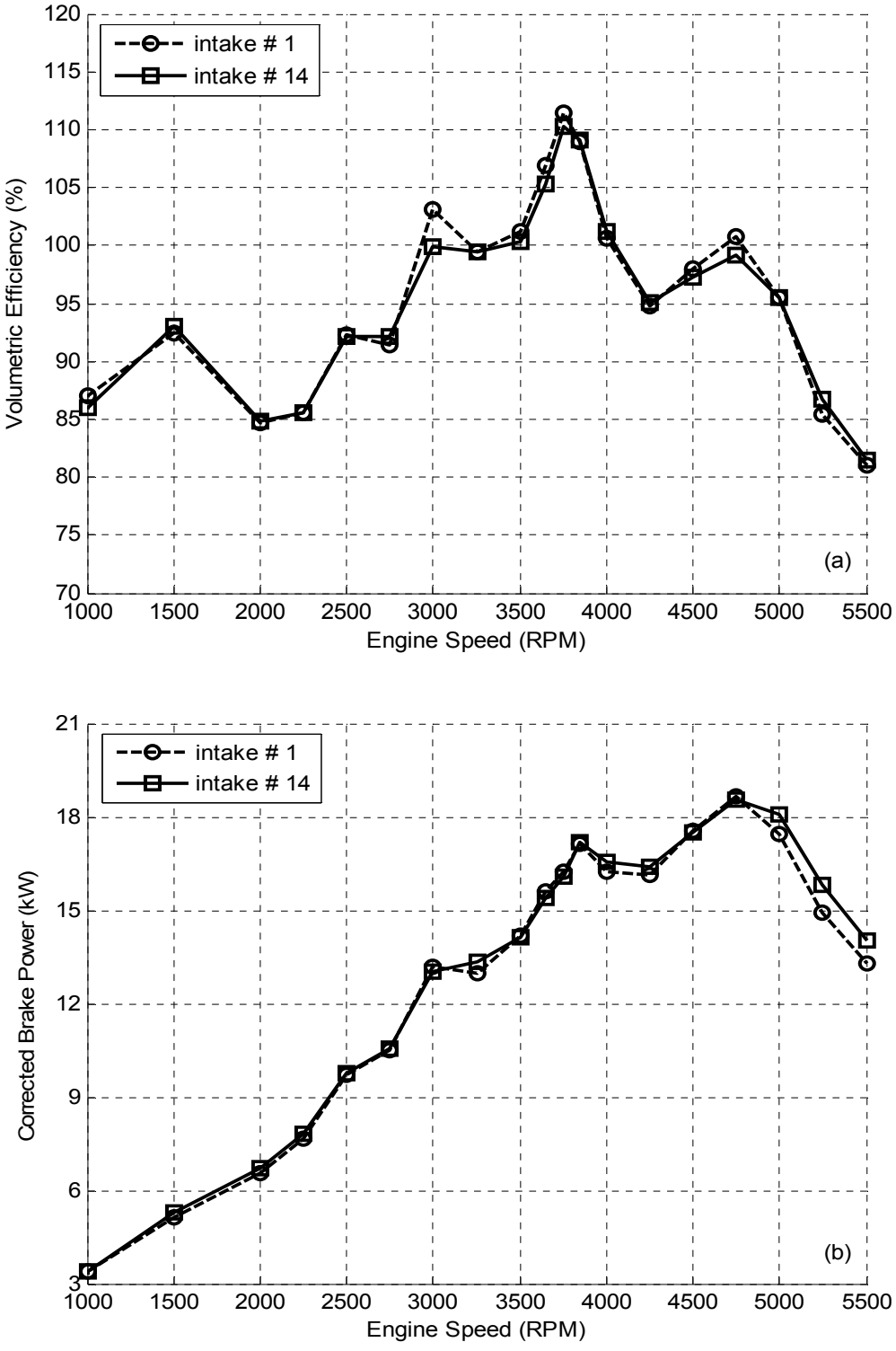

Figure 3.38: Experimental (a) Volumetric Efficiency and (b) Brake Power for Intake #1 and Intake #14.

bends of intakes #13 and 14 are around 0.215 and 0.239, respectively (Ito, 1960), a difference of 10.0%. However, using quasi-1D engine simulation code as a guide with the above loss coefficients entered into the bend region, the volumetric efficiencies for intakes #13 and 14 are predicted to be within 1%. The brake power for intakes #1 and 14 are compared in Fig. 3.38b. Since intakes #13 and 14 have similar volumetric efficiencies, it follows that they have similar powers. As observed with intake #13, intake #14 shows a slight increase in power at high speeds when compared to the straight intake #1.

The volumetric efficiency of intake #15, the tightest bend ($R_c/D = 1.0$), is compared to intake #1 in Fig. 3.39a. For intake #15, the tuning peaks at 3000, 3750, and 4750 RPM have decreased by 4.3%, 4.1%, and 3.6%, respectively, which is larger than the reduction observed with intakes #13 and 14. This is due to the increase in flow losses associated with the tighter bend of intake #15 compared to those of the baseline and the previous two larger-R_c bends. Figure 3.39b shows the corrected brake power of intakes #1 and 15. Unlike the previous two bends, the peak power of intake #15 suffers a reduction of 2.2% when compared to intake #1. However, there is still a gain in power from 5000 to 5500 RPM for this bend.

3.4.2 Intake Pressure

Figure 3.40 shows the pressure at i2 for the three bends (intakes #13, 14, and 15) and the baseline at 3000 RPM in both the (a) time domain and (b) frequency domain. The reflected compression wave peaks near IVC have reduced by about 2.9% for all bends when compared to the baseline. Also, the peak pressures during valve

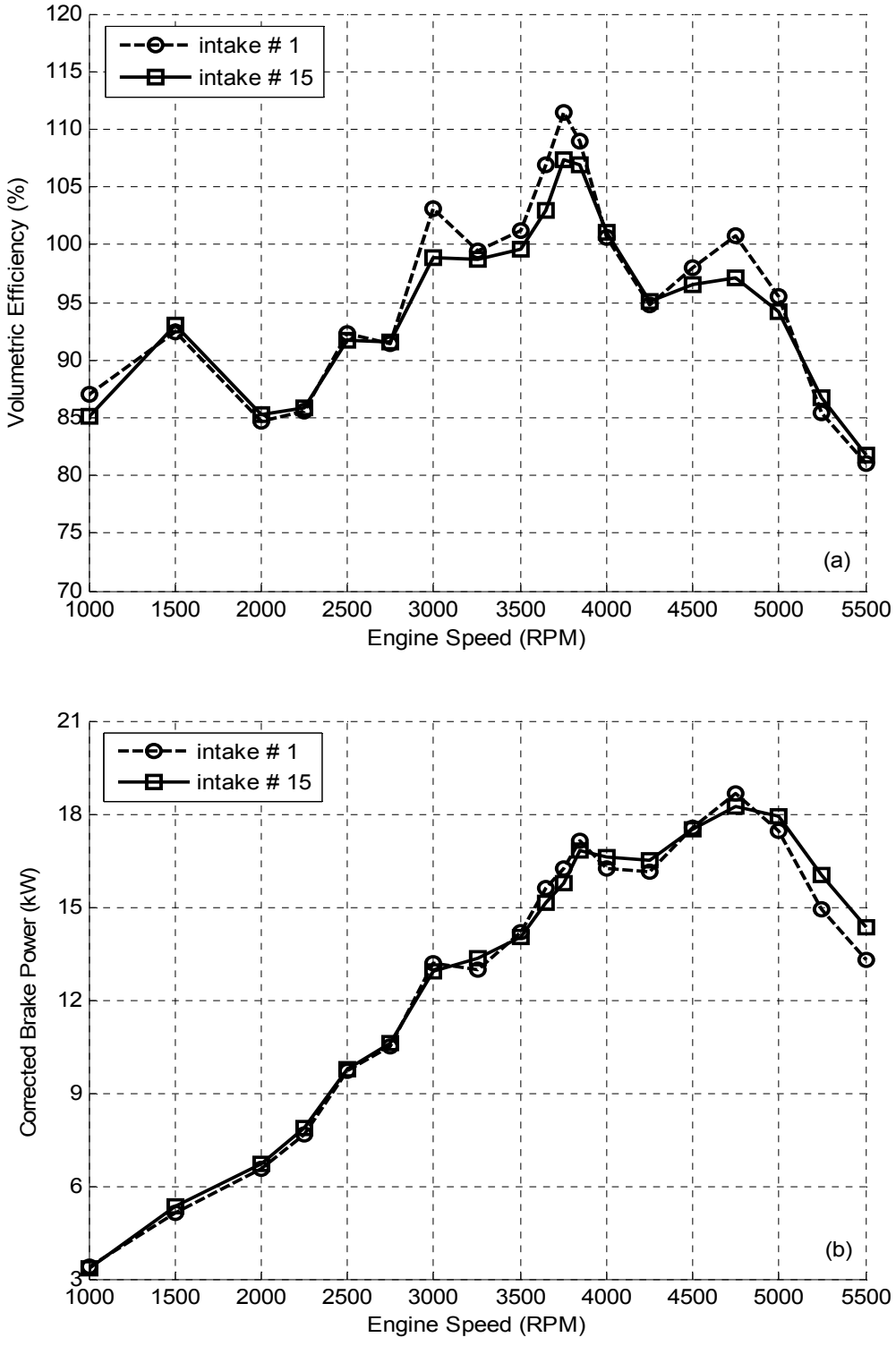

Figure 3.39: Experimental (a) Volumetric Efficiency and (b) Brake Power for Intake #1 and Intake #15.

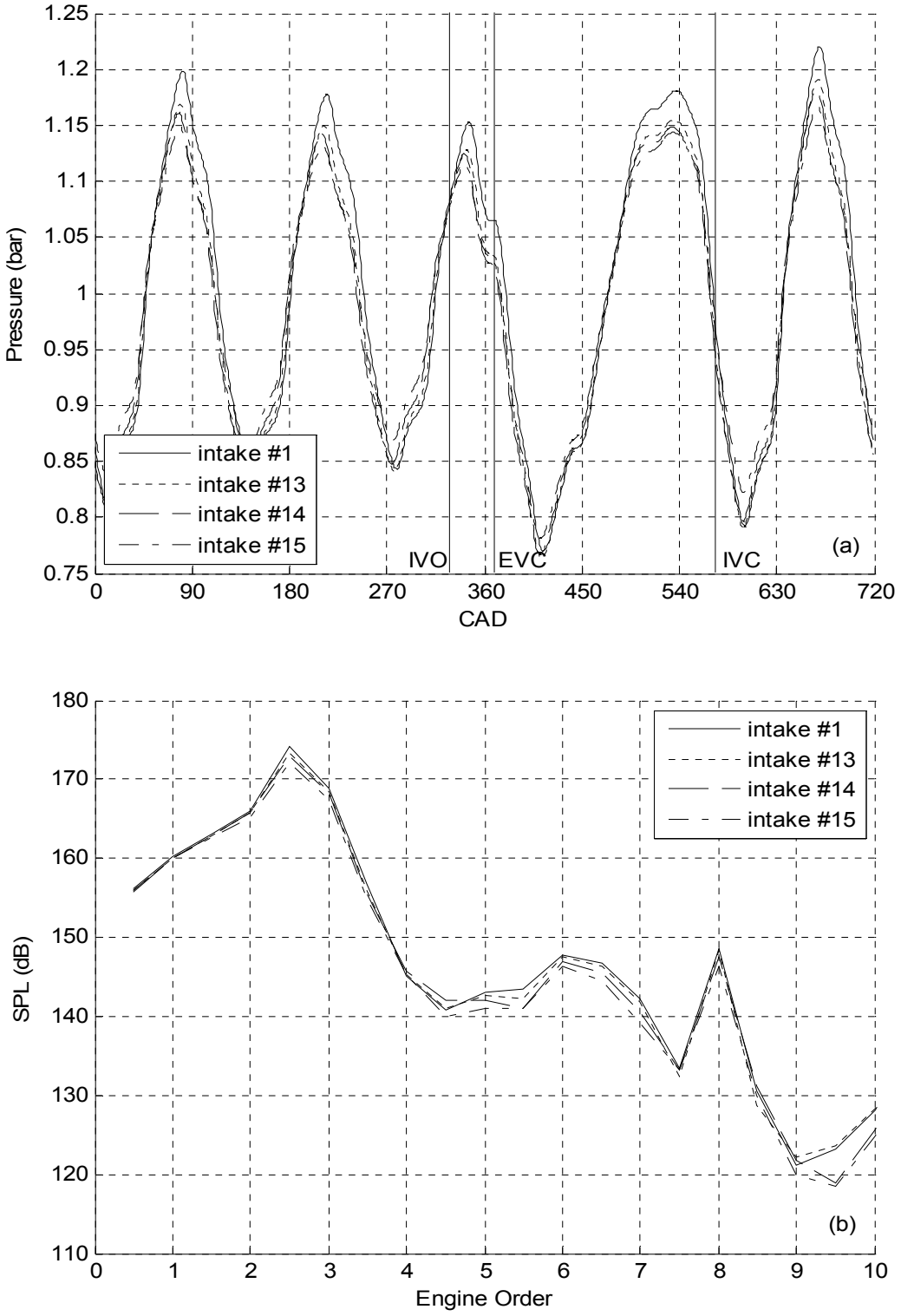

Figure 3.40: Experimental Pressure at i2 at 3000 RPM for the baseline and bend group in the (a) time domain and (b) frequency domain.

overlap have reduced by about 3.4% for all bends compared to baseline. Since the positive tuning effects both during valve overlap and near IVC have weakened similarly for all bends, it follows that the volumetric efficiencies for the bends at 3000 RPM should be similar to each other and lower than that of the baseline, as observed in Figs. 3.37-3.39. At this speed, the SPL of all the bends are within 2.6 dB of the baseline from orders 0.5 to 9.

Figure 3.41 shows intake pressure at i2 at 3750 RPM for all bends and the baseline. The peak pressures for intakes #13 and 14 are reduced by about 3.3% compared to the baseline, while that of the tightest-R_c bend, intake #15, is reduced by 4.9%. The pressure during the valve overlap period is also reduced by about 3.5% for intakes #13-15 compared to the baseline. This indicates that the volumetric efficiency for intakes #13 and 14 should be slightly lower than baseline and that of intake #15 should be slightly lower than intakes #13 and 14 at 3750 RPM. The volumetric efficiencies for intakes #13 and 14 are indeed similar and slightly less than that of the baseline, while that of intake #15 is about 4.5% less than that of the baseline (recall Fig. 3.39). The SPL for all bends are within 2.6 dB of the baseline from orders 0.5 to 5, but the spread increases to 5.5 dB from orders 5 to 10, with the largest deviations exhibited by intake #15. The spread at this speed is generally larger than that at 3000 RPM, which was within 2.6 dB from orders 0.5 to 9.

Figure 3.42 shows intake pressure at i2 for all bends compared to the baseline at 4750 RPM. The peak pressure for intakes #13 and 14 are similar and about 3.1% lower than that of the baseline. Intake #15 has a lower peak pressure than the other two bends, decreasing 5.1% from the baseline. The intake pressures during the valve overlap period

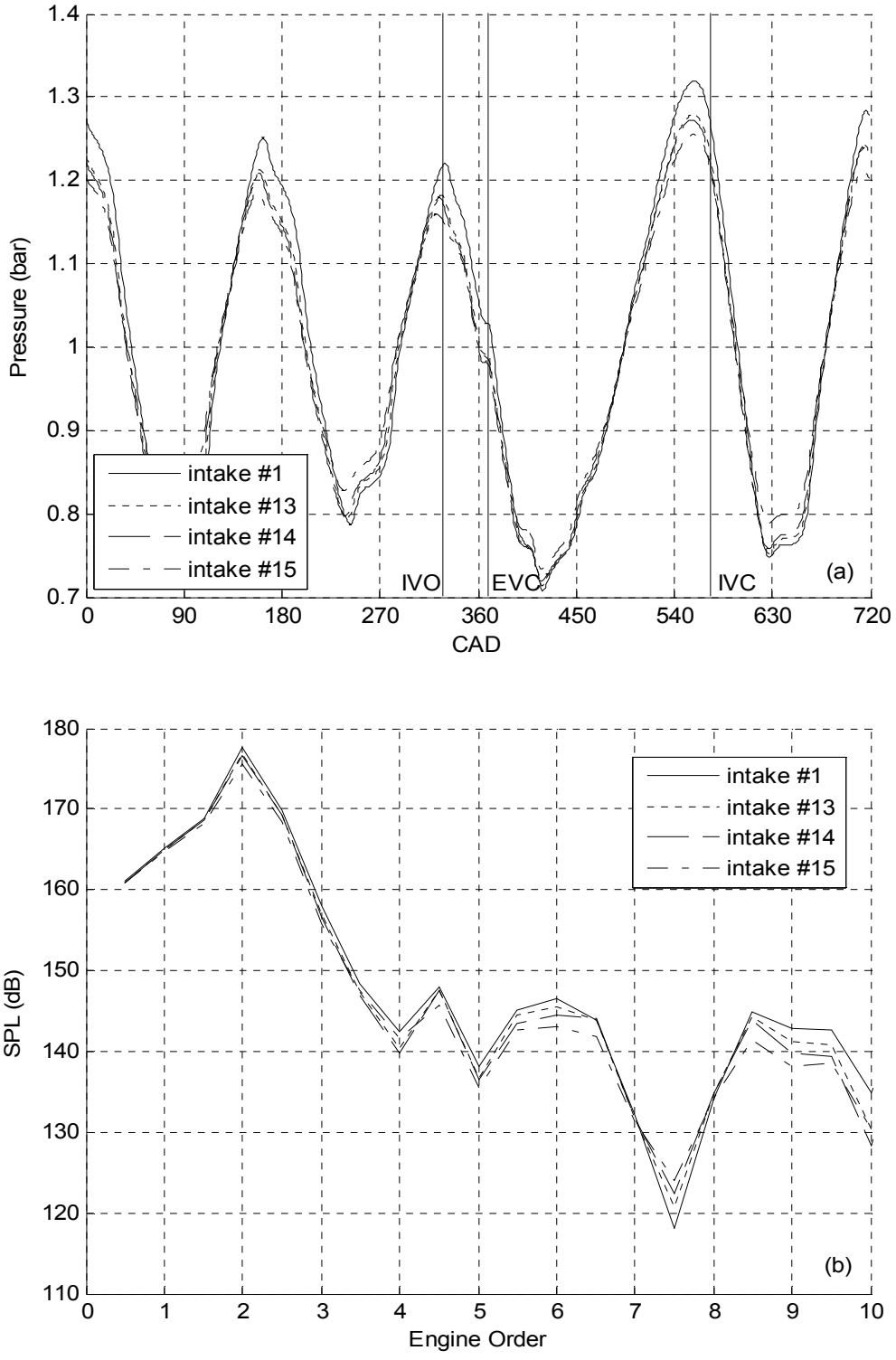

Figure 3.41: Experimental Pressure at i2 at 3750 RPM for the baseline and bend group in the (a) time domain and (b) frequency domain.

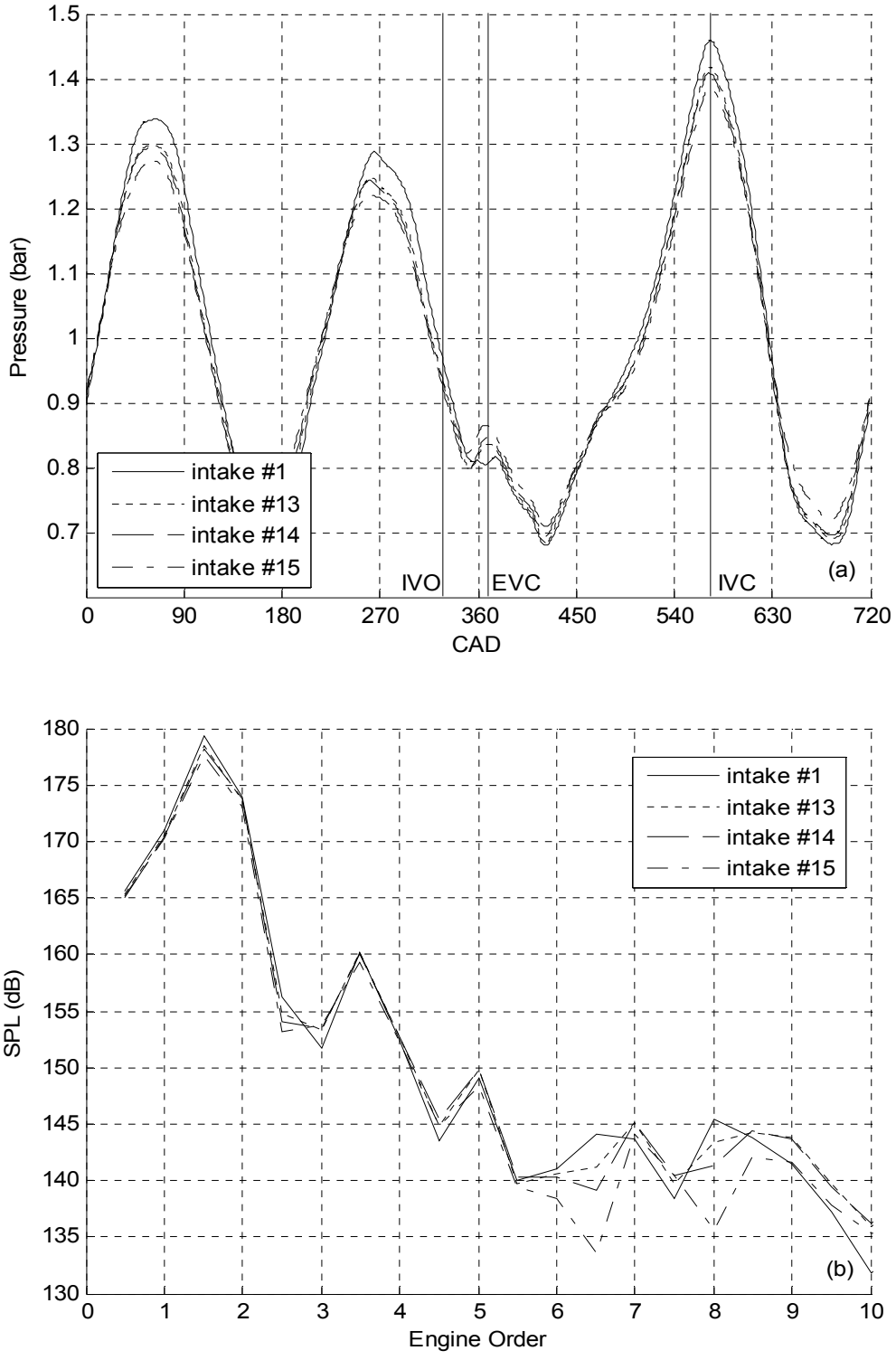

Figure 3.42: Experimental Pressure at i2 at 4750 RPM for the baseline and bend group in the (a) time domain and (b) frequency domain.

are similar for all bends and the baseline. At this speed, the volumetric efficiency follows a trend similar to that of peak pressure; intakes #13 and 14 have similar volumetric efficiencies which are about 2% lower than the baseline (Figs. 3.37 and 3.38), while intake #15 has a volumetric efficiency 3.6% lower than the baseline (Fig. 3.39). The SPL of all the bends are within 2.5 dB of the baseline from orders 0.5 to 5.5. Unlike the other two speeds, the frequency spectra after 5th order for each bend are different than the baseline, though at magnitudes 35 to 40 dB below peak SPL.

3.5 S-Bend Group

Three intakes of varying S-bend radii were tested against a baseline case using the experimental setup described in Chapter 2. The S-bend group was comprised of intakes #16 - 18, shown schematically in Fig. 2.5e. The effect of the S-bend radii on the volumetric efficiency and brake power of the engine is discussed next in Section 3.5.1. Section 3.5.2 contains comparisons of the intake pressure at i2 for the three S-bends and the baseline case.

3.5.1 Volumetric Efficiency and Brake Power

Figure 3.43a compares the volumetric efficiency of $R_c/D = 2.0$ S-bend, intake #16, and the baseline. Intake #16 seems to have little negative effect on volumetric efficiency compared to a straight pipe. Only the peak at 3000 RPM is reduced, by 2%, and the peak at 3750 RPM has decreased just slightly, but is within 1% of the baseline. Intake #16 actually seems to have a slightly enhancing effect on volumetric efficiency at high engine speeds (from 3850 to 4250 RPM and 5000 to 5500 RPM) when compared to

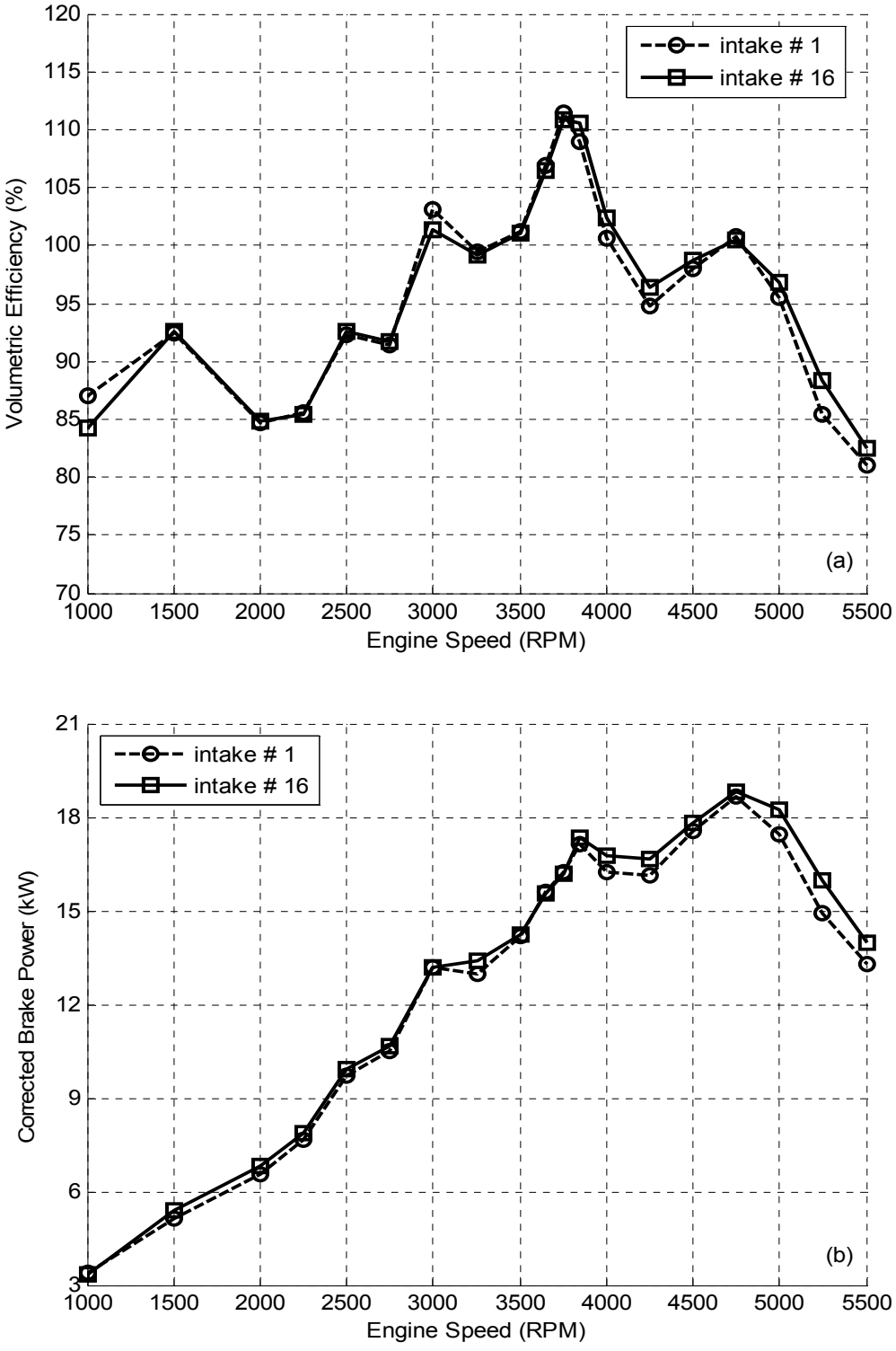

Figure 3.43: Experimental (a) Volumetric Efficiency and (b) Brake Power for Intake #1 and Intake #16.

the baseline. There are no noticeable shifts in tuning peak speeds from intake #1 to #16. The brake power comparison between intake #1 and 16 is shown in Fig. 3.43b. The differences in volumetric efficiency between these two intakes are manifested in the powers, including a slight increase in power for intake #16 from 4000 to 4500 RPM and from 5000 to 5500 RPM. The peak power for both intakes is similar.

The volumetric efficiency of the $R_c/D = 1.5$ S-bend, intake #17, is compared to baseline in Fig. 3.44a. For intake #17, the peaks at 3000, 3750, and 4750 RPM are reduced by 2.5%, 1.7%, and 1.4%, respectively. The overall shape of the volumetric efficiency for intake #17 remains similar to intake #1, as does the power, presented in Fig. 3.44b.

Figure 3.45a shows the volumetric efficiency of the tightest radius S-bend ($R_c/D = 1.0$), intake #18, and the baseline. The flow losses associated with this S-bend have a significant impact on volumetric efficiency; compared to the baseline, intake #18 shows a 5.1% reduction of the peak at 3000 RPM, effectively eliminating it as a tuning peak. The tuning peak at 3750 RPM has decreased by 3.1%, and the 4750 RPM peak by 2.6%. Again, no shifts in tuning peak speed are observed. Figure 3.45b shows the brake power for intakes #1 and 18. Intake #18 shows a slight reduction in peak power corresponding to the volumetric efficiency reduction of the tuning peak at 4750 RPM. There is a slight gain in power from 5250 to 5500 RPM, corresponding to the gain in volumetric efficiency for intake #18 across these speeds.

In general, the S-bend of a certain Rc used in this study (with bend angles of 67.5°) is equally or less detrimental to volumetric efficiency as the 135° single bend with

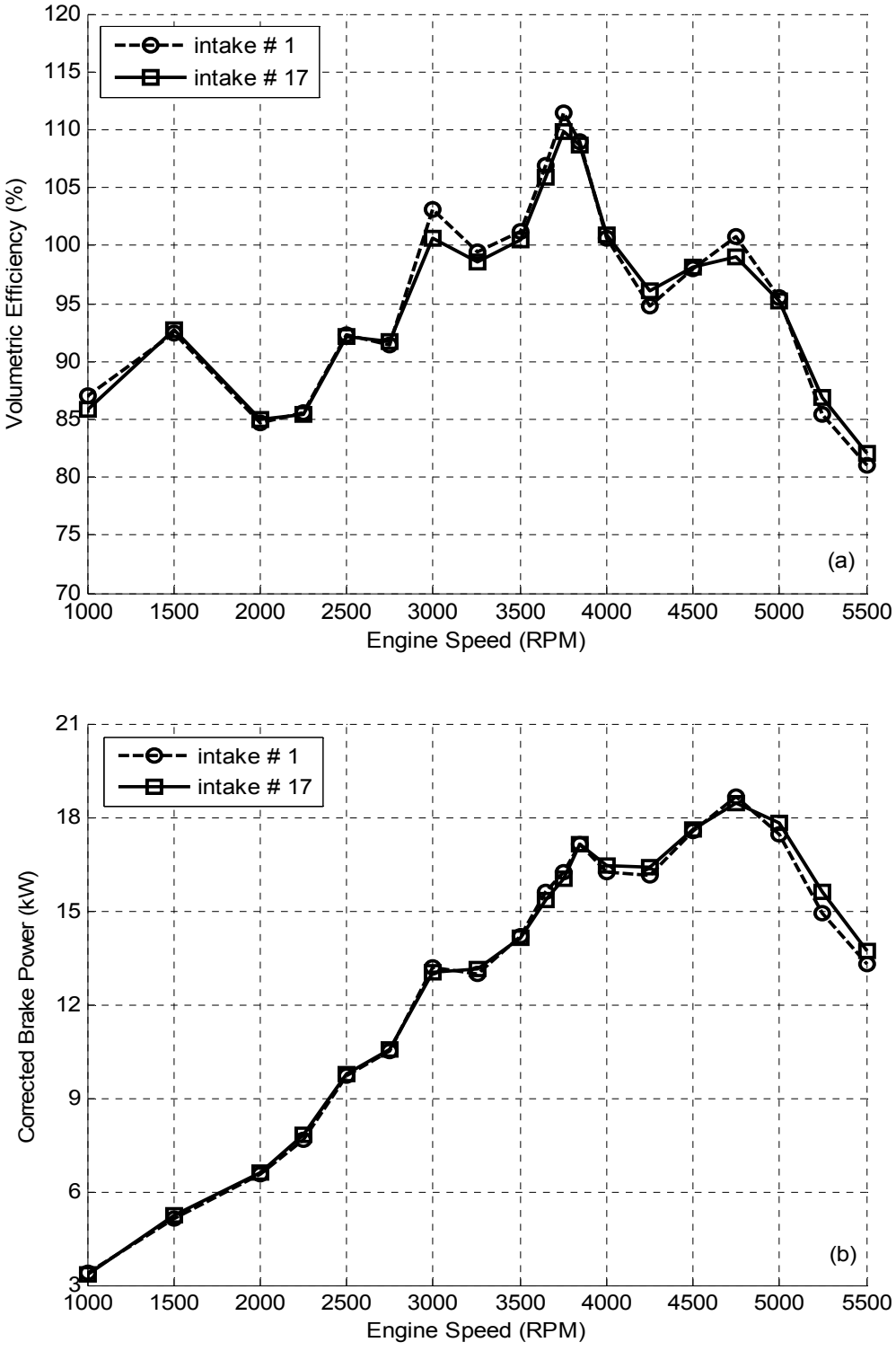

Figure 3.44: Experimental (a) Volumetric Efficiency and (b) Brake Power for Intake #1 and Intake #17.

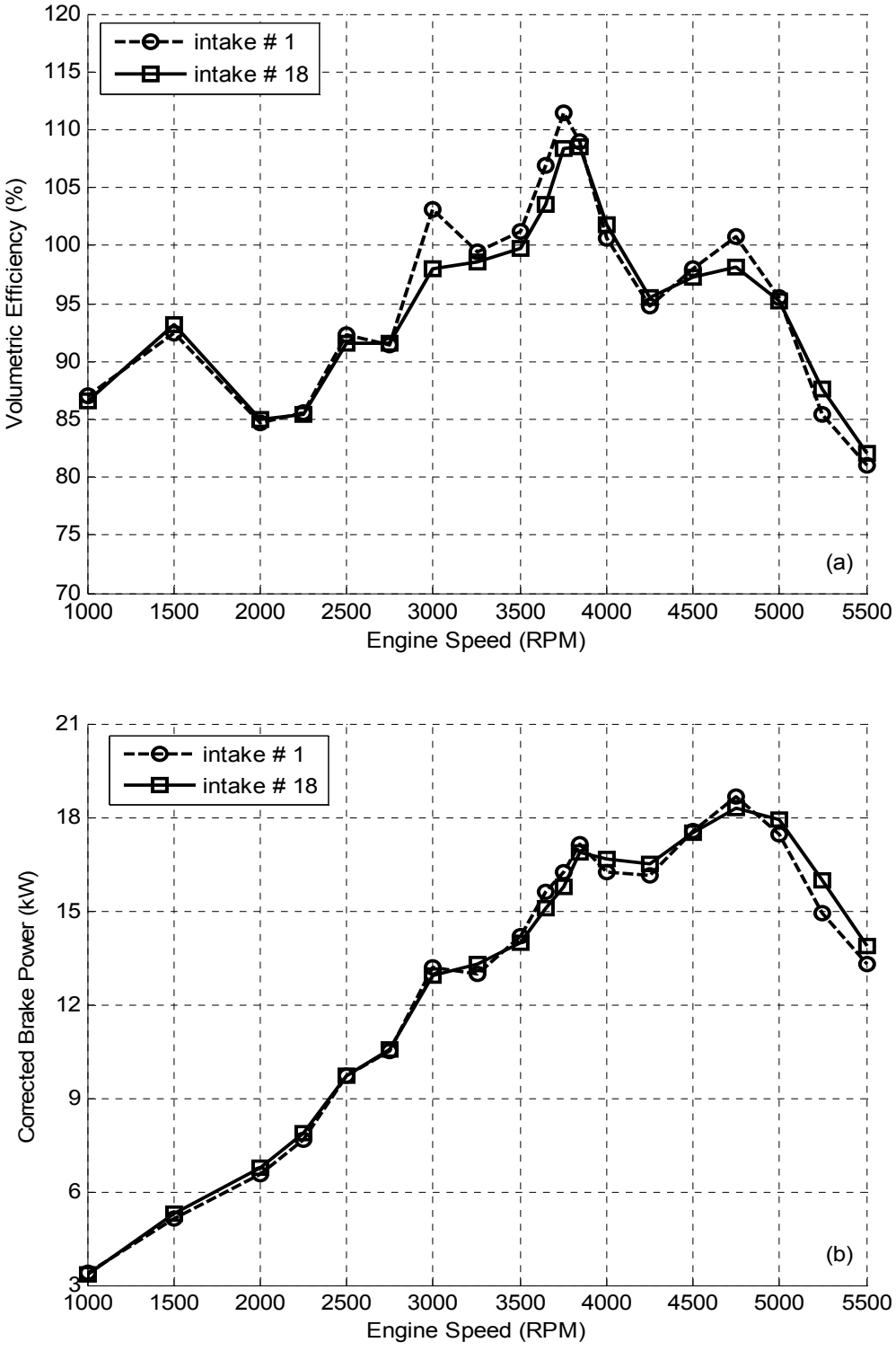

Figure 3.45: Experimental (a) Volumetric Efficiency and (b) Brake Power for Intake #1 and Intake #18.

the same R_c; this is shown in Fig. 3.46. An equation for the bend-bend interaction loss coefficient is (Miller, 1990)

$$K_{b-b} = (K_{b1} + K_{b2}) * C_{b-b}, \tag{3.4}$$

where K_{b-b} is the bend-bend loss coefficient, K_{b1} and K_{b2} are the loss coefficients of the two individual bends that comprise the S-bend, and C_{b-b} is the interaction correction factor. C_{b-b} for the exact geometry used in this study, 67.5° bends without spacers, could not be found. For S-bends comprised of two 45° bends, $C_{b-b} = 0.64$; for S-bends comprised of 90° bends without a spacer, $C_{b-b} = 1.0$. Experimental data from this study suggests that C_{b-b} for these S-bends is around 0.64. Using the $R_c/D = 1.0$ bend (intake #15) and S-bend (intake #18) as examples, the loss coefficient for the single 135° bend is approximately 0.31 (Ito, 1960) at Reynolds numbers typical of the intake breathing process for higher engine speeds. For the S-bend, which is made of two 67.5° bends, $K_{b1} = K_{b2} = 0.21$, which yields $K_{b-b} = 0.27$ using Eq. (3.4) with $C_{b-b} = 0.64$. The reduction in loss factor for the $R_c/D = 1.0$ S-bend when $C_{b-b} = 0.64$, which would result in similar or slightly higher volumetric efficiency for the S-bend compared to the single bend (as confirmed by quasi-1D simulation), suggests that C_{b-b} for the S-bends in this study is around 0.64. The loss factors for the $R_c/D = 1.5$ S-bend reduces to 0.21 from 0.24 for the single bend, and that of the $R_c/D = 2.0$ S-bend reduces to 0.19 from 0.22 for the single bend when $C_{b-b} = 0.64$.

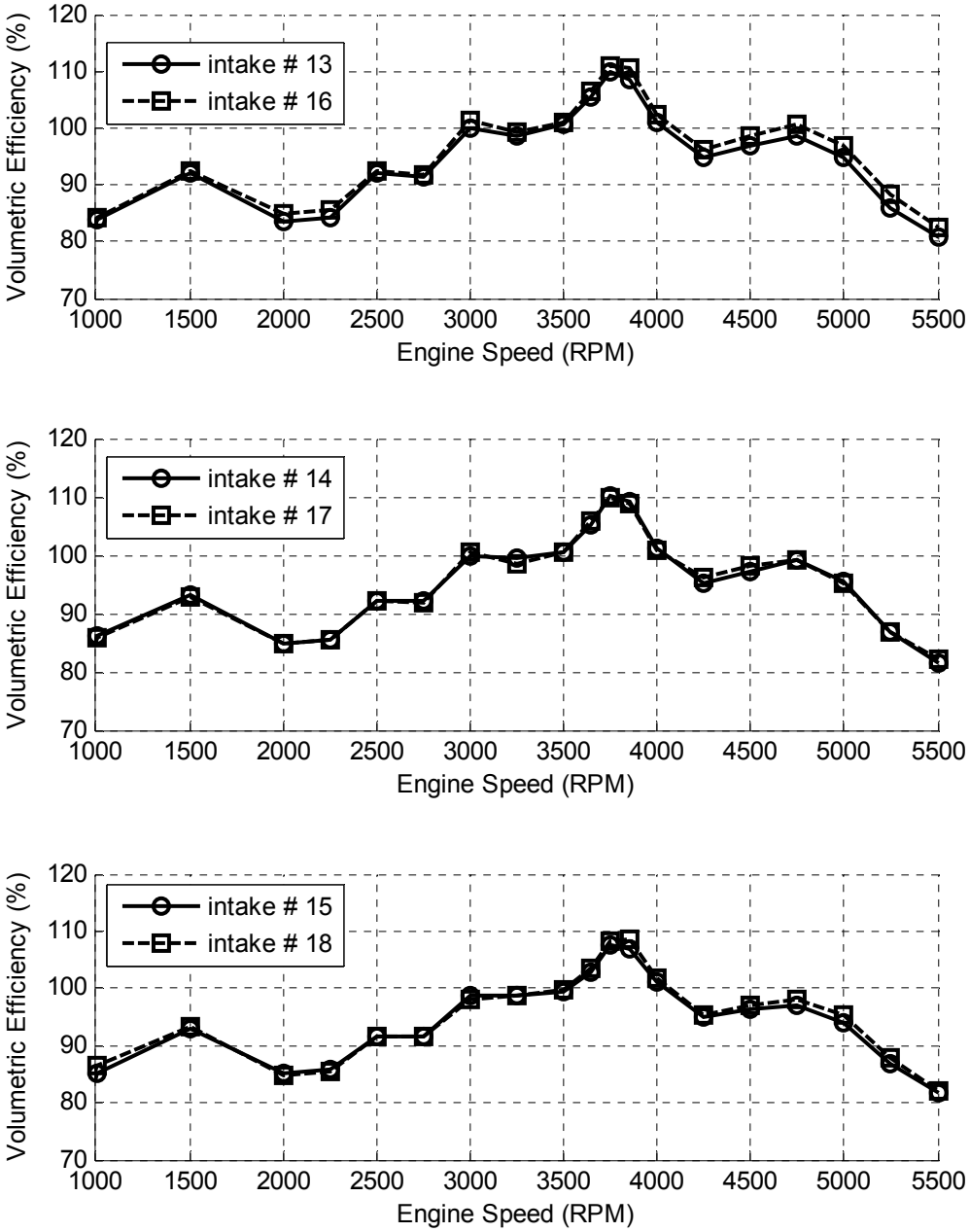

Figure 3.46: Comparison of the Effects on Volumetric Efficiency of Same-Rc Bend and S-bend Geometries Used in This Study.

3.5.2 Intake Pressures

Figure 3.47 shows the intake pressure at i2 at 3000 RPM for all of the S-bends compared to the baseline. The maximum amplitude of the compression wave near IVC is lower than that of the baseline for all S-bends; the amplitudes of intakes #16 and 17 are similar and about 2.0% lower than the baseline, while that of intake #18 is reduced by 3.5%. The peak of the compression wave during the valve overlap is similar for each S-bend and, on average, 2.0% lower than that of intake #1. Both these phenomena suggest that the supercharging effect at 3000 RPM has decreased for each S-bend compared to the baseline, with intakes #16 and 17 having similar volumetric efficiencies lower than that of intake #1 at this speed and intake #18 having the lowest volumetric efficiency, consistent with Figs. 3.43-3.45. The SPL of all S-bends are within 1.6 dB of the baseline from orders 0.5 to 4 and within 2.8 dB from order 4.5 to 9, with the larger deviations noted for intake #18, the tightest S-bend.

The pressure at i2 for each S-bend and the baseline at the main tuning peak speed of 3750 RPM are presented in Fig. 3.48. The peak pressure for each S-bend is lower than that of the baseline; intakes #16 and 17 have similar peak pressures which are 3.1% lower, while that of intake #18 is 5.5% lower. These peak pressure trends imply that the volumetric efficiencies at this speed for intakes #16 and 17 are similar and lower than that of the baseline, while that of intake #18 has decreased further. This is indeed the case as the volumetric efficiencies of intakes #16 and 17 are within 1% of each other and slightly lower than that of baseline (Figs. 3.43 and 3.44), while that of intake #18 is lower still (Fig. 3.45). The frequency spectrum for each S-bend is within 2 dB of the baseline

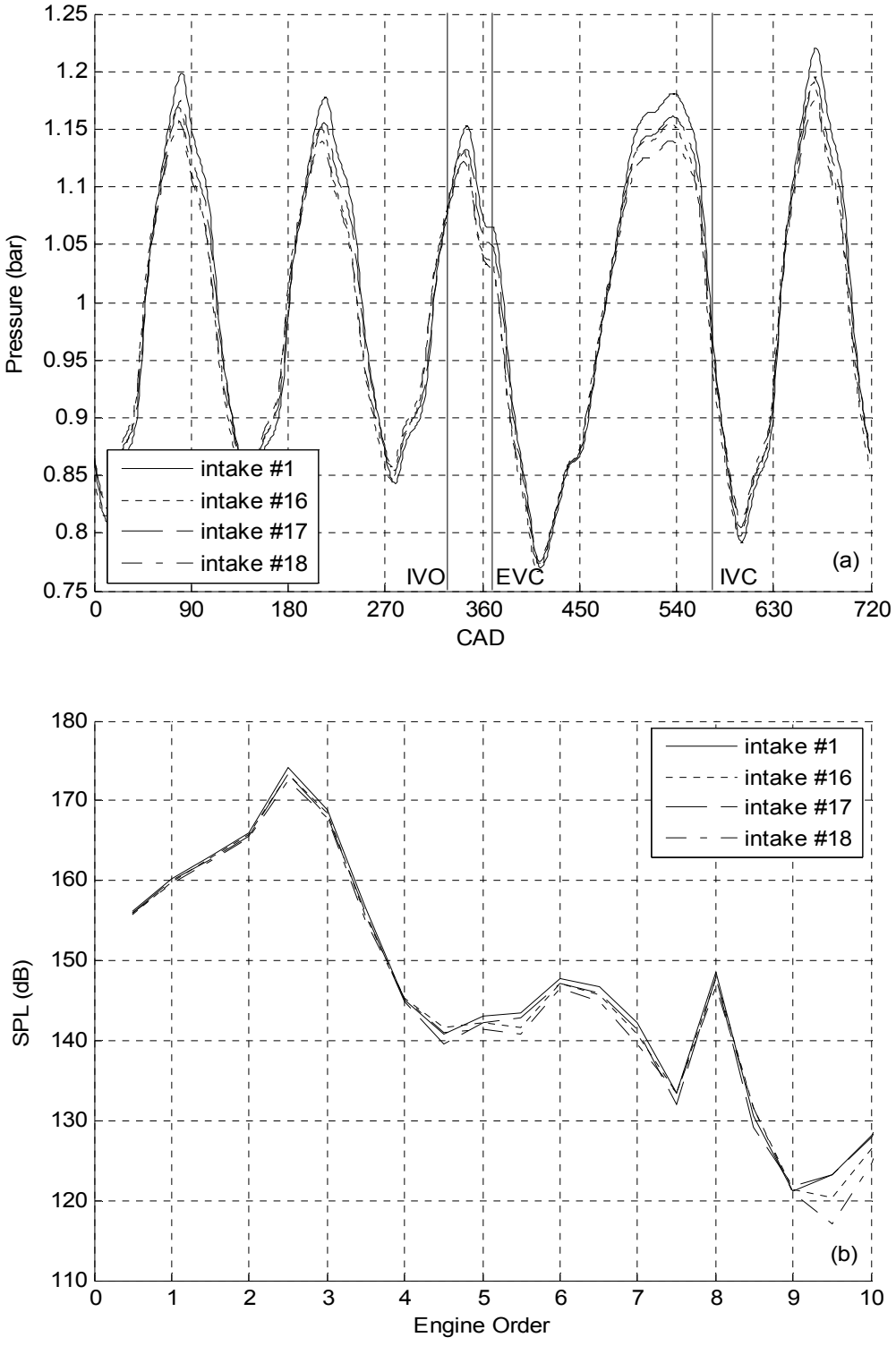

Figure 3.47: Experimental Pressure at i2 at 3000 RPM for the baseline and S-bend group in the (a) time domain and (b) frequency domain.

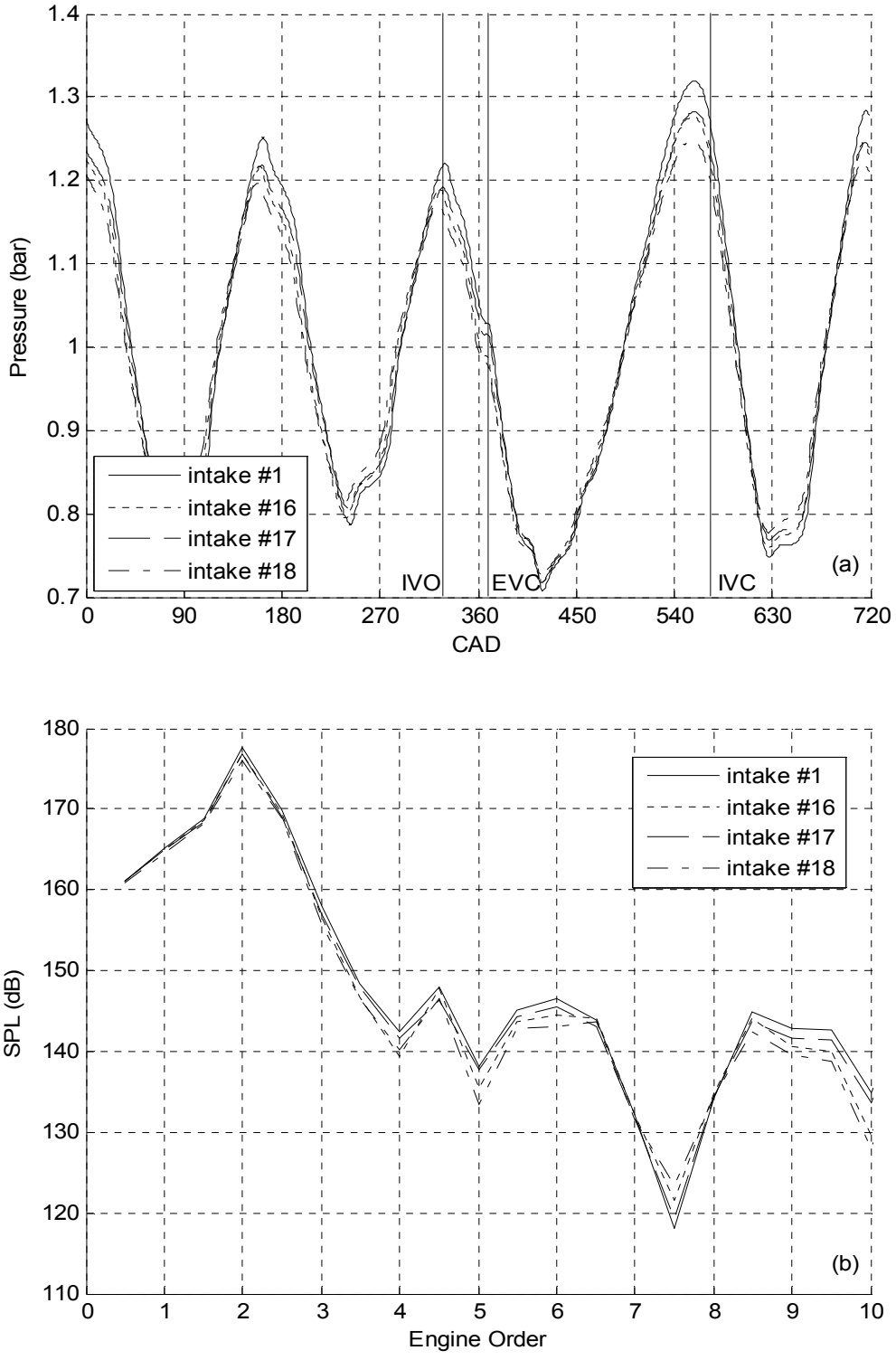

Figure 3.48: Experimental Pressure at i2 at 3750 RPM for the baseline and S-bend group in the (a) time domain and (b) frequency domain.

for the dominant engine orders, from 0.5 to 3.5; the spread increases to 5.5 dB from orders 4 to 8.5. The largest deviations from the baseline are noted for the tightest S-bend, intake #18.

Figure 3.49 shows the pressure at i2 at 4750 RPM for each S-bend and the baseline case. The peak pressure, occurring at IVC, is reduced by about 2.7% for intakes #16 and 17 compared to the baseline; that of intake #18 has reduced further, by 5.6%. The volumetric efficiencies for intakes #16 and 17 are within 1.5% of the baseline at 4750 RPM (Figs. 3.43 and 3.44), while the volumetric efficiency of intake #18 is 2.6% lower than the baseline (Fig. 3.45). The SPL of all S-bends are within 3 dB of the baseline from orders 0.5 to 6, after which the spread increases to a maximum of 7 dB for intake #18, though in the neighborhood of 140 dB as compared to peak SPL near 180 dB.

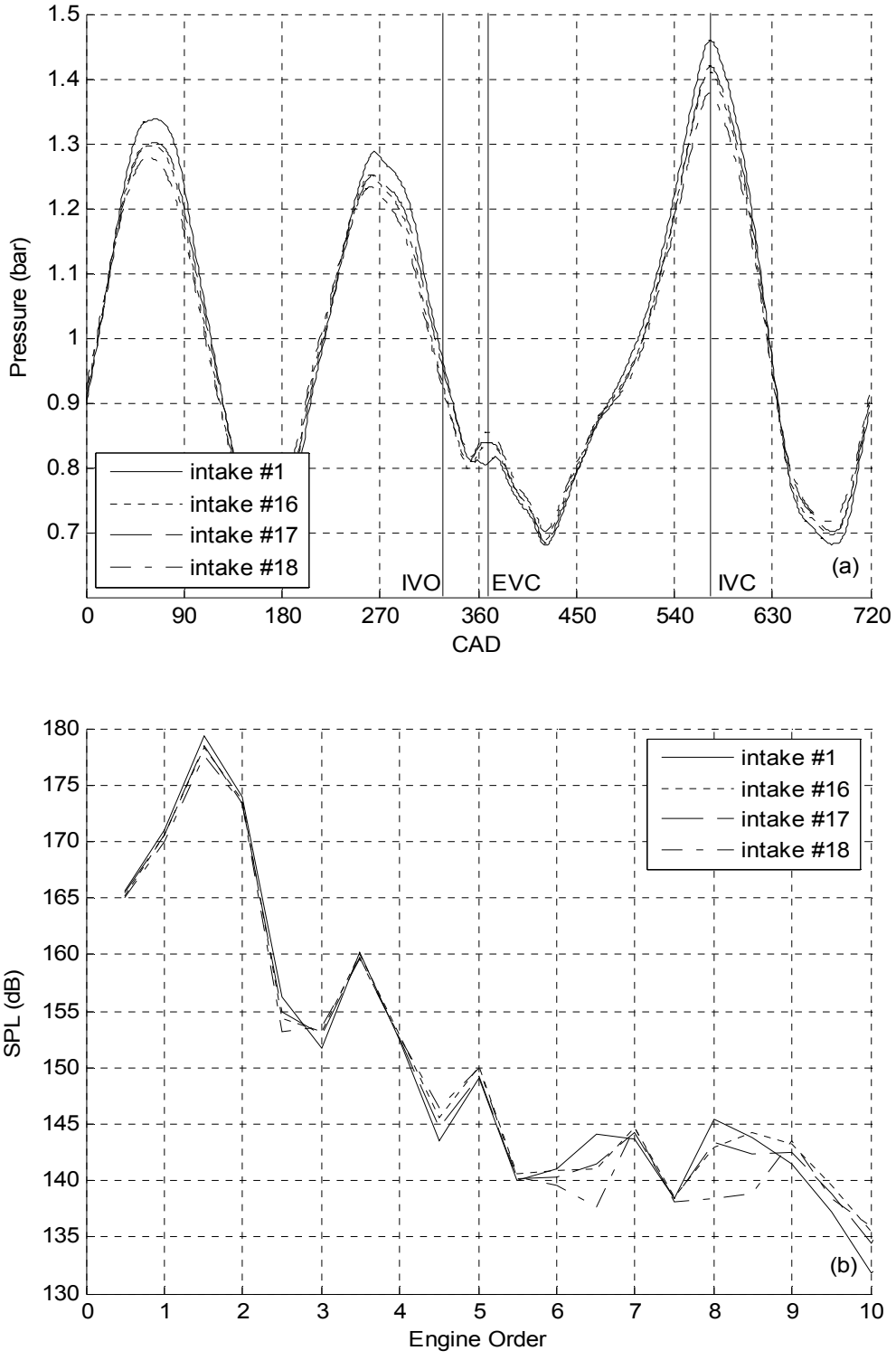

Figure 3.49: Experimental Pressure at i2 at 4750 RPM for the baseline and S-bend group in the (a) time domain and (b) frequency domain.

CHAPTER 4

COMPUTATIONAL PREDICTION METHODS

4.1 Introduction

In this study, four predictive methods for intake tuning peak locations were utilized. Three of these methods are simple, one-dimensional, linear acoustic models of the intake breathing phenomenon, and one is a complex, nonlinear, quasi-1D engine simulation code. This chapter describes these methods along with the assumptions involved. The three linear acoustic models are grouped together in Section 4.2. Section 4.3 gives some details of the quasi-1D simulation code used in this study, with its calibration to the baseline case elaborated in Section 4.3.1. The predictions of the quasi-1D simulation code for all intakes other than the baseline are presented later in Chapter 5.

4.2 One-Dimensional Linear Acoustic Models

The three linear acoustic models used for this study are the ones developed by Capetti (1929), Morse *et al.* (1933), and Engelman (1973). Capetti's method, detailed in Section 1.2, predicts that the best length of pipe is that which allows the return trip of the compression wave, traveling at the speed of sound, to reach the intake valve when the piston is at BDC. The predicted tuning speed for this case is

$$N = 7.5\frac{c}{l}, \tag{4.1}$$

where l [m] is the length of the intake pipe, c [m/s] is the speed of sound, and N [RPM] is the engine speed. Assuming the c = 348 m/s (corresponding to an average experiment ambient temperature of 302 K), and using an overall intake length of 0.6226 m from the back of the valve to the flange, the predicted tuning peak speed is 4192 RPM. The largest tuning peak for the baseline case occurs at 3750 RPM, an 11.8 % difference when compared to the predicted speed. Since there is no provision in Capetti's method for how the tuning peak location changes with changing intake area, this method will only be applied to the baseline case.

The predictive method developed by Morse *et al.* is similar to that of Capetti's in that they both assume linear, acoustic behavior in the intake duct. Recall from Section 1.2 that this method states that the QSW developed in the intake pipe between valve open periods is the cause for intake tuning. When any one of the harmonics of the engine (= RPM/120) equals one of the resonance frequencies of the intake pipe (=c/4l), intake tuning could possibly occur. It was found that when the ratio q of pipe frequency to engine frequency was equal to 3, 4, or 5, beneficial resonance would occur, leading to

$$N = \frac{30\ c}{l\ q}, \tag{4.2}$$

where c [m/s] is the speed of sound, l [m] is the length of the intake pipe, and q = 3, 4, or 5. With c = 348 m/s and l = 0.6226 m, the results of Eq. (4.2) are given in Table 4.1. It is encouraging that this method predicts three distinct intake tuning peaks, and in fact three tuning peaks are visible for the experimental baseline data, as seen in Chapter 3.

q	Predicted Peak (RPM)	Experimental Peak (RPM)	Percent Difference
3	5590	4750	17.7
4	4192	3750	11.8
5	3353	3000	11.8

Table 4.1: Morse *et al.* (1933) Method for Intake Tuning Prediction.

This method over-predicted the tuning peak speeds for all three values of q, the worse being 17.7 % too high when q = 3 and 11.8 % for both q = 4 and q = 5 cases. Much like Capetti's method, this method does not provide insight into tuning peak changes as the area of the intake duct changes. Thus, it will only be used for the baseline case.

Engelman postulated that the intake pipe and cylinder can be thought of as a lumped-parameter Helmholtz model. For his method, detailed in Section 1.2, he modeled the air in the intake pipe as a mass with no compressibility and the air in the cylinder volume as a spring with no inertia. Equations (1.3) and (1.4) give the predicted tuning peak locations, where K is a valve timing factor and is somewhere between 2.0 and 2.5 (Engelman, 1973). Taking the speed of sound as 348 m/s, the intake length as 62.26 cm, the intake area as 13.85 cm², and a preliminary guess of K = 2.1, the tuning peak location was predicted at 4314 RPM, a 15 % difference when compared to the main experimental tuning peak of the baseline case (corresponding to q = 4 in Table 4.1). Equation (1.3) was then calibrated using the actual tuning peak of 3750 RPM; K for this case is 2.416, within the range prescribed by Engelman. Engelman and Thompson also gave a method [Eq. (1.5)] for calculating an effective intake-length to intake-area ratio. Using K =

2.416, the major tuning peak location for the tapered intakes was calculated as tabulated in Table 4.2.

Intake #	$L/A\|_{effective}$ (cm^{-1})	Predicted Peak (RPM)	Experimental Peak (RPM)	Percent Difference
2	4.407	3787	3850	1.6
3	4.319	3825	3875	1.3
4	4.145	3905	4000	2.3
5	4.214	3873	4000	3.1
6	3.935	4008	4125	2.8
7	3.800	4078	4250	4.0
8	3.689	4139	4375	5.4

Table 4.2: Lumped Parameter Helmholtz Method for Intake Tuning Predictions.

As the taper became more severe, the error generally increased using this method of prediction; this Helmholtz method predicts the trend of increasing tuning peak speed with increasing intake area correctly.

4.3 Engine Simulation Code

The quasi-1D finite-difference engine simulation code used for this study was MANDY (MANifold flow DYnamics), developed by Ford Motor Company. MANDY is a continuation of the finite difference scheme initially developed by Chapman *et al.* (1982); the particular version used for this study is version 14.04. This engine simulation code is based on a FRAM finite-difference algorithm. In this method, artificial dissipation is only used in areas of large gradients, allowing it to maintain second-order accuracy elsewhere. The FRAM algorithm can be summarized as follows:

1. A provisional advanced time solution to the mass, momentum, and energy equations is calculated using a higher-order finite difference scheme.
2. Local bounds are calculated for the advanced time solution.
3. If the solution from (1) is outside of the bounds calculated in (2), then extra dissipation is added to eliminate non-physical oscillations.

In MANDY, the intake and exhaust manifolds of an engine are modeled as pipes of circular and possibly varying cross-section, junctions, plenums, and ambient conditions. The pipes are then discretized using a staggered mesh, shown in Fig. 4.1, where the vector quantities are located at node points, labeled j, and scalar quantities are located at cell midpoints, labeled j + ½.

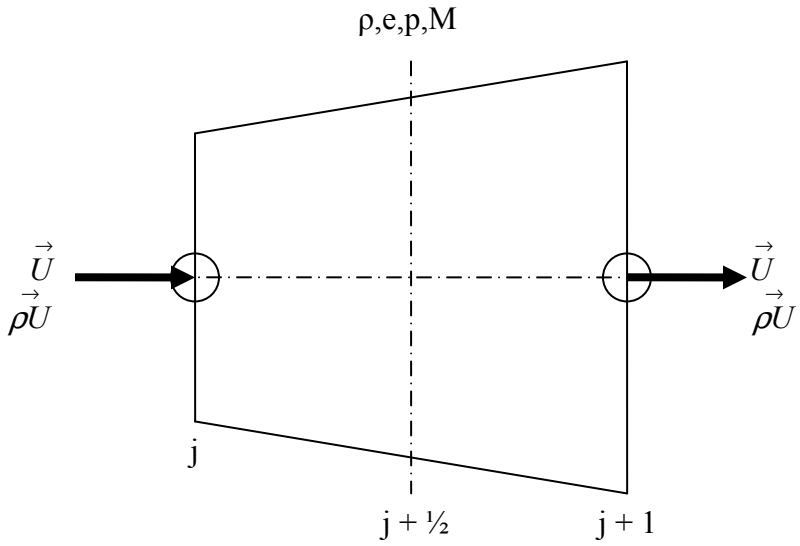

Figure 4.1: Staggered Mesh Discretization of Pipes in MANDY.

Once the pipes are discretized, the quasi-one-dimensional mass, momentum, and energy balance equations for compressible, unsteady fluid flow, shown below, can be solved when coupled with the ideal gas equation of state.

$$\frac{\partial}{\partial t}(\rho A)+\frac{\partial}{\partial x}(\rho AU)=0\,, \qquad \text{(mass)} \quad (4.3)$$

$$\frac{\partial}{\partial t}(\rho AU)+\frac{\partial}{\partial x}(\rho AU^2)+\frac{\partial}{\partial x}(pA)-\tau_w \wp=0\,, \qquad \text{(momentum)} \quad (4.4)$$

$$\frac{\partial}{\partial t}(\rho Ae)+\frac{\partial}{\partial x}(\rho AUe)+p\frac{\partial}{\partial x}(UA)+\dot{q}\wp-\tau_w \wp U=0\,, \qquad \text{(energy)} \quad (4.5)$$

$$p=(\gamma-1)\rho e\,, \qquad \text{(state)} \quad (4.6)$$

where ρ is the density, A is the cross-sectional area, U is the velocity, p is the pressure, τ_w is the wall shear stress, $\wp$ is the perimeter, e is the specific internal energy, $\dot{q}$ is the heat transfer rate, and γ is the ratio of specific heats. The chemical species in the ducts are determined by solving the species continuity equation (Selamet *et al.*, 2004)

$$\frac{\partial}{\partial t}(\rho Ay_j)+\frac{\partial}{\partial x}(\rho AUy_j)=0\,; \quad j=1,2,\ldots,N\text{-}1, \qquad (4.7)$$

where y_j is the mass fraction of species j, N is the number of species, and $\sum_{j=1}^{N} y_j=1$.

MANDY also includes the following sub-models: (1) Heat transfer to and from cylinder walls, piston motion, and combustion energy release; (2) The mass flow rate of fluids across the intake and exhaust valves as functions of the valve lift profiles based on flow tests; (3) Heat transfer models for the port and manifold walls; (4) Junctions and plenums for ducts, and (5) Flow loss models to account for wall friction, bends, sudden area changes, and user-input flow loss coefficients. For more information, the reader is

referred to publications by Chapman *et al.* (1982), Selamet *et al.* (1994), and Kothamasu (1998).

4.3.1 Model Calibration

MANDY includes provisions for several factors influencing overall engine performance, including but not limited to duct friction, cylinder wall and port temperatures, manifold wall conduction and convection coefficients, physical engine dimensions, and valve lift profiles. Some parameters such as the physical dimensions and ambient temperatures are easily measurable; other input parameters are not as well known by the user. Thus, a model calibration of the baseline case was performed to enhance the model's accuracy for the other intake configurations.

All physical dimensions and relevant experimentally measured quantities were entered into MANDY to best represent the engine and its environment. The physical measurements taken from the actual engine at The Ohio State University included valve diameter, valve lift profile, valve lash, intake and exhaust port lengths and diameters, and lengths and diameters of intake and exhaust pipes. The bore, stroke, compression ratio, connecting rod length, and displaced volume were taken from the specifications of the Jaguar 3.0L engine that the single cylinder was mimicking. The intake and exhaust port discharge coefficients were determined at Ford on a flow bench and the results were entered into the code. The experimental measurements entered into the simulation included ambient intake pressures and temperatures and air-fuel ratio.

For the model variables that were not readily known, a parametric study was performed for the variables that influence predictions the most. A working range of each

variable was given by Ford. The parameters studied were intake and exhaust wall friction factor (WF, constant), cylinder wall temperature (TWCYL, RPM-dependent), cylinder wall heat transfer constant (HFACT, constant), duct wall heat transfer constant (HTDTNC, constant), crank angle of the start of burn (CAB, RPM-dependent), and burn duration (BDUR, RPM-dependent). A list of the calibration parameters used is provided in Appendix B.

The wall friction coefficient is a variation of the Blasius correlation for fully developed turbulent flow in a smooth pipe,

$$\frac{f}{2} = \frac{\text{Blasius constant}}{2\,\text{Re}^{1/4}}, \tag{4.8}$$

where f is the Fanning friction factor, Re is the Reynolds number and the Blasius constant is 0.079. The model replaces ½ (Blasius constant) with a user-set value, WF, to account for pipe roughness, developing flow, and the fact that flow in the intake or exhaust of an engine is sometimes over the Reynolds number limit for the Blasius correlation (Re = 10^5). WF was set to 0.10 for the intake and exhaust for this study by observing the experimental volumetric efficiency and amplitude of the pressure waves at the i2 and e1 location for the baseline case. Since all test pieces were made using stereo-lithography, WF remained 0.10 for all other intakes.

TWCYL and HFACT both control the heat transfer between the fluid in the cylinder and the cylinder walls. These parameters do not affect the shape of the overall volumetric efficiency curve; they merely change its magnitudes. TWCYL is an array containing the cylinder wall temperature for each engine speed. As TWCYL is increased, air in the cylinder becomes hotter, resulting in a lower density and thus lower

volumetric efficiency. HFACT controls the amount of heat transfer occurring in the cylinder; as HFACT is increased, the volumetric efficiency decreases. Once WF was set at appropriate levels, HFACT and TWCYL were altered such that predicted volumetric efficiency matched experiment for the baseline case reasonably well while remaining physically realistic. A value of 2.5 was chosen for HFACT, and the TWCYL array is shown in Fig. 4.2. These values were used for all other intakes.

The duct wall heat transfer constant, HTDTNC, includes wall conductive resistance plus external convective resistance. HTDTNC does not have a marked effect on volumetric efficiency except where exhaust tuning plays a role. Increasing HTDTNC decreases heat transfer. Since the speed of sound is proportional to the square root of temperature ($c = \sqrt{\gamma RT}$), heat transfer has a pronounced effect on when the exhaust expansion wave caused by the reflection of the blowdown pulse returns to the valve. HTDTNC was set at 0.00002 cm².sec.K/ergs by matching the return of the predicted expansion wave in the exhaust to experiment as best as could be.

CAB and BDUR are parameters in MANDY that govern reaction rate and release of energy from fuel. This model uses a sin² curve where reaction rate, r, is defined as (Kothamasu, 1998)

$$r = \frac{2}{BDUR}\sin^2\left[\frac{(\theta - CAB)\pi}{BDUR}\right], \tag{4.9}$$

where *BDUR* is the burn duration, *CAB* is the start of ignition before top dead center, and θ is the crank angle. Changing BDUR and CAB does not have a significant effect on volumetric efficiency, but does affect indicated torque and power. For the baseline case, the phasing and magnitude of predicted in-cylinder pressure at c1 was matched to the

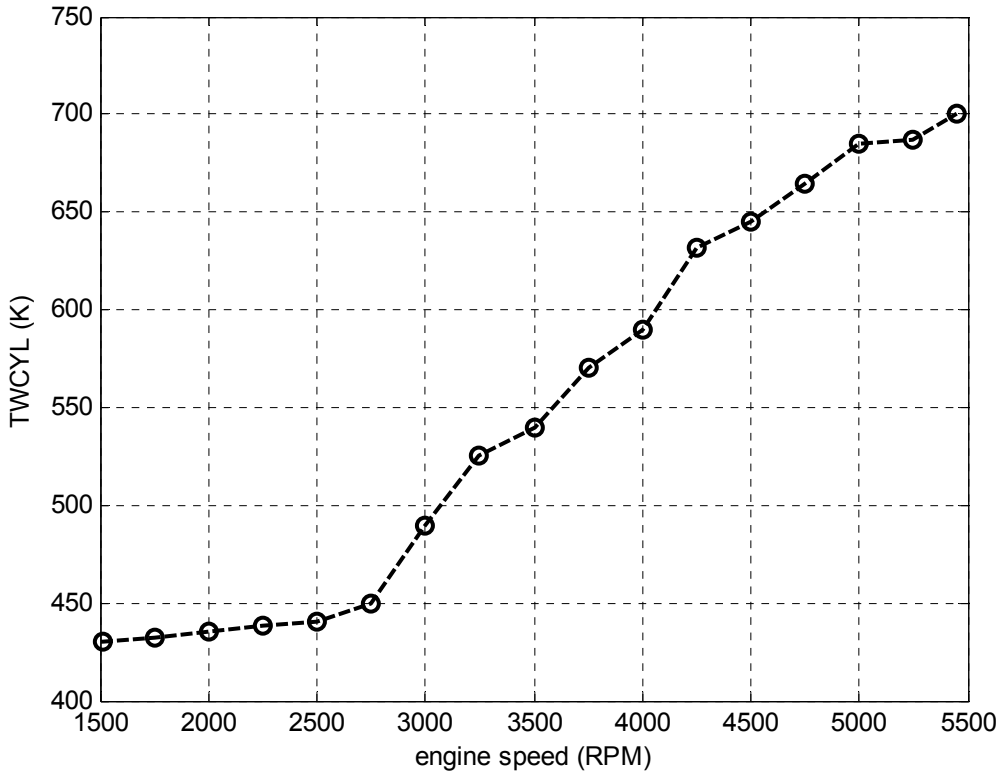

Figure 4.2: TWCYL Array Used by MANDY.

experiment. As a rule of thumb, changing CAB changes the location of the peak pressure, and increasing BDUR decreases peak pressure. This method does have the drawback of being somewhat dependent on sensor accuracy, which as discussed in Chapter 3, may suffer at WOT.

Another important parameter for model calibration is the end correction applied at the inlet of the intake duct due to inertia of the air. As described briefly in Chapter 3, the air leaving the intake pipe continues on its path for a short length as if it were still inside the duct. The pressure waves generated by the breathing process, therefore, see a longer effective length of the duct than physically exists; this extra length is accounted for in the

end correction. This end correction is important for the accurate prediction of volumetric efficiency for each of the intakes, and it is imperative that it be included in the MANDY model of the intake. Selamet *et al.* (2001) conducted a study of end corrections for bellmouthed ducts with flanged ends without mean flow. These end corrections were used as a guide. For modeling each intake, the length of the duct was ended at the start of the bellmouth, and the end correction, δ, was applied as a straight length of pipe the same diameter as the end of the physical duct as illustrated in Fig. 4.3. Each end correction was determined by comparing both the predicted volumetric efficiency and predicted frequency of the QSW at i2 to the measurements. The end corrections used for the baseline and each taper and bellmouth case are shown in Fig. 4.4. Note that for all bends and S-bends, the baseline end correction of 1.5 cm was used. For reference, approximate values of the end corrections given by Selamet *et al.* (2001) are also shown. In general, the end corrections used in this study (with mean flow) are lower than those given by Selamet *et al.* (2001) in the absence of mean flow. Mean flow is suggested by Davies *et al.* (1980) and Peters *et al.* (1993) to decrease the end corrections at low wave numbers, but a comprehensive study of end corrections for flanged pipes with mean flow in the Mach number ranges typically observed in IC engines is not available in the literature.

The predicted volumetric efficiency for the calibrated baseline is shown in Fig. 4.5a. Note that the magnitudes can be manipulated somewhat using TWCYL and HFACT, but the overall shape of the curve cannot. Thus, the model predicts the trend of the volumetric efficiency, and once TWCYL and HFACT were set, the volumetric efficiency magnitudes are within an average of 0.93% error for intake #1. Considering the experimental volumetric efficiency measurements are believed to have around 1%

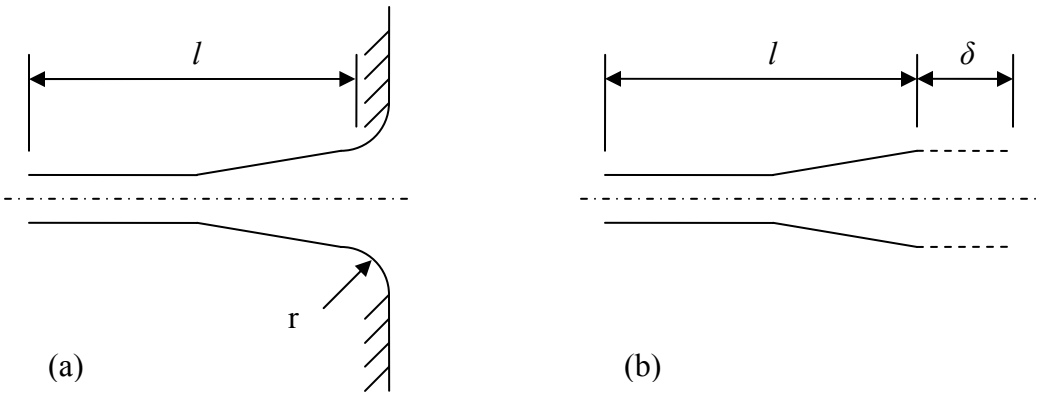

Figure 4.3: Application of End Corrections: (a) Physical Duct (b) MANDY Representation with End Correction.

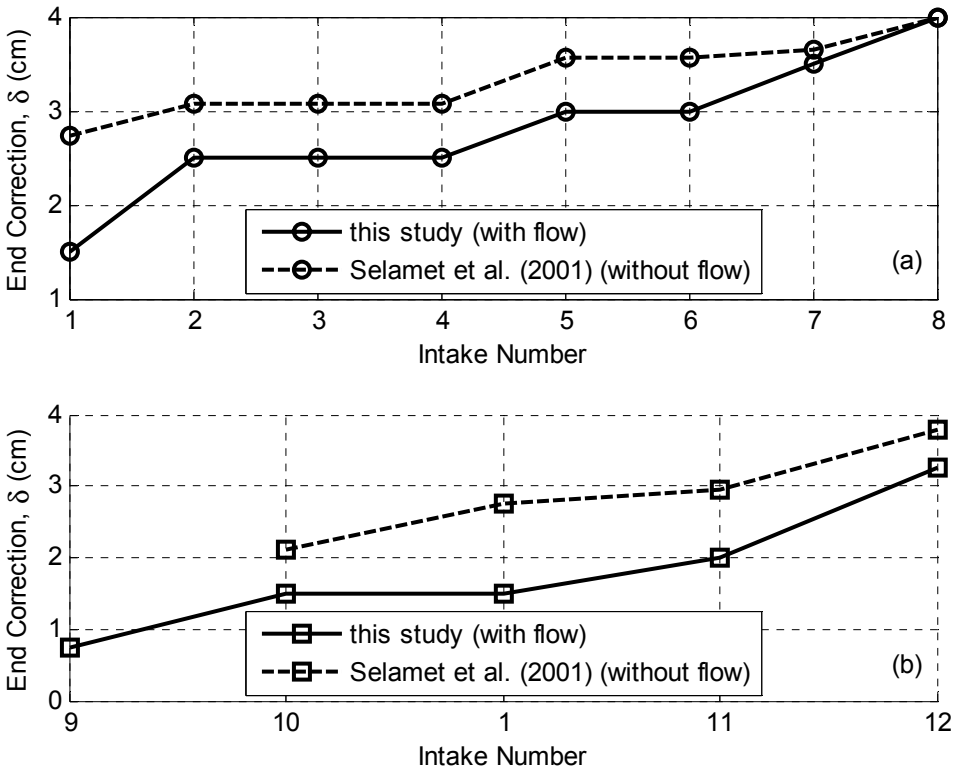

Figure 4.4: End Corrections as Determined by This Study and by Selamet *et al.* (2001) for (a) the Taper Group and (b) the Bellmouth Group.

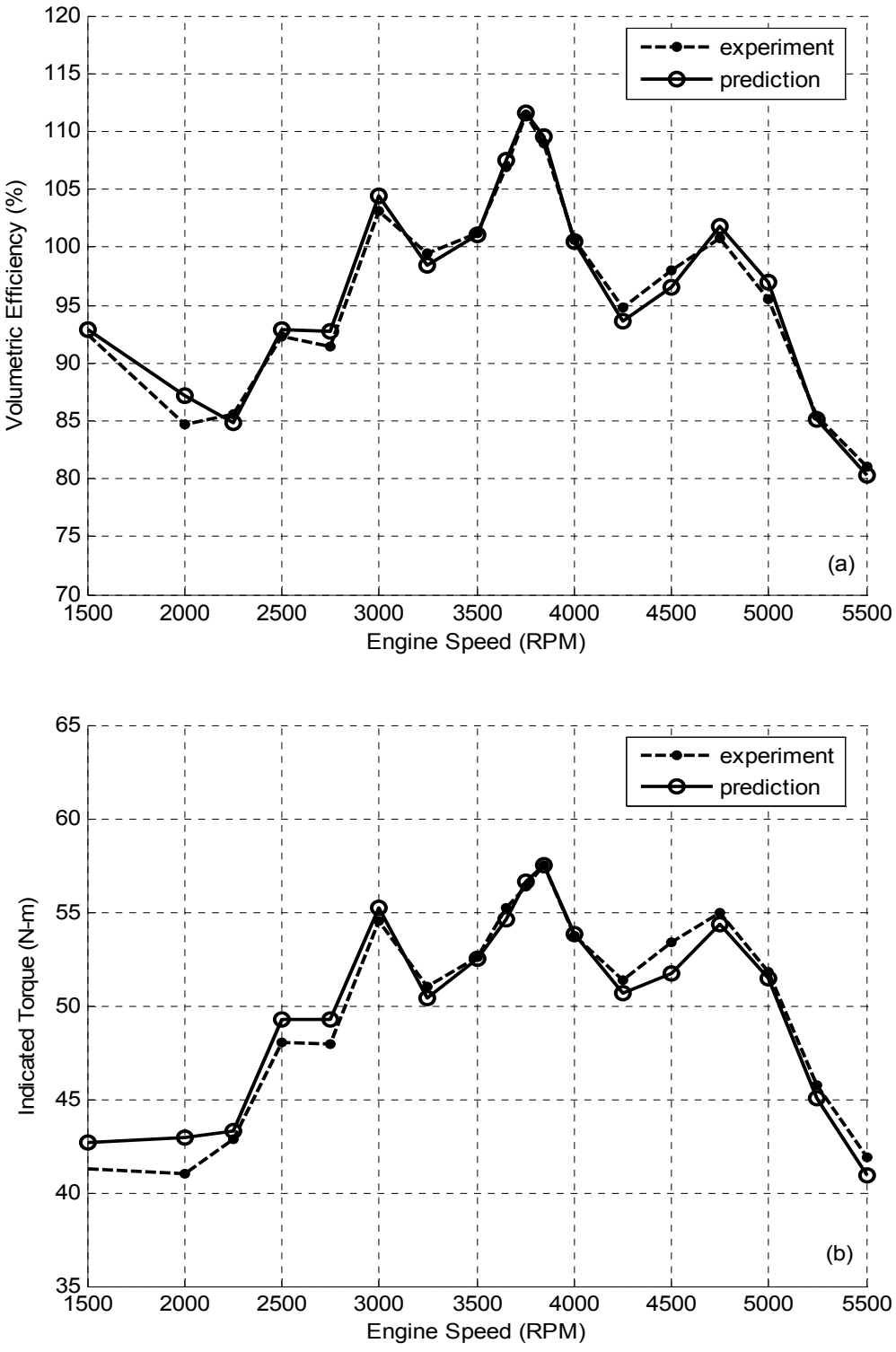

Figure 4.5: Comparison of Predicted and Measured (a) Volumetric Efficiency and (b) Indicated Torque for Intake #1.

error, the model was deemed adequate. Figure 4.5b shows the indicated torque for the baseline case. The experimental indicated torque was calculated by summing brake torque with the torque required to motor the engine at each speed. Indicated torque is predicted within 2% average error, with a maximum discrepancy of 4.7% at 2000 RPM. Once the volumetric efficiency was adequately predicted, matching the in-cylinder pressure to the experimental data gave appropriate results for indicated torque.

Figures 4.6-4.8 show predicted and experimental pressure at i2 (recall Fig. 2.1) for the baseline case at the tuning peak speeds of 3000, 3750, and 4750 RPM, respectively, in both the time (plotted every CAD) and frequency (plotted every half engine order) domain. The engine simulation predicts both the magnitude and phasing of the wave very well at 3000 RPM as can be observed in Fig. 4.6a. Figure 4.6b shows that the code predicts the frequency components that are most pivotal to engine tuning very well, with engine orders from 0.5 to 3.5 being predicted almost exactly. In general, MANDY captures the overall shape of the frequency spectrum, with a general under-prediction of the SPL from orders 3.5 to 10. However, considering the difference in magnitudes between orders 2.5 and 4, a difference of 30 dB or 10.84 kPa, these engine orders doubtfully play a significant role in engine tuning. The model predicts the pressure trace at i2 equally well for 3750 RPM as it did for 3000 RPM. The major engine orders, from 1.5 to 3, are predicted almost exactly, while the overall trend of the frequency spectrum is captured by the code. After order 7.5, MANDY tends to under-predict the magnitudes of the frequency components, with the largest discrepancy, 16 dB, at order 10. Again, these higher orders have little effect on engine tuning phenomenon. At 4750 RPM (Fig. 4.8a), there is a noticeable phase shift between the prediction

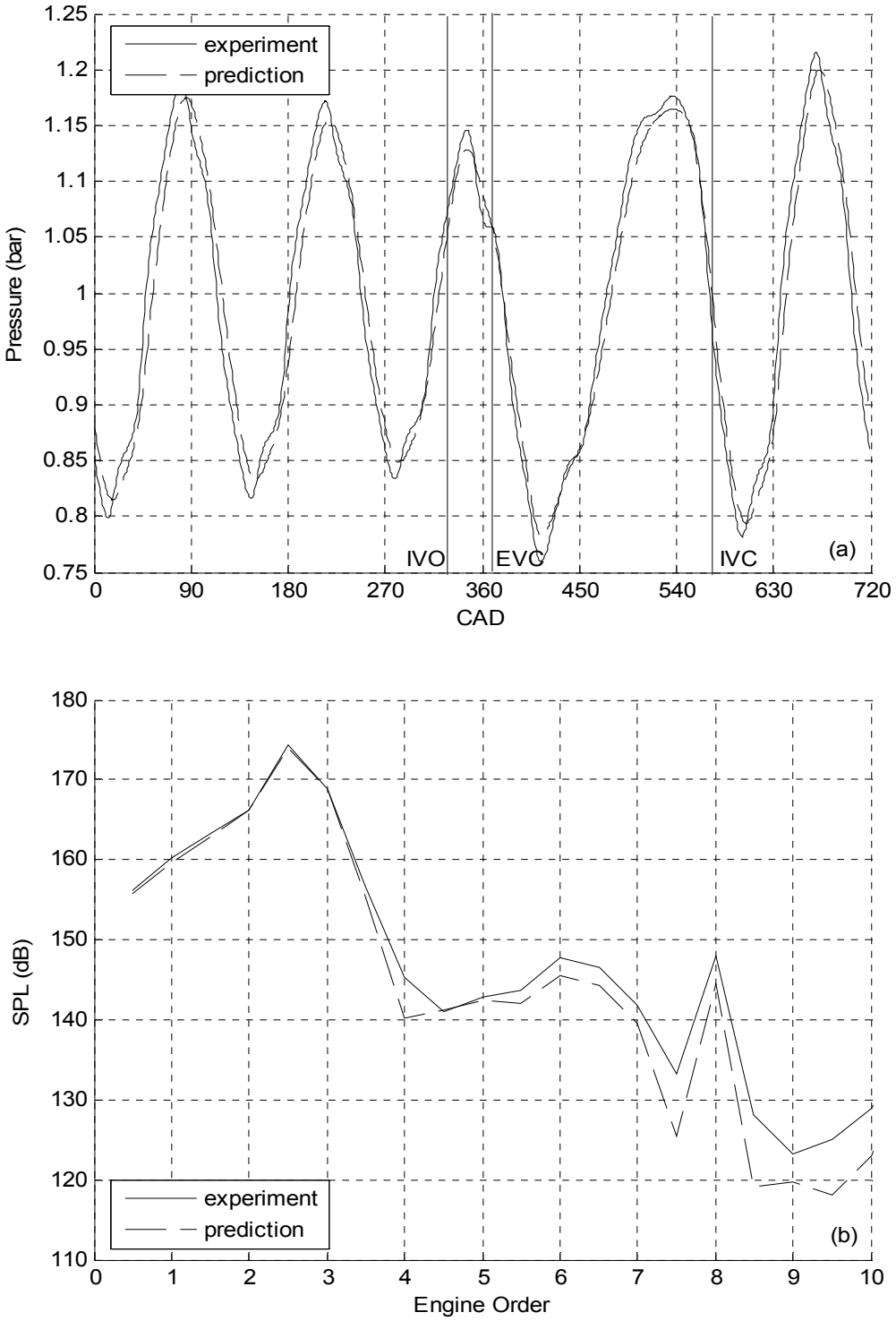

Figure 4.6: Comparison of Predicted and Measured Pressure at i2 at 3000 RPM for Intake #1 in (a) Time Domain and (b) Frequency Domain.

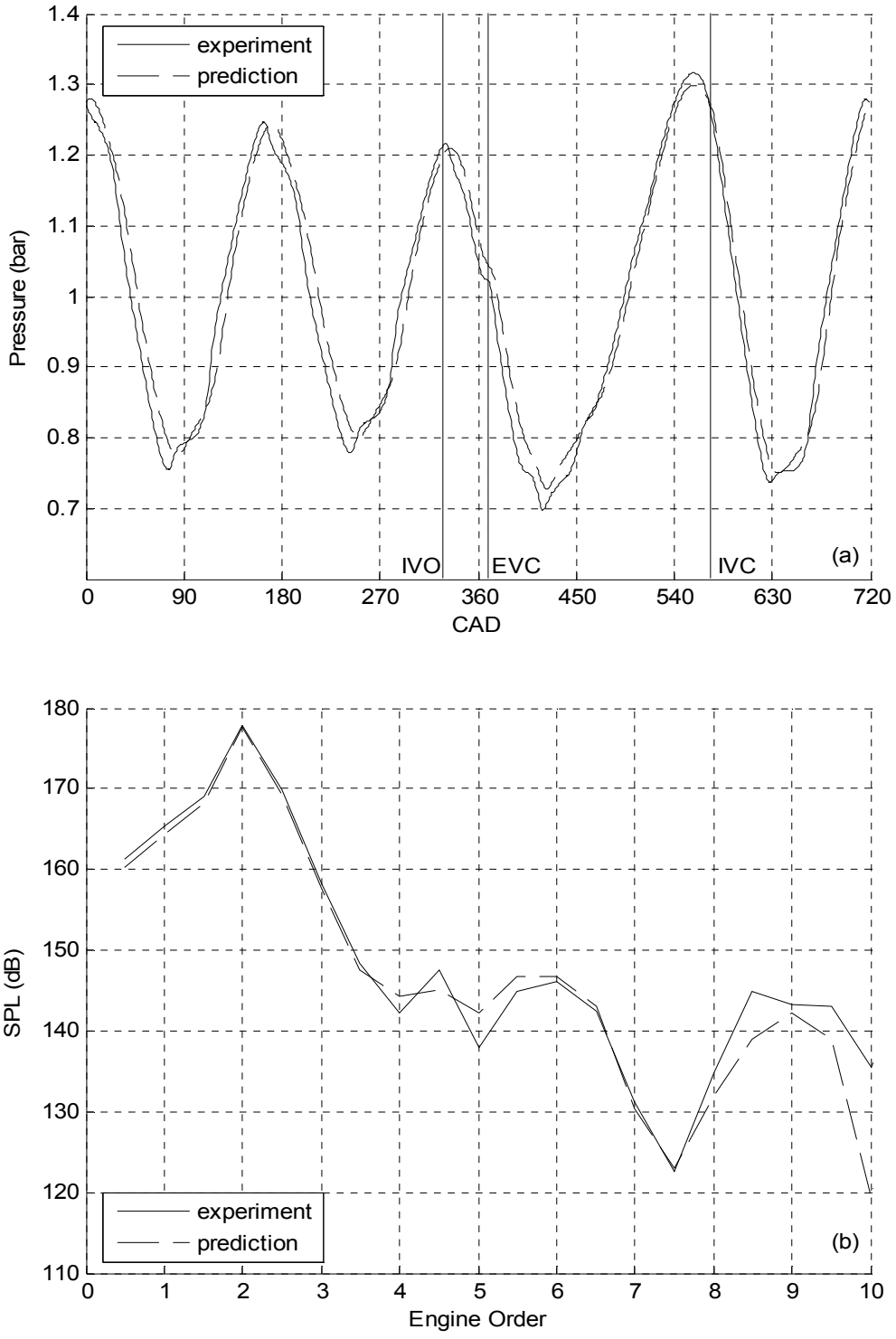

Figure 4.7: Comparison of Predicted and Measured Pressure at i2 at 3750 RPM for Intake #1 in (a) Time Domain and (b) Frequency Domain.

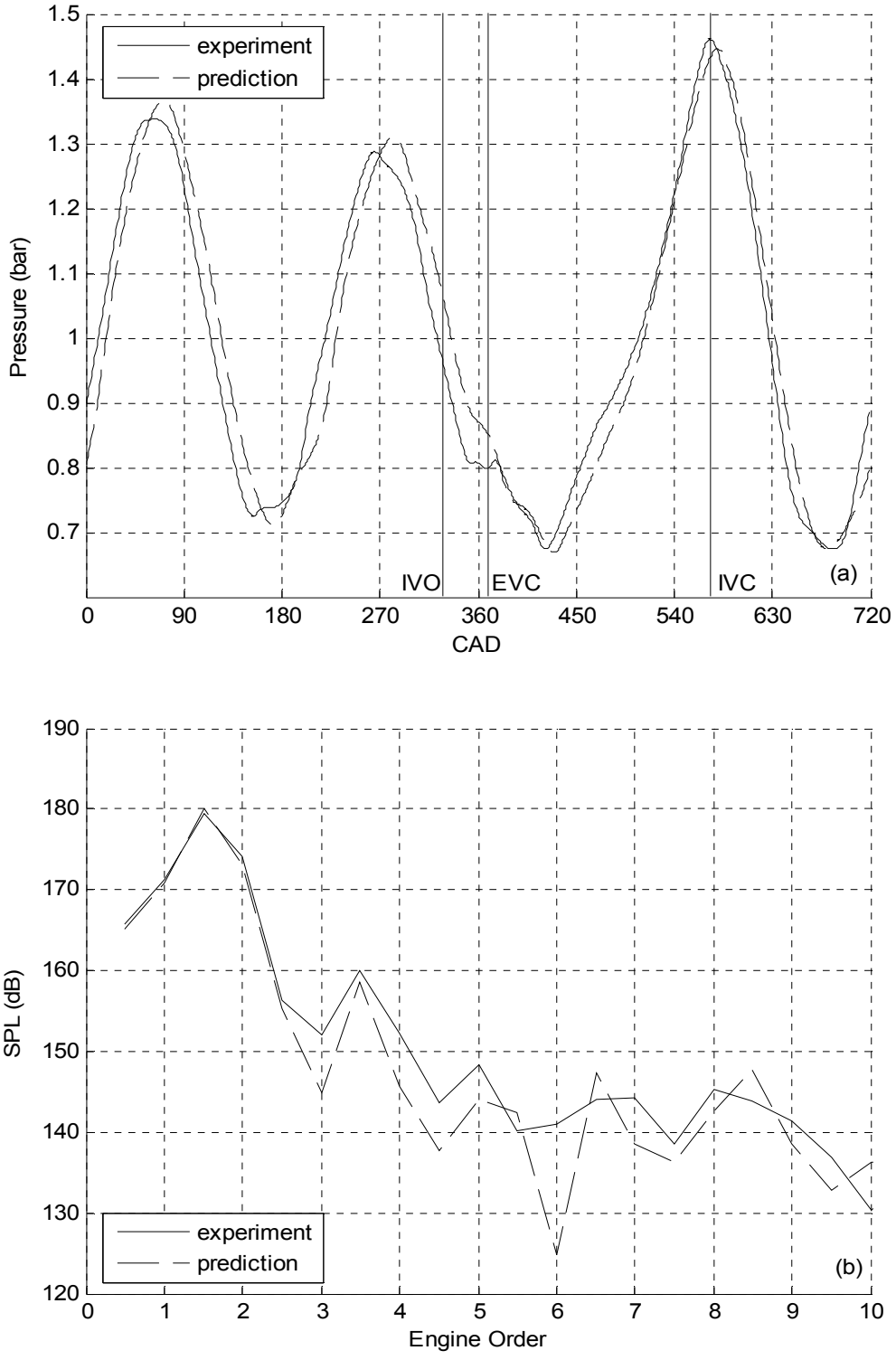

Figure 4.8: Comparison of Predicted and Measured Pressure at i2 at 4750 RPM for Intake #1 in (a) Time Domain and (b) Frequency Domain.

and the experiment; the predicted pressure trails the measurements by 5 to 10 CAD. The overall wave form and the magnitudes are captured well. Figure 4.8b shows that the most important engine orders from 0.5 to 2.5 are predicted almost exactly, and although there is a general trend of under-predicting the SPL after order 2.5, there are slight over-predictions at orders 5.5, 6.5, 8.5, and 10. The largest under-prediction, 16 dB, occurs at order 6.

Figures 4.9-4.11 show predicted and experimental pressure at the i1 location for baseline intake #1 at the tuning peak speeds of 3000, 3750, and 4750 RPM, respectively, in both the time and frequency domains. The magnitudes, phasing, and overall shape of the pressure wave at 3000 RPM, shown in Fig. 4.9a, are adequately captured by the code. However, MANDY does not capture some of the smaller details of the trace. For example, the sharp peaks at the beginning of the compression waves (at 69, 202, 336, and 656 CAD) are not captured, and instead seem to be "smeared" over the entire compression wave, and the small perturbations from 405 to 480 CAD are missed. Since the i1 location is close to the inlet, some multi-dimensional effects caused by the inlet region may be manifested in the pressure trace which are not accounted for in the inherently 1D simulation; this could be causing the discrepancies between the prediction and the experiment. Figure 4.9b shows that the prediction and the experiment show good agreement for the dominant orders, with the SPL of orders from 0.5 to 3 agreeing almost exactly. Unlike the trend seen in the frequency spectrum of the i2 location at this speed, the code tends to over-predict contributions from orders 3.5 to 5.5 (within 3 dB) and under-predict contributions from orders 5.5 to 10, the biggest discrepancy being 6 dB at order 9.5. At 3750 RPM, the code performs adequately in predicting the pressure trace at

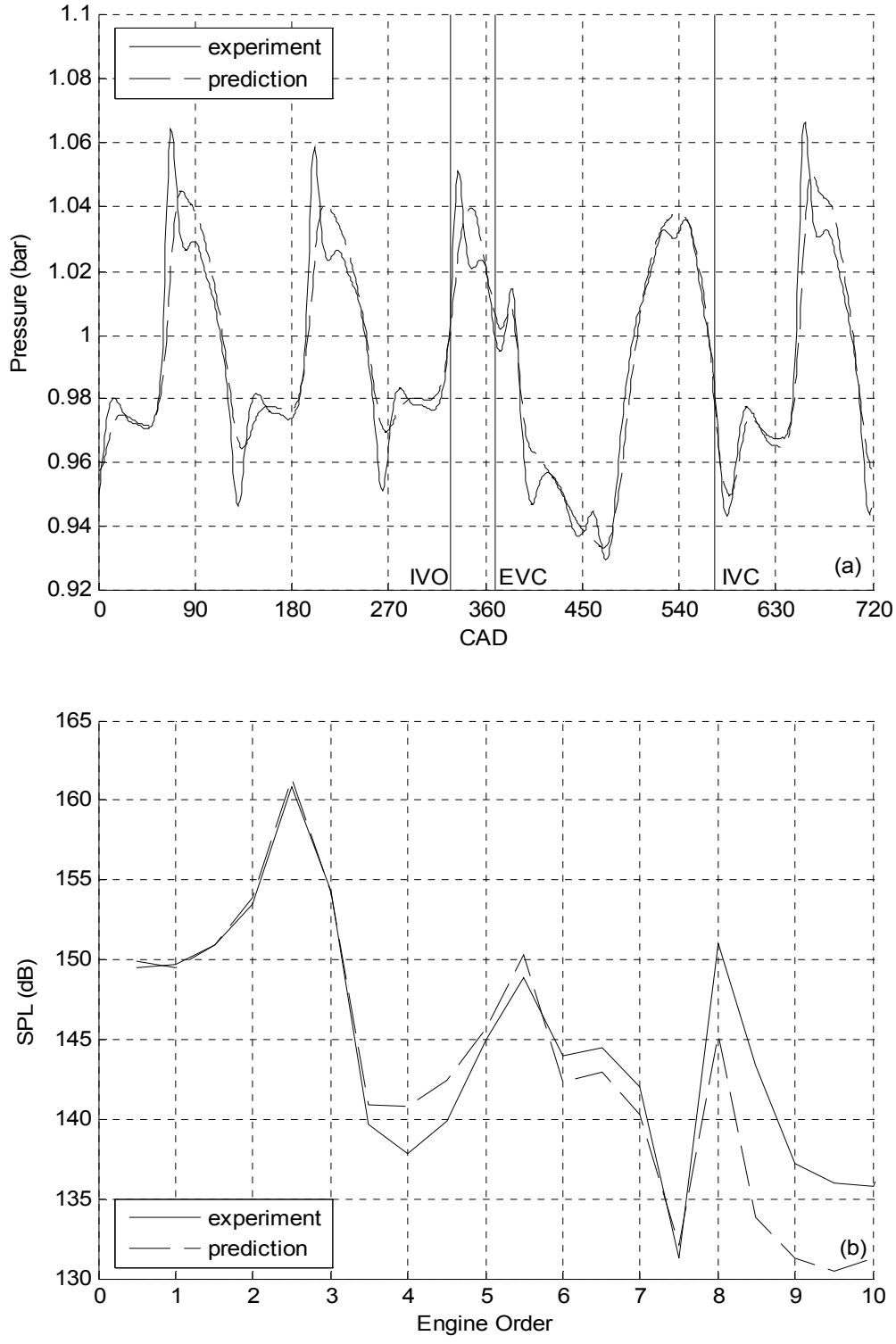

Figure 4.9: Comparison of Predicted and Measured Pressure at i1 at 3000 RPM for Intake #1 in (a) Time Domain and (b) Frequency Domain.

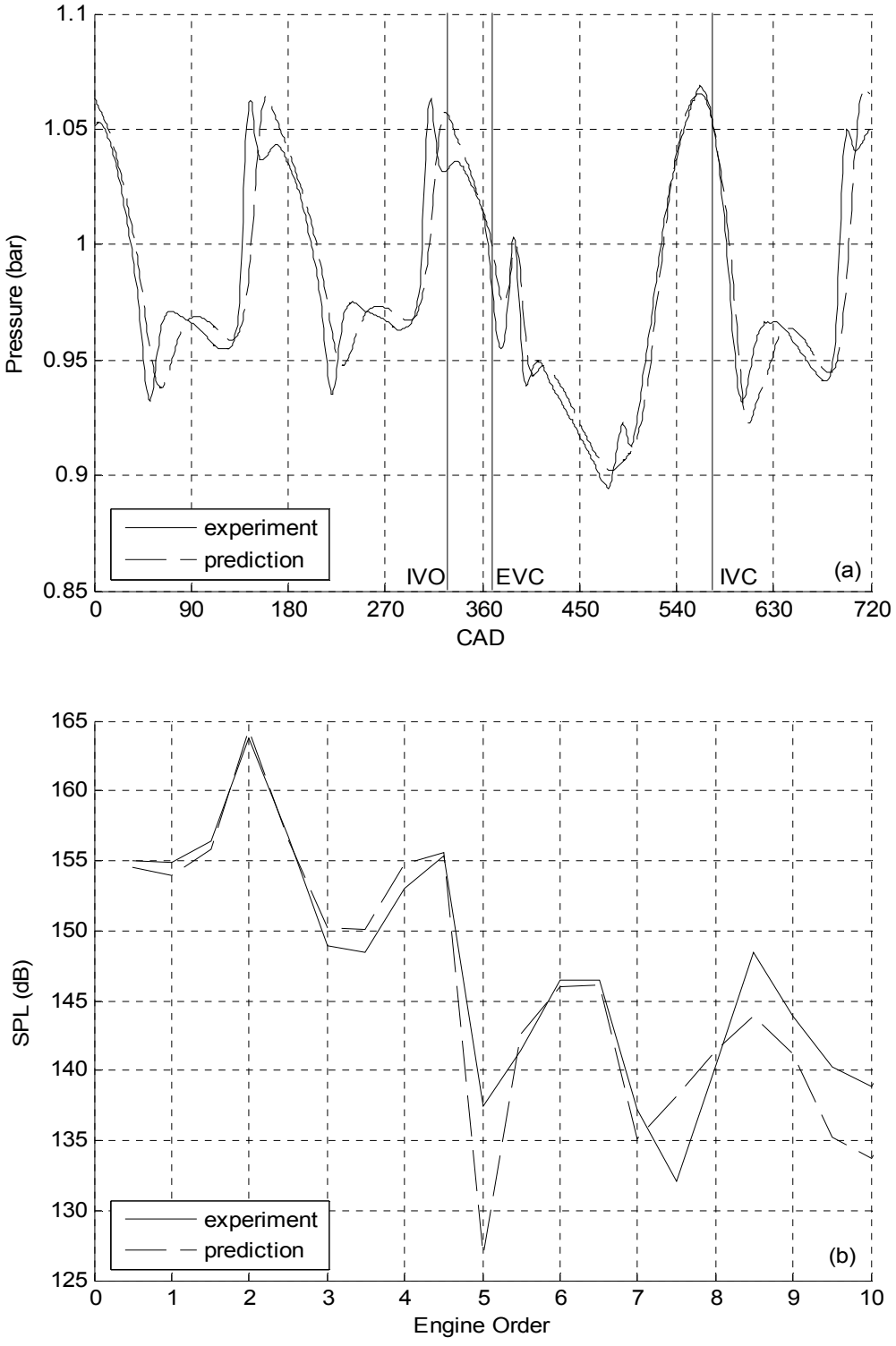

Figure 4.10: Comparison of Predicted and Measured Pressure at i1 at 3750 RPM for Intake #1 in (a) Time Domain and (b) Frequency Domain.

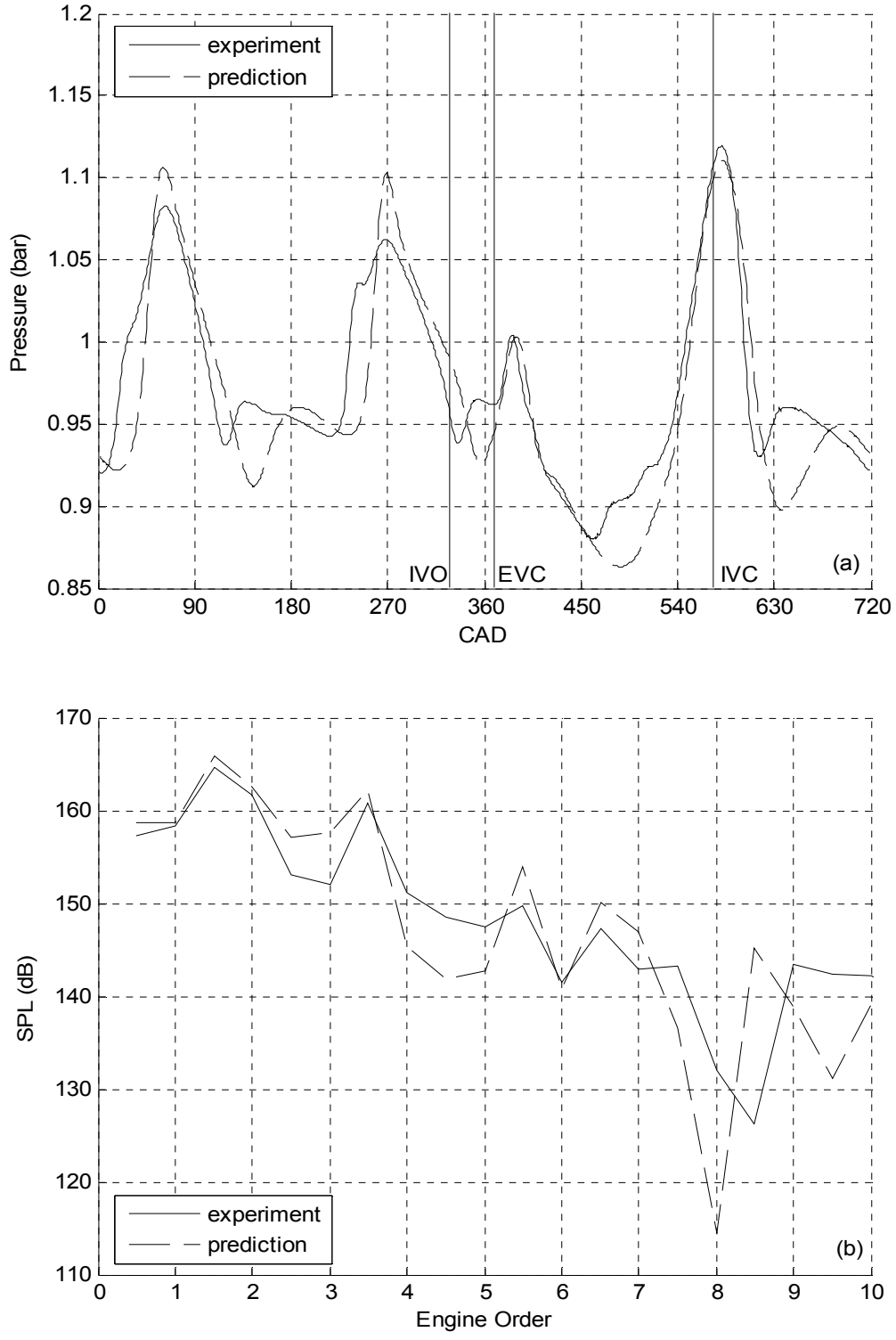

Figure 4.11: Comparison of Predicted and Measured Pressure at i1 at 4750 RPM for Intake #1 in (a) Time Domain and (b) Frequency Domain.

i1, shown in Fig. 4.10a. The wave during the IV open period is predicted very well, while again some subtle nuances of it and the QSW are missed. Again, the sharp peaks at the beginning of the crests of the compression waves are not predicted, and the valleys at 50, 210, and 595 CAD are predicted as wider than they actually are. The overall shape and frequency of the QSW is predicted well. Figure 4.10b shows that the prominent first few engine orders are predicted within 1 dB. The overall shape of the frequency spectrum is captured well, with some subtle differences at higher engine orders. The grossest under-prediction, being 10 dB, occurs at order 5. Figure 4.11a shows that the code is capturing the overall shape of the i1 wave at 4750 RPM adequately, but there is a general over-prediction of the amplitudes both in the IV open period and the QSW. The peaks of the QSW are predicted at the correct time, but the valleys have a phase shift of up to 27 CAD. Figure 4.11b shows that the shape of the frequency spectrum is captured by the code, with some subtle differences at higher orders, but the overall accuracy of the prediction is less than that of the other two speeds. This suggests that multi-dimensional effects at the inlet play a more important role as the flow velocity increases. The code generally predicts the frequency spectrum within 8 dB, with the largest error being 15 dB at order 8.

Figures 4.12-4.14 show predicted and experimental exhaust pressures for the baseline at the e1 location (recall Fig. 2.3) at the tuning peak speeds of 3000, 3750, and 4750 RPM, respectively, in both the time and frequency domain. At 3000 RPM, the shape of the exhaust pressure trace, shown in Fig. 4.12a, is predicted fairly well. In general, the predicted pressure is slightly higher than experimental pressure by about 0.05 bar. The blowdown pulse occurring while the exhaust valves are open is phased correctly

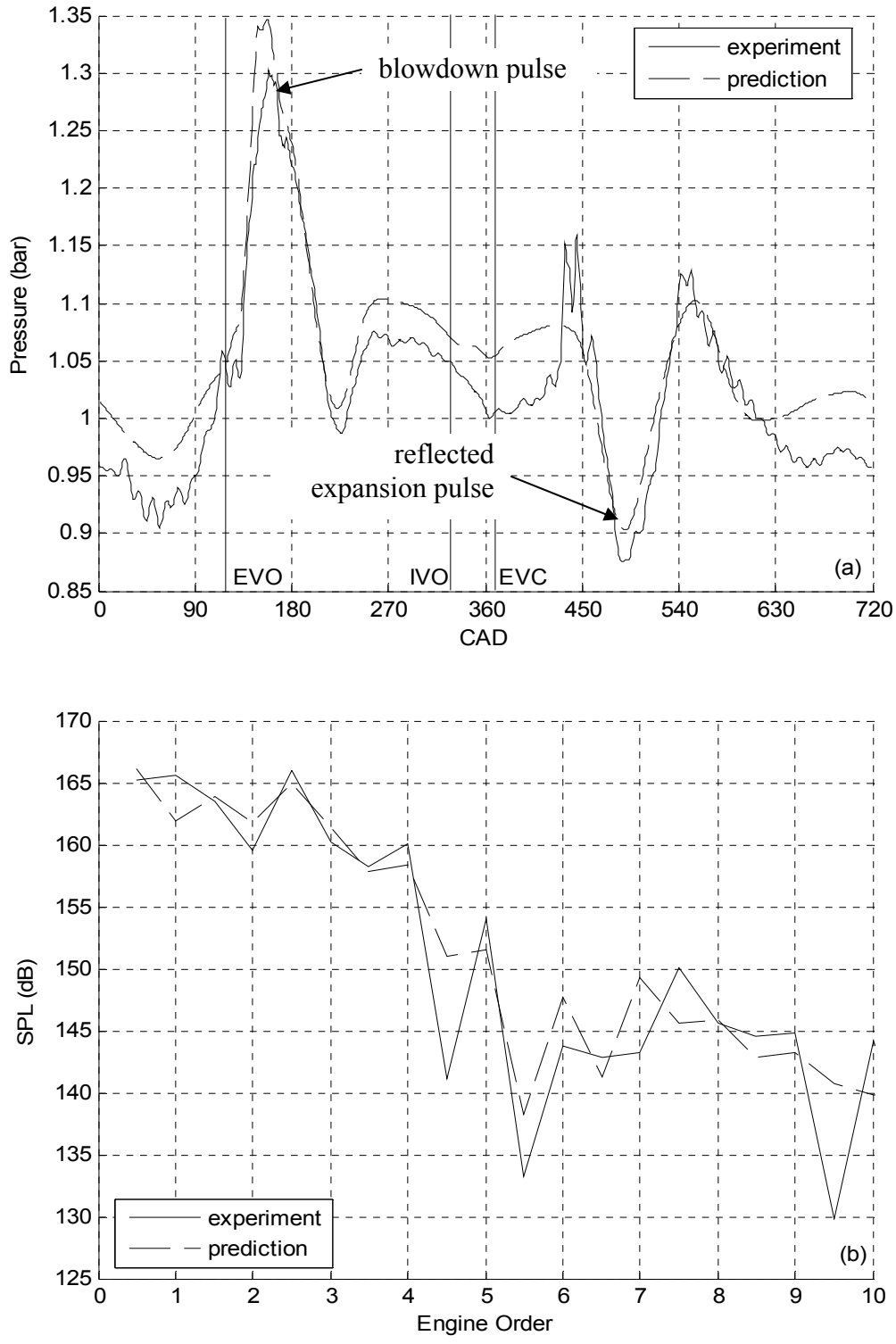

Figure 4.12: Comparison of Predicted and Measured Pressure at e1 at 3000 RPM for Intake #1 in (a) Time Domain and (b) Frequency Domain.

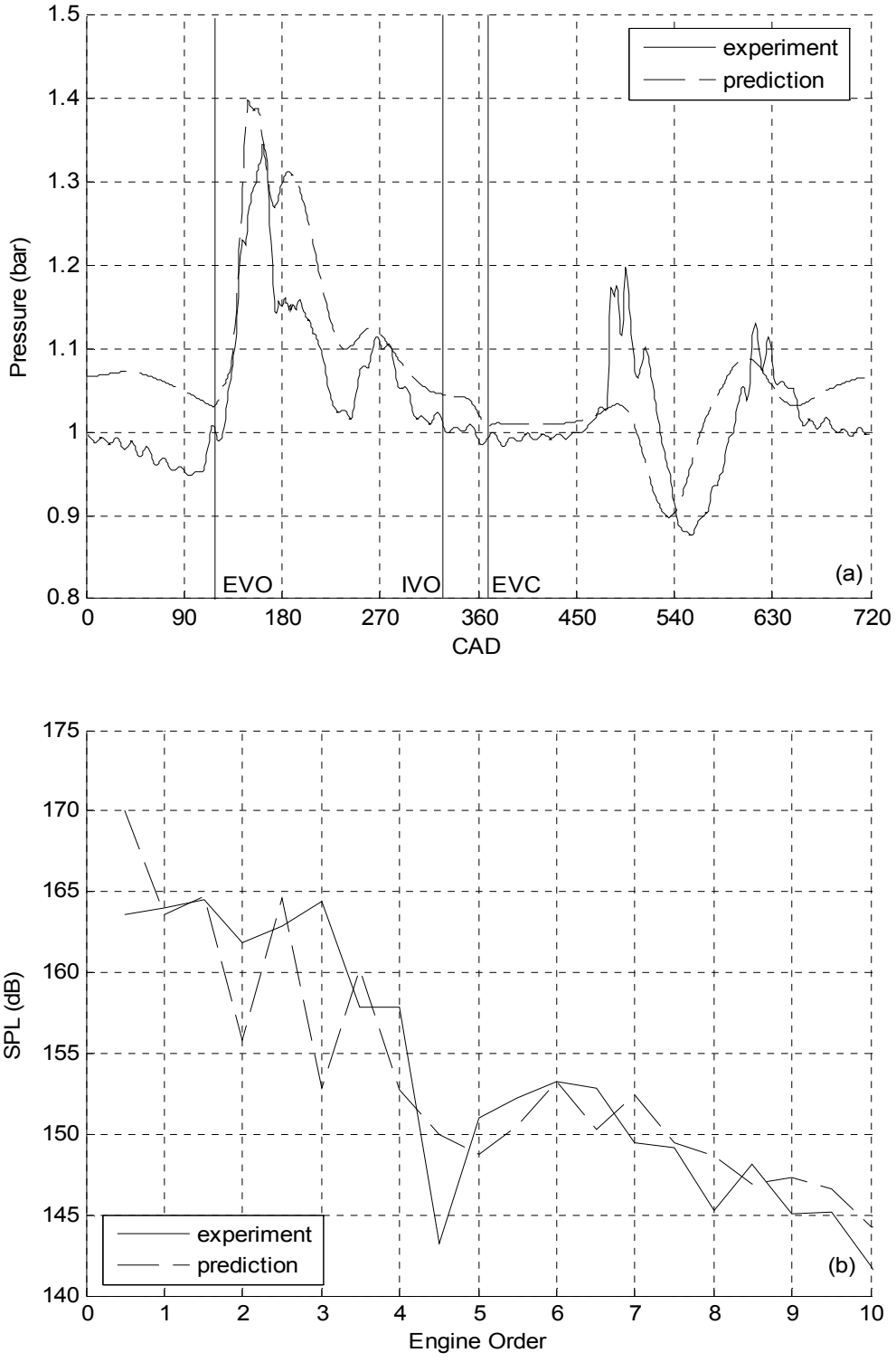

Figure 4.13: Comparison of Predicted and Measured Pressure at e1 at 3750 RPM for Intake #1 in (a) Time Domain and (b) Frequency Domain.

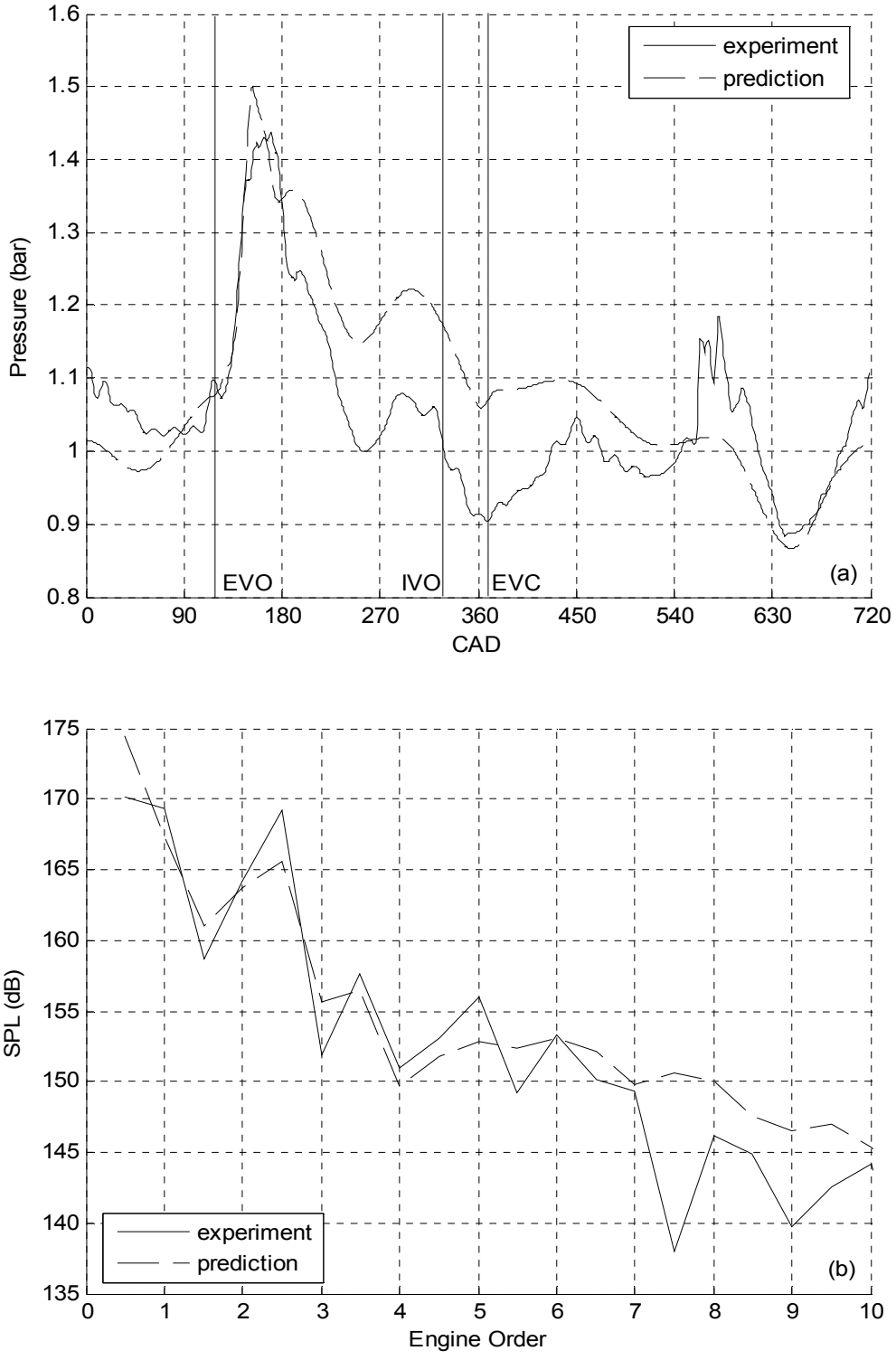

Figure 4.14: Comparison of Predicted and Measured Pressure at e1 at 4750 RPM for Intake #1 in (a) Time Domain and (b) Frequency Domain.

and has appropriate magnitude, and the reflected expansion pulse is predicted to arrive at e1 at the correct time. The blowdown and reflected expansion pulses are labeled in this figure for clarification. Figure 4.12b shows the e1 pressure at 3000 RPM in the frequency domain. The overall trend of the frequency spectrum is predicted well by the code, generally within 5 dB of the experimental data, with some slight differences at higher engine orders. Figure 4.13 shows the e1 pressure trace at 3750 RPM. Again, the average pressure is slightly over-predicted compared to experiment. Also, the reflected expansion wave does not arrive at e1 at exactly the right time. Generally, the phasing of the predicted expansion wave matches the experiment within about 5 CAD for any other engine speed; 3750 RPM is the only one with such a large discrepancy. It is unclear why this is the case, since parameters that influence exhaust heat transfer and thus the speed of sound, HTDTNC (set to 0.00002 cm^2.sec.K/ergs) and the ambient bulk fluid temperature (set to 311 K), were held constant for all speeds, and based on the timing of the reflected expansion pulse for all other speeds, they seem appropriate. Figure 4.14a shows the pressure trace at e1 at 4750 RPM in the time domain. As with the other speeds, there is a general over-prediction of the pressures in the exhaust. The largest discrepancy is 0.16 bar at 360 CAD. From the reflected expansion pulse to the blowdown pulse, there is an under-prediction of pressure. The reflected pulse is again predicted to occur at the correct time. The predicted frequency spectrum, shown in Fig. 4.14b, captures the overall trend of experimental data for the low engine orders, with a general over-prediction of sound pressure level after order 6. One reason for the discrepancies between predicted and experimental pressures at e1 may be the inclusion of a three-pass muffler in the exhaust, which causes a slightly ambiguous boundary condition between

the exhaust pipe and ambient junction in the model. Since this is primarily an intake tuning effect study, the muffler was modeled as an expansion chamber 30 cm in diameter and 30 cm long. A K-factor was applied across the expansion chamber obtained by flowing the muffler on a flow bench. A fictitious 40 cm length of pipe was attached downstream of this expansion chamber to prevent cooler ambient-temperature air from flowing into the muffler section which would have been physically unrealistic. This modeling approach provided reasonable, yet not perfect, results for the exhaust pressure.

Figures 4.15-4.17 show the predicted and experimental in-cylinder pressures for the baseline speeds of 3000, 3750, and 4750 RPM, respectively. By using only the parameters CAB and BDUR, the predicted in-cylinder pressure can be matched almost exactly to the experiment and, as shown in Fig. 4.5, gives reasonable results for the indicated torque of the actual engine. Figure 4.18 shows the overall sound pressure level (OSPL) at i2 for the baseline intake #1. The model predicts the OSPL trend well at this location. MANDY under-predicts the OSPL slightly at 2500, 3650-4500, and 5250-5500 RPM, but the discrepancy is within 2 dB. The predicted OSPL at the i1 location, shown in Fig. 4.19, captures the overall trend and magnitudes of experimental OSPL within 2 dB. Figure 4.20 shows the OSPL for the exhaust e1 location. Considering the effect of the muffler at the end of the exhaust duct, the OSPL at e1 is predicted reasonably well. The discrepancy is within 2.5 dB.

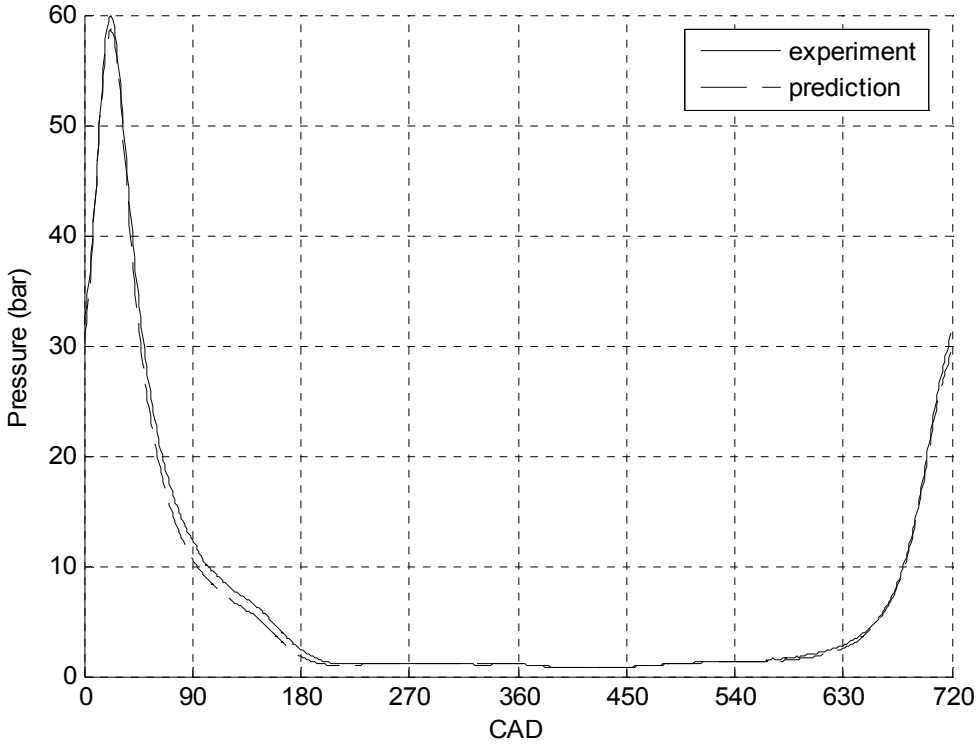

Figure 4.15: Comparison of Predicted and Measured Pressure at c1 at 3000 RPM for Intake #1.

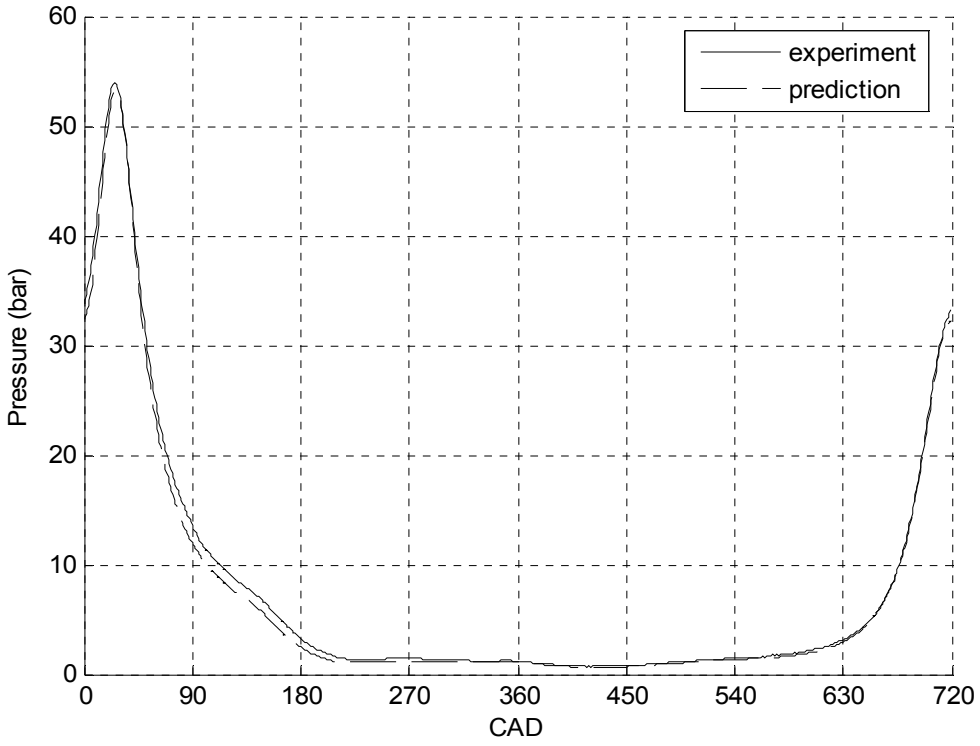

Figure 4.16: Comparison of Predicted and Measured Pressure at c1 at 3750 RPM for Intake #1.

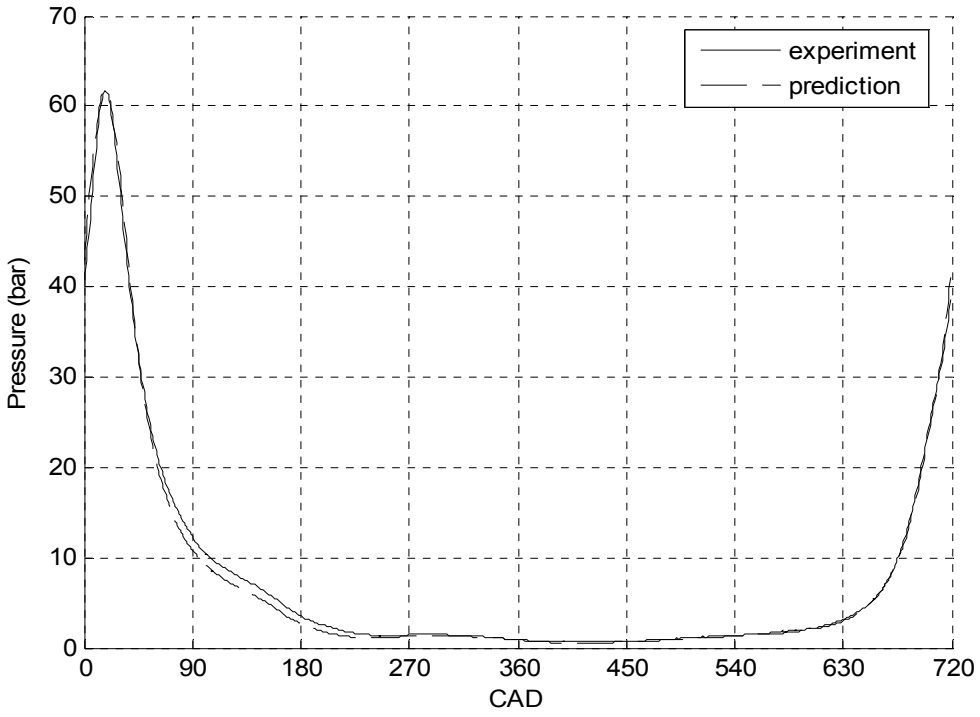

Figure 4.17: Comparison of Predicted and Measured Pressure at c1 at 4750 RPM for Intake #1.

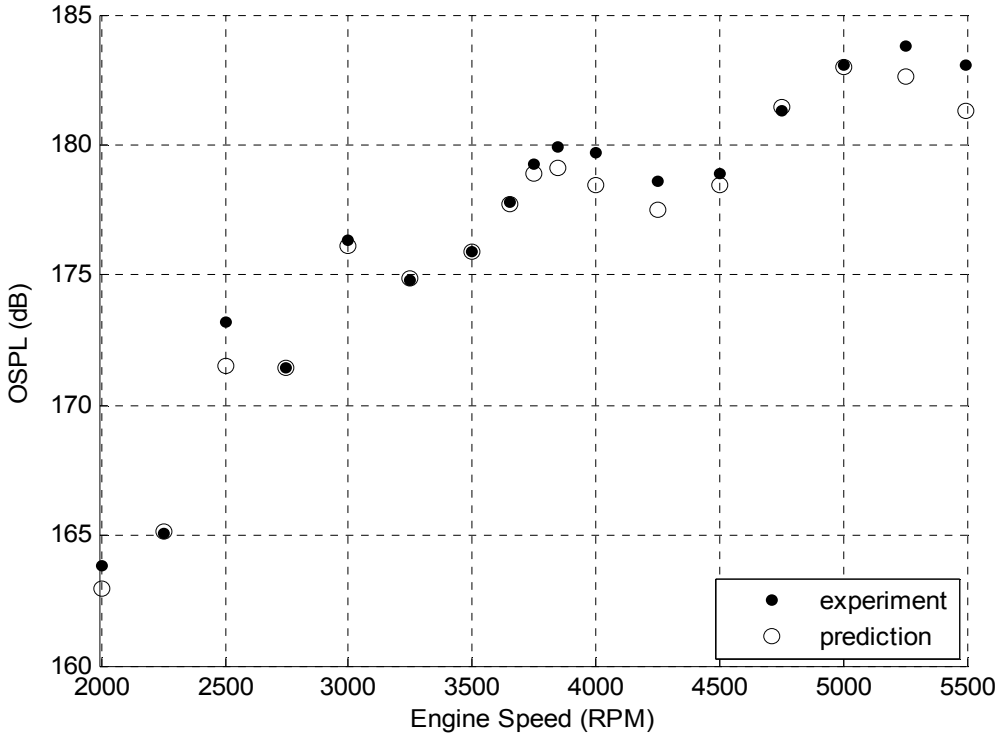

Figure 4.18: Comparison of Predicted and Measured OSPL at i2 for Intake #1.

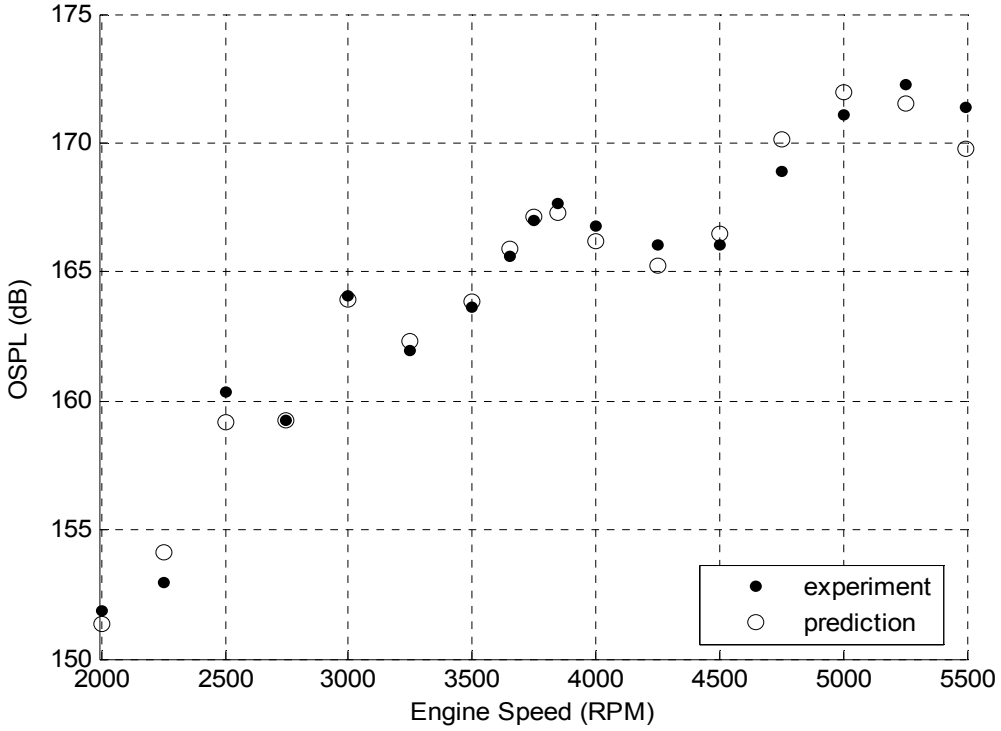

Figure 4.19: Comparison of Predicted and Measured OSPL at i1 for Intake #1.

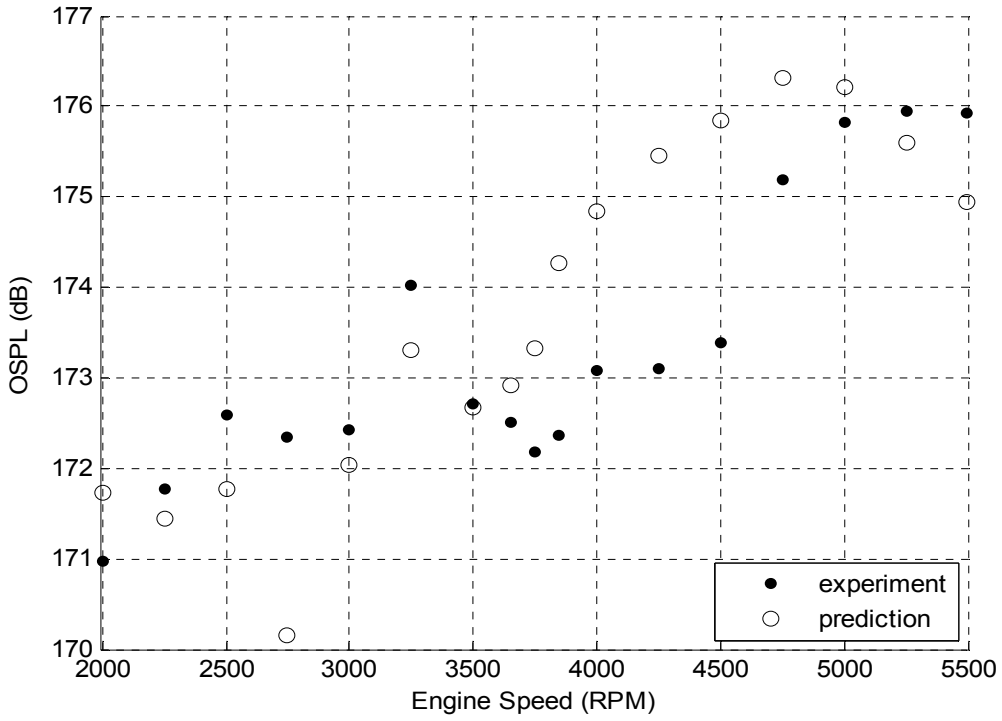

Figure 4.20: Comparison of Predicted and Measured OSPL at e1 for Intake #1.

CHAPTER 5

COMPARISON OF PREDICTIONS WITH EXPERIMENTS

The results from the quasi-1D engine simulation, described in Section 4.3, are compared to experimental data in this Chapter. For each of the 18 intake configurations, the volumetric efficiencies and intake pressures at i1 and i2 in both the CAD-resolved time domain and frequency domain are presented. Additional techniques required to model the flow losses in bends and S-bends are also described.

5.1 Taper Group Predictions

For each intake in the taper group (refer to Fig. 2.5b and Table 2.2), predicted volumetric efficiency is presented against experimental data from 1500 to 5500 RPM. The predicted intake pressure at i2 and i1 are compared to experimental data at the major intake tuning peak for each taper, shown in Table 5.1. For each taper, the average and maximum discrepancies between the predictions and the experiments are tabulated in Table 5.2. Figures 5.1-5.7 show the predicted and experimental volumetric efficiencies for intakes #2-8, respectively. Overall, the predicted and experimental shape of the curve show good agreement for every taper, and the predicted magnitudes are reasonable. For any taper, the discrepancy in volumetric efficiency is generally within 3%, the average error in predictions is less than 1.8%, and the peak volumetric efficiency is within the

Intake	Major tuning peak speed (RPM)
#2	3850
#3	3875
#4	4000
#5	4000
#6	4125
#7	4250
#8	4375

Table 5.1: Major Tuning Peak Speeds for the Taper Group.

experimental error. Considering the error associated with volumetric efficiency measurements is 1%, the code performs admirably. In general, there seems to be a trend of under-prediction of volumetric efficiency between the main tuning peak and the highest-speed peak and over-prediction of efficiency after the highest-speed tuning peak.

Intake	Average error in prediction	Maximum error in prediction	Location(s) of maximum error (RPM)
#2	1.2%	2.5%	4500, 5000
#3	1.2%	3.5%	4500
#4	1.6%	4.0%	5250
#5	1.4%	4.8%	5250
#6	1.7%	4.3%	5500
#7	1.2%	3.2%	5500
#8	1.1%	3.1%	4000

Table 5.2: Volumetric Efficiency Simulation Results for Tapered Intake Configurations.

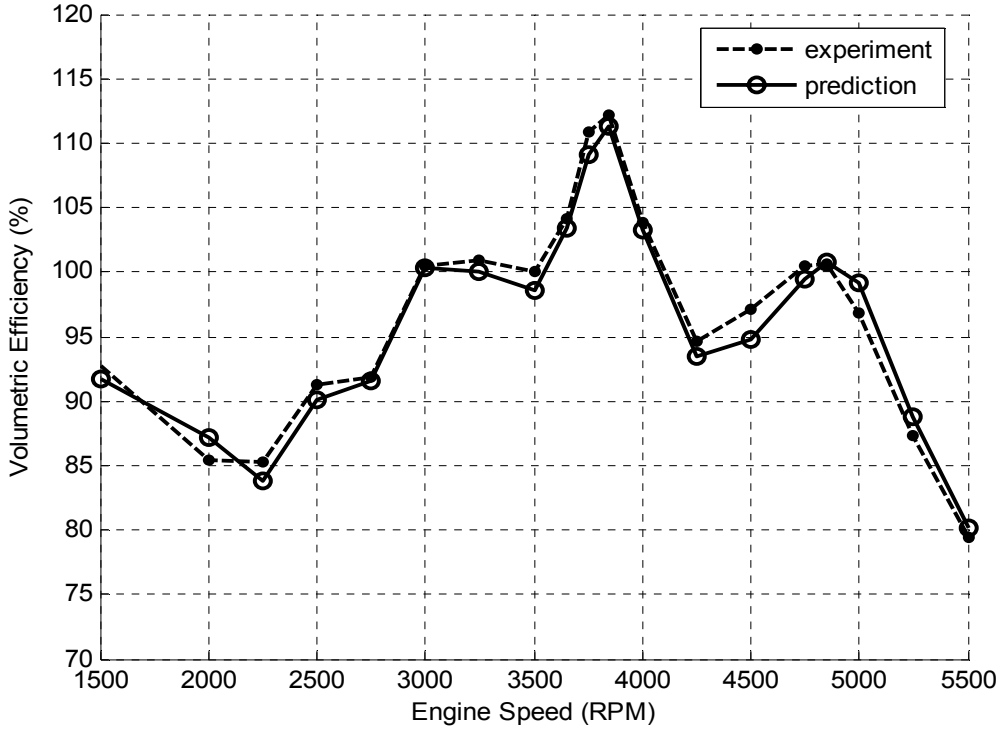

Figure 5.1: Comparison of Predicted and Measured Volumetric Efficiency for Intake #2.

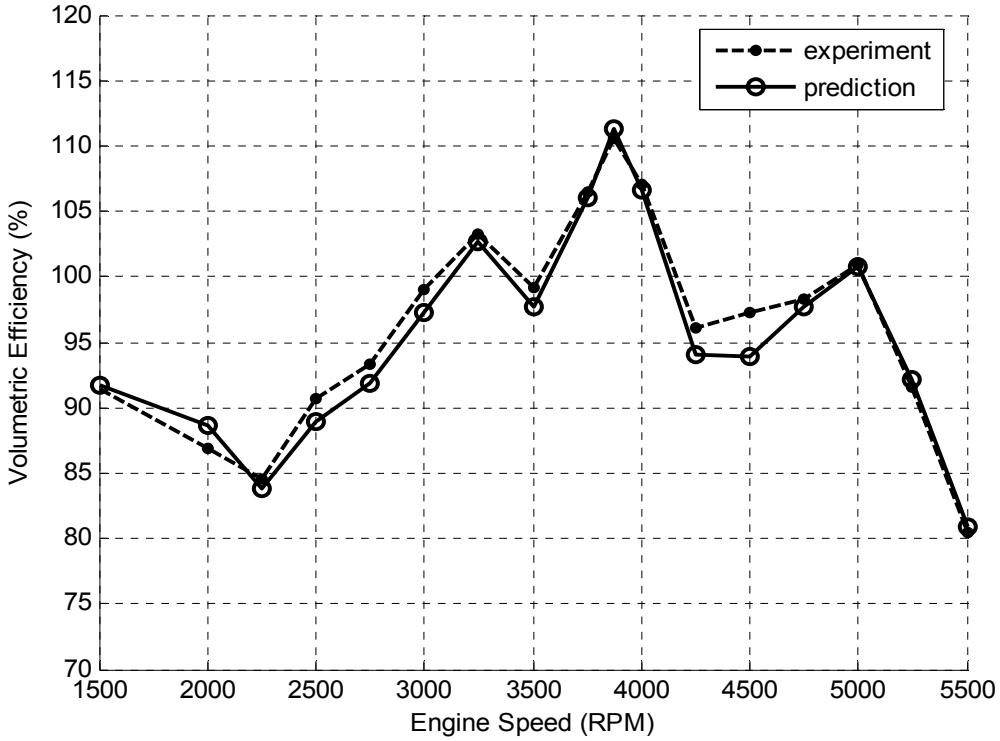

Figure 5.2: Comparison of Predicted and Measured Volumetric Efficiency for Intake #3.

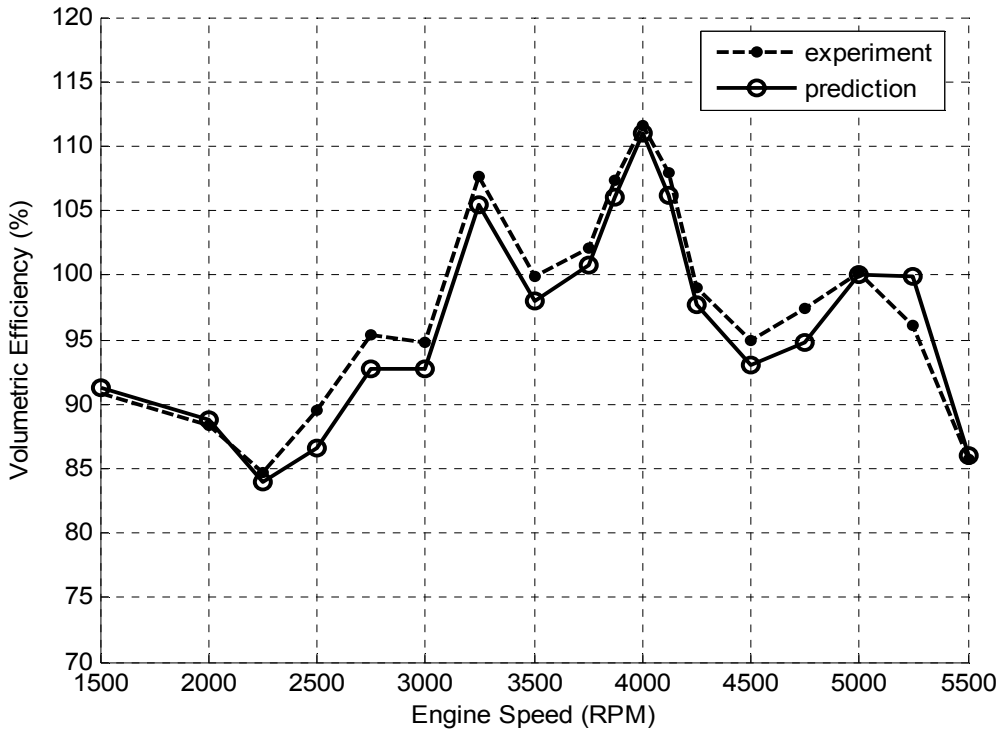

Figure 5.3: Comparison of Predicted and Measured Volumetric Efficiency for Intake #4.

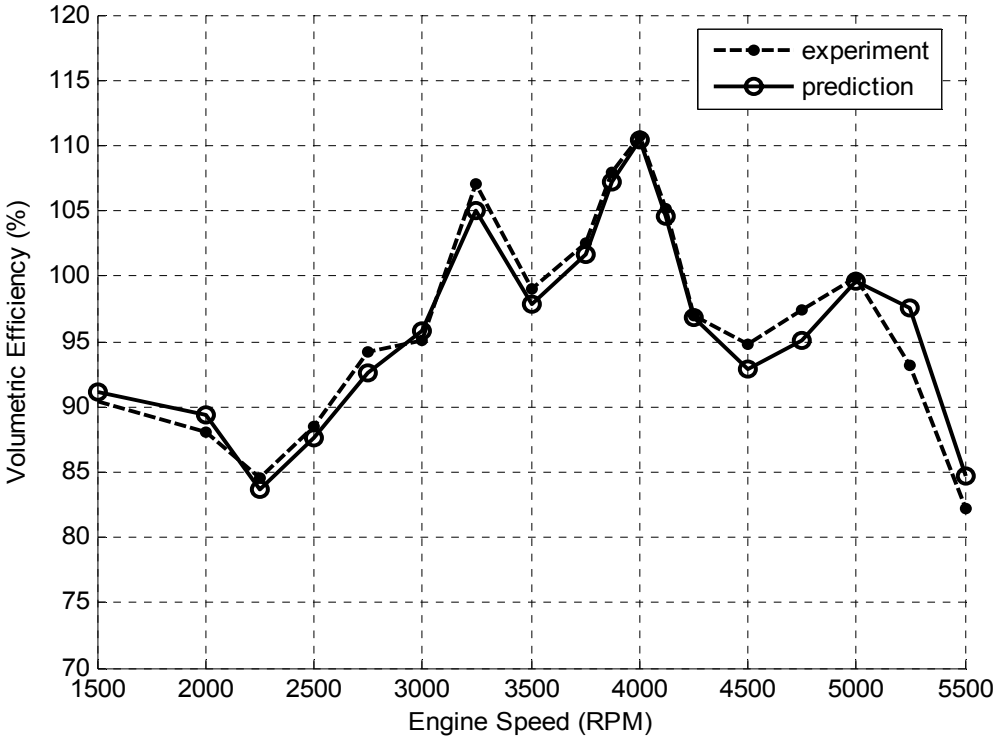

Figure 5.4: Comparison of Predicted and Measured Volumetric Efficiency for Intake #5.

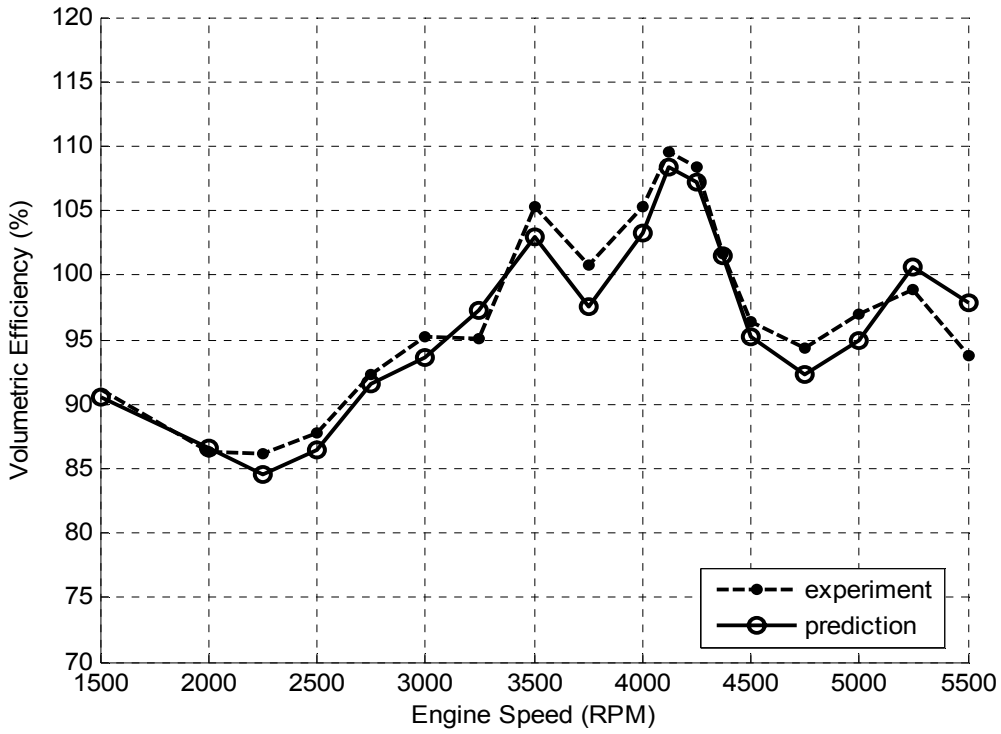

Figure 5.5: Comparison of Predicted and Measured Volumetric Efficiency for Intake #6.

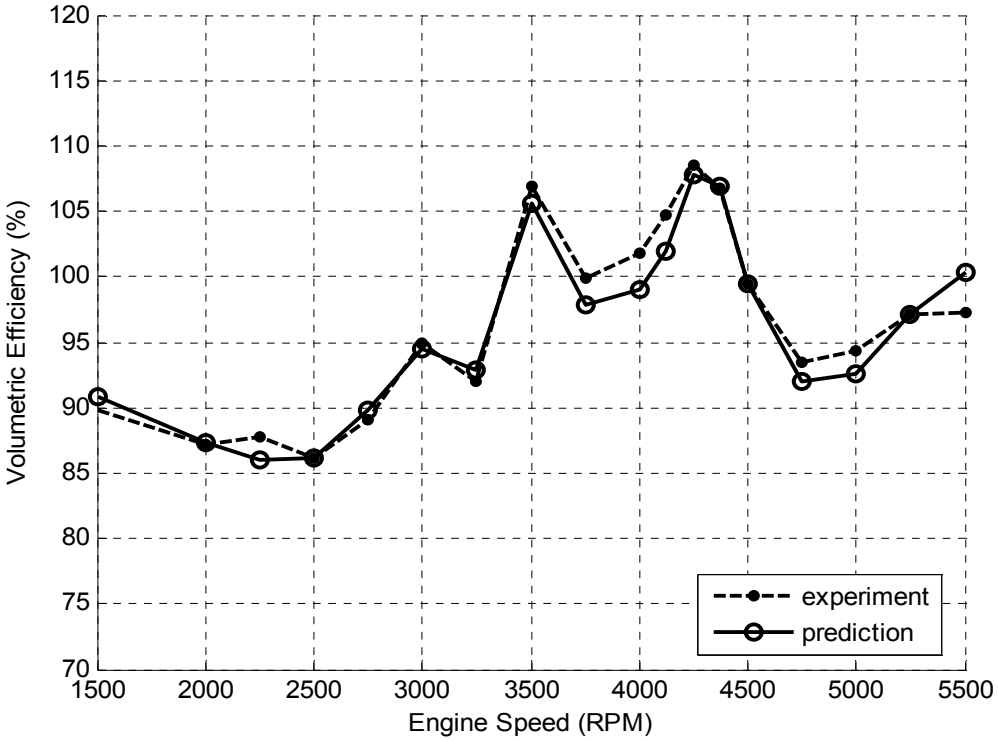

Figure 5.6: Comparison of Predicted and Measured Volumetric Efficiency for Intake #7.

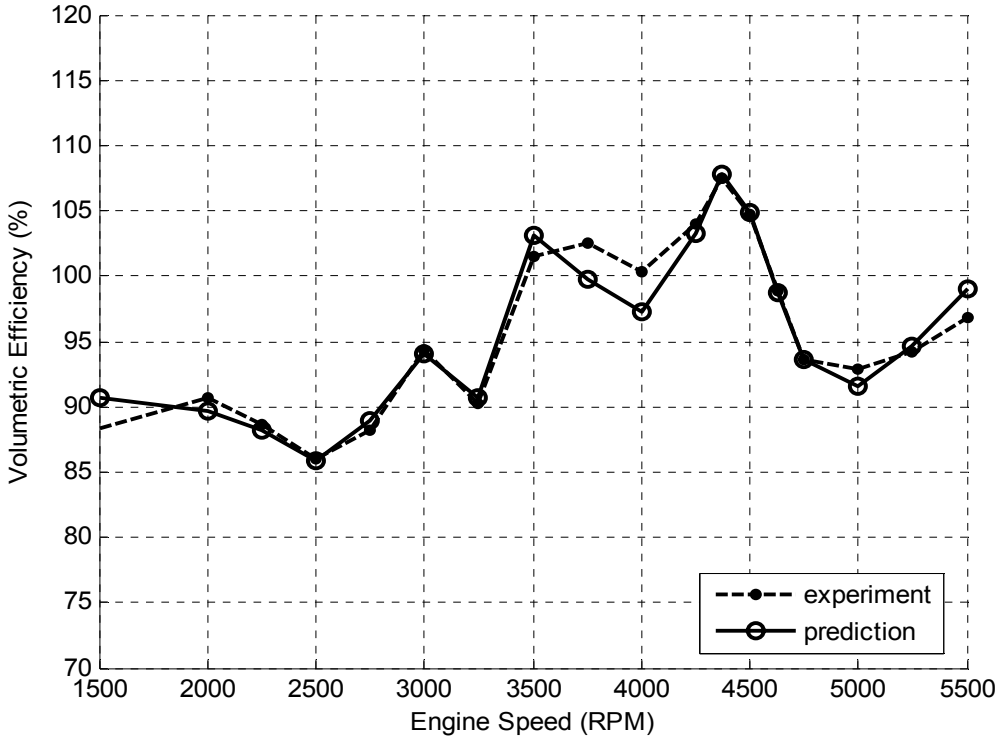

Figure 5.7: Comparison of Predicted and Measured Volumetric Efficiency for Intake #8.

The predicted pressure at i2 is compared to experimental data for intake #2 at the main tuning peak speed of 3850 RPM in Fig. 5.8 in both the (a) time domain and (b) frequency domain. The peak pressure is under-predicted by 2.9%, as are the amplitude of the QSW and the peak pressure during valve overlap. The phasing of the predicted pressure wave is within 2 CAD of the experiment. The SPL of the dominant orders, from 0.5 to 3.5, are predicted within 1 dB of experimental data. The overall trend of the frequency spectrum is predicted well with the largest deviations from experiment occurring above order 7. At the same speed, Fig. 5.9 shows the predicted and experimental pressure at i1 for intake #2. The overall shape of the pressure wave is captured well; the magnitudes and phasing are predicted appropriately; however, similar to the baseline case at this location and near this speed, the peaks of the QSW are predicted to be wider than they actually are, and perturbations around 495 CAD are missed. The frequency spectrum for this location is predicted within 1.5 dB of experimental data for the dominant orders, from 0.5 to 4.5, and follows the trend of experimental data at higher orders.

Figure 5.10 shows the predicted and experimental pressure at i2 for intake #3 at the main tuning peak speed of 3875 RPM. The peak pressure is under-predicted by 2%; as is the amplitude of the QSW. The phasing of the predicted pressure wave is within 3 CAD of experimental data. The SPL at i2 is predicted within 1 dB of the experimental data from order 0.5 to order 3.5, and follows the general trend of the experimental frequency spectrum for higher orders. The predicted and experimental pressures at i1 are compared in Fig. 5.11. The predicted pressure again shows wider peaks and valleys of the QSW than are present in experimental data, while the overall shape and magnitudes

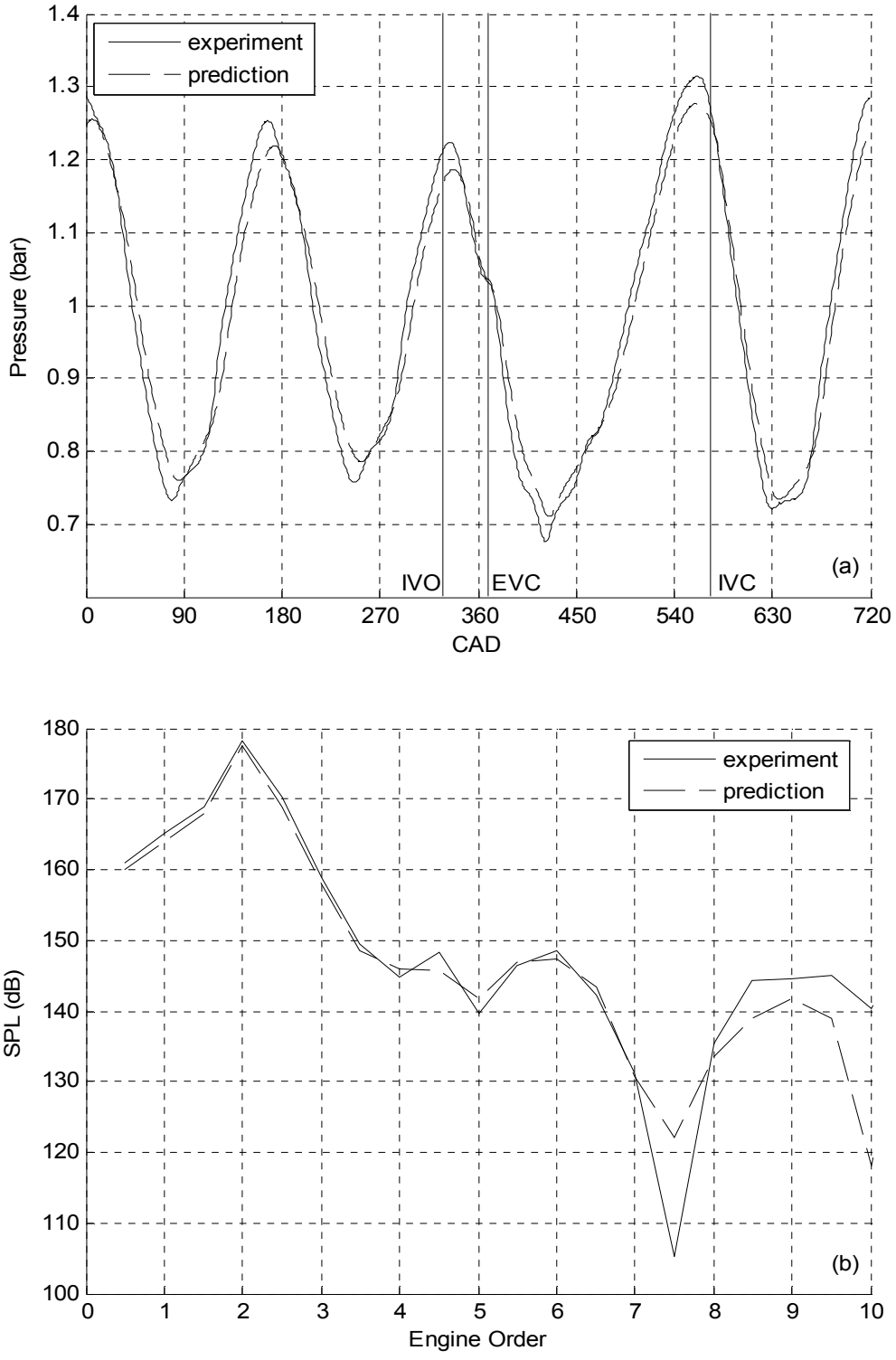

Figure 5.8: Comparison of Predicted and Measured Pressure at i2 at 3850 RPM for Intake #2 in (a) Time Domain and (b) Frequency Domain.

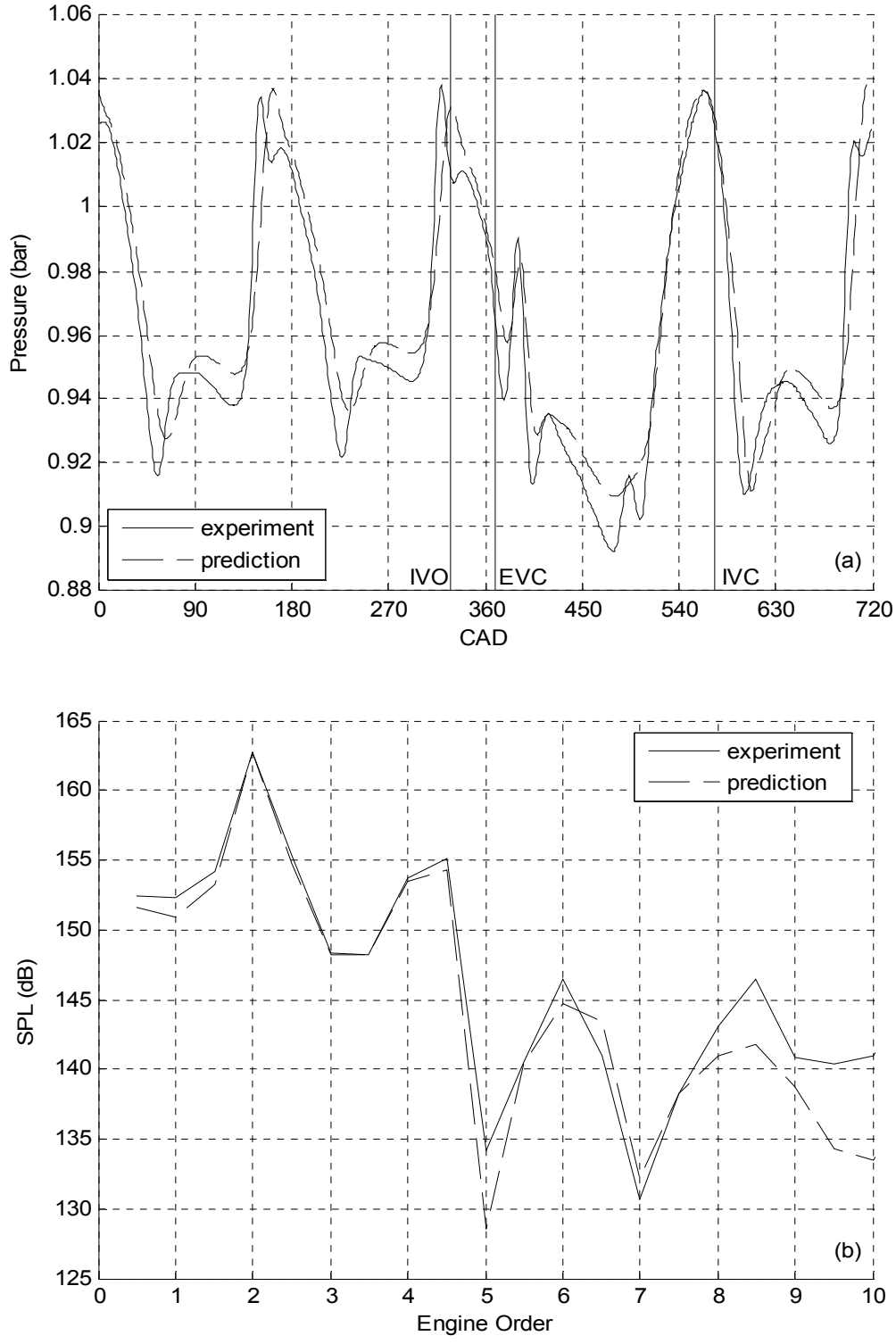

Figure 5.9: Comparison of Predicted and Measured Pressure at i1 at 3850 RPM for Intake #2 in (a) Time Domain and (b) Frequency Domain.

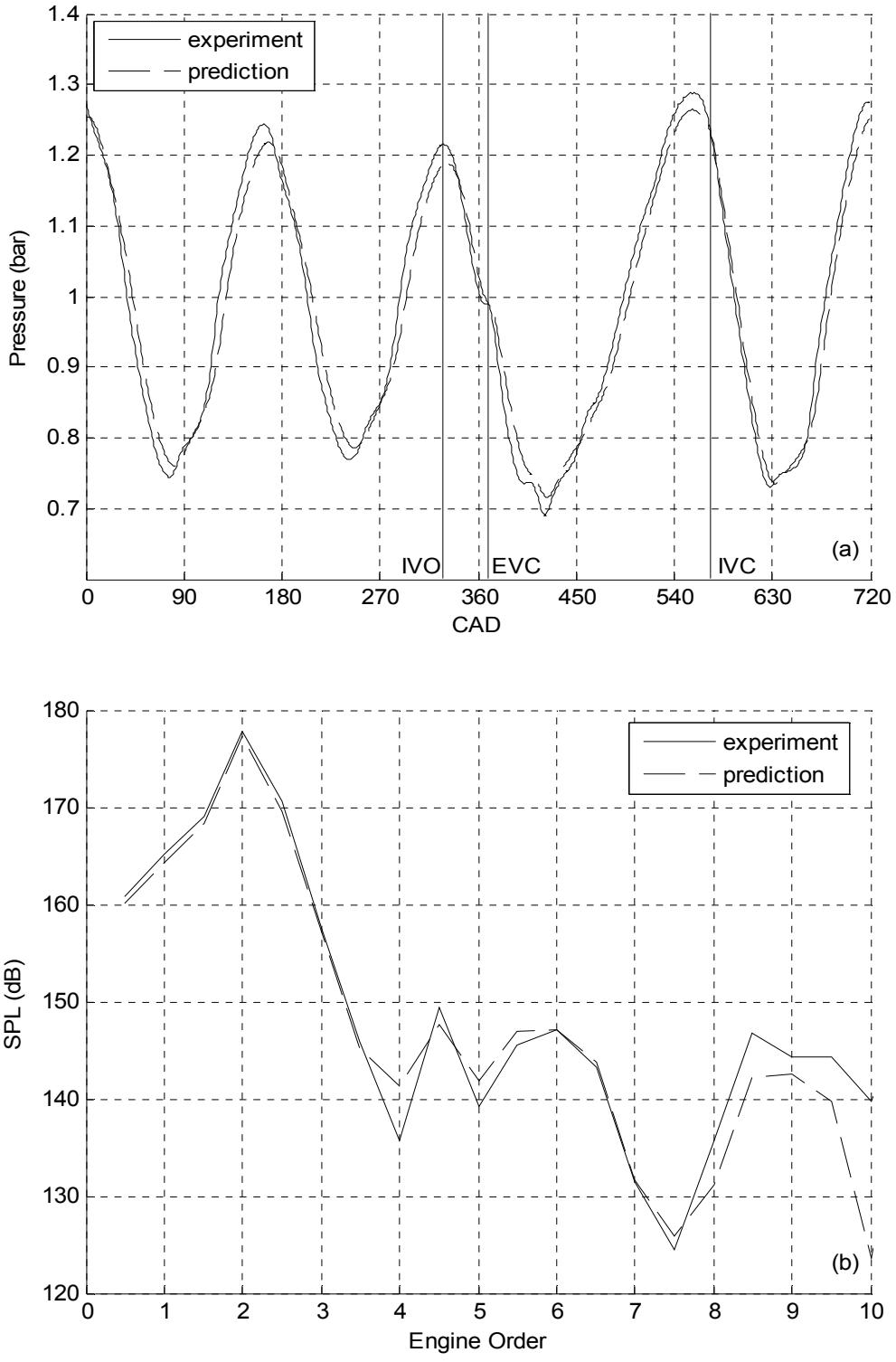

Figure 5.10: Comparison of Predicted and Measured Pressure at i2 at 3875 RPM for Intake #3 in (a) Time Domain and (b) Frequency Domain.

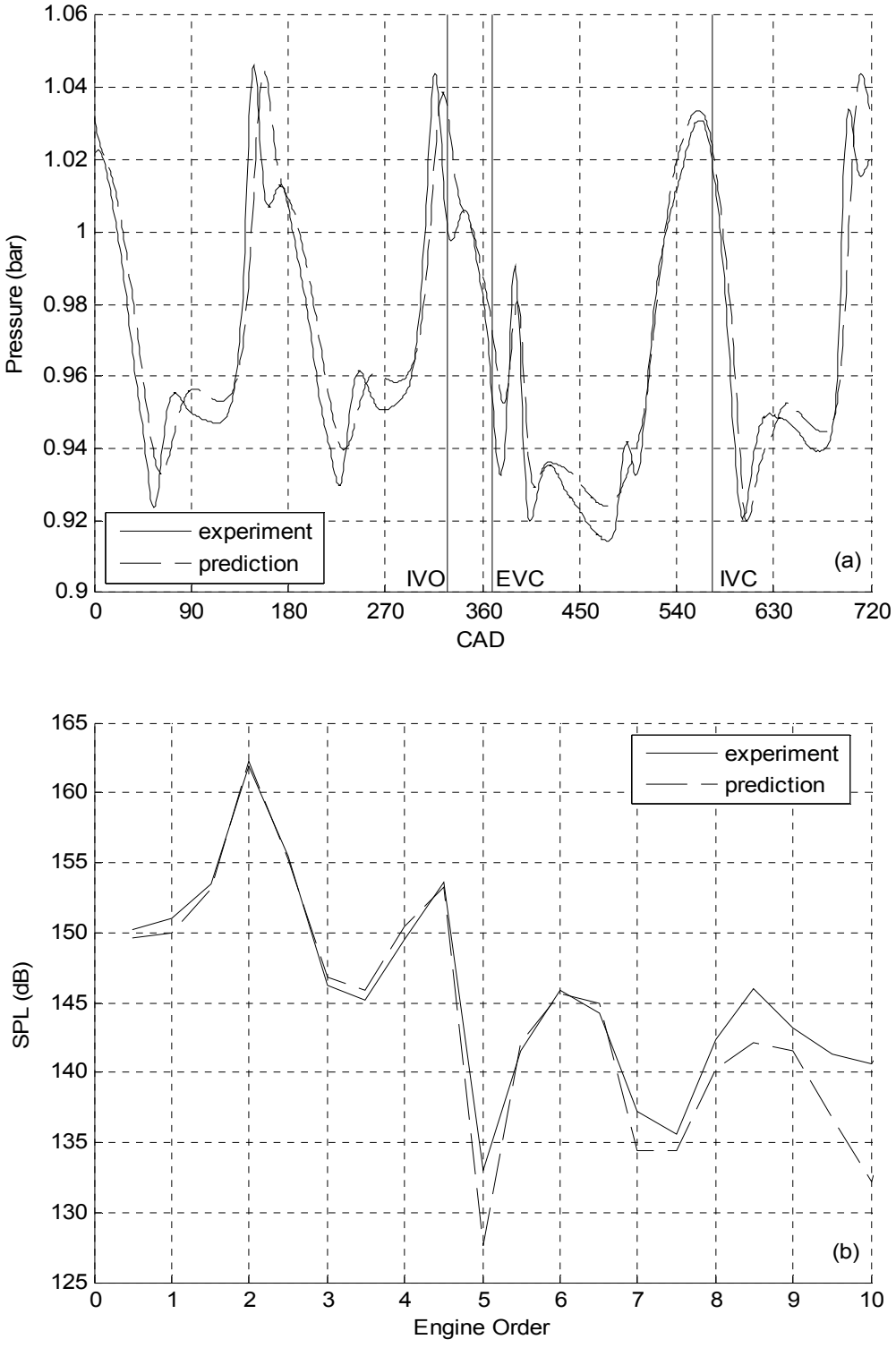

Figure 5.11: Comparison of Predicted and Measured Pressure at i1 at 3875 RPM for Intake #3 in (a) Time Domain and (b) Frequency Domain.

show good agreement. The frequency spectrum at this location is predicted within 1 dB of the experiment from orders 0.5 to 4.5 and follows the trend of the experimental data for higher orders.

The predicted intake pressure at i2 for intake #4 at the main tuning peak speed of 4000 RPM is presented against the experimental data in Fig. 5.12. The magnitude of the wave is predicted adequately, and the phasing is predicted within 3 to 8 CAD of the experiment; this phase shift is slightly larger than those for the intakes discussed in this chapter thus far. The predicted frequency spectrum at i2 is within 1 dB of the experimental data for the dominant orders, from 0.5 to 3.5, and generally follows the trend of the experimental spectrum for orders above 3.5. Figure 5.13 compares the predicted and experimental pressures at i1 at 4000 RPM for intake #4. The pressure during the IV open period is predicted very well as is the overall shape of the QSW. The phasing of the predicted wave is within 9 CAD of the experiment. The large peaks and valleys in the experimental frequency spectrum are captured well; the peaks at order 2 and 4.5 are predicted within 0.5 dB, while the peaks at orders 6 and 8.5 are under-predicted by 2 dB and 1 dB, respectively.

Figure 5.14 shows the predicted intake pressure at i2 for intake #5 at the tuning peak speed of 4000 RPM. The magnitude of the pressure wave is under-predicted by about 3%. The overall shape of the trace is predicted well, and the phasing is within 4 CAD of the experimental data. The predicted frequency spectrum at i2 for intake #5 is within 1 dB for orders 0.5 to 3.5, and follows the general trend of the experimental spectrum. The predicted and experimental pressures at i1 are shown in Fig. 5.15. As observed with intakes discussed earlier in this chapter, the predicted wave during the

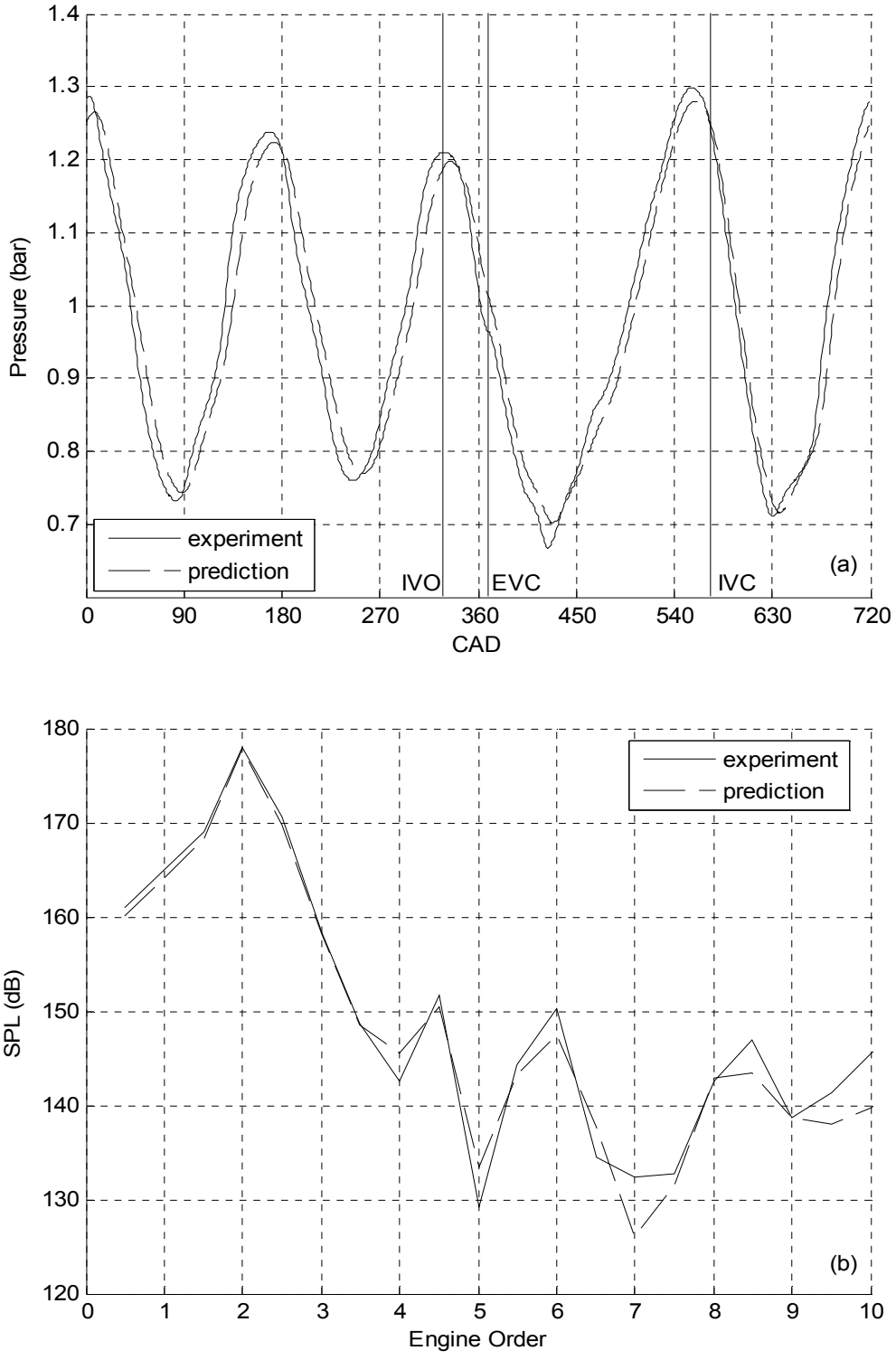

Figure 5.12: Comparison of Predicted and Measured Pressure at i2 at 4000 RPM for Intake #4 in (a) Time Domain and (b) Frequency Domain.

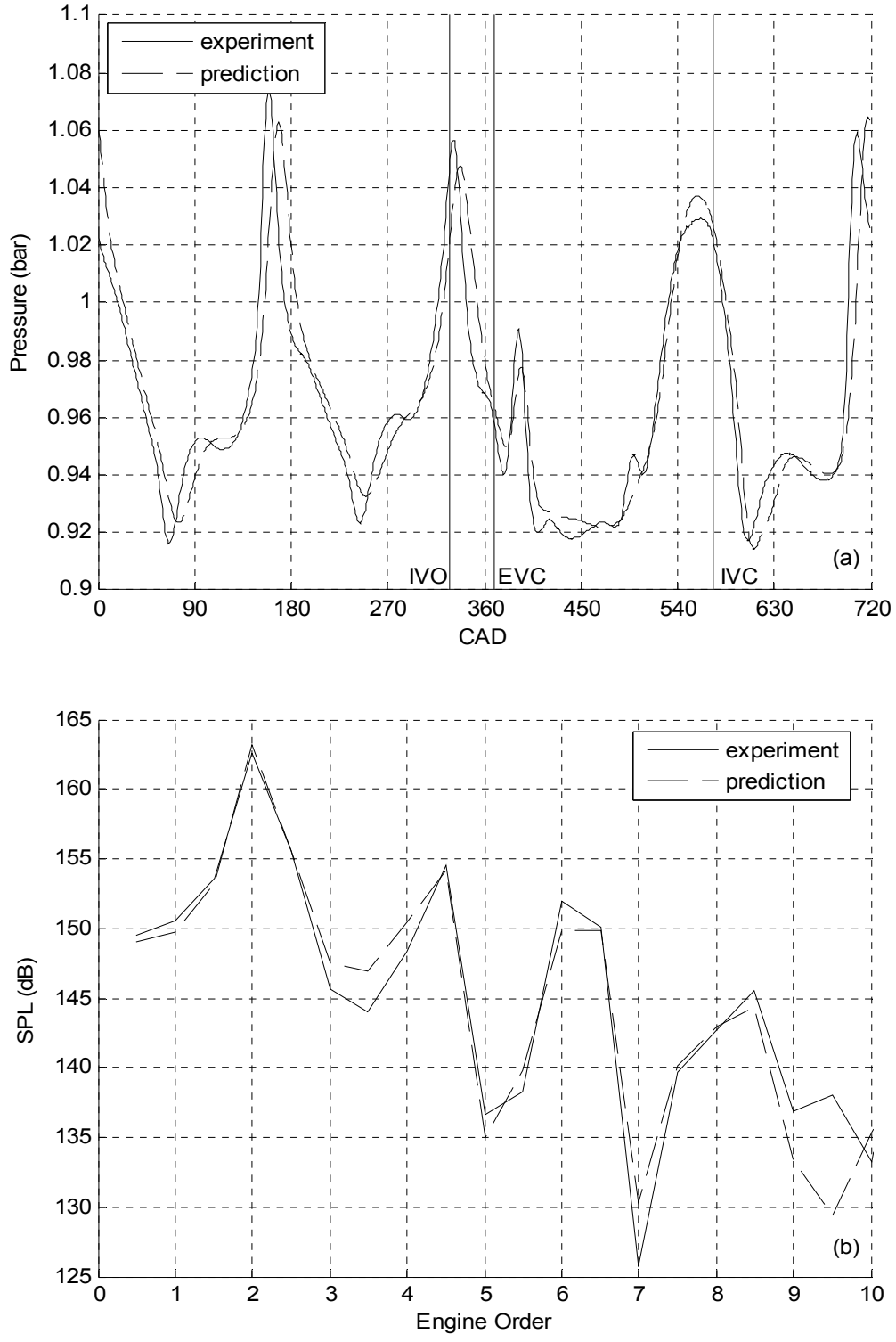

Figure 5.13: Comparison of Predicted and Measured Pressure at i1 at 4000 RPM for Intake #4 in (a) Time Domain and (b) Frequency Domain.

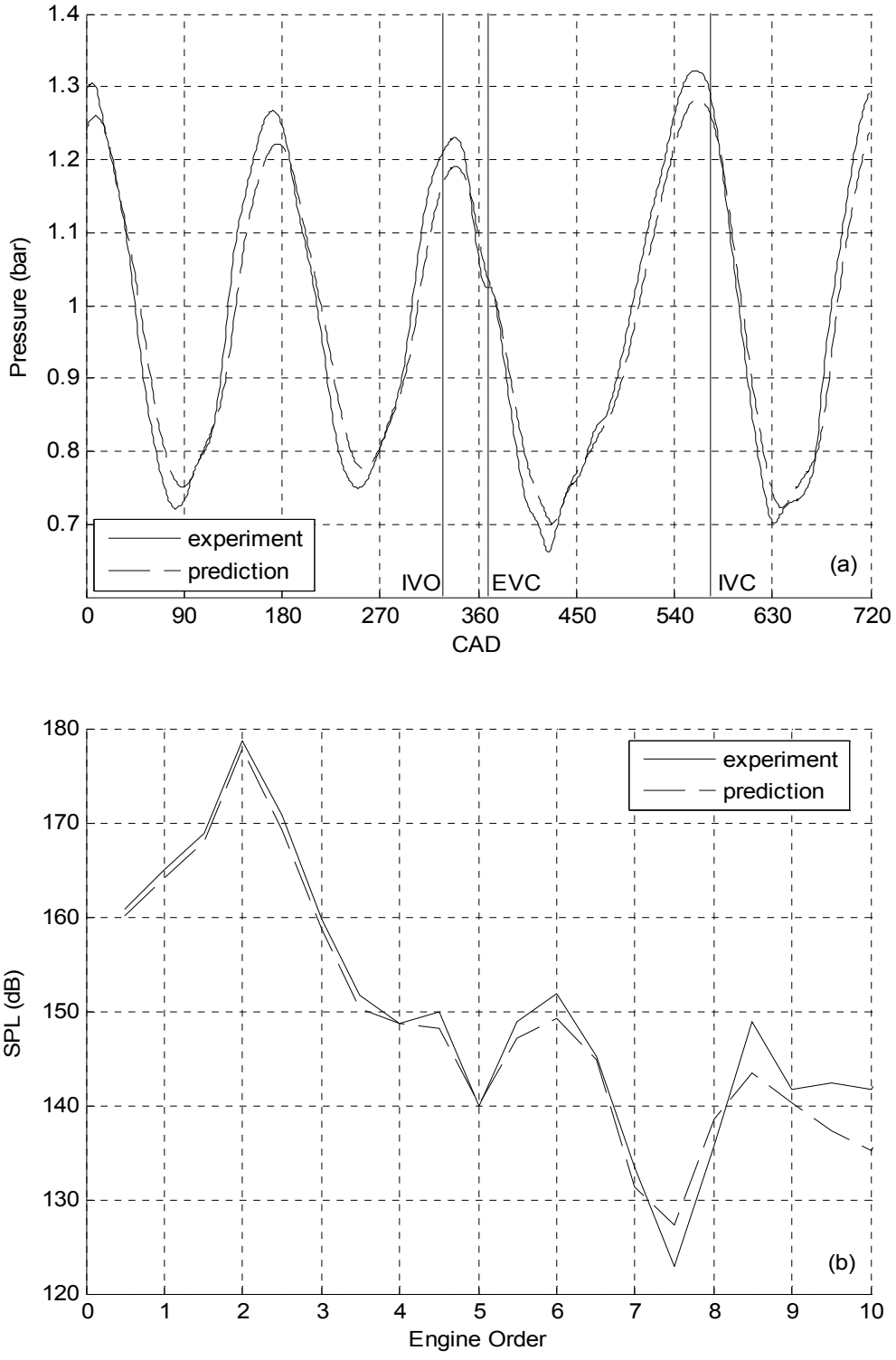

Figure 5.14: Comparison of Predicted and Measured Pressure at i2 at 4000 RPM for Intake #5 in (a) Time Domain and (b) Frequency Domain.

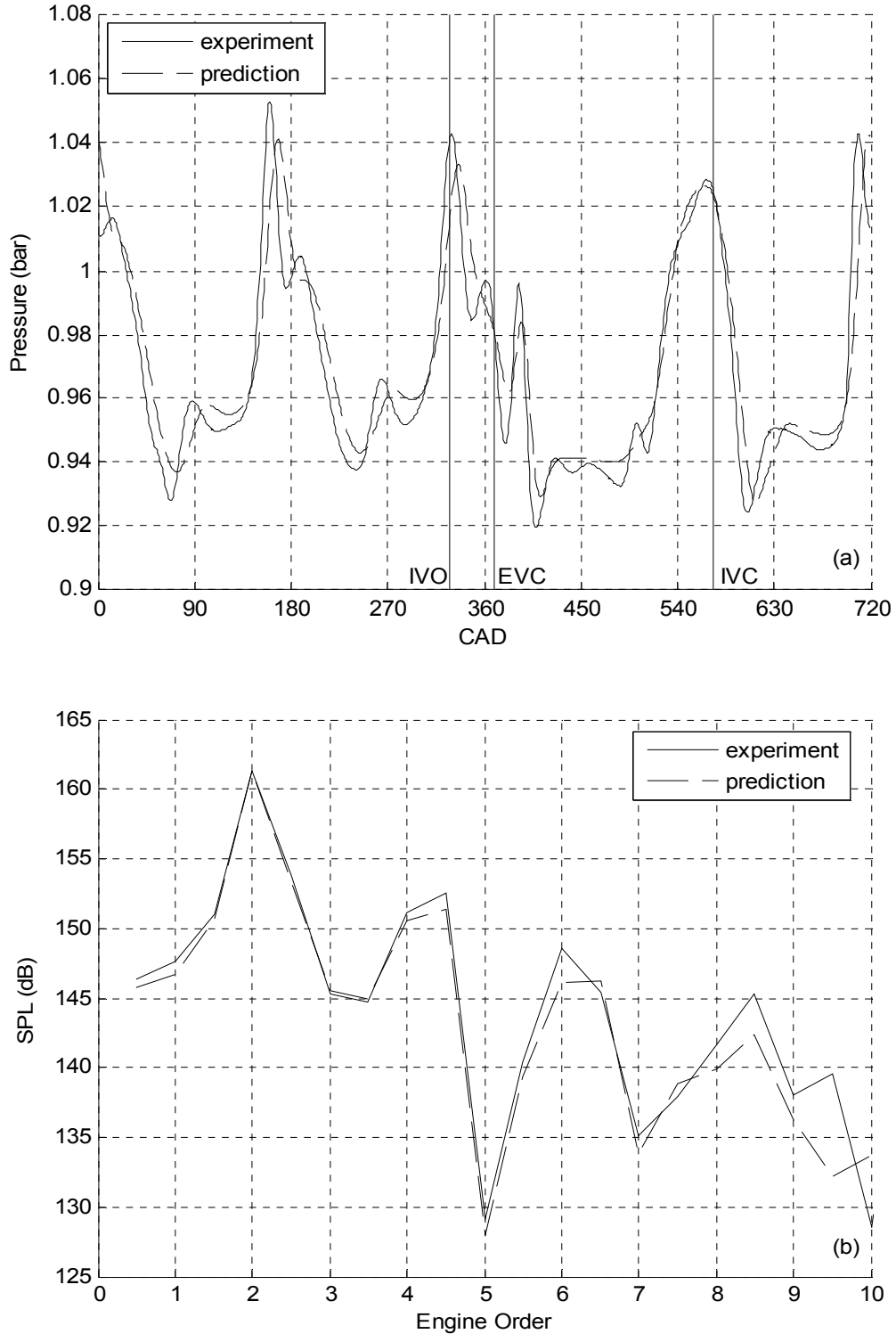

Figure 5.15: Comparison of Predicted and Measured Pressure at i1 at 4000 RPM for Intake #5 in (a) Time Domain and (b) Frequency Domain.

IV open period shows good agreement with the experimental data. Some of the details of the QSW are not predicted, such as the humps at 13, 190, and 362 CAD, and the sharp peaks of the QSW are predicted to be wider than the experimental results. The frequency spectrum at i1 is predicted within 1 dB of experimental data from orders 0.5 to 4, and the SPL of the largest order is predicted almost exactly. The overall shape of the experimental spectrum is adequately captured, with some subtle differences at higher orders.

The predicted intake pressure of intake #6 at i2 at the main tuning peak speed of 4125 RPM is shown in Fig. 5.16. The code shows good agreement with the experimental data. The magnitudes are predicted to within 1% of the pressure transducer's overall range, and the phasing of the predicted trace is within 6 CAD of the experimental wave. In the frequency domain, engine orders from 0.5 to 3 are predicted to within 0.5 dB of experimental data. The overall trend of the predicted spectrum follows that of experiment, with the largest discrepancies occurring at order 4 (15 dB), 5 (19 dB), and 7 (11 dB). For the same intake configuration, Fig. 5.17 shows the predicted and experimental pressures at the i1 location. Although some subtleties in the pressure wave are missed, the overall shape shows a good agreement with the experimental data. Generally, MANDY tends to over-predict the peak pressures at 163, 328, 552, and 712 CAD by 1 to 2%. In the frequency domain, the code over-predicts the peak SPL by 1.3 dB and generally over-predicts the contributions from orders 1.5 to 6, with the greatest over-prediction, 14 dB, occurring at order 4. The trend of the experimental frequency spectrum is captured with subtle differences at higher orders.

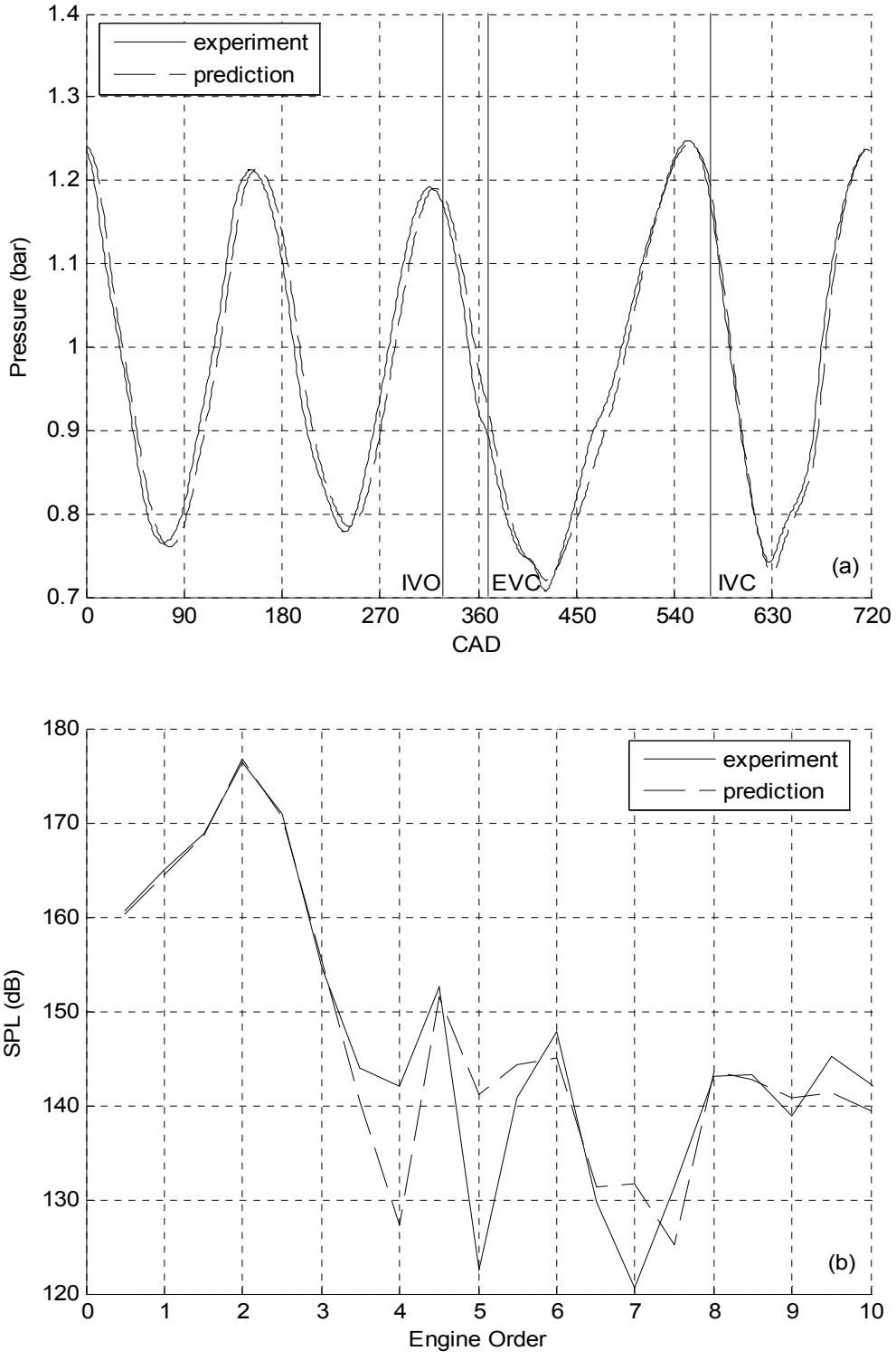

Figure 5.16: Comparison of Predicted and Measured Pressure at i2 at 4125 RPM for Intake #6 in (a) Time Domain and (b) Frequency Domain.

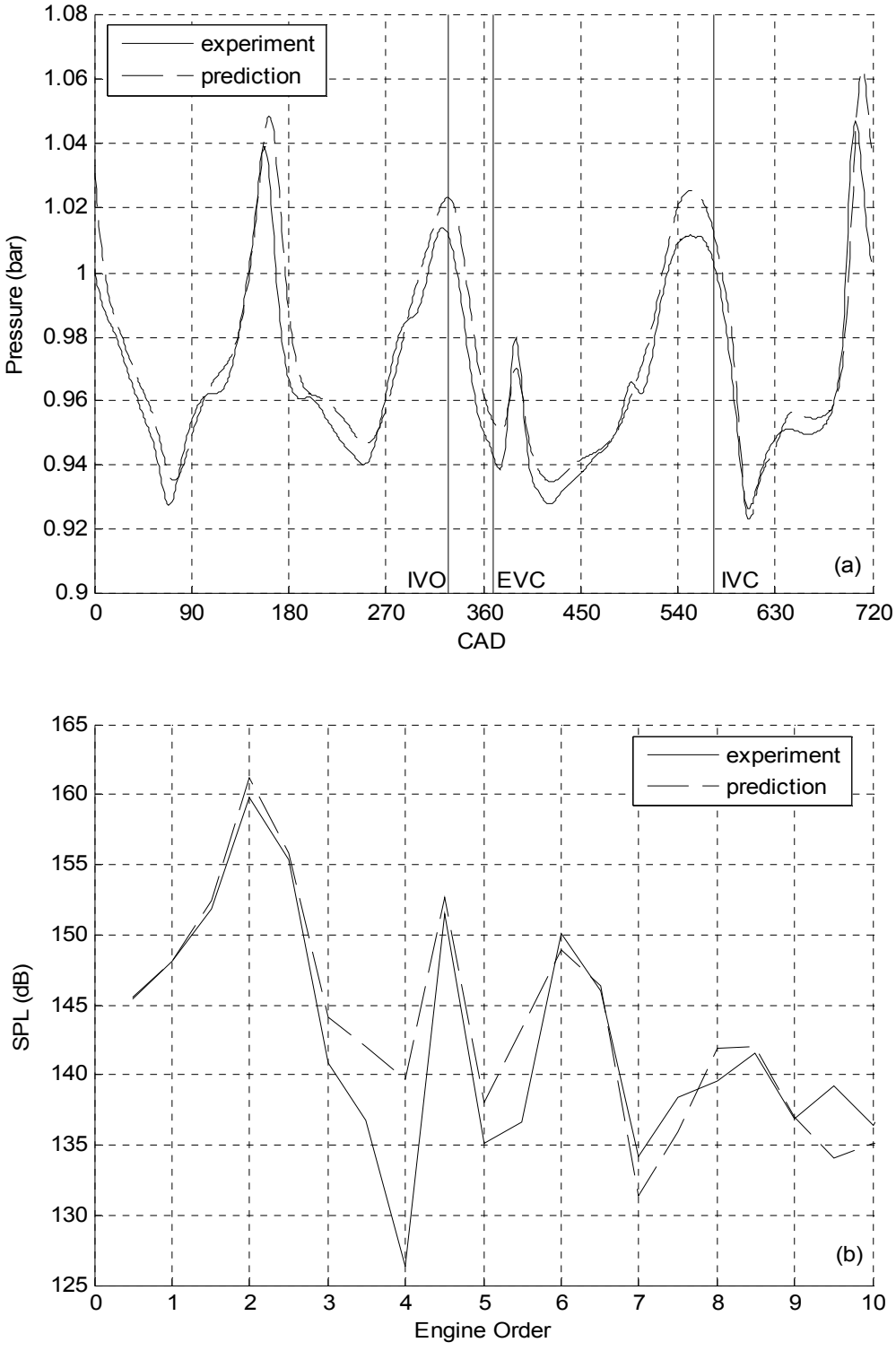

Figure 5.17: Comparison of Predicted and Measured Pressure at i1 at 4125 RPM for Intake #6 in (a) Time Domain and (b) Frequency Domain.

The predicted intake pressure for intake #7 at the i2 location at the tuning peak speed of 4250 RPM is shown against the experimental trace in Fig. 5.18. The predicted and experimental pressures show good agreement; the magnitudes at the peaks and valleys are within 1% of the experimental data, and the phasing is within 6 CAD. The predicted frequency spectrum for this intake is within 1 dB of the experimental spectrum from order 0.5 to 1.5 and nearly identical to experimental data for orders 2 to 3.5. The general trend of the rest of the experimental frequency spectrum is predicted adequately. Figure 5.19 shows the pressure at i1 for intake #7 at 4250 RPM. The general trend of the curve is captured well, although it again misses some of the smaller perturbations seen in the experiment. The magnitudes are predicted appropriately, and the phasing within 7 CAD of the experimental data. The frequency spectra show that the measured SPL is predicted within 1.3 dB of the experiment from orders 0.5 to 2.5. The overall trend of the predicted spectrum shows good agreement with measurements, however a general over-prediction of SPL is observed from orders 3 to 5.5, and an under-prediction at orders 7, 7.5, and 9.5.

The predicted and measured intake pressure at i2 for the largest taper, intake #8 is shown for the tuning peak speed of 4375 RPM in Fig. 5.20. As observed with the other tapers presented in this chapter, the magnitude and overall shape of the wave are predicted well. For this intake, the predicted pressure wave trails the experiment by 5 to 10 CAD, which is the largest shift seen at the tuning peak speed of any of the tapers at this location. Since this is the largest taper, the multi-dimensional effects may be more pronounced than they were with the other tapers, causing a larger discrepancy between the measured intake pressure and that predicted by the quasi-1D code at i2. The

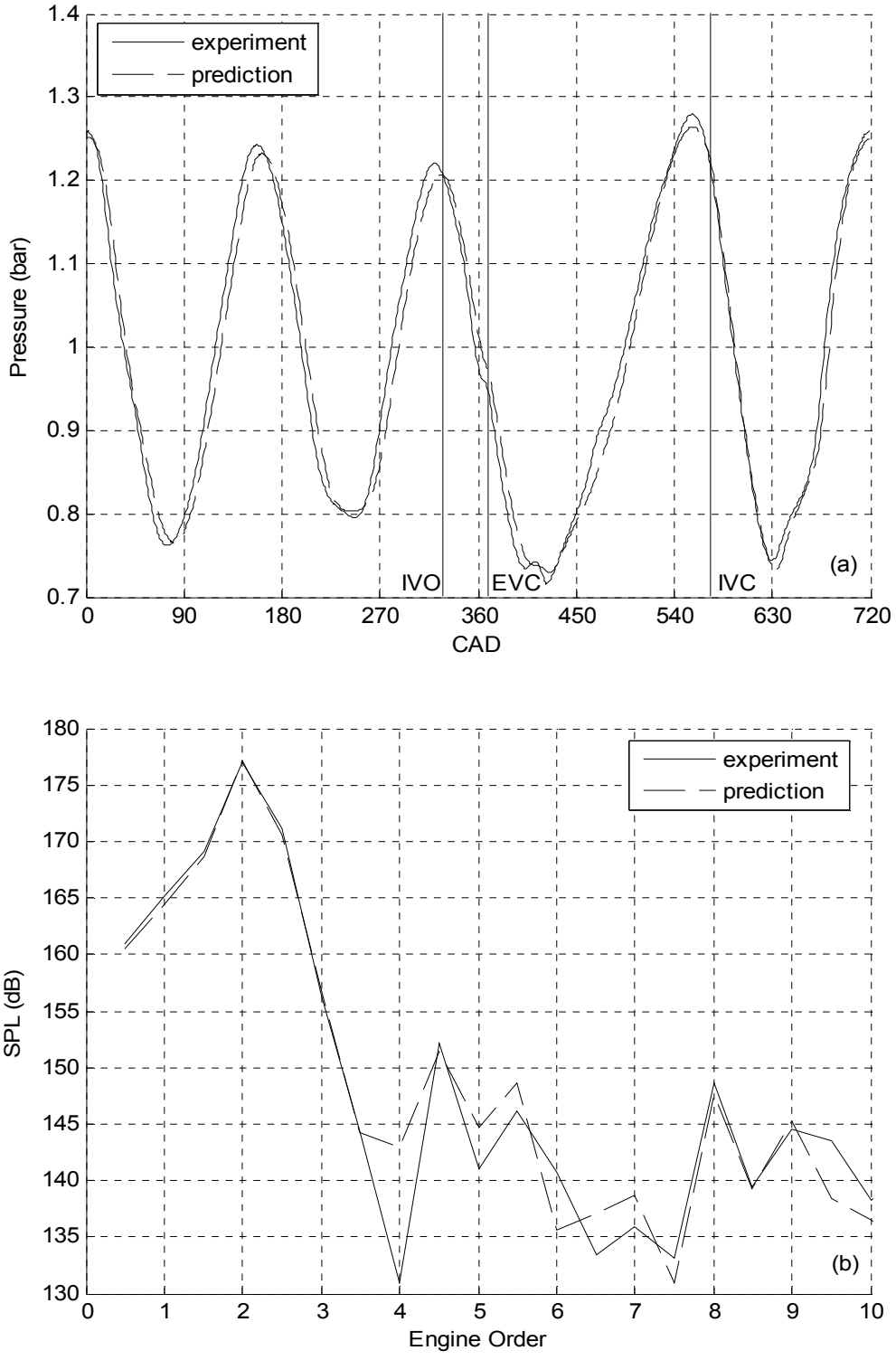

Figure 5.18: Comparison of Predicted and Measured Pressure at i2 at 4250 RPM for Intake #7 in (a) Time Domain and (b) Frequency Domain.

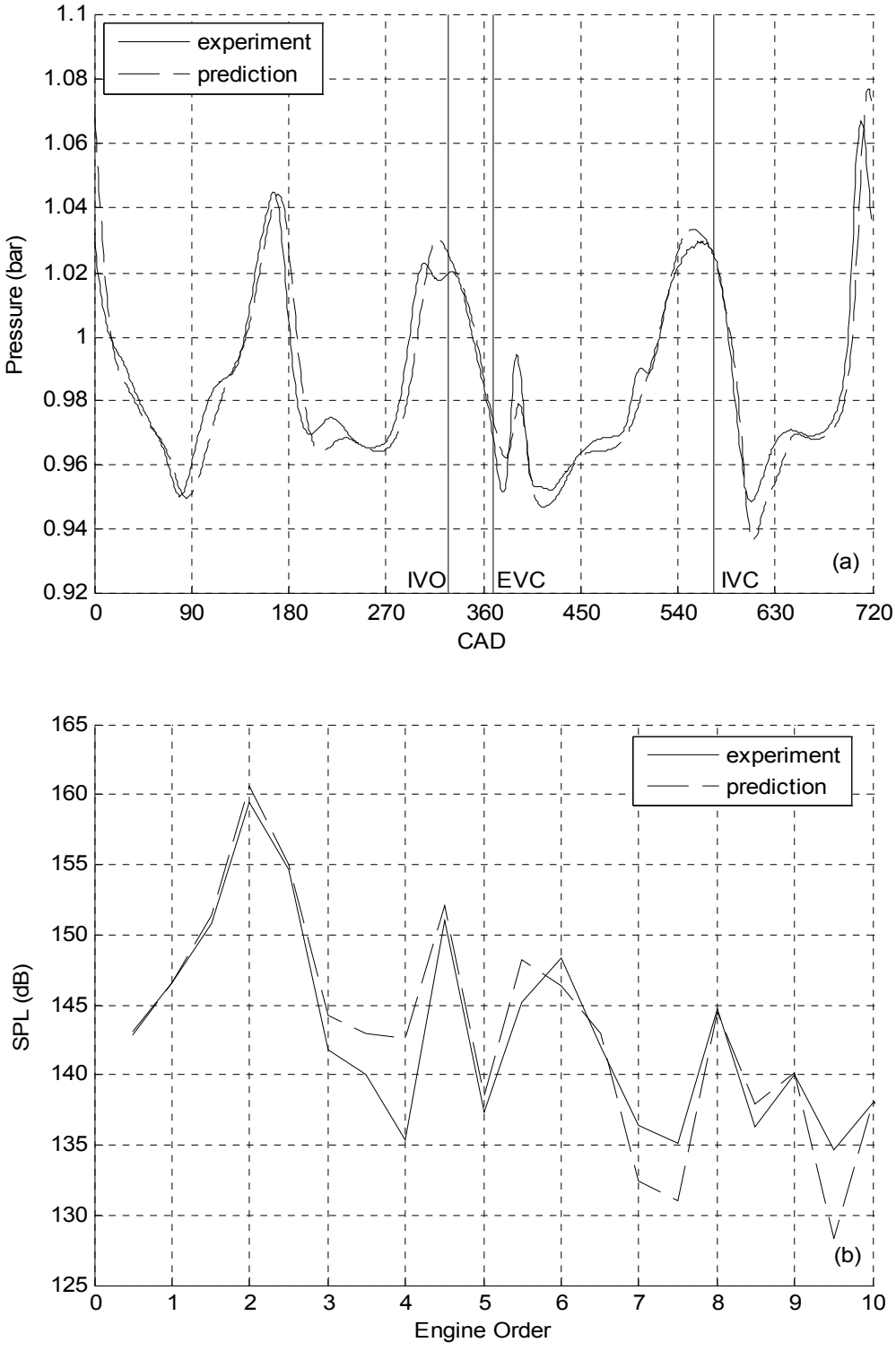

Figure 5.19: Comparison of Predicted and Measured Pressure at i1 at 4250 RPM for Intake #7 in (a) Time Domain and (b) Frequency Domain.

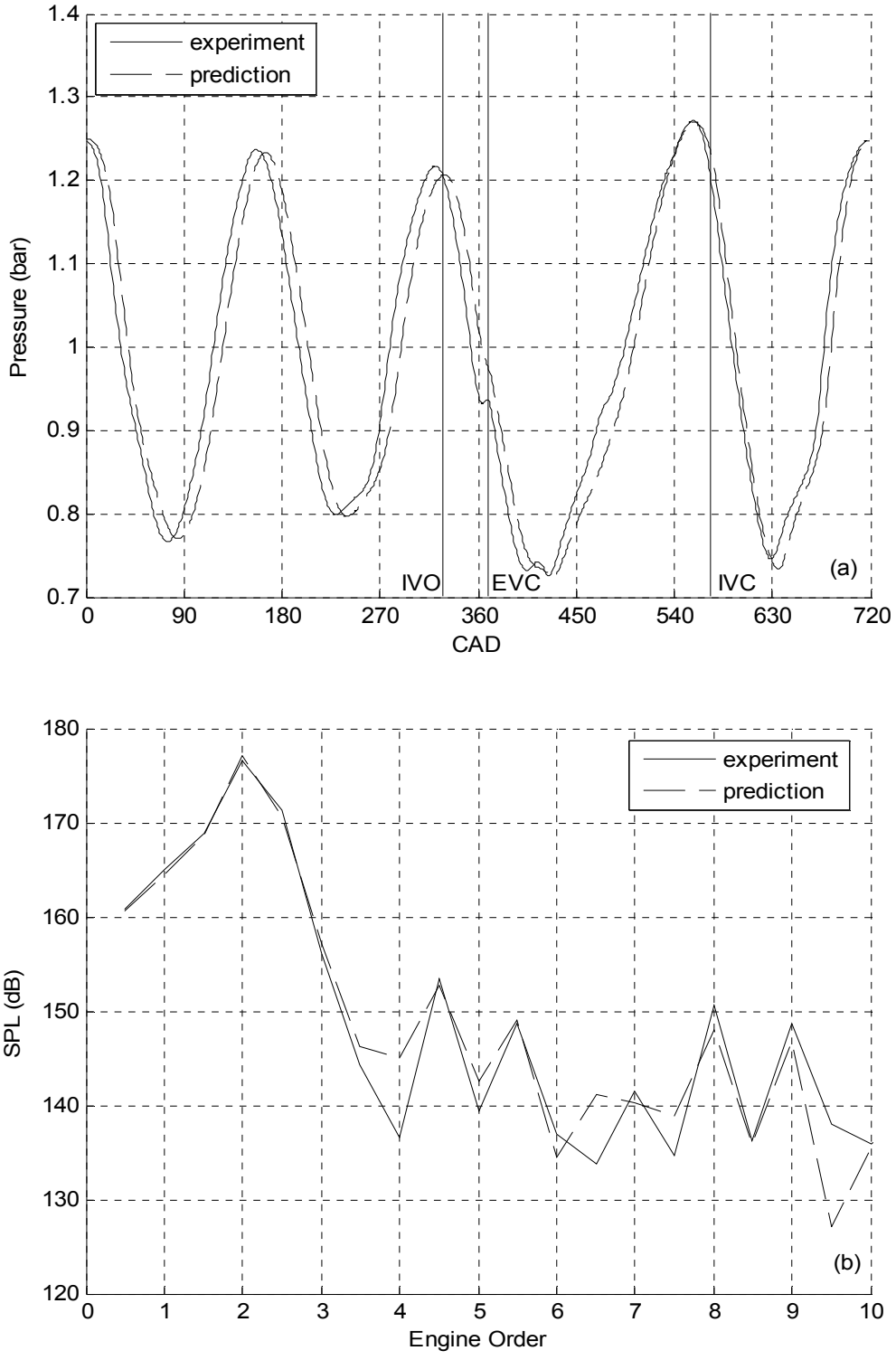

Figure 5.20: Comparison of Predicted and Measured Pressure at i2 at 4375 RPM for Intake #8 in (a) Time Domain and (b) Frequency Domain.

predicted frequency spectrum, which the phase shift does not influence, has almost the same SPL for the dominant orders, from 0.5 to 3, as the experimental spectrum. The overall trend of the measured spectrum at higher orders is predicted accurately, with some subtle differences from orders 6 to 7.5 and at order 9.5. Figure 5.21 compares the predicted and measured pressure at i1 for intake #8. The overall trend of the pressure is predicted adequately, but as with the predicted wave at the i2 location, there is a phase shift of 5 to 10 CAD. The pressure peaks are over-predicted slightly, by an average of 1.3%. The peak SPL at order 2 is over-predicted by 2 dB, and the frequency spectrum is generally over-predicted from order 1 to 5.5. The SPL at order 4 is over-predicted by 12 dB, and the peaks in SPL at orders 4.5 and 5.5 are over-predicted by 1.3 dB and 2.1 dB, respectively.

In general, intake pressure predictions from MANDY show a good agreement with experimental data for all tapers. Even for intake #8, where multi-dimensional effects seemed to be more pronounced, the phase shift in the predicted pressure is no worse than that for the baseline case at 4750 RPM (Fig. 4.8). The pressures at i2 for all tapers were predicted to have appropriate magnitudes of the peaks and valleys, and the frequencies most likely to affect the engine tuning agreed well with the experimental data. The pressure at i1 was not predicted as well, with some of the smaller nuances of the experimental waves being missed. This is understandable since multi-dimensional effects from the inlet region of the duct are more likely to be present at the i1 location, and are not accounted for in the inherently 1D code.

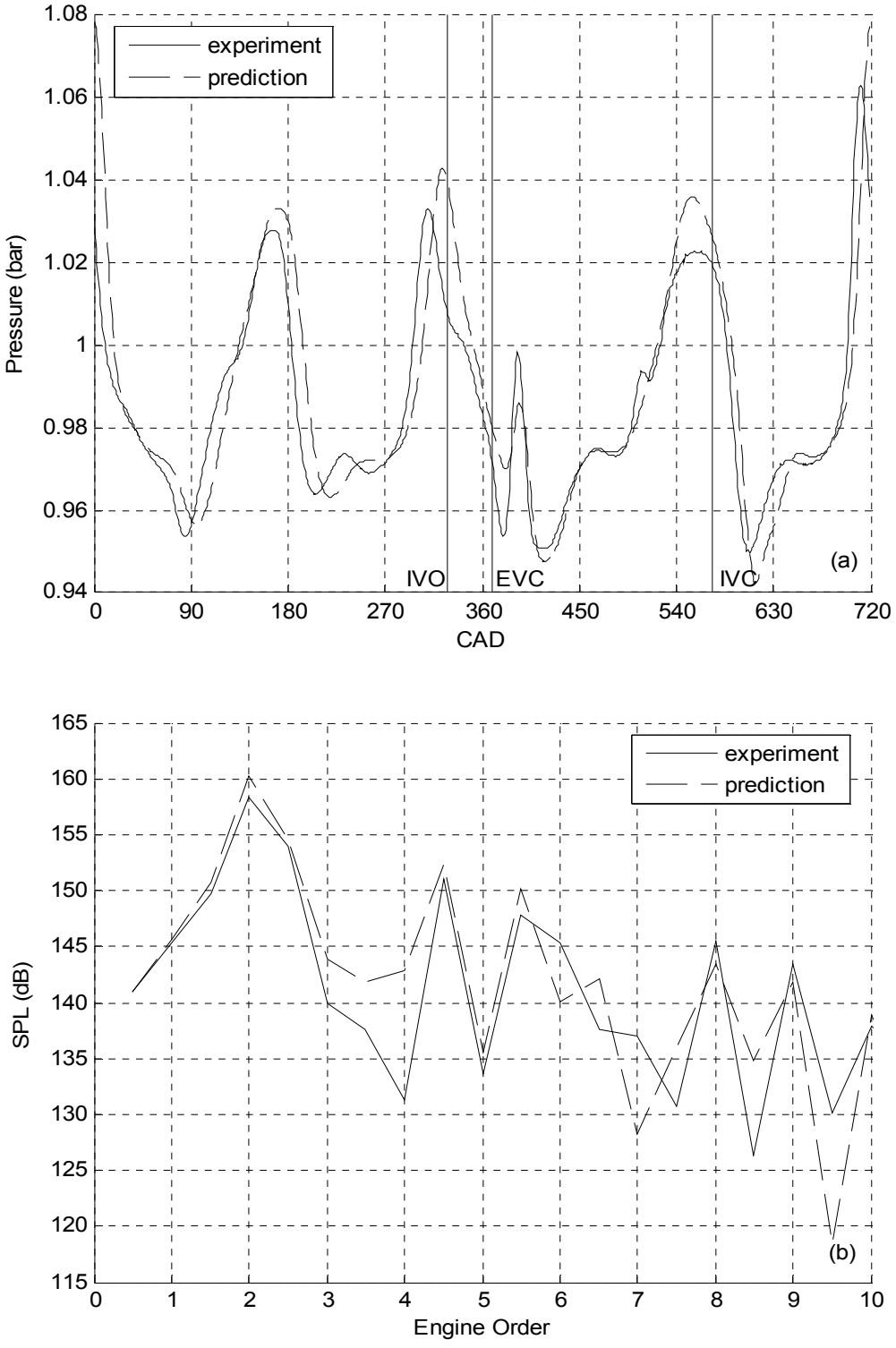

Figure 5.21: Comparison of Predicted and Measured Pressure at i1 at 4375 RPM for Intake #8 in (a) Time Domain and (b) Frequency Domain.

5.2 Bellmouth Group Predictions

For intakes #9, 11, and 12 in the bellmouth group (refer to Fig. 2.5c and Table 2.3), predicted volumetric efficiency is presented against experimental data from 1500 to 5500 RPM in this section. The predicted intake pressure at i2 and i1 are compared to experimental data at the main tuning peak speeds for each intake, shown in Table 5.3. Intake #10 is not presented because the experimental data presented in Chapter 3 shows that it is essentially equivalent to the baseline case; thus, the end correction for intake #10 is the same as that of the baseline, and it would be modeled exactly like the baseline.

Intake	Major Tuning Peak Speed (RPM)
#9	3850
#11	3750
#12	3650

Table 5.3: Major Tuning Peak Speeds for the Bellmouth Group.

Figure 5.22 shows the comparison of predicted and experimental volumetric efficiency for the smallest-radius bellmouth ($R_i/D = 0.05$), intake #9. To account for the sharp inlet radius, a loss factor of 0.2 (Miller, 1990) was applied to the first 2 cm of the duct after the ambient junction. Experimental data suggests that for all other intakes, the inlet radius is large enough to make inlet losses negligible; thus, an inlet loss factor was only used for intake #9. The predicted volumetric efficiency is within 1.0% average error of the experimental data. The largest discrepancies occur at 2000 RPM (over-prediction of 3.0%), and 4250 RPM (under-prediction of 2.7%). The peak volumetric efficiency is predicted within the error of experimental measurement. Without the loss factor

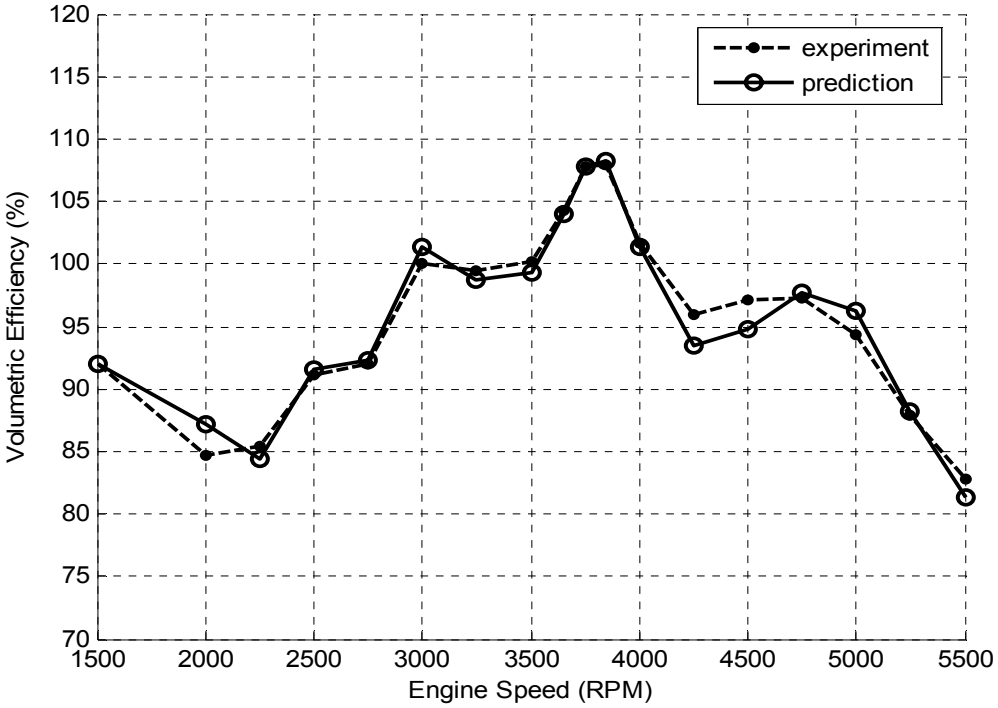

Figure 5.22: Comparison of Predicted and Measured Volumetric Efficiency for Intake #9.

applied, the average error increases to 1.8% and the maximum error to 3.8%. The predicted volumetric efficiency of intake #11 is compared to experiment in Fig. 5.23. The volumetric efficiency for this intake is predicted within 2.5% of experimental data everywhere, and with an average error of 1.1%. The main tuning peak is predicted within the error of experimental volumetric efficiency measurement. Figure 5.24 shows predicted versus experimental volumetric efficiency for the largest-radius bellmouth ($R_i/D = 1.0$), intake #12. The volumetric efficiency is generally predicted within 2.0% for all speeds, with an average error less than 1.0%.

Figure 5.25 shows the intake pressure at the i2 location for intake #9 at the peak volumetric efficiency location of 3850 RPM. Overall, the predicted pressure shows good agreement with the experiment, indicating that applying the loss coefficient to the inlet is an appropriate way to model sharp entrance regions. The peak pressure during the IV open period is under-predicted by 2.7%, while the QSW amplitude is over-predicted slightly. Without the inlet loss factor applied, the peak pressure matches the experiment; however, the peaks of the QSW are over-predicted by 5.6%. The peaks and valleys of the predicted QSW are within 5 CAD of the measured wave. The peak SPL is predicted very close to the experiment as are neighboring orders. The general form of the predicted frequency spectrum follows that of the measured data with subtle differences present at higher engine orders. The intake pressure at i1 for intake #9 is shown in Fig. 5.26. The predicted pressures during the IV open period matches very well with the experiment. The shape of the predicted QSW is similar to that of the measured wave; the most noticeable difference is the dip at the beginning of each expansion wave (at 73, 246, and 613 CAD) that is not present in the experimental data. The predicted frequency

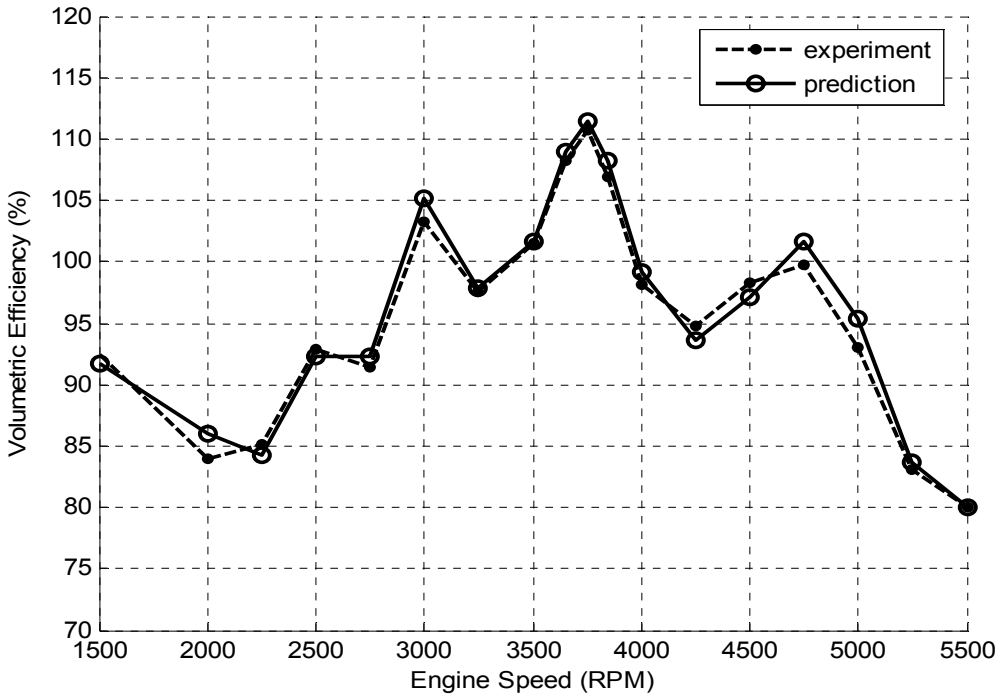

Figure 5.23: Comparison of Predicted and Measured Volumetric Efficiency for Intake #11.

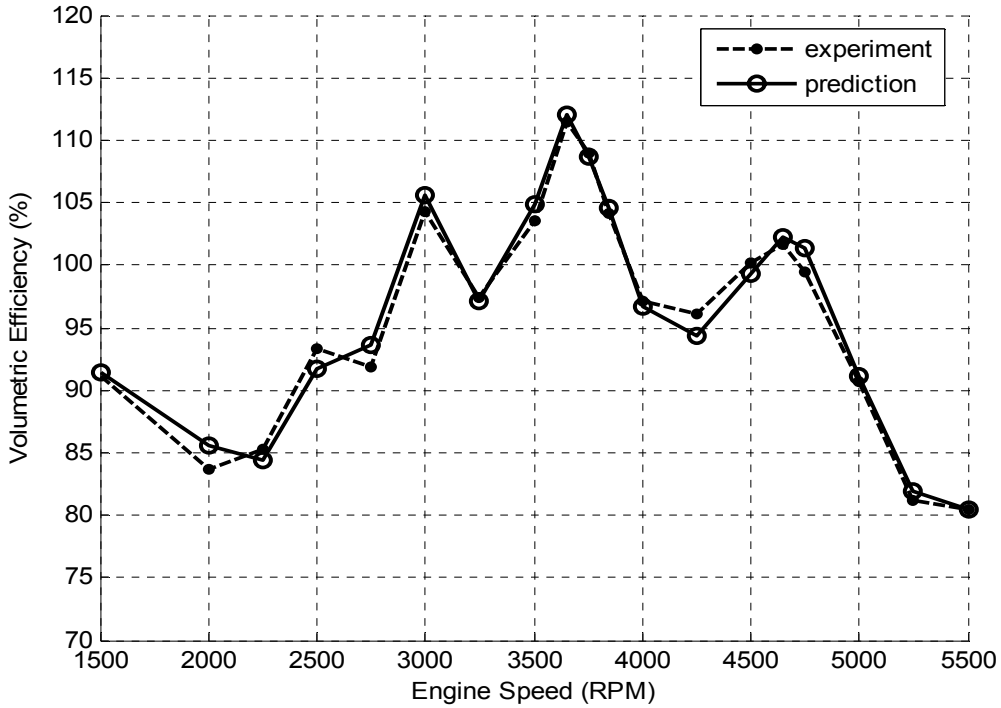

Figure 5.24: Comparison of Predicted and Measured Volumetric Efficiency for Intake #12.

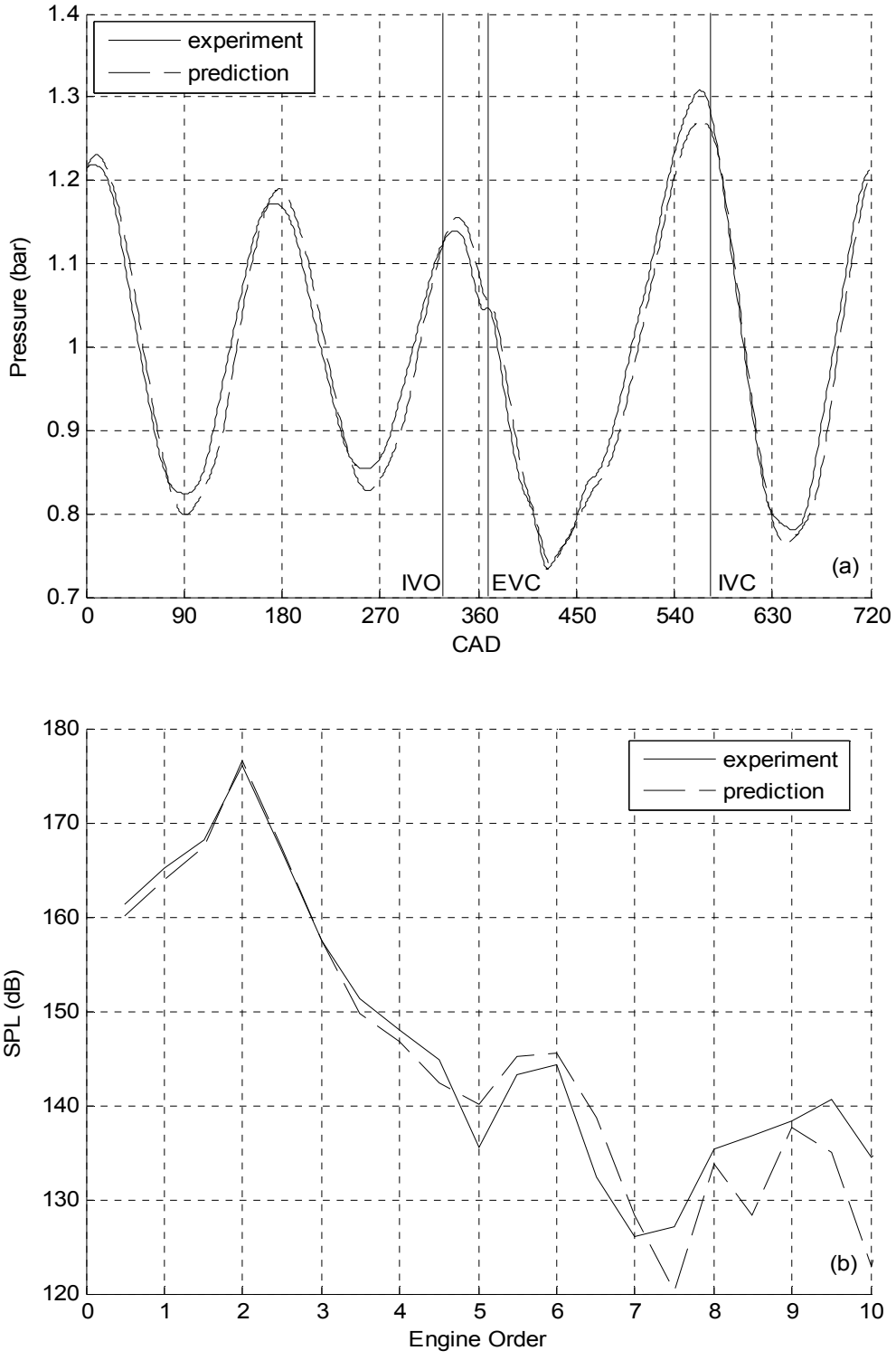

Figure 5.25: Comparison of Predicted and Measured Pressure at i2 at 3850 RPM for Intake #9 in (a) Time Domain and (b) Frequency Domain.

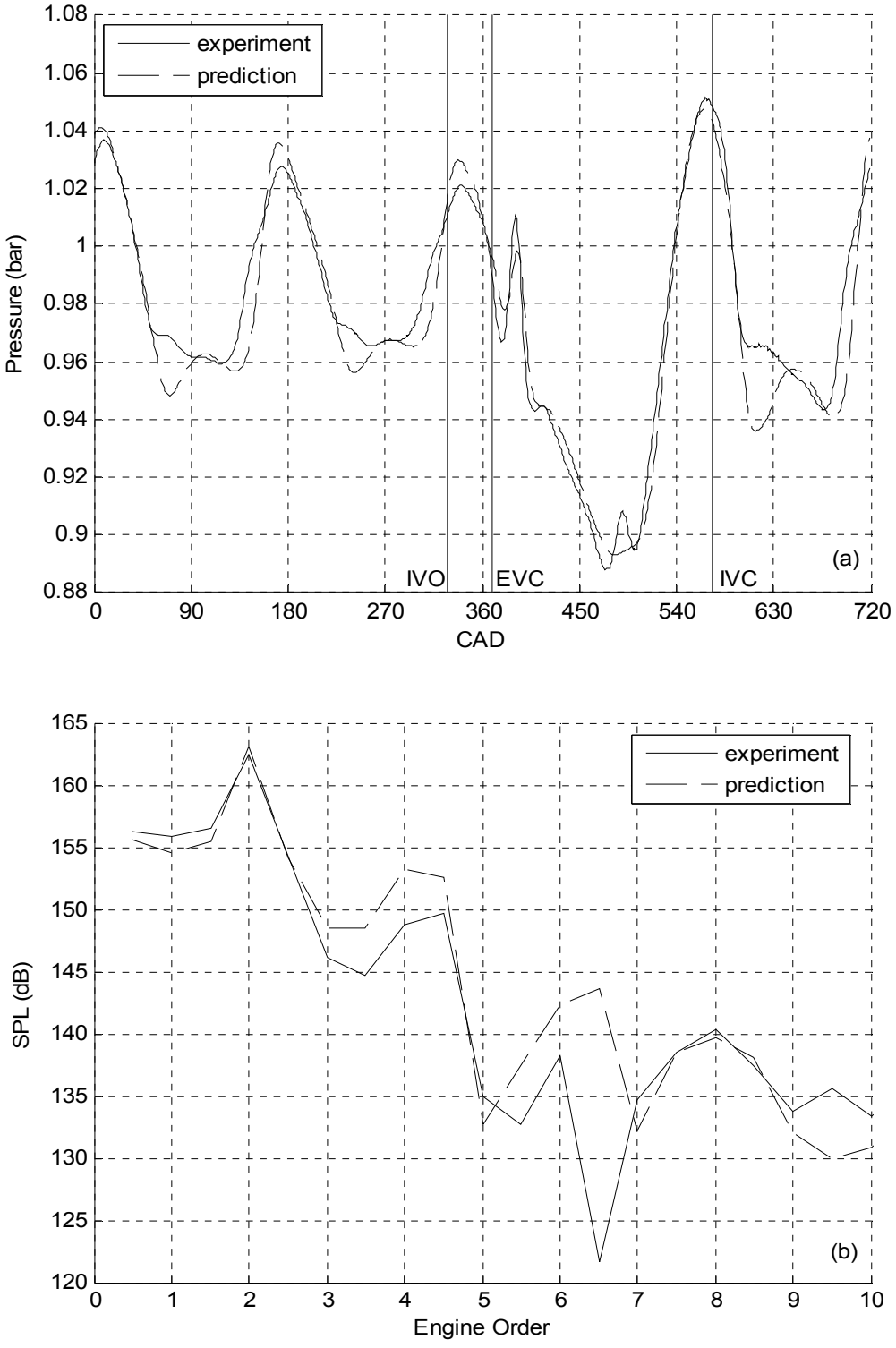

Figure 5.26: Comparison of Predicted and Measured Pressure at i1 at 3850 RPM for Intake #9 in (a) Time Domain and (b) Frequency Domain.

spectrum shows good agreement with the experiment for the dominant orders, from 1.5 to 2.5. Elsewhere, there are some deviations from the overall trend, with an over-prediction of around 5 dB from order 3 to 4.5, and the largest being a 22 dB over-prediction at order 6.5.

The predicted intake pressure at i2 at the peak volumetric efficiency speed of 3750 RPM is presented for Intake #11 in Fig. 5.27. The peak pressure is under-predicted by 2.9%, and the amplitude of the QSW is slightly under-predicted; there is a slight phase shift, as the predicted pressure wave trails its experimental equivalent. The predicted frequency spectrum matches experimental data within 3 dB from order 0.5 to 7.5, with the largest SPL, at order 2, being predicted within 0.5 dB. The predicted pressure is compared to the experiment for intake #11 at the i1 location at the same speed in Fig. 5.28. Both the predicted and experimental waves are similar to those of intake #1 at this speed (Fig. 4.10). As with intake #1, the code predicts the sharp dips in pressure at the end of the compression waves of the QSW as being wider than they are, and appears to "smear" the spikes at the beginning of the compression waves across the crest of each compression wave. The predicted and measured SPL of orders 1.5 to 2.5 agree within 0.5 dB. The overall trend of the experimental frequency spectrum is captured with larger differences occurring as engine order increases.

Figure 5.29 shows the comparison between the predicted and experimental intake pressures at i2 for intake #12 at the tuning peak location of 3650 RPM. The overall shape of the predicted pressure shows a good agreement with the experiment. The amplitudes are slightly under-predicted, and there is a 3 to 5 CAD phase lag from the experimental results. Again, the SPL of the dominant orders is predicted within 1 dB, with the peak

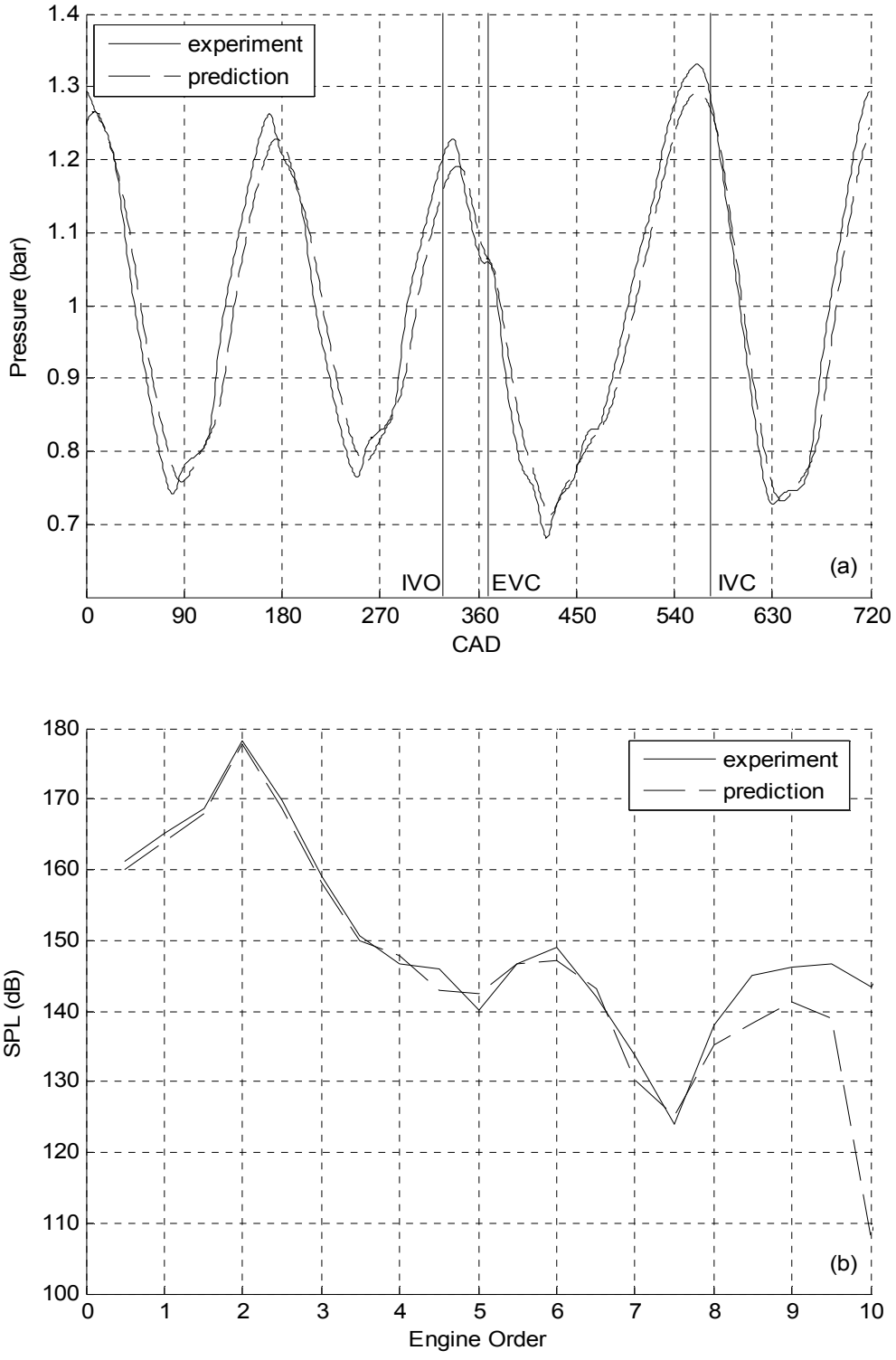

Figure 5.27: Comparison of Predicted and Measured Pressure at i2 at 3750 RPM for Intake #11 in (a) Time Domain and (b) Frequency Domain.

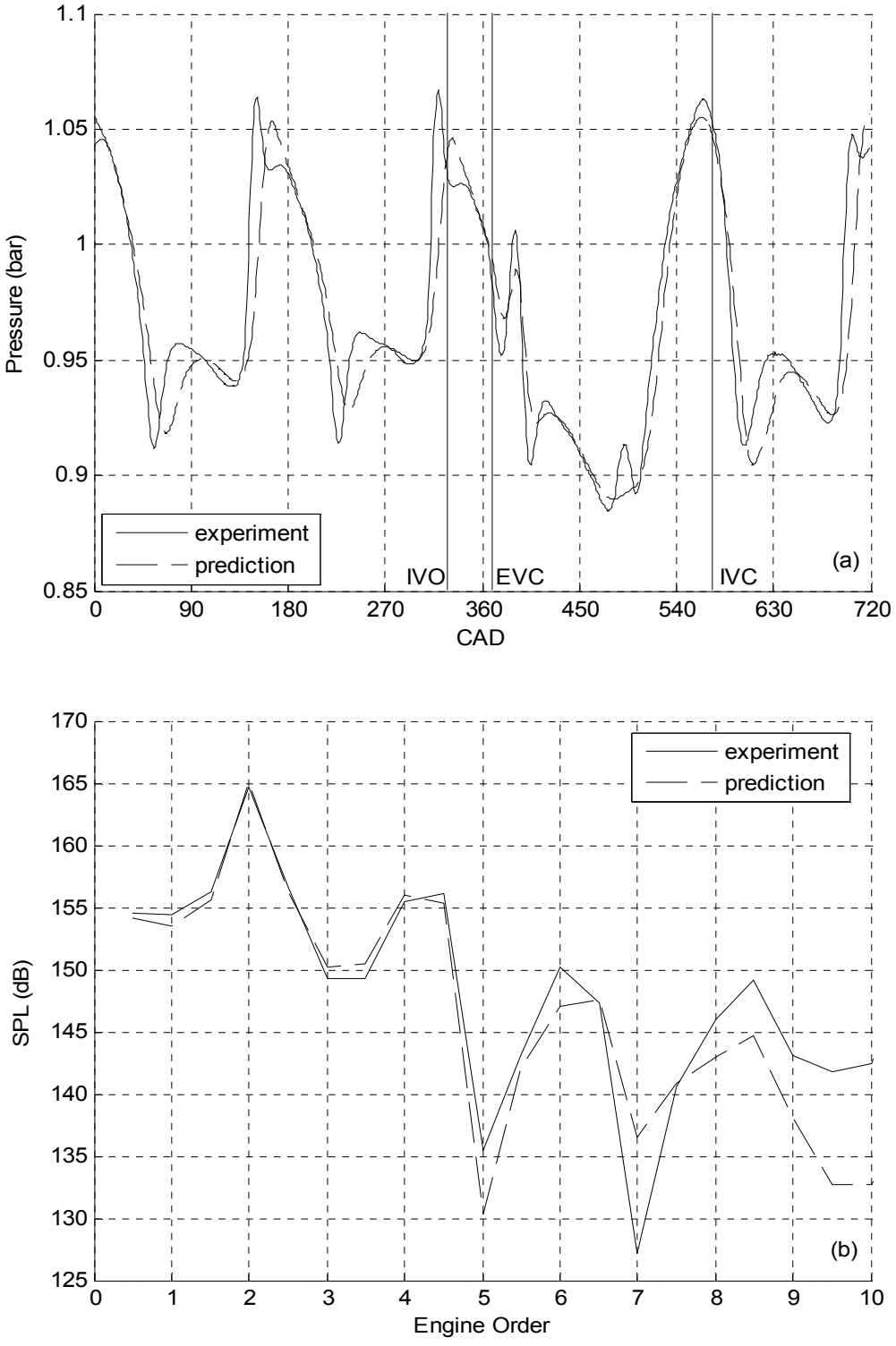

Figure 5.28: Comparison of Predicted and Measured Pressure at i1 at 3750 RPM for Intake #11 in (a) Time Domain and (b) Frequency Domain.

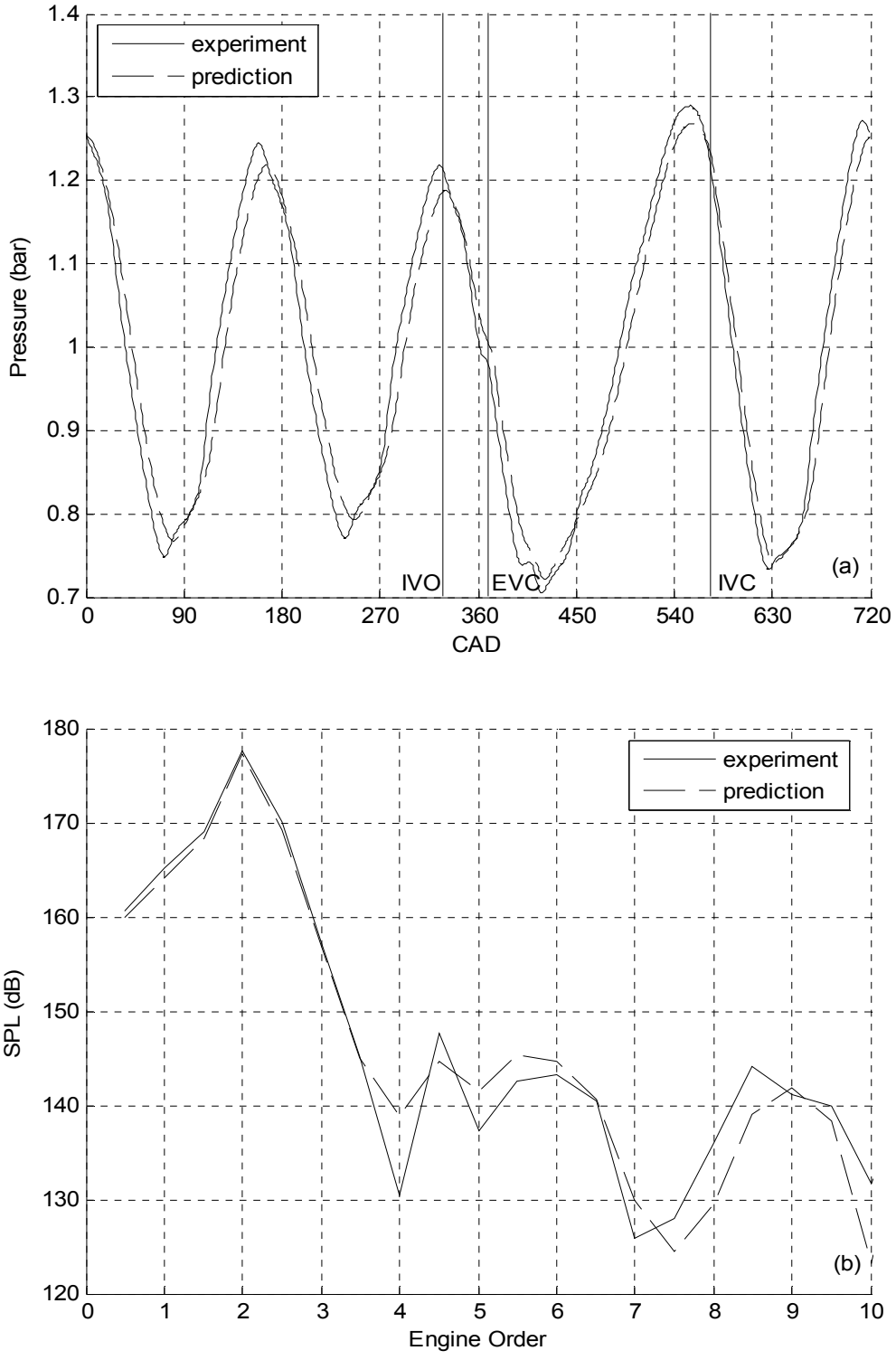

Figure 5.29: Comparison of Predicted and Measured Pressure at i2 at 3650 RPM for Intake #12 in (a) Time Domain and (b) Frequency Domain.

SPL at order 2 being within 0.5 dB. The general trend of the frequency spectrum is captured, with small differences at high engine orders. The predicted pressure at i1 for intake #12 at the same speed, shown in Fig. 5.30, shows good agreement with experimental data, while exhibiting discrepancies similar to those of intakes #1 and #11 at i1 near this speed. The predicted frequency spectrum shows excellent agreement with the experimental data from orders 0.5 to 3, while the overall trend of the rest of the measured SPL is captured reasonably well.

In general, MANDY predicts the experimental volumetric efficiency for the bellmouth group nearly as well as it did for the baseline case, which was carefully calibrated. The predicted volumetric efficiency of Intake #9 deviates furthest from experiment; this may be due to approximating the effect of the sharp-edged inlet with a steady flow loss factor smeared across the first 2 cm of the inlet. By only applying an appropriate end correction, and the loss factor in the case of intake #9, the intake pressures at both the i2 and i1 locations were predicted for each intake in this group nearly as well as they were predicted for the baseline case at 3750 RPM.

5.3 Bend Group Predictions

For each intake in the bend group (refer to Fig. 2.5d and Table 2.4), predicted volumetric efficiency is presented against experimental data from 1500 to 5500 RPM in this section. The predicted intake pressure at i2 and i1 are also compared to experimental data at the peak volumetric efficiency speed of 3750 RPM in both the (a) time domain and (b) frequency domain. The bend section of the intakes in this group had to be modeled in 1D: A loss factor including the local loss from the bend itself and the wall

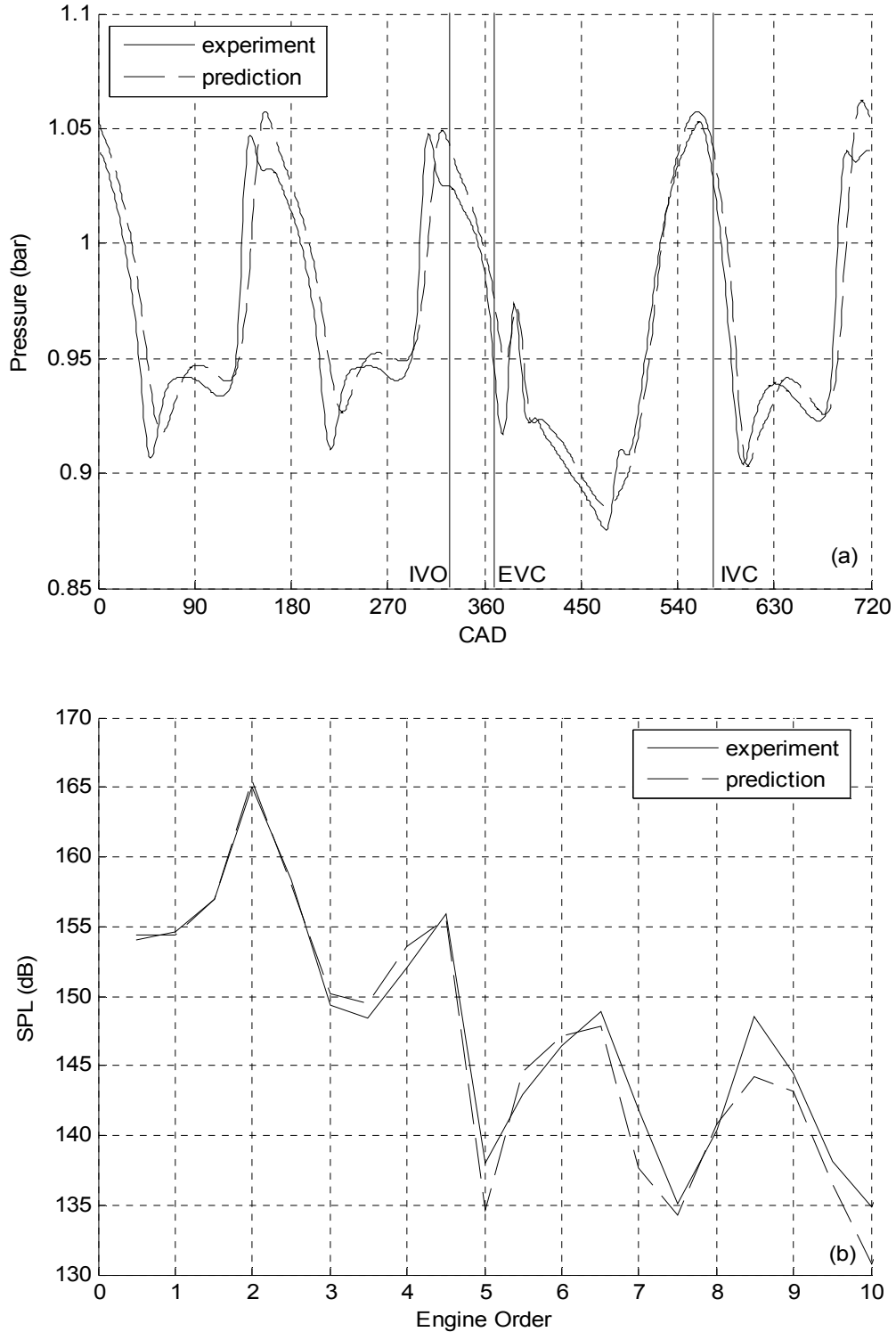

Figure 5.30: Comparison of Predicted and Measured Pressure at i1 at 3650 RPM for Intake #12 in (a) Time Domain and (b) Frequency Domain.

friction was applied to the section of pipe corresponding to the physical bend. For smooth bends, an empirical expression for the loss factor is given by (Ito, 1960)

$$k_t = 0.00241\alpha\theta\,\mathrm{Re}^{-0.17}\left(\frac{R_c}{r}\right)^{0.84}, \tag{5.1}$$

where *Re* is the Reynolds number, R_c is the bend radius of curvature, r is the radius of the duct, θ [deg] is the bend angle, and

$$\alpha = 0.95 + 17.2\left(\frac{R_c}{r}\right)^{-1.96} \tag{5.2}$$

for θ = 90°. Unfortunately, Ito did not give expressions for bends other than 45°, 90°, and 180°. However, there is a correction factor, C_θ, presented in the *SAE Aero-Space Applied Thermodynamics Manual* (1960) for bends angles other than those three as

$$C_\theta = \frac{K_\theta}{K_{90}}, \tag{5.3}$$

where K_θ is the loss coefficient of the desired bend angle, and K_{90} is the loss coefficient of the 90° bend at a given radius and Reynolds number. For θ = 135°, C_θ is about 1.22. Note that Ito did not separate friction from the bend loss, thus k_t is the total loss of the bend. Also, when specifying a loss factor in MANDY, the code turns off wall friction in that section. Thus, the k_t found using Eq. (5.1) was directly applied to the bend section. In order to use Eq. (5.1), appropriate Reynolds numbers had to be determined. Using MANDY as a guide, the Reynolds numbers at i2 were calculated as a function of crank angle for each speed. Representative speeds are presented in Fig. 5.31. For simplicity, a single Reynolds number of $2.4\text{x}10^5$ was chosen to insert into Eq. (5.1) because it is typical of Reynolds numbers during the intake breathing process for higher engine

speeds, where flow losses matter more (Heywood, 1988). The loss coefficients used for each bend are shown in Table 5.4.

Single Bend R_c/D	Loss Coefficient
2.0 (intake #13)	0.215
1.5 (intake #14)	0.239
1.0 (intake #15)	0.310

Table 5.4: Bend Loss Coefficients Used in MANDY.

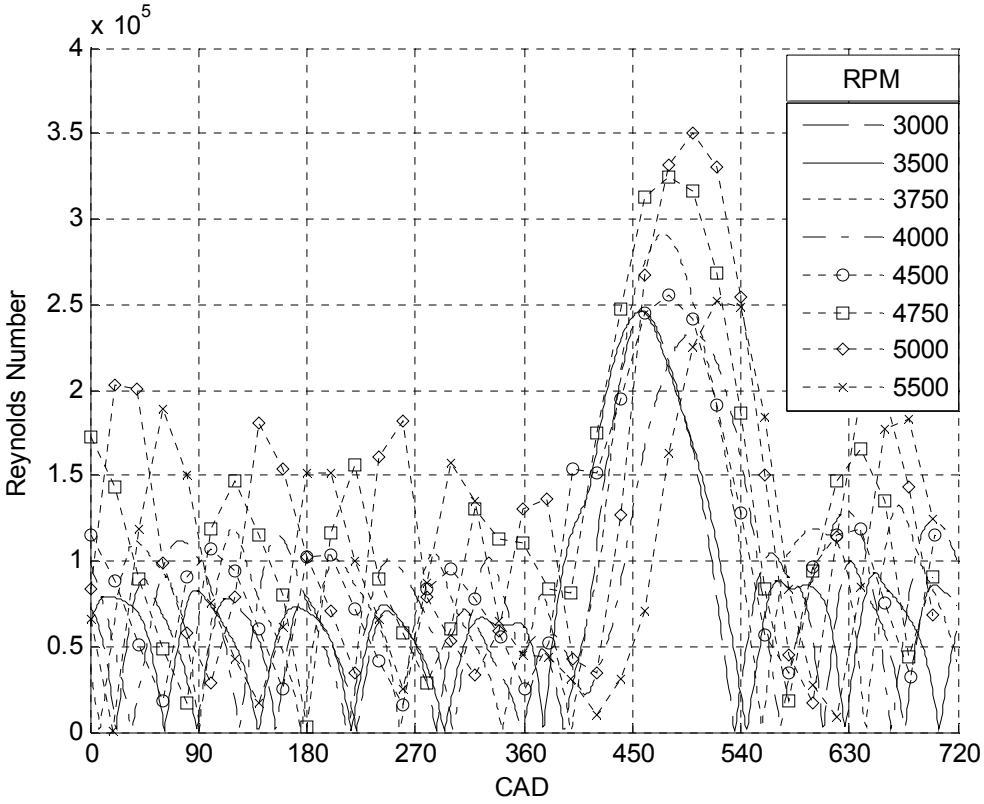

Figure 5.31: Predicted Reynolds Numbers versus Crank Angle at i2 for Various Engine Speeds.

Figure 5.32 shows the predicted and experimental volumetric efficiency for intake #13. The discrepancy between the prediction and experimental results is generally under 2%. The largest error is around 4% and occurs at 3000 RPM; the full extent of the detrimental effect that the bend had on this particular tuning peak was not captured. The loss factor for the bend seems appropriate as the magnitudes of the tuning peaks at 3750 and 4750 RPM are both predicted within 1.5% of the experimental data; without the loss factor applied, the discrepancies increase to 1.7% and 3.2%, respectively. The predicted volumetric efficiency for intake #14 is compared to experimental data in Fig. 5.33. As with intake #13, the volumetric efficiency for intake #14 was generally predicted within 2% of the experimental data, and the detrimental effect on the peak at 3000 RPM was again not captured; the deviation at 3000 RPM is 3.4%. The agreement between experimental and predicted volumetric efficiency for intakes #13 and 14 confirm the earlier discussion in Section 3.4.1, that these two intakes have a similar effect on volumetric efficiency despite their different bend radii. Figure 5.34 shows the comparison between predicted and experimental volumetric efficiency for the tightest bend ($R_c/D = 1.0$), intake #15. The effects of this bend are not predicted quite as well as the first two. The average error of this bend is 1.4%; intakes #13 and 14 both had an average error of 1.2%. The largest error, 4.0%, is again at 3000 RPM. The volumetric efficiency is over-predicted at 3650 RPM by 2.7% and under-predicted at 4250 RPM by 2.2%. Elsewhere, the prediction is within 2% of the experimental data. The accurate prediction of the volumetric efficiency indicates that the loss factor chosen for this bend is appropriate.

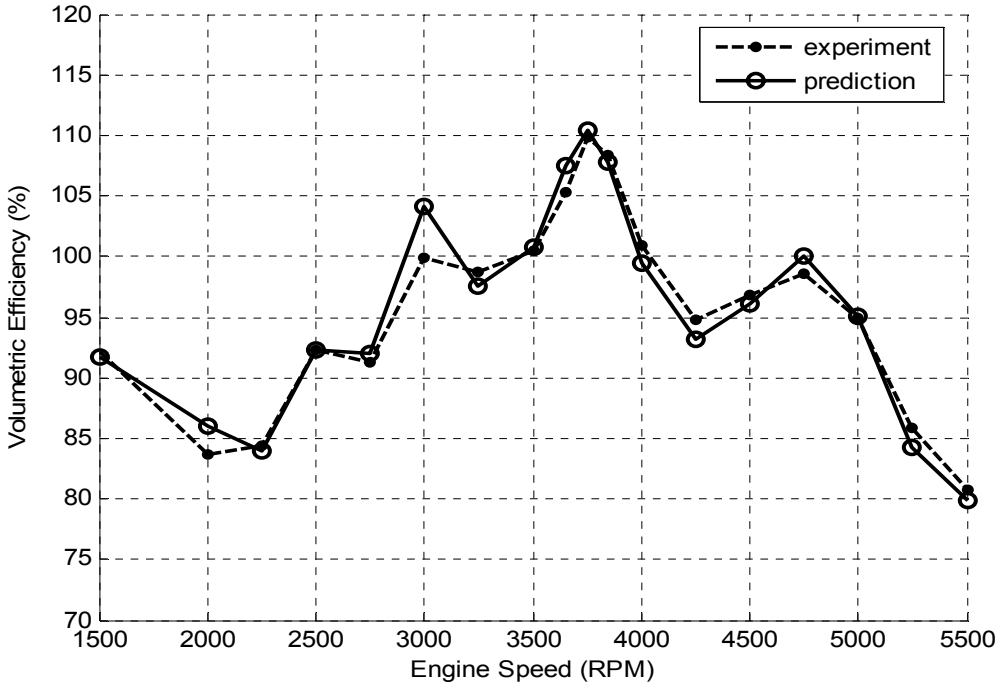

Figure 5.32: Comparison of Predicted and Measured Volumetric Efficiency for Intake #13.

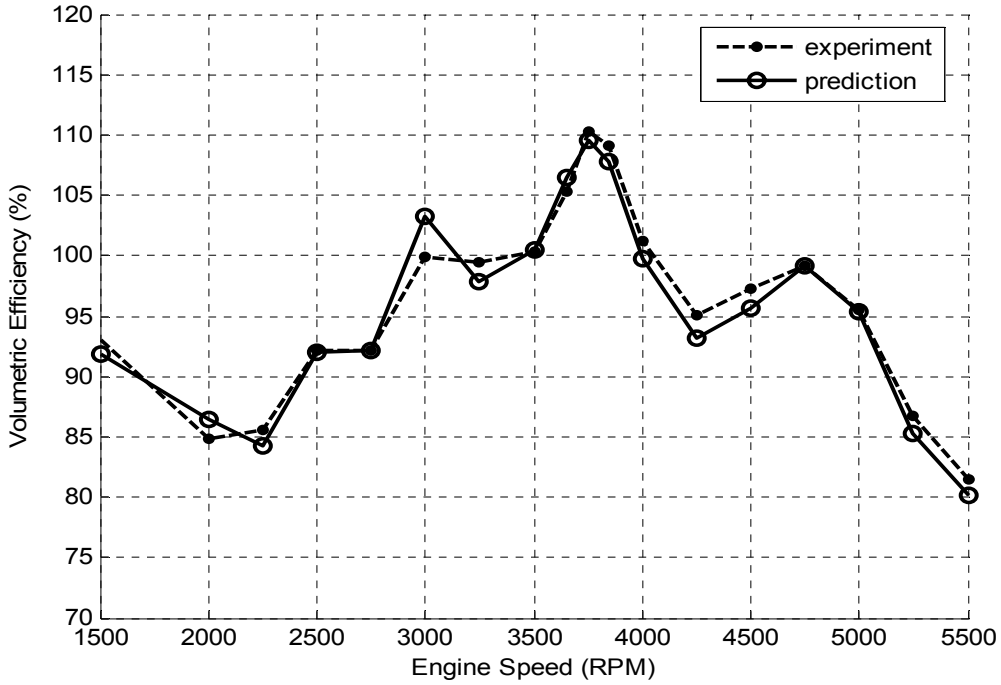

Figure 5.33: Comparison of Predicted and Measured Volumetric Efficiency for Intake #14.

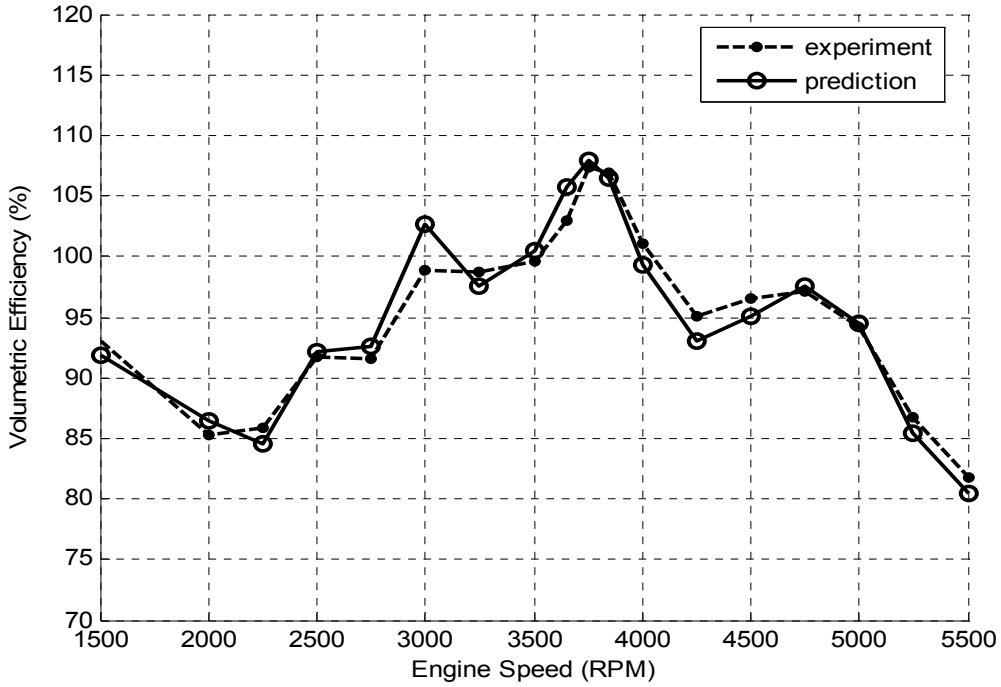

Figure 5.34: Comparison of Predicted and Measured Volumetric Efficiency for Intake #15.

Figure 5.35 shows the predicted and measured intake pressure at i2 for intake #13 at the main tuning peak speed of 3750 RPM. The predicted peak pressure and magnitude of the QSW show good agreement with experimental data. The overall form of the experimental wave is captured by the code, with a slight phase shift (3 to 7 CAD). The predicted frequency spectrum is within 1 dB of the experiment from orders 0.5 to 3.5 with the largest SPL, at order 2, predicted within 0.5 dB. The overall trend of the experimental spectrum is captured for less important orders. The predicted and experimental intake pressure at i1 is shown for intake #13 in Fig. 5.36. The magnitudes and overall shape of the experimental wave are captured, but as observed with most pressures thus far at i1, the code misses some of the finer details. The phase shift between experiment and prediction at this location for intake #13 is larger than that of the baseline prediction. The SPL peak at order 2 is over-predicted by 1 dB. From orders 0.5 to 3, the predicted spectrum is within 1 dB of experiment. At higher orders, the predicted SPL is generally within 5 dB of experiment, with the largest deviation of 8 dB at order 5.

Figure 5.37 shows the predicted and measured intake pressure at i2 for intake #14 at the tuning peak speed of 3750 RPM. The amplitudes of the wave are under-predicted just slightly. As observed with intake #13, intake #14 has a slight phase shift with respect to the experiment. The experimental frequency spectrum is predicted within 1 dB from order 0.5 to 1.5, and within 0.5 dB from order 1.5 to 3.5. Elsewhere, the predicted spectrum generally agrees within 6 dB of experiment with the worst error, 20 dB, occurring at order 10. The predicted pressure at i1 for intake #14 at the same speed, shown in Fig. 5.38, has an overall shape and magnitude similar to that of the measured wave. Again, the sharp peaks (at 140, 307, and 695 CAD) of the QSW are not predicted

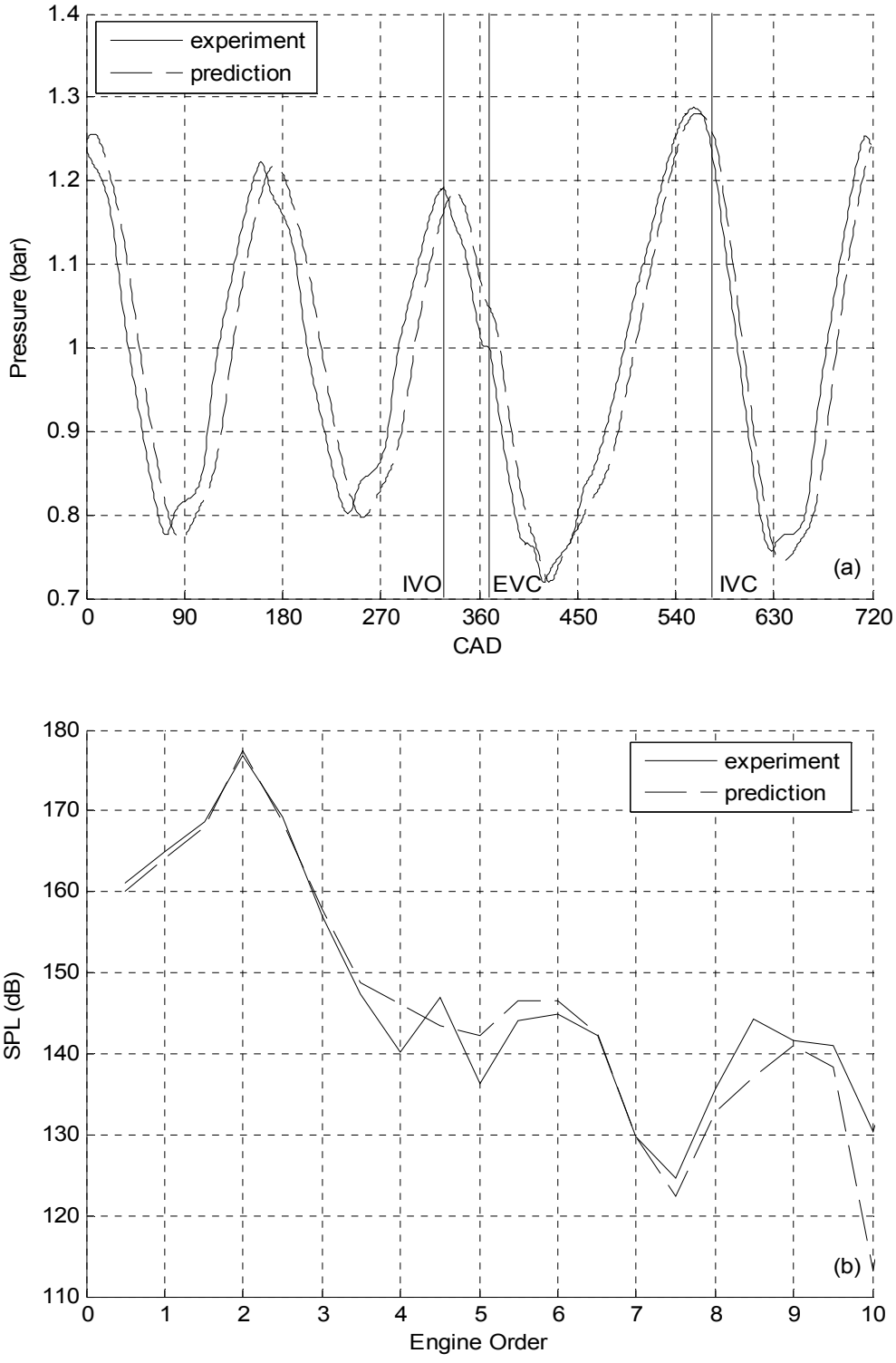

Figure 5.35: Comparison of Predicted and Measured Pressure at i2 at 3750 RPM for Intake #13 in (a) Time Domain and (b) Frequency Domain.

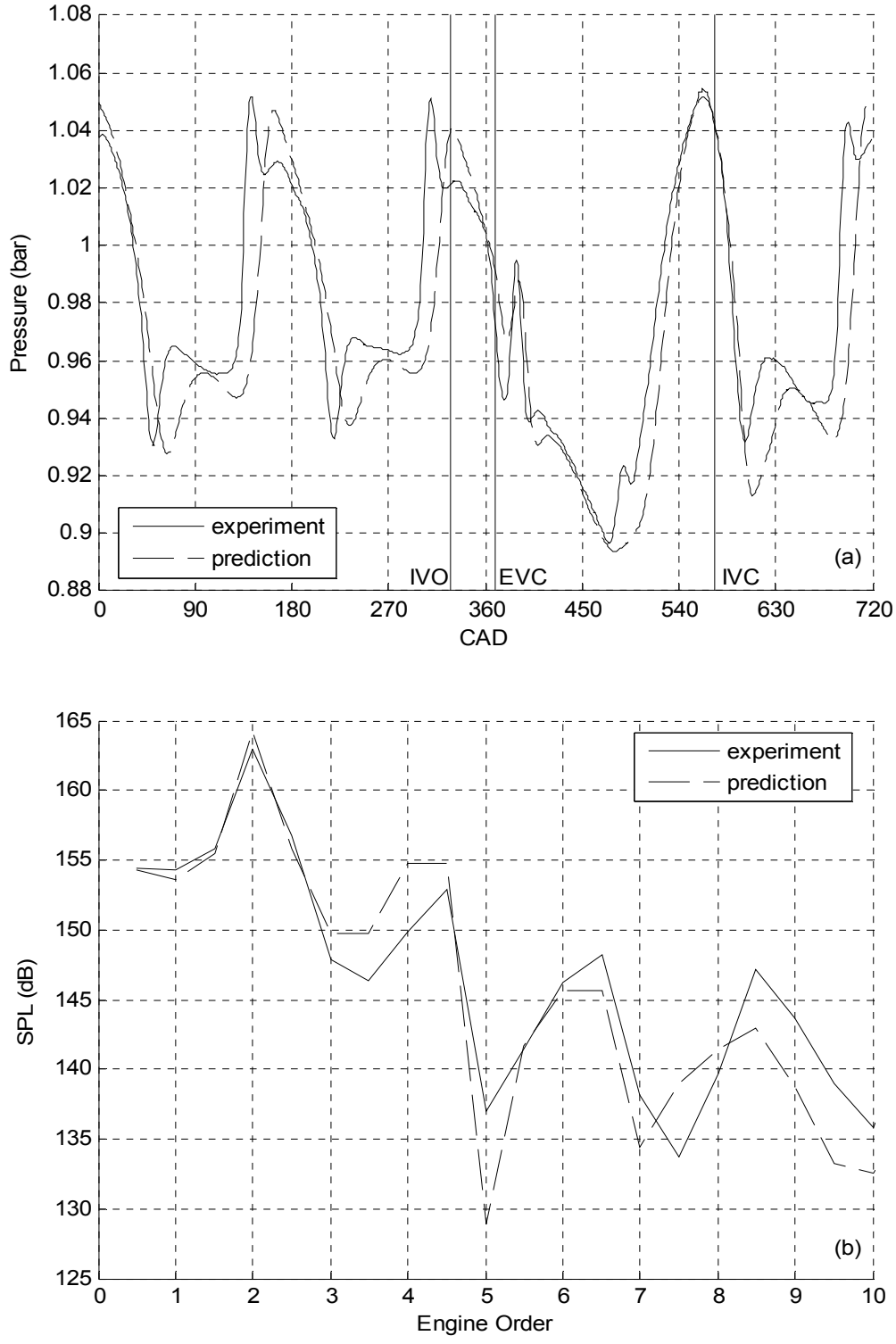

Figure 5.36: Comparison of Predicted and Measured Pressure at i1 at 3750 RPM for Intake #13 in (a) Time Domain and (b) Frequency Domain.

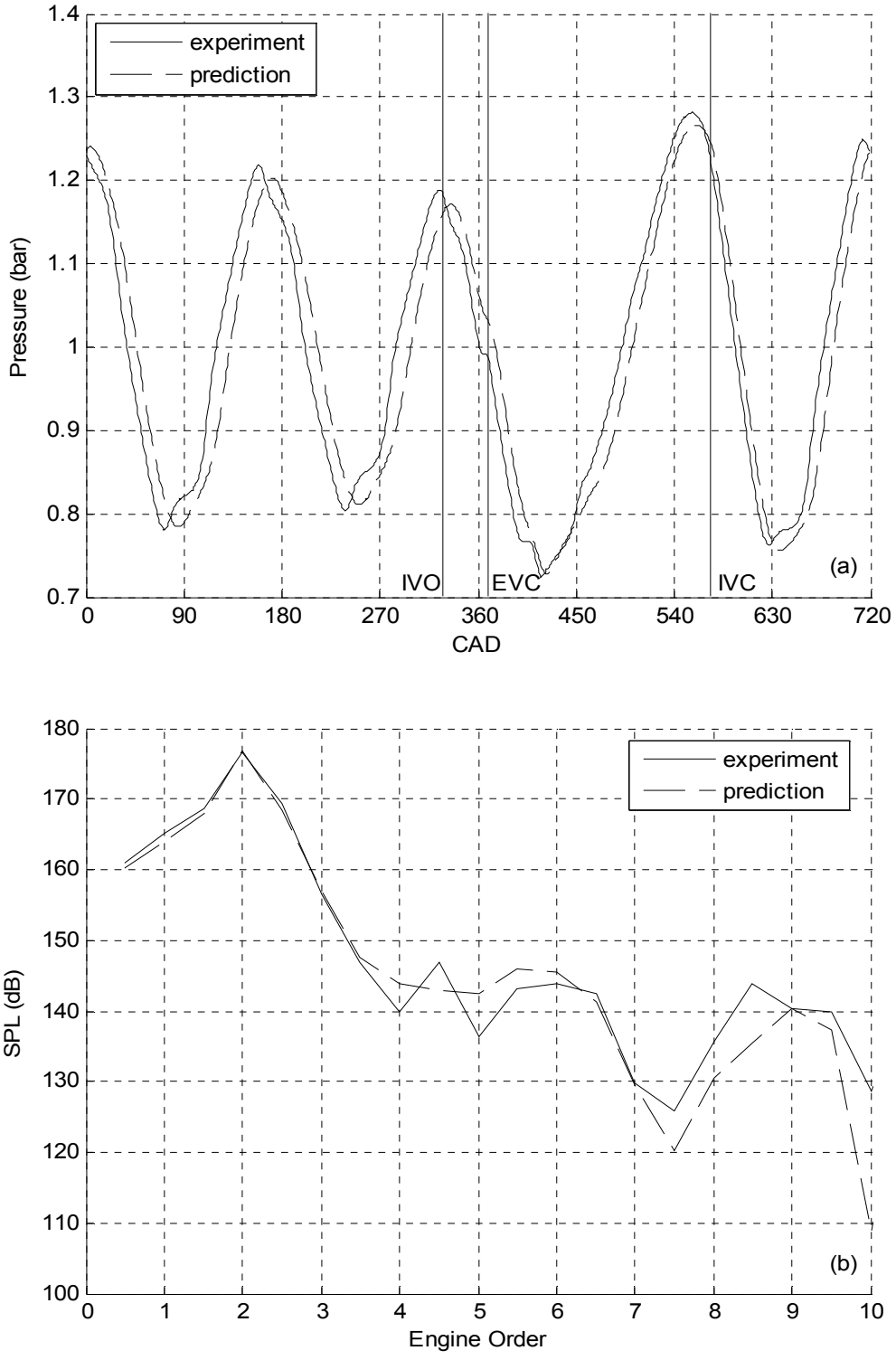

Figure 5.37: Comparison of Predicted and Measured Pressure at i2 at 3750 RPM for Intake #14 in (a) Time Domain and (b) Frequency Domain.

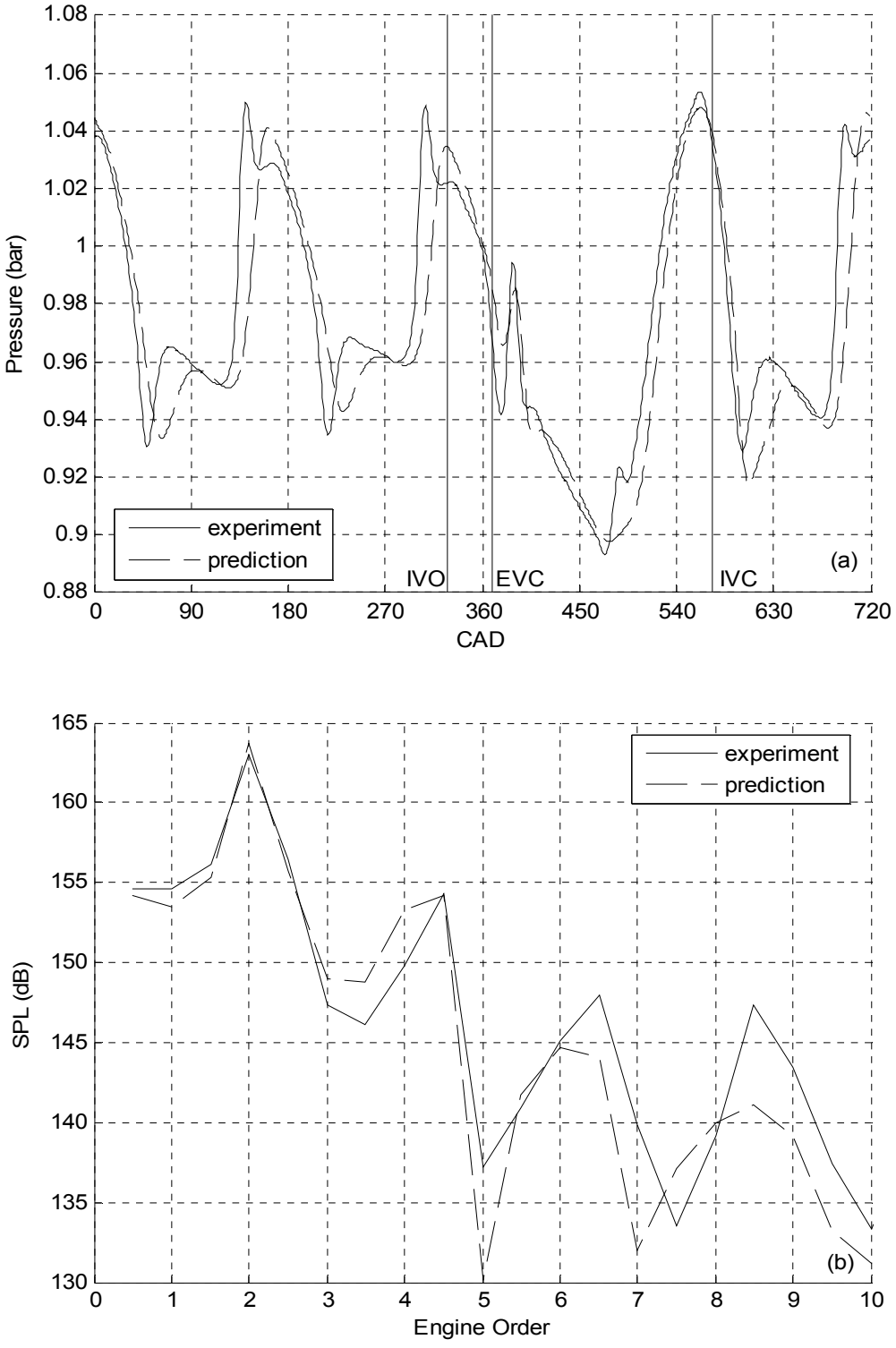

Figure 5.38: Comparison of Predicted and Measured Pressure at i1 at 3750 RPM for Intake #14 in (a) Time Domain and (b) Frequency Domain.

and the valleys (at 49, 217, and 601 CAD) are somewhat wider than the experiment. As observed with intake #13, the phase shift between prediction and experiment is slightly larger than it was for the baseline at this location. The dominant engine orders, from 1.5 to 2.5, are predicted within 0.5 dB of experiment. The overall shape of the experimental frequency spectrum is more or less captured by the code, with some differences above order 5.5.

Figure 5.39 shows the predicted and experimental pressure at i2 for the tightest bend ($R_c/D = 1.0$), intake #15, at the tuning peak speed of 3750 RPM. The overall shape and amplitudes of the measured pressure show good agreement with the prediction, and as observed with each bend in this group, a slight phase shift of 3 to 7 CAD is present. The frequency spectrum is predicted within 1 dB of the experiment from order 0.5 to 1.5 and within 0.5 dB from order 1.5 to 3.5. The predicted spectrum follows the trend of the measured spectrum at higher orders with an error generally under 7 dB. The predicted and experimental pressures at the i1 location for intake #15 are shown in Fig. 5.40. The magnitudes and overall shape of the wave are predicted adequately, and as observed with the other bends, some of the smaller details are missed by the code. Also, the phase lag between measured and predicted waves at this location is larger for intake #15 than it was for the baseline. The peak SPL is over-predicted by 1 dB when compared to the experiment. In general, the trend of the measured spectrum is captured by the code with some differences observed above order 5.

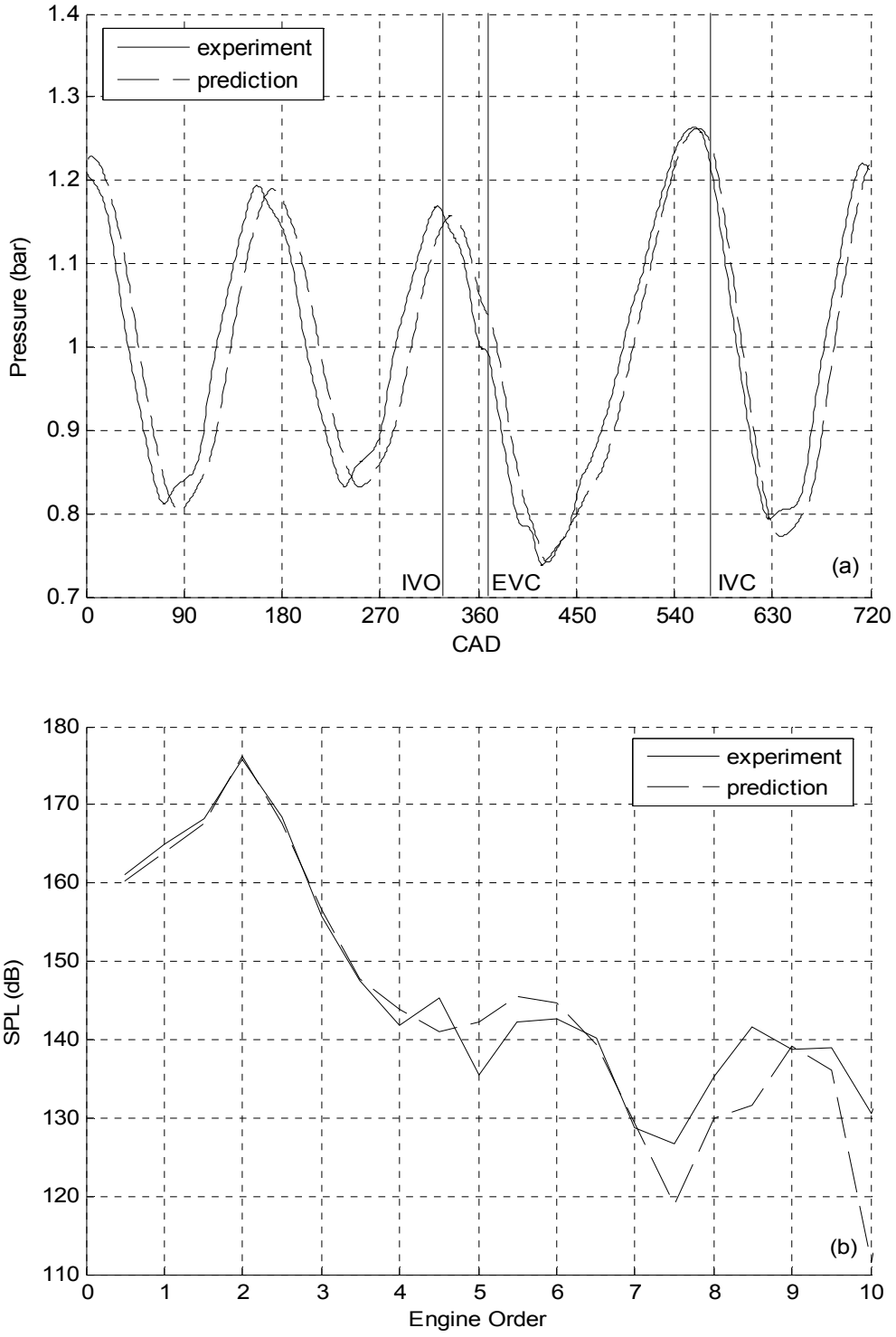

Figure 5.39: Comparison of Predicted and Measured Pressure at i2 at 3750 RPM for Intake #15 in (a) Time Domain and (b) Frequency Domain.

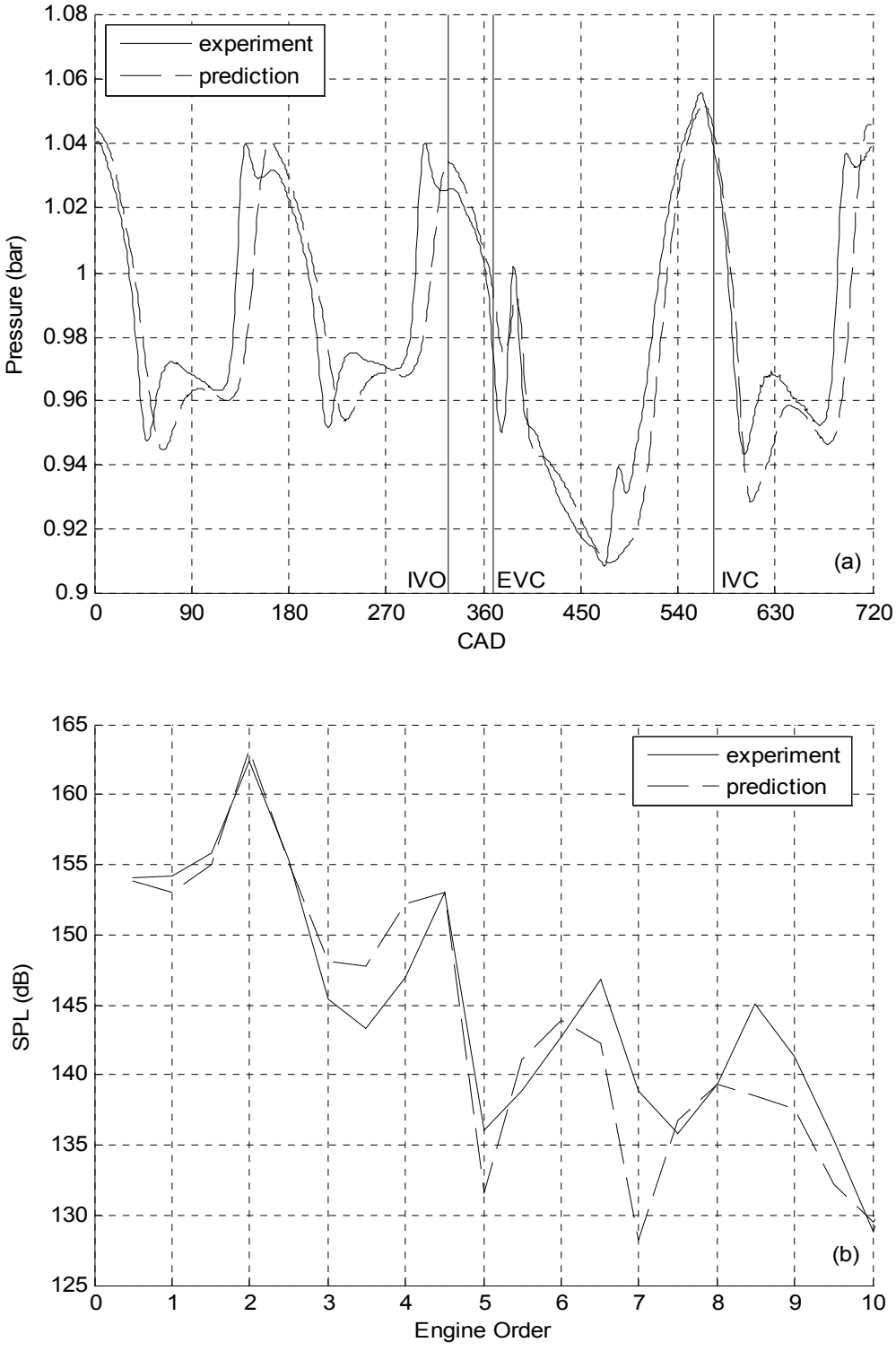

Figure 5.40: Comparison of Predicted and Measured Pressure at i1 at 3750 RPM for Intake #15 in (a) Time Domain and (b) Frequency Domain.

5.4 S-Bend Group Predictions

For each intake in the S-bend group, predicted volumetric efficiency is presented here against experimental data from 1500 to 5500 RPM. The predicted intake pressure at i2 and i1 are also compared to experimental data at the three baseline tuning peak speeds, 3000, 3750, and 4750 RPM. As with the bend group, an appropriate loss factor was applied across the S-bend section of the intake. The loss factor for the bend-bend interaction is not simply the addition of the loss factor of each individual bend. There is an interaction factor that should be multiplied to this sum, as given by Eq. (3.4) (Miller, 1990). For each S-bend, the single-bend loss coefficients for R_c = 8.4, 6.3, and 4.2 cm and a bend angle of 67.5° were found using Eqs. (5.1-5.3) where C_θ is now 0.83 instead of 1.22. These single-bend loss coefficients, shown in Table 5.5, were then plugged into Eq. (3.4) for K_{b1} and K_{b2} with $C_{b\text{-}b}$ = 0.64 based on the discussion of same-R_c bend / S-bend pairs in Section 3.5, and the resultant S-bend loss factors, also shown in Table 5.5, were determined.

S-Bend R_c/D	Single 67.5° Bend Loss Coefficient	S-Bend Loss Coefficient
2.0 (intake #16)	0.146	0.188
1.5 (intake #17)	0.163	0.208
1.0 (intake #18)	0.211	0.270

Table 5.5: S-Bend Loss Coefficients Used in MANDY.

Figure 5.41 shows the comparison between predicted and measured volumetric efficiency for intake #16. The prediction is generally within 2% of experimental data with the largest deviations being 2.8% (over-prediction) at 3000 RPM and 3.0% (under-

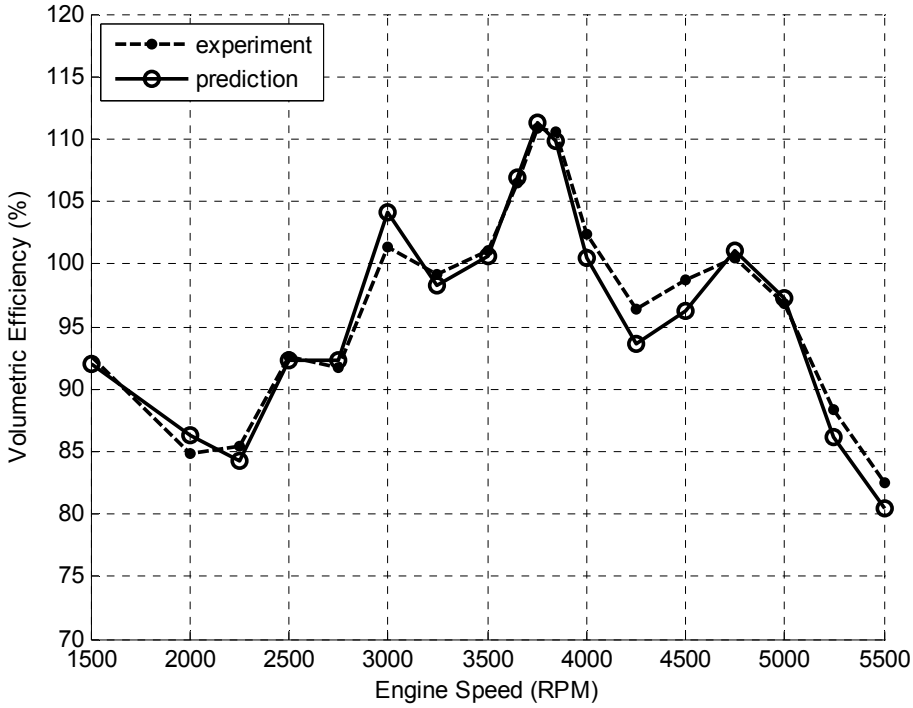

Figure 5.41: Comparison of Predicted and Measured Volumetric Efficiency for Intake #16.

prediction) at 4250 RPM. The largest tuning peak is predicted within experimental error, as is the peak at 4750 RPM. The predicted and measured volumetric efficiency for intake #17 is shown in Fig. 5.42. The predicted volumetric efficiency is generally within 2% of the experimental data. The largest deviations are again an over-prediction at 3000 RPM and under-prediction at 4250 RPM. The prediction of volumetric efficiency for the tightest S-bend, intake #18, is shown against experimental data in Fig. 5.43. The volumetric efficiency is generally predicted within 2% of experiment. The largest deviation, 4.9%, occurs at 3000 RPM. The tuning peaks at 3750 and 4750 RPM are predicted within experimental error. In general, MANDY predictions show good agreement with the experiments for most speeds. The largest differences for each S-bend are at 3000 RPM; MANDY does not predict that the S-bends will be as detrimental as they were experimentally to the tuning peak there when compared to the baseline. The prediction accuracy of the tuning peaks at 3750 and 4750 RPM suggest that the $C_{b\text{-}b}$ chosen based on comparison with experimental data is appropriate.

Figure 5.44 shows the predicted and measured intake pressure at i2 for intake #16 at 3750 RPM. The magnitude and overall shape of the predicted pressure show good agreement with the experiment. As observed with the single bend predictions, a slight phase shift persists. The SPL from orders 0.5 to 1.5 are predicted within 1 dB, and the most dominant orders, 1.5 to 2.5, are within 0.5 dB. The overall shape of the experimental spectrum is captured well, with discrepancies generally under 6 dB. The predicted and measured intake pressures of intake #16 at i1 at the same speed are compared in Fig. 5.45. The overall shape and magnitudes of the wave are predicted

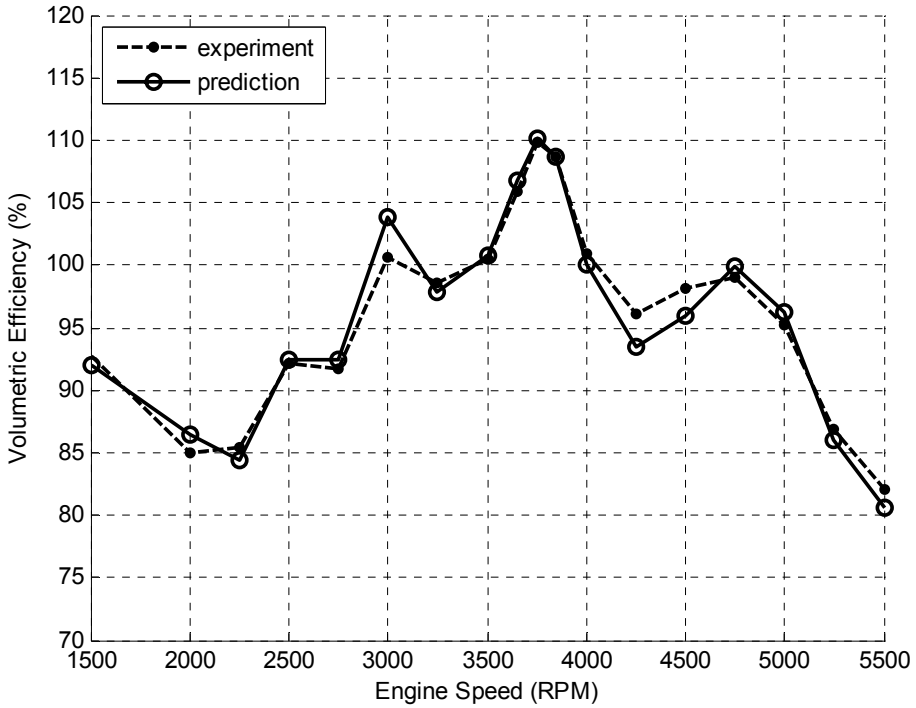

Figure 5.42: Comparison of Predicted and Measured Volumetric Efficiency for Intake #17.

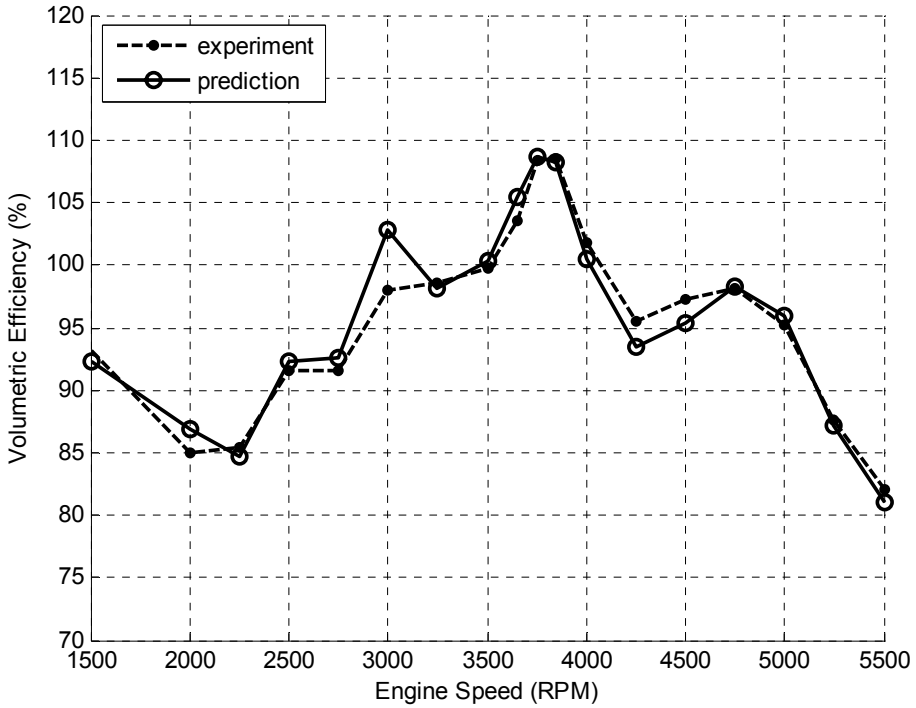

Figure 5.43: Comparison of Predicted and Measured Volumetric Efficiency for Intake #18.

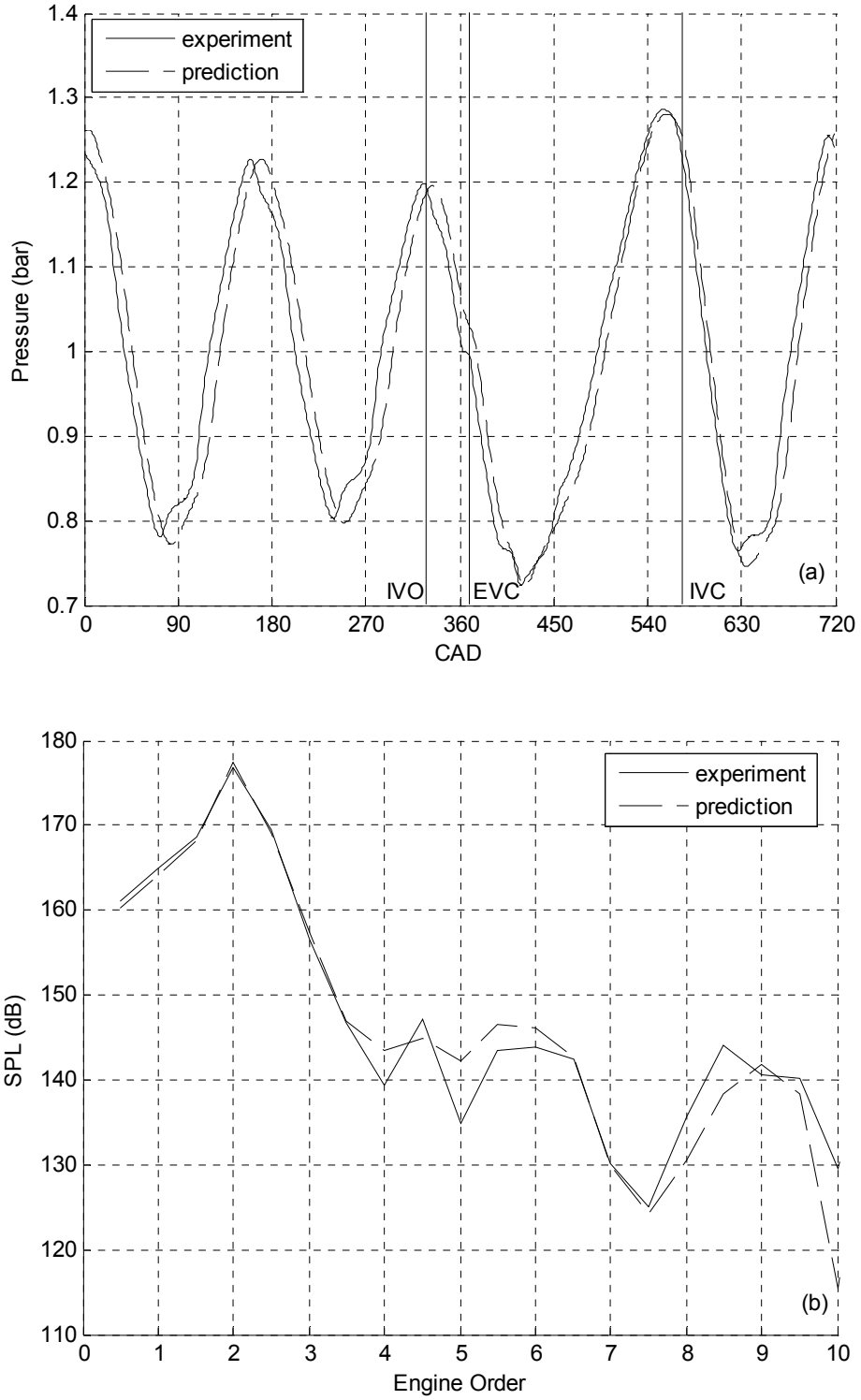

Figure 5.44: Comparison of Predicted and Measured Pressure at i2 at 3750 RPM for Intake #16 in (a) Time Domain and (b) Frequency Domain.

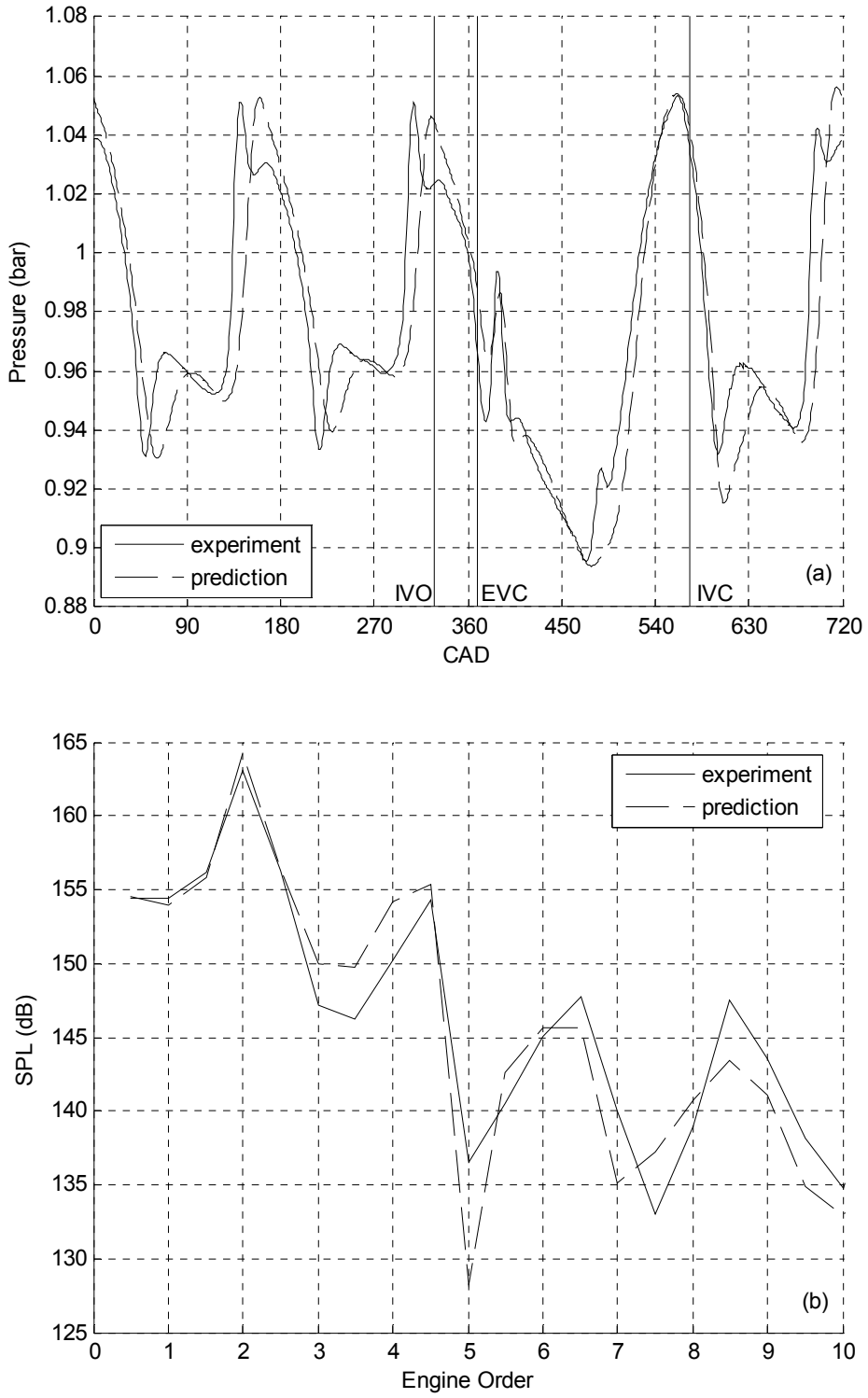

Figure 5.45: Comparison of Predicted and Measured Pressure at i1 at 3750 RPM for Intake #16 in (a) Time Domain and (b) Frequency Domain.

appropriately, with discrepancies similar to those of the baseline case at this location at this speed. The predicted SPL is within 1 dB of the experimental data for order 0.5 to 2.5; the overall trend is captured with some subtle differences at higher orders.

Figure 5.46 shows the predicted and measured pressures at i2 for intake #17 at 3750 RPM. Again, the magnitudes and overall shape are predicted adequately, with a 2 to 5 CAD phase shift present. The SPL prediction is within 1 dB of the experiment from orders 0.5 to 3.5, with the peak SPL predicted almost exactly. For higher orders, the overall trend of the spectrum is predicted well. Predicted and measured pressures at i1 for intake #17 at the same speed are compared in Fig. 5.47. The predicted pressure matches the experiment well both during the IV open period and the QSW, while some detailed features are missed. The SPL predictions are within 1 dB of the measured spectrum for orders 0.5 through 2.5; elsewhere the overall trend of the spectrum is captured adequately.

Predicted and experimental pressure at i2 at 3750 RPM are compared for the tightest S-bend ($R_c/D = 1.0$), intake #18, in Fig. 5.48. As with the other S-bends, the magnitudes of the wave are predicted well, as is the overall structure, but a slight phase shift is present. The frequency spectrum is predicted within 0.5 dB from order 0.5 to 3.5, with discrepancies in less relevant orders generally under 9 dB. Figure 5.49 compares the predicted pressure at i1 of intake #18 with the experimental data at the same speed. There are some small discrepancies at the expansion wave at 475 CAD. Elsewhere, the predicted pressure is similar to that of other S-bends and the baseline at this speed. The

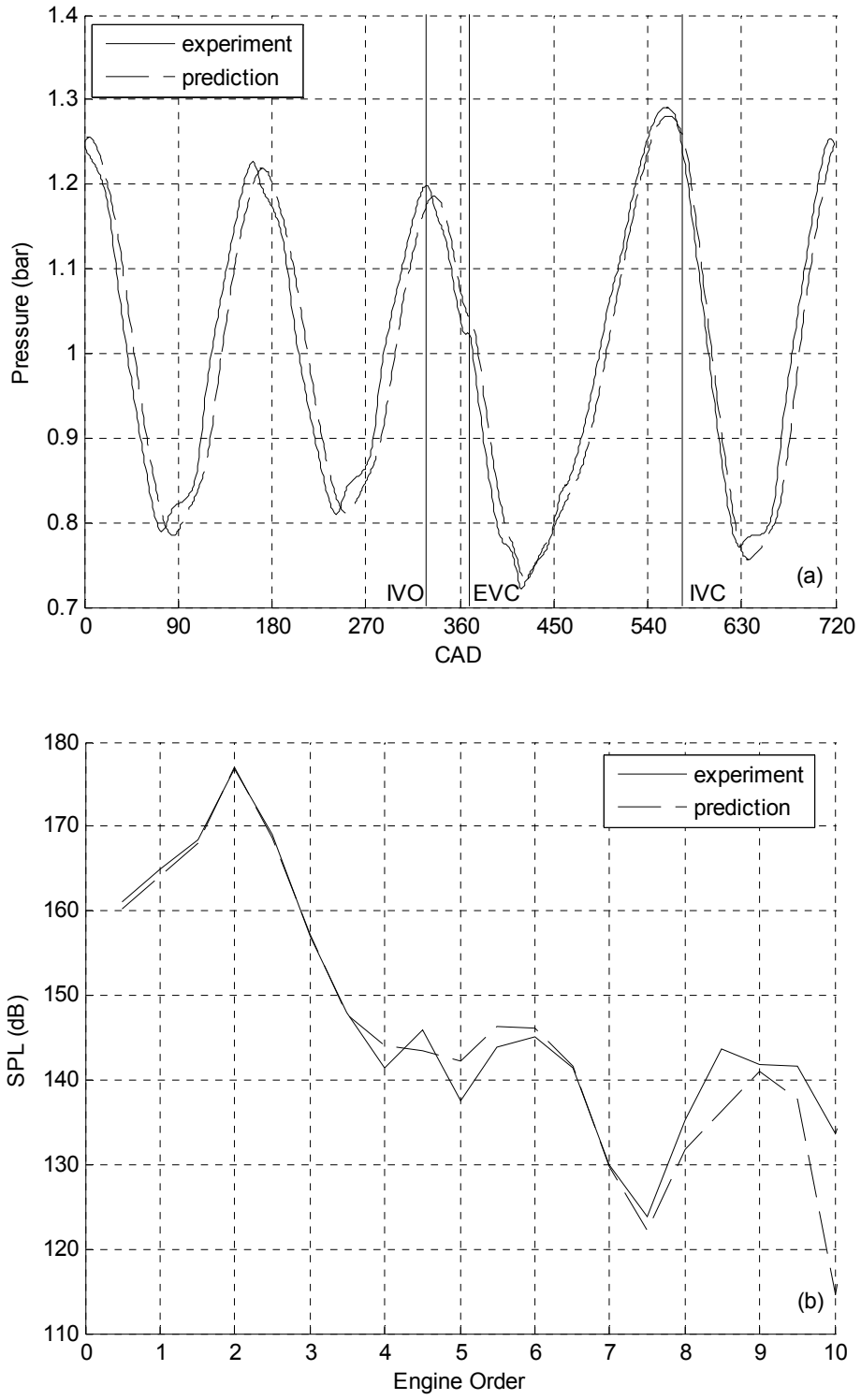

Figure 5.46: Comparison of Predicted and Measured Pressure at i2 at 3750 RPM for Intake #17 in (a) Time Domain and (b) Frequency Domain.

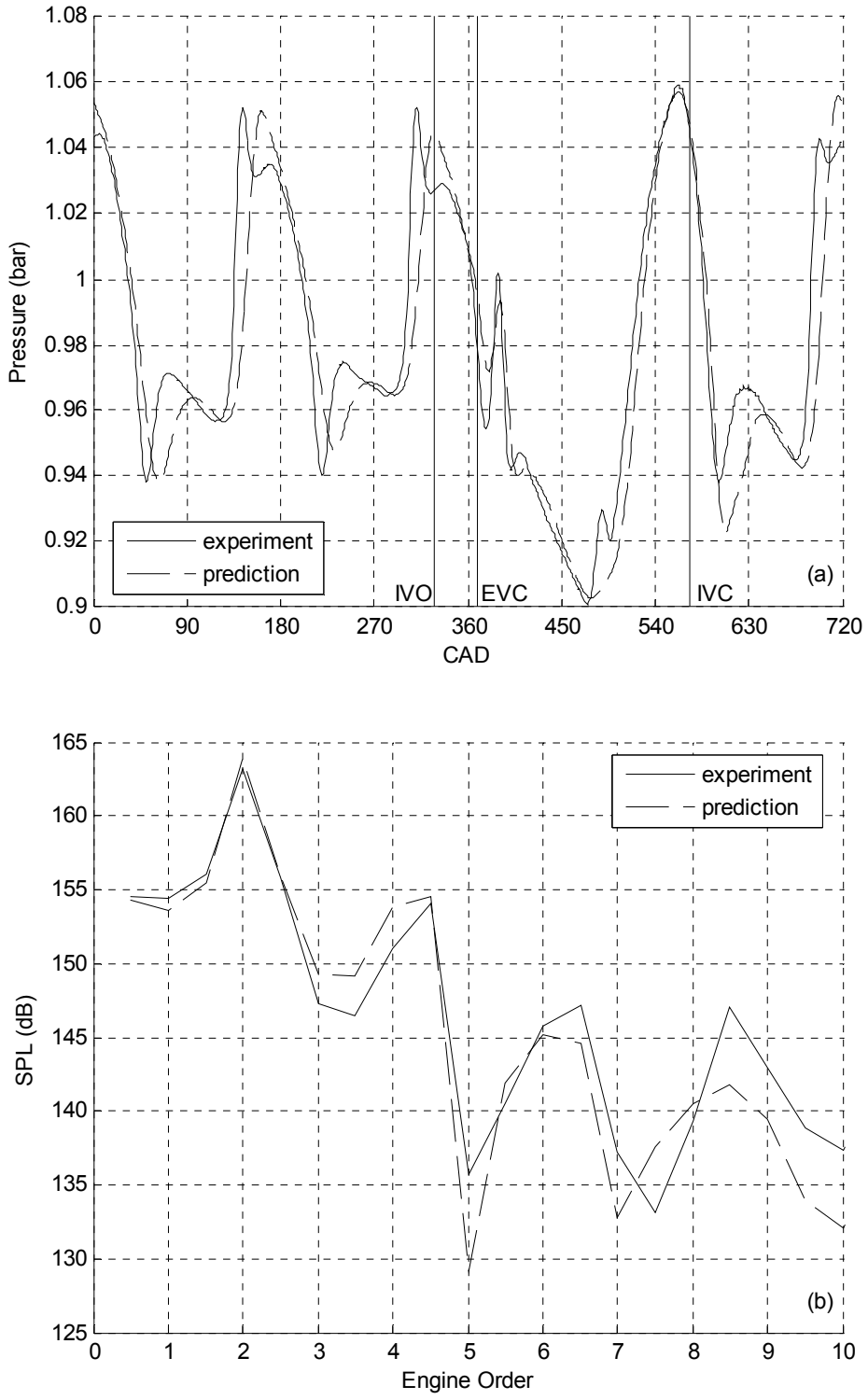

Figure 5.47: Comparison of Predicted and Measured Pressure at i1 at 3750 RPM for Intake #17 in (a) Time Domain and (b) Frequency Domain.

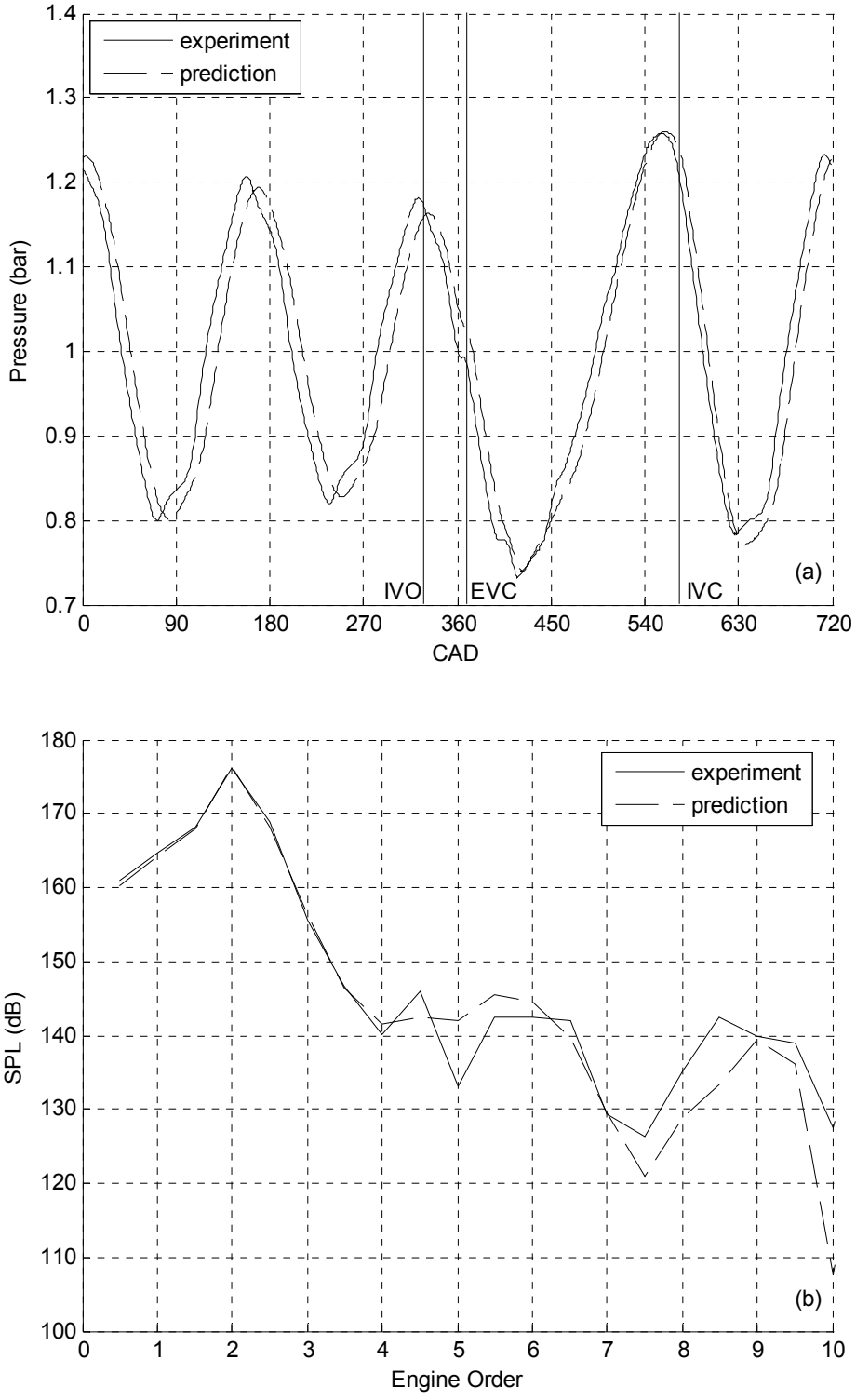

Figure 5.48: Comparison of Predicted and Measured Pressure at i2 at 3750 RPM for Intake #18 in (a) Time Domain and (b) Frequency Domain.

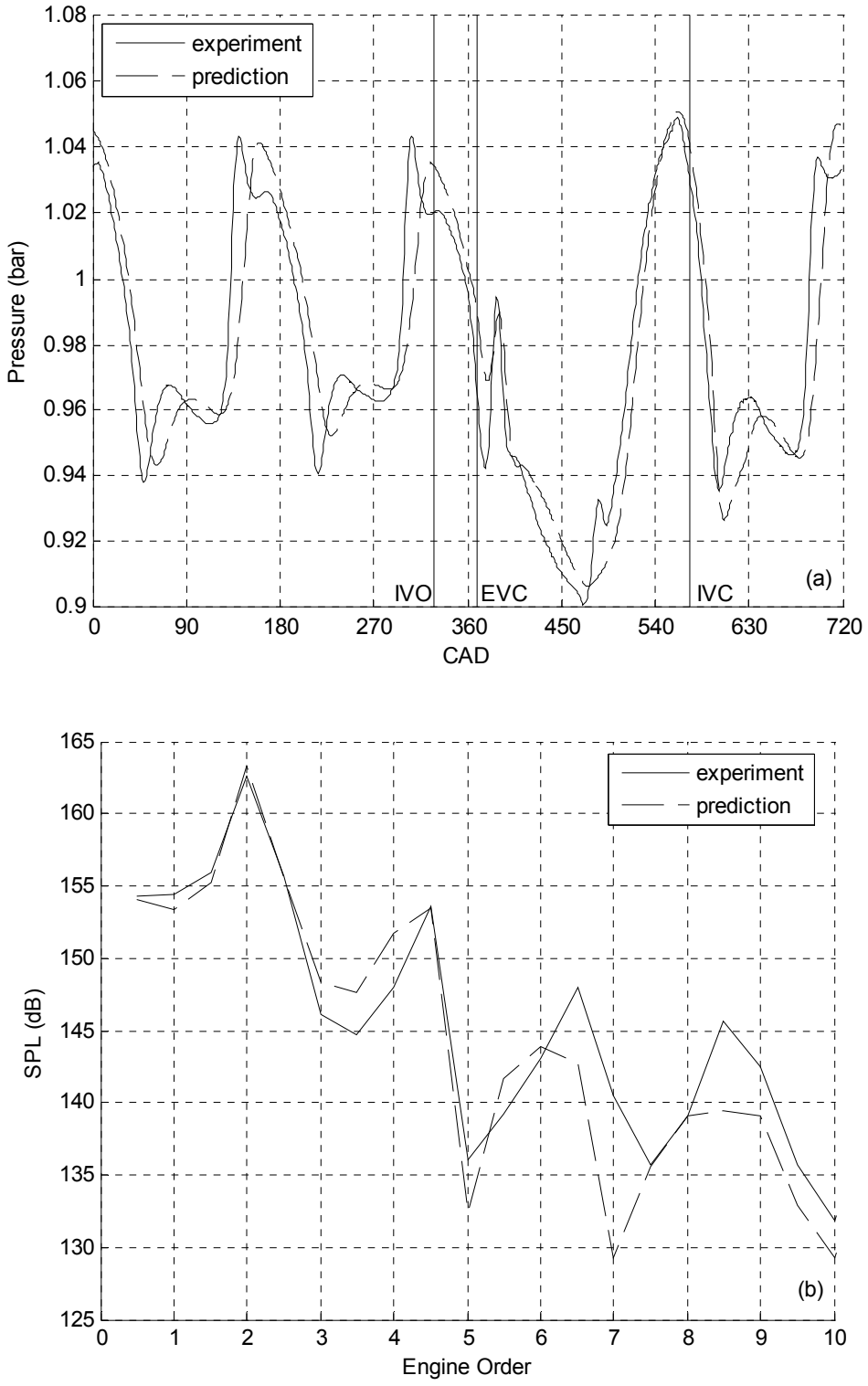

Figure 5.49: Comparison of Predicted and Measured Pressure at i1 at 3750 RPM for Intake #18 in (a) Time Domain and (b) Frequency Domain.

SPL prediction is within 1 dB of the experiment from orders 0.5 to 1.5 and within 0.5 dB for the dominant orders, from 1.5 to 2.5. Elsewhere, the overall trend of the spectrum is captured, with the largest differences at orders 7 and 8.5.

CHAPTER 6

CONCLUDING REMARKS

An experimental and computational investigation of intake geometry on engine performance was presented in this study. The experiments were performed on a firing single cylinder research engine with 18 different intake configurations, which included a straight baseline case, tapers, inlet bellmouths, 135° bends, and S-bends. For each configuration, volumetric efficiency, brake power, and intake and exhaust pressures were presented. The computational approach used for this study was a non-linear, finite-difference-based quasi-1D engine simulation code. This model was calibrated to the baseline and then applied to all other intake configurations to asses the program's ability to accurately capture the effects of the various geometries on engine performance.

The volumetric efficiency of the taper group shows the trend of increasing tuning peak speeds with increasing $L/A_{effective}$. This trend is accurately predicted by the lumped Helmholtz approximation of the intake system developed by Engelman (1973). As the taper area ratio is increased above 1.5, the peak volumetric efficiency begins to deteriorate. The shape of the power curves followed a similar trend to the volumetric efficiency, with intake #8 making the highest power of all tapers. The compression wave returning to i2 near IVC is known to cause intake tuning. However, the location of its

peak must be taken into account as the wave takes about 17° to travel from i2 to the back of the valves at speeds typical of peak volumetric efficiency for this group. If the peak of the compression wave for the baseline was closer to IVC than that of any taper and within 17° of IVC, then a significant decrease in volumetric efficiency was observed for the baseline even if the taper had a lower peak pressure magnitude. For example, intake #4 had a lower peak pressure at 4000 RPM, but it occurred 18° earlier than that of the baseline, which contributed to an 11% increase in volumetric efficiency for the taper. If the compression wave peaks of the baseline and any taper were both an ample time ahead of IVC, then the difference in peak pressures was of the same order of magnitude as the difference in volumetric efficiency. For example, the pressures for intakes #6 and 8 were 13.8% and 10.6% lower than the baseline at 3750 RPM and volumetric efficiencies were 11.0% and 9% lower. For the tapered intakes, the dominant frequency of the QSW at i2 increased compared to the baseline, which is an effect similar to shortening the length of a closed-end quarter-wave silencer. The largest difference in exhaust pressure was seen between intakes #1 and 8, but magnitude differences were generally within 0.05 bar and phasing within 7 CAD. The differences in exhaust pressure were largest between these two intakes; thus, they were not presented for any other intake configuration.

The volumetric efficiency of the bellmouth group showed slight movement of tuning peaks to lower speeds as R_i/D increased. The lumped Helmholtz approach indicates that this is caused by increasing intake effective length. The trend of increasing effective intake length with increasing R_i/D was echoed in the pressures at i2; the phase shifts from the baseline indicated if the end correction for any particular intake configuration in this group increased or decreased with respect to that of the baseline. If

the pressures led the baseline, a smaller end correction was needed, and if the pressures trailed the baseline, a larger. A reduction in volumetric efficiency was observed at the tuning peaks for intake #9 ($R_i/D = 0.05$) most likely due to inlet flow losses. When $R_i/D \geq 0.20$, no losses were evident, as the tuning peak volumetric efficiencies of intakes #10 – 12 were similar. Brake power trends generally followed the volumetric efficiency. The pressure peak trend at i2 before IVC was generally indicative of the volumetric efficiency behavior, although the timing of the peak was an important factor for intake #12.

The volumetric efficiency of the bend group had the same tuning peak locations as the baseline case, with some amplitude reductions of the tuning peaks. Intakes #13 and 14 ($R_c/D = 2.0$ and 1.5, respectively) behaved similarly, while intake #15 ($R_c/D = 1.0$) was slightly more detrimental to engine performance. For each of the bends, brake power increased at 5250 and 5500 RPM over the baseline case despite having similar volumetric efficiencies at those speeds. The reductions in amplitude of the pressure waves at i2 were similar for intakes #13 and 14, while those of intake #15 had reduced further when compared to the baseline.

The volumetric efficiency of the largest-curvature S-bend ($R_c/D = 2.0$), intake #16, showed little reduction from that of the baseline. Intake #17 ($R_c/D = 1.5$) was slightly more detrimental, while intake #18 ($R_c/D = 1.0$) was the most detrimental. The brake power for each S-bend generally followed the trend of volumetric efficiency. In general, the S-bend of a certain R_c was equally or less detrimental to engine performance than the single-bend with the same R_c for the geometries used in this study. Pressures at i2 for the S-bends were similar to those of the single bends; for intakes #16 and 17 had similar reductions in amplitudes, while intake #18 had the largest reductions.

MANDY predictions for the tapered cases, in general, agreed well with the experimental data. Volumetric efficiency was predicted within an average error of 1.7% for all tapers and was generally within 3% at any speed. MANDY predicted the location of the tuning peaks well, and peak volumetric efficiencies were all within experimental error. The predicted intake pressures at i2 for the tapers were generally of the same accuracy as that of the baseline; with the exception of the largest taper (intake #8) which had a 5 to 10 CAD shift. The pressures at i1 were predicted adequately as the overall shape and magnitudes matched the experiment, but some of the finer details were missed.

MANDY predicted the volumetric efficiencies of the bellmouth group nearly as well as the baseline, which was carefully calibrated. By adding a loss factor to the inlet of intake #9 ($R_i/D = 0.05$), both the volumetric efficiency and intake pressure magnitudes were predicted well. The other intake configurations in this group had ample inlet radii, and a loss factor at the inlet was not used. Predicted intake pressures at both i1 and i2 matched the experimental data, in general, as well as they did for the baseline case.

Following an introduction of local flow losses into the intake model, the predicted volumetric efficiencies for each bend were generally within 2% of the experiments with the tuning peaks at 3750 and 4750 RPM predicted within 1.5%. The predicted pressures at i1 and i2 for this group showed agreement with the experiments similar to that observed for the baseline.

Through comparisons with the experimental data for each same-R_c bend / S-bend pair, a $C_{b\text{-}b} = 0.64$ was chosen to model the S-bend group. Using this $C_{b\text{-}b}$, the volumetric efficiencies for all S-bends were predicted generally within 2% of the experiments. As observed with the single bends, the predicted intake pressures at i1 and i2 for all S-bends

had appropriate magnitudes and agreed with the experiments nearly as accurately as the baseline model.

For this study, each intake configuration was only modeled in quasi-1D. Some of the more extreme intake configurations from this study, such as the taper with area ratio of 3 or the $R_c/D = 1.0$ bend and S-bend, could be modeled using the coupled 1D-3D approach mentioned in Section 1.2. Using this method, predictions may be improved over the quasi-1D model alone since multi-dimensional effects are likely to play an important role, and the flow effects in the intakes can be visualized to aid in the improvement of the quasi-1D code.

When searching for appropriate loss factors for the bends and S-bends, it was difficult to find information on the 135° bends and 67.5° S-bends without spacers used for this study. Most data found was for 45°, 90°, and 180° single bends and S-bends comprised of two 90° bends only. The total bend loss coefficients could be determined for the bend and S-bend geometries using a method similar to that used by Christian (2003) and Paul (2005) for right-angled tee junctions. A project more broad in scope could also be defined where the loss coefficients for a number of different bend angles, radii, and S-bend configurations similar to those seen on production IC engines are determined.

The next phase of engine work should introduce a plenum-like structure around the inlet of each intake configuration to force the flow to turn into it, much like the intake manifold of a multi-cylinder engine is typically designed. The tradeoff between the flow effects at the tee junction and the wave dynamics could then be investigated.

APPENDIX B

MANDY CALIBRATION PARAMETERS

Variable	Value
BDUR	47.0, 52.0, 50.0, 46.0, 44.0, 44.0, 46.0, 53.0, 50.0, 54.0, 50.0, 45.0, 47.0, 48.0, 54.0, 59.0, 55.0, 58.0, 62.0
BDURRPM	1000, 1500, 2000, 2250, 2500, 2750, 3000, 3250, 3500, 3650, 3750, 3850, 4000, 4250, 4500, 4750, 5000, 5250, 5500
CAB	-2.5, 4.0, 0.0, -1.5, -5.0, -5.0, -6.0, -5.0, -5.0, -6.0, -3.0, -6.0, -8.0, -10.0, -12.0, -15.0, -13.0, -14.0, -10.0
CABRPM	1000, 1500, 2000, 2250, 2500, 2750, 3000, 3250, 3500, 3650, 3750, 3850, 4000, 4250, 4500, 4750, 5000, 5250, 5500
CRNTDT	0.4
DXEXH	2.0
DXINT	1.0
HFACT	2.5
HTDTNC	2.00e-05
HTDUCT	1.0
IBKFLO	0
IVTTYP	0
LASHEC	0.032
LASHEO	0.032

LASHIC	0.023
LASHIO	0.023
MXCYCL	30
PEX	1013000.0
PWSR	1.0
TEX	311
TOLRNC	0.0005
TPORT	361.0 (intake), 361.0 (exhaust)
TPORTL	10.0 (intake), 8.3 (exhaust)
TWCYL	430, 430, 435, 438, 440, 450, 490, 525, 540, 570, 590, 632, 645, 665, 685, 687, 700
TWRPM	1000, 1500, 2000, 2250, 2500, 2750, 3000, 3250, 3500, 3750, 4000, 4250, 4500, 4750, 5000, 5250, 5500
WF	0.10 (intake), 0.10 (exhaust)

BIBLIOGRAPHY

Arias, J. R., Moreno, E., Navarro, E. and Varela, E., 2000, "Using 1-D and 3-D Models for the Simulation of Gas Exchange Processes," *SAE Paper 2000-01-0658.*

Benson, R. S., Garg, R. D., and Woollatt, D., 1964, "A Numerical Solution of Unsteady Flow Problems," *International Journal of Mechanical Sciences*, 6: 117-144.

Borghi, M., Mattarelli, E. and Montorsi, L., 2001, "Integration of 3D-CFD and Engine Cycle Simulations: Application to an Intake Plenum," *SAE Paper 2001-01-2512.*

Capetti, A., 1929, "Effect of Intake Pipe on the Volumetric Efficiency of an Internal Combustion Engine," *NACA Technical Memorandum 501* (translated from *Ann. R. Scuola d'Ingegneria di Padova,* Dec. 1927).

Chapman, M., Novak, J. M., and Stein, R. A., 1982, "Numerical Modeling of Inlet and Exhaust Flows in Multi-Cylinder Internal Combustion Engines," *Flows in Internal Combustion Engines,* T. Uzkan, editor. ASME Winter Annual Meeting.

Chapman, M., Novak, J. M. and Stein, R. A., 1983, "A Nonlinear Acoustic Model of Inlet and Exhaust Flow in Multi-Cylinder Internal Combustion Engines," *ASME Paper 83-WA/DSC-14.*

Christian, A. M., 2003, "The Effect of Interface Geometry on Flow losses in Right-Angled Tee Junctions," MS Thesis, The Ohio State University.

Davies, P. O. A. L., Bento Coelho, J. L., and Bhattacharya, M., 1980, "Reflection Coefficients for an Unflanged Pipe with Flow," *Journal of Sound and Vibration*, 72: 543-546.

DeHaller, P., 1945, "The Application of a Graphic Method to some Dynamic Problems in Gases," *Sulzer Technical Review*: 1: 6-24.

Dennison, E. S., 1933, "Inertia Supercharging of Engine Cylinders," *Transactions of the ASME*, 55: 53-64.

Driels, M. R., 1975, "Dynamics of I.C. Engine Induction Systems," *Journal of Sound and Vibration,* 43(3): 499-510.

Engelman, H. W., 1973, "Design of a Tuned Intake Manifold," *ASME Paper 73-WA/DGP-2.*

Heywood, J. B., 1988, *Internal Combustion Engine Fundamentals.* McGraw-Hill, Inc., New York.

Howard, T. M., 2003, "Tapered Intakes on a Single Cylinder Engine," MS Thesis, The Ohio State University.

Ito, H., 1960, "Pressure Losses in Smooth Pipe Bends," *Transactions of the ASME. Journal of Basic Engineering,* 82: 131-143.

Kadenacy, M., 1935, British Patent 431,856.

Koester, E. W., 1904, "Luftkompressoran," *Zeitschrift. Verein Deutscher Ingenieure,* 48: 109-118.

Kothamasu, V., 1998, "Effect of Intake and Exhaust Elements on Sound Attenuation and Engine Performance: An Experimental and Computational Investigation," MS Thesis, The Ohio State University.

Lakshminarayanan, P. A., Janakiraman, P. A., Gajendra-Babu, M. K. and Murthy, B. S., "Prediction of Gas Exchange Process in a Single Cylinder Internal Combustion Engine," *SAE Paper 790359.*

Ledger, J. D., 1975, "A Finite-Difference Approach for Solving the Gas Dynamics in an Engine Exhaust," *Journal of Mechanical Engineering Science*, 17: 125-132.

Lichty, L.C., 1951, *Internal Combustion Engines.* McGraw-Hill Book Company, Inc., New York.

Matthews, R. and Gardiner, A. W., 1924, "Increasing the Compression Pressurein an Engine by Using a Long Intake Pipe," *NACA Technical Memorandum 180.*

Maynes, B. D. J., Kee, R. J., Kenny, R. G., Fleck, R., Mackey, D. O. and Foley, L., 2002, "Prediction of Formula 1 Engine and Airbox Performance using Coupled Virtual 4-Stroke and CFD Simulations," *SAE Paper 2002-01-3318.*

Miller, D. S., 1990, *Internal Flow Systems, 2nd Edition.* BHRA Information Services, Cranfield.

Morse, P. M., Boden, R. H., Schecter, H., 1938, "Acoustic Vibrations and Internal Combustion Engine Performance I: Standing Waves in the Intake Pipe System," *Journal of Applied Physics,* 9: 16-23.

Mucklow, G. F., 1940, "Exhaust-Pipe Effects in a Single-Cylinder Four-Stroke Engine," *Proceedings of the Institution of Mechanical Engineers*, 143: 109-125.

Paul, J., 2005, "The Effect of Interface Geometry on Dividing and Combining Flow Losses in Right-Angled Tee Junctions," MS Thesis, The Ohio State University.

Pearson, R. J. and Winterbone, D. E., 1990, "A Rapid Wave Action Simulation Technique for Intake Manifold Design," *SAE Paper 900676.*

Peters, M. C. A. M., Hirschberg, A., and Reijnen, A. J., 1993, "Damping and Reflection Coefficient Measurements for an Open Pipe at Low Mach and Low Helmholtz Numbers," *Journal of Fluid Mechanics*, 256: 499-534.

Randolf, Andrew, L., 1994, "Cylinder-Pressure-Based Combustion Analysis in Race Engines," *SAE Paper 942487.*

Riegler, U. G. and Bargende, M., 2002, "Direct Coupled 1D/3D-CFD-Computation (GT-Power/Star-CD) of the Flow in the Switch-Over Intake System of an 8-Cylinder SI Engine with External Exhaust Gas Recirculation," *SAE Paper 2002-01-0901.*

SAE Aero-Space Applied Thermodynamics Manual, 1960, Society of Automotive Engineers, New York.

Selamet, A., Ji, Z. L. and Kach, R. A., 2001, "Wave Reflections from Duct Terminations," *Journal of the Acoustical Society of America*, 109: 1304-1311.

Selamet, A., Dickey, N. S., Novak, J. M., 1994, "The Herschel-Quincke Tube: A Theoretical, Computational, and Experimental Investigation," *Journal of the Acoustical Society of America,* 96: 3177-3185.

Selamet, E. E., Selamet, A., Novak, J. M., 2004, "Predicting Chemical Species in Spark-Ignition Engines," *Journal of Energy,* 29: 449-465.

Takizawa, M., Uno, T., Oue, T. and Yura, T., "A Study of Gas Exchange Process Simulation of an Automotive Multi-Cylinder Internal Combustion Engine," *SAE Paper 820410.*

Thompson, M. P., 1968, "Non-Mechanical Supercharging of a Four-Stroke Diesel Engine," MS Thesis, The Ohio State University.

Winterbone, D. E. and Pearson, R. J., 1999, *Design Techniques for Engine Manifolds: Wave Action Methods for IC Engines,* Professional Engineering Publishing, London.